AD

USAAVLABS TECHNICAL REPORT 65-72

STUDY OF TANDEM ROTOR HELICOPTER DYNAMICS FOLLOWING POWER FAILURE AT HIGH SPEED

By

J. M. Davis
J. F. Kannon
P. F. Leone
H. A. McCafferty

November 1965

U. S. ARMY AVIATION MATERIEL LABORATORIES
FORT EUSTIS, VIRGINIA

CONTRACT DA 44-177-AMC-239(T)

VERTOL DIVISION
THE BOEING COMPANY
MORTON, PENNSYLVANIA

BLANK PAGES
IN THIS
DOCUMENT
WERE NOT
FILMED

DEPARTMENT OF THE ARMY
U S ARMY AVIATION MATERIEL LABORATORIES
FORT EUSTIS, VIRGINIA 23604

This report has been reviewed by the U. S. Army Aviation Materiel Laboratories and is considered to be technically sound. It is published for the exchange of information and stimulation of ideas.

Task 1D121401A14203
Contract DA 44-177-AMC-239(T)
USAAVLABS Technical Report 65-72
November 1965

STUDY OF TANDEM ROTOR HELICOPTER DYNAMICS FOLLOWING POWER FAILURE AT HIGH SPEED

R-383

by

J. M. Davis
J. F. Kannon
P. F. Leone
H. A. McCafferty

Prepared by

VERTOL DIVISION
THE BOEING COMPANY
Morton, Pennsylvania

for

U.S. ARMY AVIATION MATERIEL LABORATORIES
FORT EUSTIS, VIRGINIA

ABSTRACT

This report covers a parametric study of tandem rotor helicopter dynamics following power failure at high speed (200 knots plus).

It was concluded that complete loss of power on a high-speed helicopter results in hazardous flight conditions. Installation of auxiliary propulsion and incorporation of high-inertia rotor blades greatly relieve the situation by increasing the time available for the pilot to initiate recovery. Installation of a collective pitch rate limiter and an engine failure warning horn are recommended, to assist the pilot in taking corrective action. Provided collective pitch inputs are limited to safe values, no serious problems arise in the structural design of rotor blades to meet the conditions encountered in recovery from high-speed power failure. Dualization of engines and fuel systems provides an adequate margin of safety against sudden and complete power failure.

CONTENTS

LIST OF ILLUSTRATIONS

LIST OF TABLES

LIST OF SYMBOLS

Symbol	Definition	Unit
A	Rotor disc area	ft^2
a_1	First harmonic longitudinal flapping angle with respect to rotor shaft normal plane; hence, longitudinal tilt of the rotor cone, positive for rearward tilt	rad
a_{1_α}	Change in longitudinal flapping angle with angle of attack	
a_{1_μ}	Change in longitudinal flapping angle with advance ratio	rad
$a_{1_{\theta_c}}$	Change in longitudinal flapping with collective pitch	
B_{1T}	Longitudinal cyclic trim	rad
b	Number of blades per rotor	
b_1	First harmonic lateral flapping angle with respect to rotor shaft normal plane; hence, lateral tilt of the rotor cone, positive for tilt toward advancing side	rad
c_ℓ	Airfoil section lift coefficient	
c_d	Airfoil section drag coefficient	
C_T	Rotor thrust coefficient $[T \div \rho\pi R^2(\Omega R)^2]$ where T is parallel to shaft axis	
C_{T_α}	Change in thrust coefficient with angle of attack	rad^{-1}

Symbol	Definition	Unit
$\frac{C_T}{\sigma}$	Blade loading parameter	
c	Blade chord	ft
c_o	Blade preload about lag hinge	ft-lb
c_1	Blade damping about lag hinge	ft-lb/ rad/sec
c.g.	Center of gravity	
D/L	Ratio of fuselage drag to overall lift	
e	Rotor flap hinge offset	ft
e/R	Flap hinge offset ratio	
f_c	Centrifugal force	lb
G.W.	Gross weight	lb
g	Acceleration due to gravity	ft/sec^2
h	Height of rotor hub above c.g., parallel to the helicopter Z axis	ft
I_X, I_Y, I_Z	Helicopter moments of inertia about the X, Y and Z axis, respectively	$sl-ft^2$
I_F	Blade moment of inertia about the flap hinge	$sl-ft^2$
I_L	Blade moment of inertia about the lag hinge	$sl-ft^2$
I_R	Polar moment of inertia of rotating components	$sl-ft^2$
i	Angle of incidence of rotor shaft in the helicopter X-Z plane, positive for a forward tilt	deg

Symbol	Definition	Unit
J_{ZX}	Helicopter product of inertia	sl-ft^2
k_1	Kinematic ratio between blade pitch and its own flapping angle	
k_2	Kinematic ratio between blade pitch and the flapping angle of the following blade	
k_3	Kinematic ratio between blade pitch and the flapping angle of the preceding blade	
ℓ	Distance from helicopter center of gravity to the projection of rotor hub on the helicopter X axis	ft
M_α	Change in helicopter pitching moment with angle of attack	ft-lb/rad
$(M_\alpha)_e$	Change in helicopter pitching moment with angle of attack due to flap hinge offset	ft-lb/rad
$(M_\alpha)_{h_R}$	Change in helicopter pitching moment with angle of attack due to height of rear rotor	ft-lb/rad
M_{θ_C}	Change in helicopter pitching moment due to collective pitch	ft-lb/rad
M_F	Blade weight moment about flapping hinge	ft-lb
M_L	Blade weight moment about lag hinge	ft-lb
M_T	Advancing blade tip Mach number	
R	Rotor radius	ft
V	Forward speed	knots

V_t	Rotor tip speed (ΩR)	ft/sec
XYZ	Coordinate system fixed to helicopter fuselage at center of gravity	
X_c	Blade root cutout ratio	
Ω	Rotor rotational speed	rad/sec
α	Angle of attack of fuselage with respect to free stream	rad
β	Angle of sideslip of fuselage with respect to free stream	rad
θ_c	Mean root collective pitch of blade around the azimuth	rad
λ	Inflow ratio with respect to rotor shaft normal plane	
μ	Advance ratio with respect to rotor shaft normal plane	
σ	Rotor blade solidity $(\frac{bc}{\pi R})$	
ψ	Rotor blade azimuth position measured from downwind position in the direction of rotation	deg

NOTE: Subscripts F and R are used to denote front and rear rotors

SUMMARY

An analytical investigation of power failure during high-speed flight has provided an insight into the effects that various rotor configurations and control inputs have on rotor behavior, fuselage motions, and blade loads. The investigation was carried out at 200 knots, except for a few cases at 250 knots.

Realistic tandem rotor helicopter configurations were analyzed, with drag/lift (D/L) ratios from 0 to 0.15. The effects of flapping hinge offset, blade twist, Lock number, longitudinal cyclic pitch, and relative rotor spacing were investigated. Configurations having delta-three flapping hinges, tip path plane controllers, and teetering rotors were also analyzed. All configurations were assumed to be equipped with a stability augmentation system (SAS) providing rate damping about all three helicopter axes, as well as static directional stability.

A serious problem arises following complete power failure on helicopters with no auxiliary thrust (D/L = 0.15). The allowable delay time before collective reduction is only 1.5 seconds, and a precise collective input schedule must be adhered to closely. The situation is not so critical for complete failure on aircraft with large auxiliary thrust (D/L = 0). Allowable delay times are greater than 4.0 seconds, and fairly mild collective reduction rates can be used. Likewise, for partial power failure, allowable delay times are longer, and low collective reduction rates are satisfactory.

Large improvements in helicopter and rotor behavior after power failure can be obtained by an increase in rotor blade inertia and/or incorporation of pitch-flap coupling on the forward rotor.

A satisfactory collective recovery technique was found to consist of an initial rapid reduction for 50 percent of the total reduction, changing to a slower rate for the remainder of the input. A large simultaneous aft longitudinal stick input will maintain altitude, reduce forward velocity, and restore rotor speed.

Experience with existing tandem rotor helicopters indicates that prompt warning of complete power failure will be given by the change in transmission noise level which results from

rotor speed decay; however, for adequate warning of partial failure, a horn is required. A collective dump rate limiter will enable the necessary rapid collective rates to be obtained manually without exceeding safe limits of blade-fuselage clearance, negative load factor, and blade loading. With the installation of these two devices (warning horn and dump rate limiter), automatic equipment for reducing collective pitch independent of pilot action will not be necessary.

An analysis of the peak transient vibratory flapwise and chordwise bending stresses, added to the steady-state vibratory flapwise and chordwise bending stresses for the trim condition before power failure, shows that the particular rotor blade structural design employed in the study will satisfactorily withstand the loads encountered during all anticipated recovery maneuvers.

CONCLUSIONS

Loss of engine power in a high-speed helicopter can become a flight safety hazard. Reduction of driving torque immediately causes rotor speed to decay during pilot reaction time. The decreased rotor speed increases the retreating-blade angle of attack, and soon both rotor flapping and aircraft attitude become divergent. Higher advance ratios and thrust coefficients, which are critical factors in determining blade airloads, are also produced. The pilot can take alleviating action by reducing collective pitch to initiate autorotational entry. However, a control input executed too rapidly can produce negative thrust, high negative normal acceleration, and blade-fuselage interference. Since rotor loads encountered during safe recovery from complete power failure at high speed are such that conventional rotor blades can be designed to withstand the stresses imposed, the problem is mainly one of determining a safe pilot technique for autorotational entry.

The most critical feature of helicopter response to complete power failure is rotor speed decay. The only configuration modifications which have an appreciable effect thereon are large reductions in drag/lift ratio and in blade Lock number. The rotor speed decay which results from these modifications will provide a longer delay time between power failure and initiation of recovery action, and will permit slower rates of collective reduction. The autorotational entry is less severe, resulting in lower blade loads. For example a 50-percent reduction in Lock number produces a 20-percent reduction in flapwise bending moment*and a 40-percent reduction in chordwise bending moment*for the same pilot recovery technique.

Peak blade loading as indicated by $C_{T/\sigma}$ is mainly governed by pilot technique during recovery. For a given collective reduction rate, the peak blade loading can be reduced by incorporating rotor stabilization devices such as: (1) Delta-three coupling**,(2) Pitch-flap out-of-phase coupling** and (3) Pitch-cone coupling**. For example, a 30-degree delta-

*Oscillatory
**Defined in Section 1 of the discussion.

three coupling on the forward rotor reduces the flapwise bending moment* 15 percent and the chordwise bending moment* 40 percent. Negative swashplate dihedral was found to produce high peak loading, $C_{T/\sigma}$, on both rotors.

Normal acceleration loads are also determined by pilot technique. However, for a given collective reduction rate, the negative normal acceleration load can be somewhat reduced by incorporating delta-three or pitch-cone coupling on the forward rotor. In contrast, large flapping hinge offset produces large negative normal acceleration.

Adequate blade-fuselage clearance during recovery from power failure is a matter of concern because of the transient flapping and negative coning of the rotors. The problem can obviously be relieved by changing aft rotor cyclic pitch or by increasing aft rotor height. An optimum cyclic pitch schedule for minimum flapping of both rotors produced higher blade bending moments, while variations in the relative aft rotor height showed only negligible change in bending moments. The teetering rotor was also found to have merit in regard to blade-fuselage clearance since the total flapping is diminished because one rotor blade restrains the other.

The best rotor design is one that suppresses the peak responses during pilot reaction time and autorotational entry. The following modifications, listed in decreasing order of effectiveness, have beneficial effects during the period between engine failure and collective reduction:

1. Reduced drag (auxiliary propulsion)
2. Reduced Lock number (higher blade inertia)
3. Pitch-flap out-of-phase coupling on the forward rotor
4. Forward longitudinal cyclic pitch on both rotors
5. Negative swashplate dihedral

The following modifications have a favorable influence on helicopter dynamics during and after collective reduction. The transient rotor flapping, normal acceleration, and blade loading were reduced by these modifications, while minimum rotor speed and blade-fuselage clearance were improved. These modifications are listed in decreasing order of effectiveness as follows:

---

*Oscillatory

1. Reduced drag
2. Reduced Lock number
3. Aft longitudinal cyclic pitch on both rotors
4. Delta-three coupling on the forward rotor
5. Pitch-cone feedback on the forward rotor
6. Pitch-flap out-of-phase coupling on the forward rotor.

Note that reduced drag, reduced Lock number, and pitch-flap out-of-phase coupling reduce the divergences in both modes. Forward cyclic pitch on both rotors diminishes the divergence during pilot reaction time, and aft cyclic pitch on both rotors is helpful during autorotational entry. Delta-three on the forward rotor not only reduces divergence during pilot recovery but also significantly improves the static stability of the tandem helicopter with angle of attack.

A study of the effects of various autorotational entry techniques led to the following conclusions concerning collective and longitudinal control inputs:

1. The smoothest recovery is achieved by combining an aft longitudinal stick input with a collective reduction that starts at 20 degrees per second and is converted to 4 degrees per second at 50 percent travel. The aft longitudinal stick input relieves peak negative normal acceleration, maintains rotor tip speed and conserves altitude during autorotational entry.

2. The maximum pilot delay times between complete power failure and initiation of recovery control are limited to 1.5 seconds on most configurations having no auxiliary thrust. For aircraft with large auxiliary thrust, delay times of up to 4.0 seconds could be tolerated. For configurations optimized to relieve rotor speed decay and excessive transient flapping, the above maximum allowable delay times become greater than 2.0 seconds and 5.0 seconds, respectively.

3. Adequate warning of complete power failure will be given by rotor speed decay and the resultant change in transmission and rotor noise, provided special efforts are not made to irolate the cockpit from these noises. For configurations without auxiliary propulsion, approximately one-quarter second is required after power failure for the rotors studied to

lose sufficient speed to give warning. For configurations with auxiliary thrust, the required time is approximately one-half second. The lack of audible warning of partial power failure may necessitate a warning horn for this condition. The horn would also serve to give additional warning of a complete power failure.

4. A collective dump rate limiter should be incorporated on configurations without auxiliary propulsion. Because of the limited allowable delay time and the high initial collective reduction rates, there is danger that the collective input may be continued too far, causing blade-fuselage contact. Aft longitudinal stick should not be applied until after the initiation of the reduced collective rate, which is after the occurrence of peak flapping. This is to preclude an excessive rate of collective reduction on the aft rotor, which could cause rotor-fuselage interference.

The following conclusions apply to recovery from complete power failure at 250 knots. To assure safe recovery from complete rotor power failure, drag/lift ratio must be considerably less than 0.15. If auxiliary thrust is incorporated for other reasons on 250-knot helicopters, this consideration will present no additional design requirement at these speeds. Assuming D/L = 0 at 250 knots, the responses to complete rotor power failure are considerably milder than for configurations having D/L = 0.15 at 200 knots, and recovery should therefore present no great problem.

RECOMMENDATIONS

The results of this investigation form the basis for the following recommendations concerning the design and operation of high-speed tandem rotor helicopters:

1. Dual engines with completely independent fuel and control systems should be provided, to minimize the chances of complete power failure.

2. Auxiliary propulsion should be installed, to reduce rotor speed decay and improve delay time.

3. Rotor blades with large moments of inertia should be utilized, for the same reasons.

4. A collective dump rate limiter should be installed, to allow collective pitch to be reduced at the fastest safe rate for the configuration in question.

5. An engine failure warning horn should be installed, to reduce pilot reaction time in the event of single-engine failure.

6. Consideration should be given to the installation of pitch-flap out-of-phase coupling on the forward rotor, and the reduction of forward longitudinal cyclic pitch on the aft rotor, in order to stabilize the helicopter and increase blade-fuselage clearance.

In the course of conducting the study, several significant avenues of investigation became apparent, but were not pursued because they were beyond the scope of this report. It is therefore recommended that consideration be given to further investigation as follows:

1. Investigation of the effects of rotor flap-lag coupling on rotor behavior.

2. Investigation of the highly divergent tendencies of rotors with large hinge offset.

3. Investigation of the effects of fuselage stability characteristics on helicopter and rotor responses.

INTRODUCTION

Engine failure at high speed on a tandem rotor helicopter can lead to the development of dangerous flight conditions, as a result of the rapid loss of rotor speed. During recovery, which in the case of complete failure involves entry into autorotation, blade-fuselage clearance may become critical because of large rotor flapping angles, while excessive loads on the rotor blades may cause them to fail.

To reduce the uncertainty regarding the seriousness of the problem, an exploratory analytical investigation of the tandem lifting rotor type with realistic fuselage and rotor aerodynamic characteristics was conducted. It was assumed that the maximum rotor stresses would be associated with the largest blade excursions in the flapping and lead-lag degrees of freedom. Hence, the object of the investigation was the determination of these excursions, as influenced by various parameters and control inputs, and interpretation of the results in terms of airloads.

The work was accomplished using Vertol Division's transient analysis program, as documented in Appendix I, and aeroelastic analyses performed on 20 selected cases.

The accuracy of the automatic data-plotting equipment used for this program has been investigated. Comparison of plotted values with printed computer results indicates a plotting accuracy of approximately $\pm$ 1 millimeter, or 1/5 of a grid division, for each parameter. The accuracy of the transient analyses in estimating the time histories is discussed in Appendix II where the estimated data are correlated with flight test data.

The analysis was conducted over the range of parameter combinations shown in Table 1, wherein the parameter combinations are identified by a configuration number. Throughout this report, reference will be made to configuration numbers when comparing configurations. A baseline case (Configuration 6) was selected, and systematic variations thereto were made to obtain other configurations.

TABLE 1

TABULATION OF CONFIGURATIONS

Airspeed (Knots)	200	200	200	200	200	250
Drag/Lift	0	0.075	0.15	0.15	0.15	0
Blade Linear Twist	0°	-4°	-4°	-8°	-12°	-12°
Articulated Rotor: e/R = 0	1	2	3	--	--	--
Articulated Rotor: e/R = 0.05	4	5	6*	7	8	45
Articulated Rotor: e/R = 0.15	9	10	11	--	--	--
Teetering Rotor	12	13	14	--	--	--
Delta Three on Fwd Rotor : e/R = 0.05	15	--	16	--	17	46
Tip Path Controller on Fwd Rotor; e/R = 0.05						
Pitch-Cone	18	--	19	--	20	47
Pitch-Flap Out-of-Phase	21	--	22	--	23	--
Pitch-Flap In-Phase	--	--	24	--	--	--
All Three	--	--	25	--	--	--
50% Lower Lock Number : e/R = 0.05	26	27	28	--	--	48
Cyclic Pitch Variation: e/R = 0.05						
2° Aft	29	--	--	--	--	--
4° Fwd	--	--	30	--	--	--
10° Fwd	31	--	--	--	--	--
14° Fwd	--	--	32	--	--	--
Swashplate Dihedral: e/R = 0.05						
5.5°	33	--	--	--	--	--
1.5°	--	--	34	--	--	--
-6.5°	--	--	35	--	--	--
-10.5°	36	--	--	--	--	--
Rotor Overlap: e/R = 0.05						
20%	37	--	38	--	--	--
0%	39	--	40	--	--	--
Aft Rotor Height : e/R = 0.05						
20%	41	--	42	--	--	--
30%	43	--	44	--	--	--

* BASELINE CONFIGURATION

The aircraft configuration analyzed in this investigation was of the tandem lifting rotor type, the characteristics of which are described in Appendix III. These data represent the best estimate of a realistic tandem rotor transport helicopter at the time the contract was awarded.

Time histories, generally five seconds in length, were plotted. Significant time histories will be found in Appendix IV. The motions recorded included the following:

1. Cockpit control positions (an input)
2. Rotor blade motions: Flapping and lead-lag, with special indication of blade-fuselage proximity, for both rotors
3. Rotor tip speed
4. Height loss
5. Airspeed
6. Normal acceleration at helicopter center of gravity
7. Fuselage angle of attack
8. Fuselage sideslip angle
9. Fuselage attitudes: pitch, roll, and yaw
10. Collective and cyclic pitch on the rotor heads
11. Blade loading parameters
12. Rotor advance and inflow ratios.

The analysis conducted during this program is reported in five sections, as follows:

1. Aircraft Response to Power Failure at 200 Knots

   In this section the divergent characteristics of the various configurations under the condition of no corrective control inputs are compared.

2. Development of Recovery Techniques

   In this section various control inputs are made on the baseline configuration (Configuration 6) described in Table 1, in order to develop a satisfactory, but not necessarily optimum, technique. The argument for a dump rate limiter is developed.

3. Controlled Recovery from Power Failure

The recovery technique developed for Configuration 6 is applied to the remaining configurations. The results, including blade loadings, are discussed.

4. Analysis at 250 Knots

The results of 10 cases run at 250 knots are discussed in this section.

5. Aeroelastic Considerations

The theoretical flapwise and chordwise moment distributions obtained by the aeroelastic analysis of 20 selected time histories are presented.

DISCUSSION

1. AIRCRAFT RESPONSE TO POWER FAILURE AT 200 KNOTS

The responses of the various configurations to power failure at 200 knots, in the absence of corrective control inputs, are compared in this section of the report, in order to determine which features of a given configuration contribute to rapid divergence in both rotor and helicopter motions after power failure, and what modifications can be made to alleviate these problems.

In order to compare the response of one configuration with another, the following divergence criteria are used:

1. Time to Attain Rotor Flapping Amplitudes of ± 0.20 Radian (Peak-to-Peak) - The flapping amplitude criterion corresponds roughly to the greatest peak-to-peak flapping values obtained in flight tests of two current tandem rotor helicopter types.

2. Time for Rotor Tip Speed to Diminish to 550 Feet per Second - This rotor tip speed criterion represents a 25-percent loss of rotor speed, which is about 5 percent greater than the maximum allowable transient rotor speed loss for typical tandem rotor helicopters currently in operation.

3. Time to Attain Sinking Speed of 1500 Feet per Minute, Time to Attain Fuselage Sideslip Angle of ± 10 Degrees, and Time to Attain Fuselage Roll, Pitch, and Yaw Rates of ± 10 Degrees per Second - The sinking speed, sideslip angle, and fuselage divergence rate criteria represent the approximate demarkation between normal mild maneuvers and more severe maneuvers. The rate criteria also correspond to the maximum rates allowed within 3 seconds of a stability augmentation system failure, as set forth in Reference 1.

4. Time to Attain Fuselage Angle of Attack of 20-Degree Nose-Up or 10-Degree Nose-Down - The fuselage angle of attack criterion corresponds to rotor angles of attack of approximately ± 20 degrees (taking into account the rotor shaft incidences); this is well

within the demonstrated capability of present rotary wing aircraft. These values were selected in order to obtain a measurement of differences between configurations, within the 5-second duration of the time histories.

5. Time to Attain Blade Loading Parameters, C_T/σ, of 0 or +0.12 - The criterion for blade loading parameter is a rough representation of the maximum blade stress levels obtained in normal operations with tandem helicopters.

These criteria were chosen to indicate the time required for the helicopter to approach critical values of rotor flapping amplitude, rotor rpm loss, and blade load, or time to reach uncomfortable attitudes and rates.

TYPICAL BEHAVIOR OF THE TANDEM HELICOPTER FOLLOWING POWER FAILURE (NO CONTROL INPUTS)

The characteristics typical of the behavior of a tandem rotor helicopter following complete power failure at 200 knots, with no corrective pilot inputs, are detailed below. Reference is made to Figures 57 and 58, which describe the behavior of Configurations 6 and 4, respectively.

Complete loss of driving torque causes the rotors to decelerate rapidly, losing as much as 25 percent of the cruise rpm in 1.5 seconds (D/L = 0.15) or in 4 seconds (D/L = 0). As the rotor speed falls, centrifugal force on the blades is reduced and μ is increased, giving rise to divergent aft longitudinal flapping, and blade stall (through the rotor derivative a_{1_μ}). Rotor sensitivity to angle of attack (a_{1_α}) also increases rapidly with μ.

The development of severe blade stall is indicated by the rate of divergence of rotor flapping. Analysis of a number of representative time histories indicates that a higher-order divergence will commence at rotor tip speeds between 500 and 550 feet per second for configurations with D/L = 0.15, and between 550 and 600 feet per second for configurations with D/L = 0. Typically, these tip speeds occur between 1.3 and 2.2 seconds after engine failure for the higher drag cases, and between 2.5 and 4.5 seconds for the zero-drag cases.

As rotor thrust decays, forward velocity falls slowly, provided the helicopter remains approximately level. If the helicopter pitches up, however, a sharp deceleration occurs as the thrust vectors are rotated aft.

Rate of sink increases rapidly as the rotors lose thrust, and normal acceleration may fall to 0.5g within 2 seconds, the most rapid decrease occurring instantaneously with power loss.

As the rate of sink builds up, angle of attack increases, thereby contributing to rotor flapping divergence through the positive rotor derivative a_{1_α}, which is, itself, increasing with μ. Also, if the helicopter as a whole is unstable because of a positive M_α, a divergent pitching moment results. Divergences in roll, yaw, and sideslip are generated by lateral flapping of the rotors. Typically, these divergences do not become serious until 3 to 4 seconds after power failure for the high-drag cases. For the low-drag cases, which do not undergo such large changes in rotor speed and μ, these divergences will not appear until well beyond 5 seconds.

ANALYSIS OF COMPLETE POWER FAILURE

Using the criteria previously discussed, the responses of the various configurations to complete power failure at 200 knots are compared in Tables 11 to 14, for cases without corrective action by the pilot.

Effect of Blade Twist

From the tabulated data, it is evident that rotor blade twist has only a small effect on the rates of divergence of both the helicopter and the rotors. Except for a slight increase in the rate of sink, higher blade twist results in a small reduction in the rate of divergence for all parameters.

Effect of Flapping Hinge Offset

The effects of rotor flapping hinge offset for D/L = 0.15 may be obtained by comparing Figures 57, 59, and 60, the tabulated data from which are plotted in Figure 1.

The strong adverse influence of hinge offset on the rates of divergence is due mainly to the unstable hub moments generated by large offset and high longitudinal flapping. The

200 KT, D/L = 0.15, COMPLETE POWER FAILURE, NO INPUTS

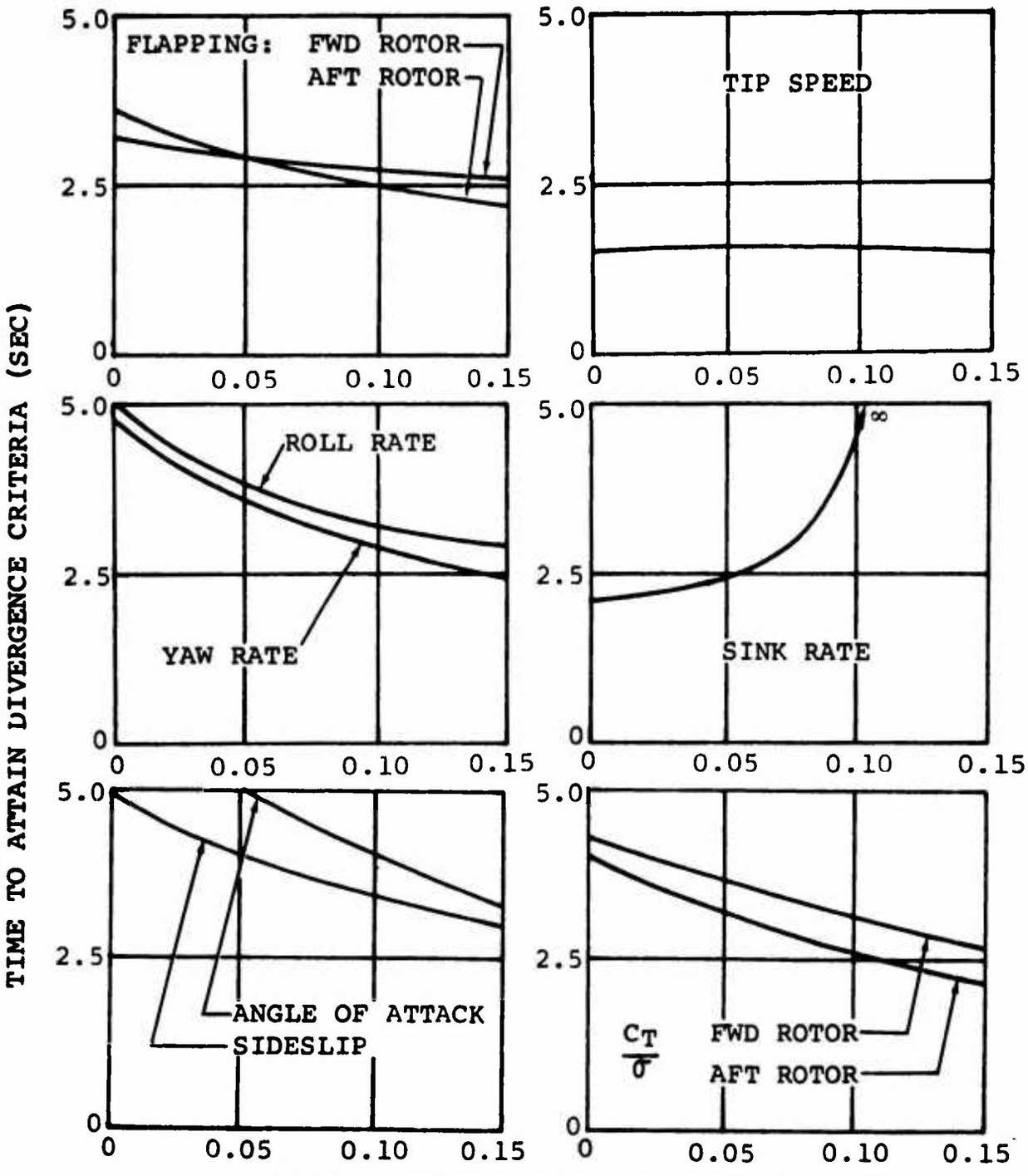

Figure 1. Effect of Rotor Flapping Hinge Offset on Helicopter and Rotor Divergence.

contribution of hinge offset to the static longitudinal stability of a tandem helicopter is given approximately by

$$(M_\alpha)_e = \frac{f_c eb}{2} \quad (a_{1F_\alpha} + a_{1R_\alpha}) \qquad (1)$$

Taking typical values from a stability analysis of the configurations and flight conditions considered, the relationship of hinge offset to pitching moment parameters is given in Table 2.

TABLE 2

VARIATION OF PITCHING MOMENT PARAMETERS WITH HINGE OFFSET

e/R	0	0.05	0.15
$\frac{f_c eb}{2}$ (ft-lb)	0	226,000	679,000
a_{1F_α}	0.698	0.803	0.880
a_{1R_α}	0.532	0.598	0.670
$(M_\alpha)_e$ (ft-lb/rad)	0	317,000	1,052,000
$\frac{(M_\alpha)_e}{I_Y}$ (rad/sec^2)	0	1.92	6.37

Hence, configurations with appreciable hinge offset have to contend with a large destabilizing contribution to longitudinal stability. Figure 2 shows the variation with hinge offset of M_α/I_Y resulting from all contributions.

Hinge offset initially has little effect on the rotor and helicopter rates of divergence up to about 1.5 seconds. However, as the angle of attack builds up as the result of the increasing

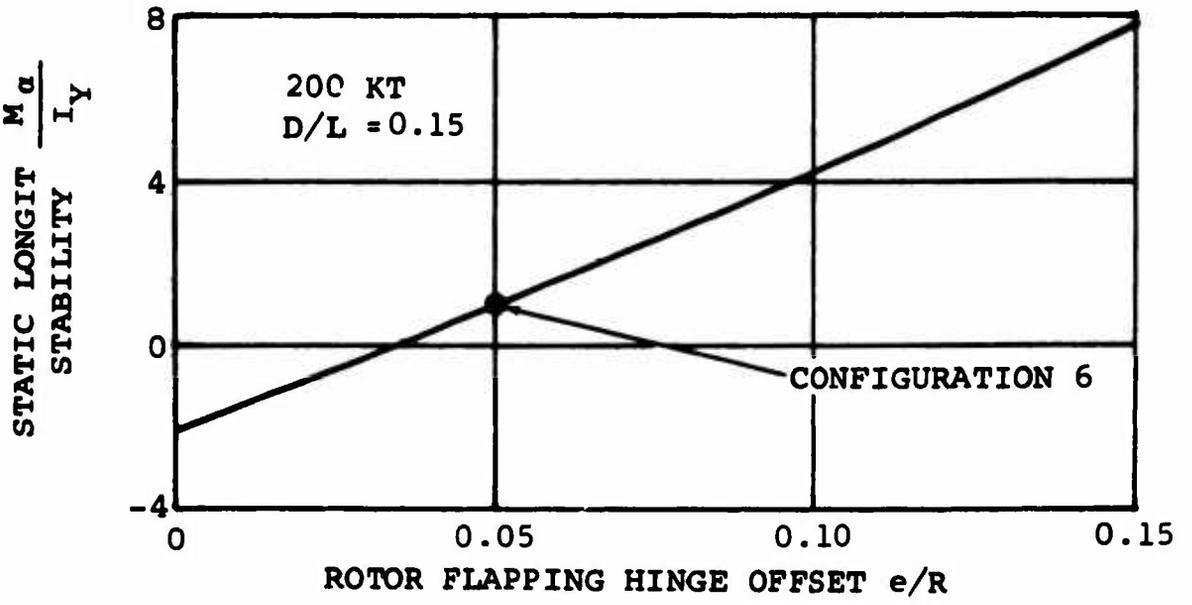

Figure 2. Effect of Rotor Flapping Hinge Offset on Static Longitudinal Stability Derivative.

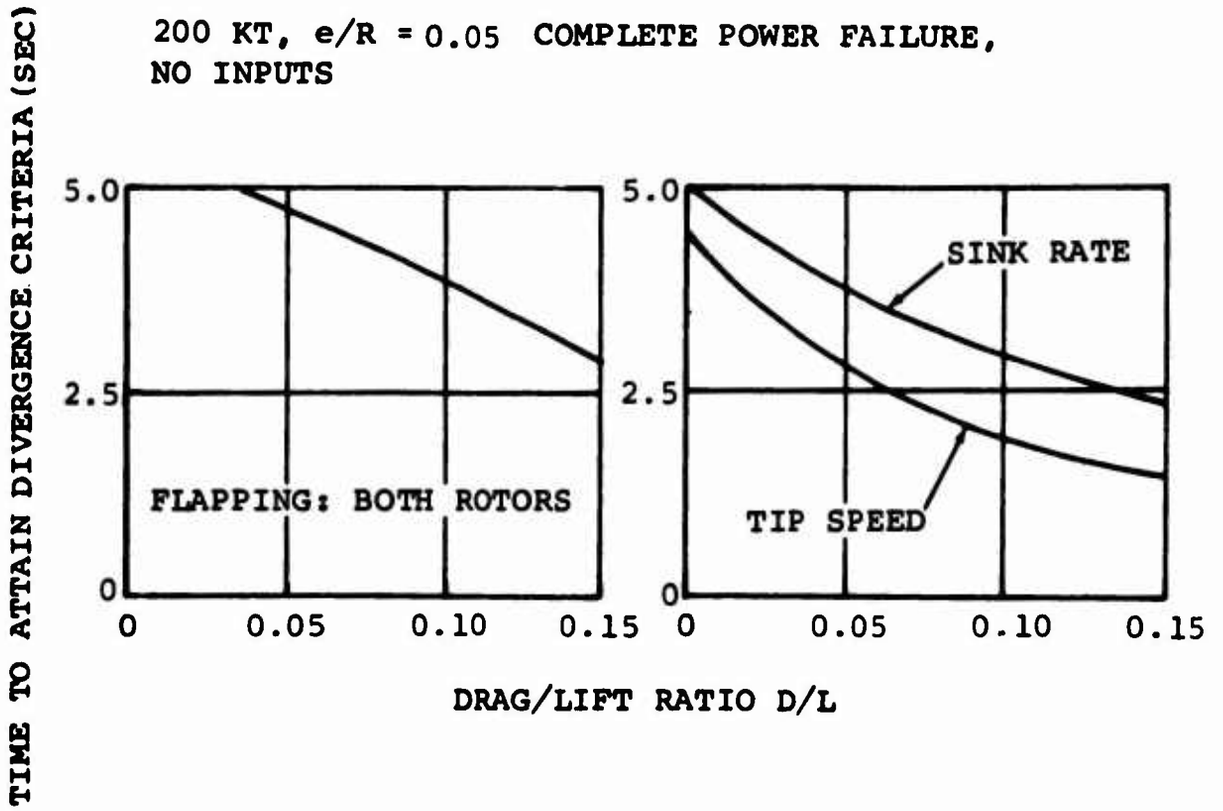

Figure 3. Effect of Drag/Lift Ratio on Helicopter and Rotor Divergence.

sink rate, the differences in a_{1F_α} and in a_{1R_α} begin to be felt in the greater longitudinal flapping of the higher-offset rotors. At the same time the large, unstable value of $(M_\alpha)_e$ at e/R = 0.15 results in a rapid pitch-up, which does not occur for the other two configurations. This pitch-up produces a positive increment in rotor inflow, which causes further longitudinal flapping divergence and blade stall. Lateral flapping will also be induced due to the increasing μ, leading to divergences in roll, yaw, and sideslip. The same trends are evident in the tabulated data for D/L = 0.075 and D/L = 0, but the divergences are less severe for reasons discussed in the following paragraphs.

Effect of Drag/Lift Ratio

Comparison of the time histories presented in Figures 57, 58, and 61 shows the effect of decreasing the drag/lift ratio, by drag cleanup and/or by addition of auxiliary propulsive units. The tabulated data are plotted in Figure 3 for e/R = 0.05.

The favorable effects of reduced drag on the rates of divergence arise from the lower rotor torque (power) requirements indicated in Table 14. The lower drag and the lower torque required cause both the helicopter and the rotor to decelerate more slowly. Consequently μ increases at a much slower rate, and the onset of large-amplitude flapping and rotor stall is delayed.

Because rotor speed decays more slowly, thrust levels are maintained for a longer time, rotor and SAS damping is improved, control is retained for a longer period, and rate of sink is reduced; hence, the angle of attack increases more slowly. Helicopter instabilities due to angle of attack are therefore reduced, and pitch, roll, and yaw divergences are much less severe.

Effect of Longitudinal Cyclic Pitch

Figures 62 and 63, together with Figure 57, show the effects of varying longitudinal cyclic pitch between 4 degrees forward and 14 degrees forward on both rotors simultaneously, for D/L = 0.15. Figures 4 and 5 show the favorable influence of forward cyclic pitch on helicopter behavior and on longitudinal stability. This effect is largely explained by referring to

Table 3, which shows the significant derivatives for the configurations considered.

TABLE 3

VARIATION OF LONGITUDINAL DERIVATIVES WITH LONGITUDINAL CYCLIC PITCH

B_{1T}	4°	8°	14°
$\frac{M_\alpha}{I_Y}$ (rad/sec^2)	6.53	0.94	-3.77
C_{TF_α} (rad^{-1})	0.042	0.041	0.036
C_{TR_α} (rad^{-1})	0.034	0.042	0.044
a_{1F_α}	0.755	0.803	0.860
a_{1R_α}	0.768	0.598	0.529
a_{1F_μ} (rad)	0.292	0.161	-0.031
a_{1R_μ} (rad)	0.450	0.239	0.064

The large change in M_α/I_Y is attributable mainly to variations in the rotor thrust contribution to static longitudinal stability, given approximately by

$$(M_\alpha)_{thrust} = (C_{TF_\alpha} \ell_F - C_{TR_\alpha} \ell_R) \rho A(\Omega R)^2 \qquad (2)$$

These two terms form the dominant contribution to M_α. Since they are of opposite sign and of approximately equal magnitude, moderate variations in C_{TF_α} and C_{TR_α} will result in large changes in M_α. Such moderate variations in C_{TF_α} and C_{TR_α} arise from rotor stall effects, which reduce the thrust

response of the rotor to angle-of-attack changes. With B_{1T} = 4 degrees, the aft rotor at trim is operating on the verge of stall (α_{270} = 14.1 degrees); the same is true of the forward rotor with B_{1T} = 14 degrees (α_{270} = 13.8 degrees). The resultant variations in C_{TF_α} and C_{TR_α} produce the large change in M_α/I_Y with longitudinal cyclic pitch. However, normal helicopter operations are usually carried out with the rotors somewhat removed from stall conditions, in which case the influence of longitudinal cyclic pitch may not be as large as is apparent in this study.

The behavior of the helicopter following engine failure may be explained by referring to the tabulated derivatives. As rotor speed falls rapidly from the instant of power failure, μ increases quickly, and the effects of the large differences in a_{1F_μ} and a_{1R_μ} are seen in the immediate divergence of longitudinal flapping for the configuration with B_{1T} = 4 degrees compared to the initial convergence shown by the configuration having B_{1T} = 14 degrees. The greater longitudinal flapping for B_{1T} = 4 degrees generates a positive pitching moment, which increases the angle of attack and thus excites both the rotor instabilities represented by a_{1F_α} and a_{1R_α}, and the helicopter instability M_α. Flapping and angle of attack then rapidly diverge, and the helicopter pitches up, yielding a positive increment in rotor inflow which further accentuates the flapping divergence. Large-amplitude lateral flapping then develops, leading to lateral and directional divergences.

For the configuration with B_{1T} = 14 degrees, the stable value of M_α greatly reduces the angle-of-attack increase, and, therefore, does not excite rotor divergence through a_{1F_α} and a_{1R_α}. However, this improvement is obtained at the cost of large-amplitude forward flapping at trim, which may not be allowable in a practical design because of stress considerations.

The higher trim power required with B_{1T} = 4 degrees is attributable to the high fuselage drag associated with the large negative angle of attack of the fuselage (-8.4 degrees). This higher power requirement results in greater rotor deceleration, a faster increase in μ, and, consequently, a more rapid divergence in rotor flapping.

The initial convergence of rotor flapping shown in Figure 63 for 14 degrees of forward cyclic pitch is due to the large-

amplitude forward flapping at trim. After engine failure, the rotors begin to flap aft, converging to zero longitudinal flapping before finally diverging.

All the trends discussed above are also valid for rotor shaft incidence changes of equal magnitude, since cyclic and shaft tilt are interchangeable, to a first approximation. These trends also appear in the data for D/L = 0, but the divergences are much milder because of lower drag.

Effect of Swashplate Dihedral

The effects of varying swashplate dihedral* are indicated by a comparison of Figures 64 and 65 with Figure 57. For the high-drag case (D/L = 0.15), the dihedral was varied between 1.5 degrees and -6.5 degrees. Figures 6 and 7 show the large adverse effect of positive dihedral. This adverse effect can be explained on the same basis as the effect of cyclic pitch, using values obtained from a stability analysis of the configurations considered. Table 4 shows the relationship of swashplate dihedral to the significant longitudinal derivatives.

As with the longitudinal cyclic data considered in Table 3, the large variation in M_α/I_Y with swashplate dihedral is caused by the sensitivity of M_α to changes in C_{TF_α} and C_{TR_α}. Similarly, the variation of M_μ/I_Y arises from the sensitivity of M_μ to small changes in C_{TF_μ} and C_{TR_μ}. However, the variation of these thrust derivatives with swashplate dihedral is not readily attributable to rotor stall in this case, since the maximum blade angles of attack are less than those encountered in the study of longitudinal cyclic effects; for example, α_{270} = 13.2 degrees (dihedral = 1.5 degrees) and α_{270} = 13.9 degrees (dihedral = -6.5 degrees) for the aft and forward rotors, respectively. Consequently, the effects of swashplate dihedral variation obtained herein will be valid for normal helicopter operation

*Swashplate dihedral is defined as one-half the included angle between the forward and aft swashplate axes. Negative swashplate dihedral is also termed "cathedral".

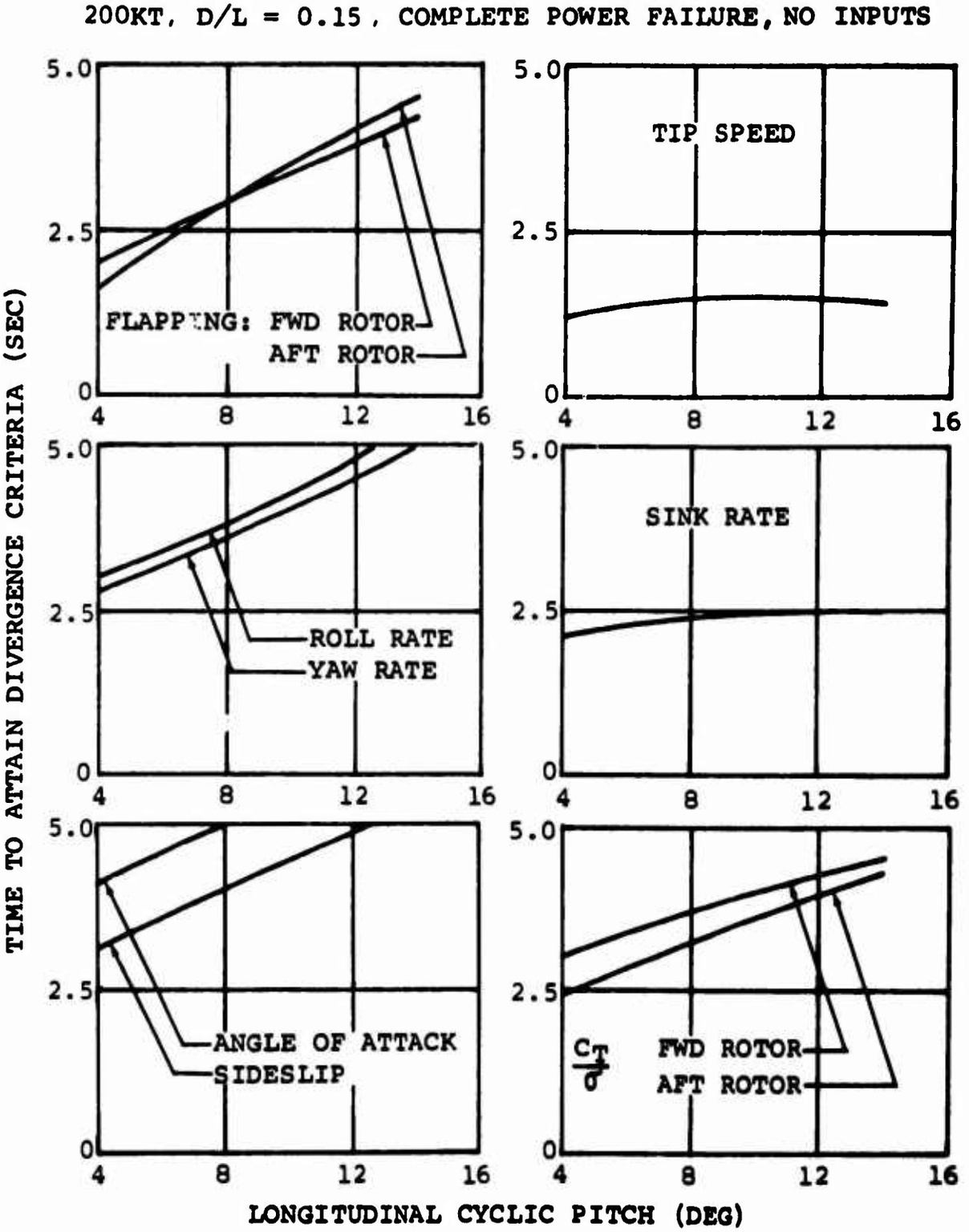

Figure 4. Effect of Longitudinal Cyclic Pitch on Helicopter and Rotor Divergence.

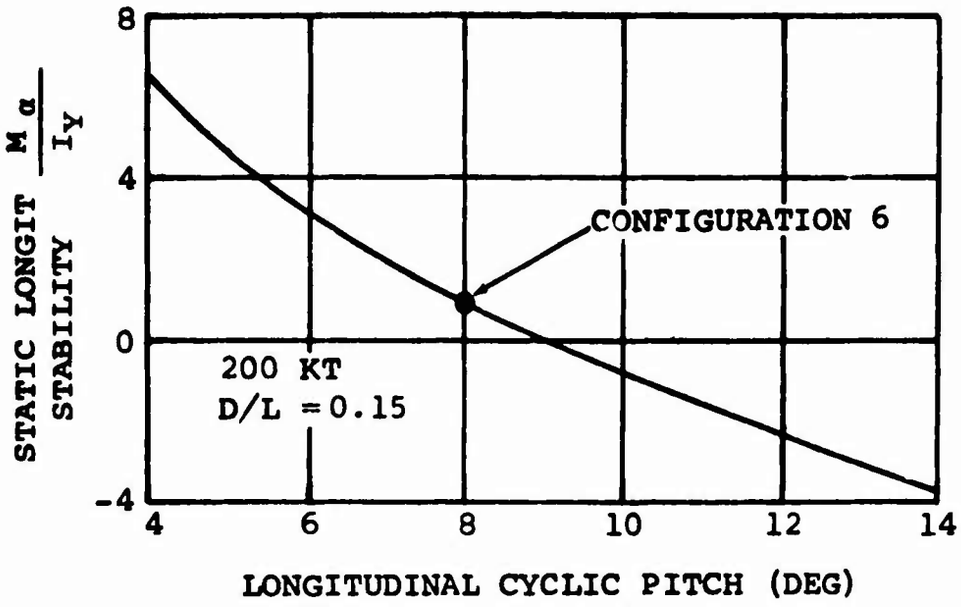

Figure 5. Effect of Longitudinal Cyclic Pitch on Static Longitudinal Stability Derivative.

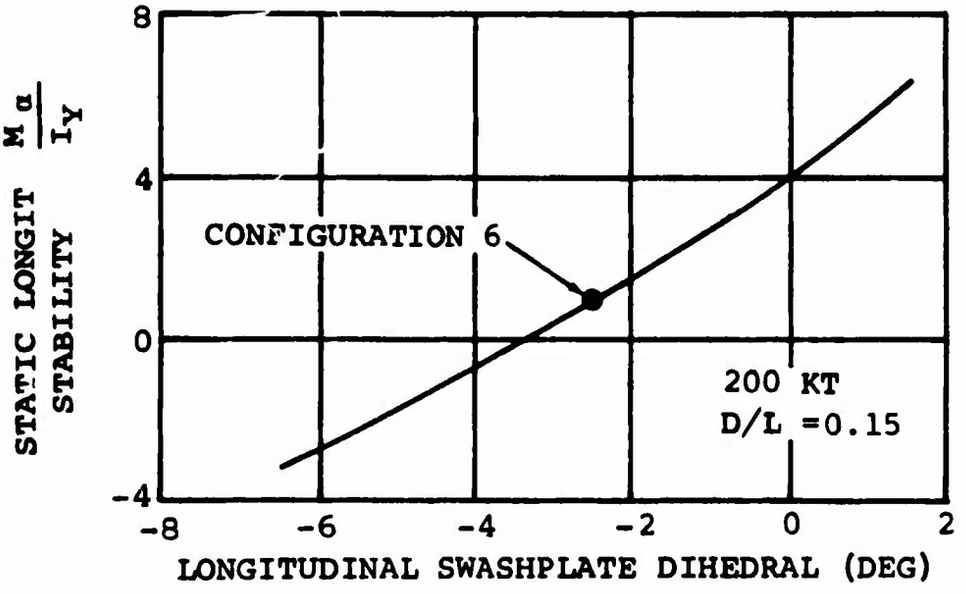

Figure 6. Effect of Swashplate Dihedral on Static Longitudinal Stability Derivative.

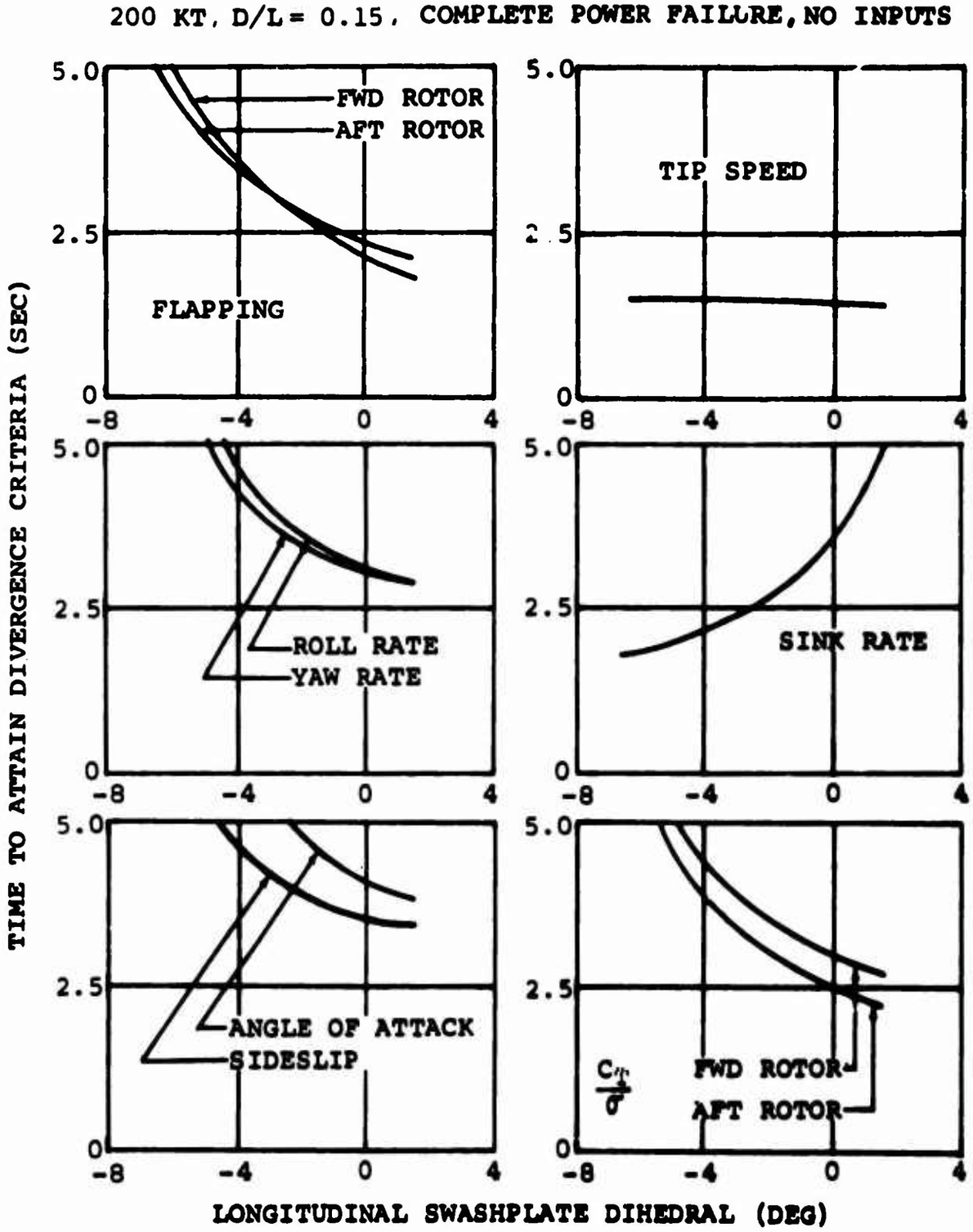

Figure 7. Effect of Swashplate Dihedral on Helicopter and Rotor Divergence.

TABLE 4

VARIATION OF LONGITUDINAL DERIVATIVES WITH SWASHPLATE DIHEDRAL

Dihedral	1.5°	-2.5°	-6.5°
$\frac{M_\alpha}{I_Y}$ (rad/sec^2)	6.350	0.940	-3.160
C_{TF_α} (rad^{-1})	0.046	0.041	0.036
C_{TR_α} (rad^{-1})	0.035	0.042	0.047
a_{1F_α}	0.728	0.803	0.839
a_{1R_α}	0.690	0.598	0.528
$\frac{M_\mu}{I_Y}$ (rad/sec^2)	1.970	-1.860	-5.470
C_{TF_μ}	-0.008	-0.012	-0.016
C_{TR_μ}	-0.009	-0.004	0.002
a_{1F_μ} (rad)	0.204	0.161	0.100
a_{1R_μ} (rad)	0.224	0.239	0.240

Using these tabulated data, the behavior of the helicopter after engine failure may be explained as follows. As rotor speed falls and μ increaares, all three configurations initially experience mild longitudinal flapping divergence, because of the small, and roughly comparable, values of a_{1F_μ} and a_{1R_μ}. The helicopter derivative M_μ gives rise to a nose-up moment for the configuration with 1.5 degrees of dihedral. This results in an increasing angle of attack, which acts through the derivatives a_{1F_α}, a_{1R_α}, and M_α to produce divergent rotor

flapping and pitch attitude. Large-amplitude lateral flapping will then follow as μ continues to increase, giving rise to roll, yaw, and sideslip divergences.

The configuration with -6.5 degrees of dihedral (6.5 degrees of cathedral) experiences a strong nose-down moment due to M_μ, which, in combination with the stable M_α, virtually eliminates the angle of attack divergence. Longitudinal flapping and fuselage attitude therefore diverge very slowly. The reduction in angle of attack also results in lower values of rotor thrust, so that a somewhat greater height loss is experienced by this configuration.

The benefits of negative swashplate dihedral are obtained without the penalty of high flapping angles at trim, which were encountered with large forward cyclic pitch. The undesirable stick position gradient with speed, which arises from the negative value of M_μ associated with negative dihedral, may be overcome by a stick positioning device sensitive to airspeed. The differential collective pitch trim (DCPT) system, which is already standard on contemporary tandem rotor helicopters, fulfills this function.

Installation of this device on the configurations investigated would not significantly affect the time histories, since the forward velocity changes very little in 5 seconds. Similarly, the tabulated μ-derivatives at trim would not be changed, since they are really derivatives with respect to tip speed, not forward velocity.

The above trends, which are also valid for equivalent shaft incidence variations, appear in the data for D/L = 0 as well, but are much less severe because of the lower drag involved.

Effect of Tip Path Controllers and Delta-Three

The four basic types of pitch-flap coupling considered in this report are:

1. Pitch-cone feedback - The pitch of each blade changes in proportion to the rotor coning angle.

2. Pitch-flap out-of-phase feedback - The pitch of each blade changes in proportion to the tip path plane tilt

about an axis in the rotor disc plane perpendicular to the flapping axis of the blade.

3. Pitch-flap in-phase feedback - The pitch of each blade changes in proportion to tip path plane tilt about an axis in the rotor disc plane parallel to the flapping axis of the blade.

4. Delta-three feedback - The pitch of each blade changes in proportion to its own flapping angle.

The exact kinematic ratios involved in each feedback are defined in Table 10, Appendix III. The ratio for the delta-three feedback produces the same response of blade pitch to blade flapping angle as would be obtained with a delta-three flapping hinge angle of 30 degrees (i.e. a ratio of -0.5774 to 1). The kinematic ratios involved in the other types of coupling were then chosen to provide this same ratio of blade pitch response to rotor coning angle, to rotor flapping angle 90 degrees ahead of the blade azimuth, and to rotor flapping angle at the blade azimuth.

These feedback devices have the effect of changing the natural frequency of the blade flap motion. However, no rephasing of the cyclic control input or increase in the control kinematic ratios to retain equivalent non-feedback control effectiveness has been considered. The effect of each form of feedback, alone and in combination, is considered below. The devices are used only on the forward rotor.

Pitch-Cone Coupling - As indicated by a comparison of Figures 57 and 66, and by a review of the tabulated data, a pitch-cone feedback is not effective in controlling either the rotor or fuselage divergences. The main effect of pitch-cone coupling is to improve the helicopter longitudinal stability through a reduction in front rotor thrust and coning response. Less pitch SAS input is required with the coupling to maintain the same pitch attitude and angle of attack variation. Since only the coning angle can be controlled by this type of feedback, the excessive flapping and lateral-directional fuselage motions (resulting from large μ and α changes) shown in Figure 57 also appear in the pitch-cone data of Figure 66.

Pitch-Flap Out-of-Phase Coupling - Significant improvements in rotor and fuselage stability result from the use of stable out-of-phase pitch-flap feedback, as can be seen in Figure 67. The flapping amplitude shows only a small rate of divergence over the entire time interval. This high degree of effectiveness can be attributed to the 90-degree phase lead of the corrective cyclic input which, with the blade flapping response characteristic, reduces flapping excursions all around the azimuth. This in turn stabilizes the otherwise divergent changes in a_{1F} and b_{1F} with increasing μ. The stable forward rotor flapping has the additional effect of controlling the fuselage motions. The aft rotor also remains relatively stable even without any stabilizing device, because of the absence of large fuselage excursions. The strong longitudinal stability of this configuration results in a lower angle of attack, which in turn reduces rotor thrust and hence increases height loss somewhat.

Pitch-Flap In-Phase Coupling - Figures 57 and 68 and the tabulated data show that, as with pitch-cone coupling, no improvements are obtained with pitch-flap in-phase coupling; in fact, the fuselage divergences occur sooner, leading to increased SAS inputs and flapping amplitudes after two seconds. The ineffectiveness of this coupling is due to the blade flap response characteristic of the rotor, i.e., the maximum flap response lags the maximum corrective pitch input by approximately 90 degrees. Hence, the corrective input does not stabilize the longitudinal flapping, but rather excites the lateral flapping.

All Three Coupling Modes - Comparison of Figures 67 and 69 reveals that a combination of all three types of coupling is almost as effective as the pitch-flap out-of-phase coupling alone. This was to be expected, since the pitch-cone coupling had virtually no effect, and the pitch-flap in-phase coupling had a slight adverse influence. The slight deviation in fuselage attitude at the end of the time interval is due to the in-phase coupling influence.

Delta-Three - As might be expected in view of the foregoing discussions, flapping feedback through a delta-three hinge, being a combination of pitch-cone and pitch-flap in-phase coupling, is not an effective rotor stabilizing device. Comparison of Figure 70 with Figure 68 shows that the delta-three configuration has virtually the same response as the

pitch-flap in-phase configuration, because of the negligible effect of pitch-cone coupling on rotor divergence.

Examination of the data for D/L = 0 indicates that the same trends prevail for the low-drag configurations involving tip path controllers and delta-three. However, the excursions are reduced on account of the smaller power deficiency and consequent slower deceleration of the rotors.

Effect of Lock Number

A reduction in rotor Lock number from 4.38 to 2.19, accomplished by doubling the blade inertias, results in a great improvement in the behavior of the helicopter and rotor system following power failure, as shown in Figure 71.

The data in Table 11 indicate that, because of the greater angular momentum of the rotating components, initial rotor deceleration is reduced by one half. Hence, μ increases at a much slower rate, with the effect of greatly improving rotor flapping divergence and decreasing the unstable rotor contribution to pitching moment. In addition, rotor speed and damping are maintained at a high level; this enables control of the helicopter to be maintained for a longer time. The same trends with Lock number are evident in the data for configurations having lower drag/lift ratios.

Effect of Rotor Overlap* and Relative Rotor Height**

Overlap - Comparison of Figures 57, 72, and 73, together with review of the data in Tables 11 to 14, indicates that the effects of rotor overlap on helicopter and rotor behavior after complete power failure are small. The configurations represented by these figures have progressively decreasing overlap,

*Rotor overlap is defined as the difference between rotor diameter and the distance between rotors, expressed as a percentage of rotor diameter.

**Relative rotor height is the distance that the aft rotor is above the forward rotor expressed as a percentage of rotor diameter.

obtained by lengthening the fuselage. The helicopter inertias are increased according to the fuselage extensions considered, while the rotor contributions to pitching moment increase approximately in proportion to the change in distance between rotors. These relationships are presented in Table 5.

TABLE 5

VARIATION OF STABILITY PARAMETERS WITH ROTOR OVERLAP

Overlap (%)	I_Y (sl-ft^2)	$\ell_F + \ell_R$ (ft)	% Increase (I_Y)	% Increase ($\ell_F + \ell_R$)
35	165,000	38.9	0	0
20	284,000	48.0	72%	23%
0	437,000	60.0	165%	54%

The inertia increases with fuselage extension at a faster rate than the destabilizing rotor pitching moment terms. This accounts for the slight improvement in helicopter divergence, and hence in rotor flapping, observed with decreased overlap. Changes in rotor interference are not significant, since at 200 knots the rotor downwash angles are small (about 0.75 degree), and the changes therein resulting from varying overlap are even smaller.

In view of the demonstrated minor influence of rotor overlap on helicopter and rotor behavior, overlap effects are eliminated from further consideration in this report. The responses of Configuration 6 (35-percent overlap) to various inputs will in all cases be very similar to the responses of Configurations 38 and 40 (20-percent and 0-percent overlap), and any conclusions drawn with respect to Configuration 6 will also be valid for Configurations 38 and 40.

Relative Rotor Height - The effect of relative rotor height may be determined by comparing Figures 57, 74 and 75, the tabulated data from which show only very small changes. The configurations considered have progressively higher aft rotor pylons, the helicopter inertias being increased accordingly.

The aft rotor height contribution to static longitudinal stability is given, approximately, by

$$(M_\alpha)_{h_R} = \rho A(\Omega R)^2 \; h_R \left[C_{TR_\alpha} \; (a_{1R} - i_R) + C_{TR} \; a_{1R_\alpha} \right] \tag{3}$$

The second bracketed term is always destabilizing, whereas the first will be destabilizing only if $(a_{1R} - i_R)$ is positive.

For the configurations considered, $(a_{1R} - i_R)$ is negative, and the two terms virtually cancel, yielding a negligible effect of aft rotor height on longitudinal stability. For other values of aft shaft incidence or longitudinal cyclic pitch, the height of the aft rotor may have some influence.

In view of the negligible aft rotor height effects shown in the referenced figures, no further consideration will be given them in this report. The behavior of Configuration 6 (8-percent aft rotor height) is considered to be representative of the behavior of Configurations 42 and 44 (20-percent and 30-percent aft rotor height).

Effect of Teetering Rotors

The data in Figure 76 refer to a helicopter with D/L = 0.15 having two-bladed teetering rotors of the same solidity and Lock number as the articulated rotors of Configuration 3. This latter configuration is the correct one for comparison with the teetering rotor, since both have zero hinge offset. The figure and tabulated data indicate that the teetering rotor has somewhat lower rates of divergence. This difference is attributable mainly to the higher-order flapping harmonics of the articulated rotor, which cannot exist on a teetering rotor. The absence of higher harmonics reduces the peak-to-peak flapping; this gives rise to slightly milder rotor and helicopter divergences.

There is a large oscillation in the blade loading parameter, which almost reaches the divergence criterion of $C_T/\sigma = +0.12$ while still at trim. The rather mild divergence after engine failure immediately increases the blade loading beyond this criterion, which accounts for the short divergence times listed in Table 14 for the teetering rotor.

The oscillations evident in the normal acceleration and blade-loading traces are characteristic of teetering rotors at high speed. They are the result of a large-amplitude single-blade two-per-rev airload acting on a two-bladed configuration. This two-per-rev airload is created by the high μ and large degree of longitudinal cyclic pitch. This condition also exists for each blade of the articulated rotor, but is largely cancelled out in the net rotor C_T/σ parameter because of the three-bladed configuration. In a practical design, the teetering rotors would be isolated from the fuselage by a system of vibration absorbers, and the oscillations would be transmitted to the fuselage with greatly reduced amplitude. In addition, blade flexing (not accounted for in the present analysis) would relieve some of the calculated oscillatory airloads.

The same characteristics are evident in the data for teetering rotor configurations with lower drag/lift ratios, but the divergences are less pronounced.

ANALYSIS OF PARTIAL POWER FAILURE

Examination of a number of time histories of response to partial power failure at 200 knots, with no corrective pilot action, indicates that the resulting rotor and helicopter divergences will be mild for all configurations. For the purposes of this report, partial power failure is defined as the sudden loss of exactly one half of the trim power of the helicopter, after which the power of the remaining engine stays constant. Comparison of Figure 77 with Figure 57 shows the differences between partial- and complete-power-failure responses for Configuration 6. It is evident that, within the 5-second limit of the time histories, none of the parameters in Figure 77 attains the divergence criteria values. This is generally true for partial failure on all configurations, except Configurations 11 and 24.

In view of the comparative mildness of the partial-power-failure time histories, in comparison with those for complete power failure, it is evident that, for the purposes of this investigation, very little is to be learned from a study of partial failure that is not demonstrated more clearly and forcefully in the complete-power-failure data. Consequently, with the exception of Figure 77, no specific time histories of partial power failure are included or discussed in this report. However, based on the data that were examined, the following general observations on partial power failure at 200 knots are made.

Within the first 1.5 seconds after partial failure, no configuration will experience a rotor speed loss greater than 11 percent, a flapping change greater than 2 degrees, or an attitude change greater than 1 degree. These changes are not excessive, and recoveries therefrom have been repeatedly demonstrated during simultaneous engine failure tests on current tandem rotor helicopters (see Appendix II).

If a twin-turbine helicopter operating at maximum available power suffers the loss of one engine, the remaining engine will lose some available power, as well, because of the rpm decay of its power turbine, which is geared directly to the rotors. Since the rotor speed loss is normally about 20 percent or less, as shown in Figure 77, Reference 2 indicates that the associated power loss will be less than 5 percent for a typical helicopter gas turbine. Hence, the assumption, that the power available from the remaining engine is 50 percent of the total trim power of both engines, is sufficiently accurate for the purposes of this report.

If a twin-turbine helicopter operating at somewhat less than maximum available power suffers the loss of one engine, the remaining engine will immediately run up to full power, subject to the loss in available power discussed above. Hence, the net power loss may be less than 50 percent of the total trim power. This situation occurs with the configurations having D/L = 0.075 and D/L = 0, since hover requirements necessitate installed power of about 4000 shaft horsepower, while considerably less than this is required for cruise at 200 knots (per Table 14).

It was noted that the partial-power-failure time history for each high-drag configuration was quite similar to the time history for complete failure on the corresponding zero-drag configuration. For example, Figure 77 (D/L = 0.15, partial failure, Configuration 6) is very similar to Figure 58 (D/L = 0, complete failure, Configuration 4). This is due primarily to the coincidence that the trim power with zero drag is roughly one half of the trim power for the corresponding high-drag configuration, as shown in Table 14. The power deficiencies after the respective partial and complete failures are therefore similar, so that the two configurations will undergo comparable rotor decelerations, yielding similar divergences.

2. DEVELOPMENT OF RECOVERY TECHNIQUES

The destructive nature of the responses encountered by many configurations discussed in Section 1 can be radically altered by appropriate control inputs. To provide a basis for determining the more favorable inputs, a systematic array of collective and longitudinal stick inputs were applied to Configuration 6, following complete power failure at 200 knots. From an examination of the resulting time histories, the summary plots in Figure 8 through 13 were prepared. The array of inputs consisted generally of three groups:

1. Twelve linear collective reductions of 10-degree magnitude, with various rates and delay times after engine failure.

2. Eighteen compound collective reductions of 10-degree magnitude, with several initial and final rates and various delay times.

3. Eight longitudinal stick pulses of 1-degree magnitude per rotor, having various durations and delay times. Two of these pulses were applied simultaneously with a linear collective input of 10 degrees.

In addition to the above, two compound collective reductions with 2.0-second and 3.0-second delays were applied to Configuration 6, as were two longitudinal stick steps made simultaneously with a compound collective reduction initiated at 1.0 second. These last two simultaneous collective and longitudinal stick inputs are the most realistic of all the inputs considered,

since they most closely represent the probable pilot action following complete power failure.

The magnitude of the collective reductions studied was chosen to approximate a full down collective input which would be applicable to all configurations having D/L = 0.15. Since the trim collective pitch at 75-percent radius ranged between 12 degrees and 14 degrees for all these configurations, a standard collective reduction input magnitude of 10 degrees was selected.

In analyzing the various responses of Configuration 6 to the above inputs, the following flight safety limitations are used as a basis for comparing the resulting time histories.

1. Maximum rotor flapping amplitude: $\pm$ 0.20 radian

2. Minimum aft rotor blade angle over fuselage: -0.21 radian

3. Minimum rotor tip speed: 550 feet per second

4. Minimum normal acceleration: -0.50g

The rotor flapping and tip speed limitations have been discussed in the previous section. The criterion for minimum aft rotor blade angle over the fuselage represents the condition for blade-fuselage contact for all configurations except those with increased aft rotor height. The minimum normal acceleration criterion is consistent with the load factor limitations on current production helicopters.

LINEAR COLLECTIVE REDUCTIONS

The 12 linear collective reductions of 10-degree magnitude applied to Configuration 6 are listed in Table 6.

The 4-degree-per-second rate was chosen to represent a slow collective reduction, while the 50-degree-per-second rate is representative of the highest collective rates ever achieved during flight testing of two current tandem rotor helicopter types. The results are summarized in Figures 8 through 13. A typical time-history plot is presented in Figure 78 for a collective rate of 20 degrees per second with a delay time of 1.0 second.

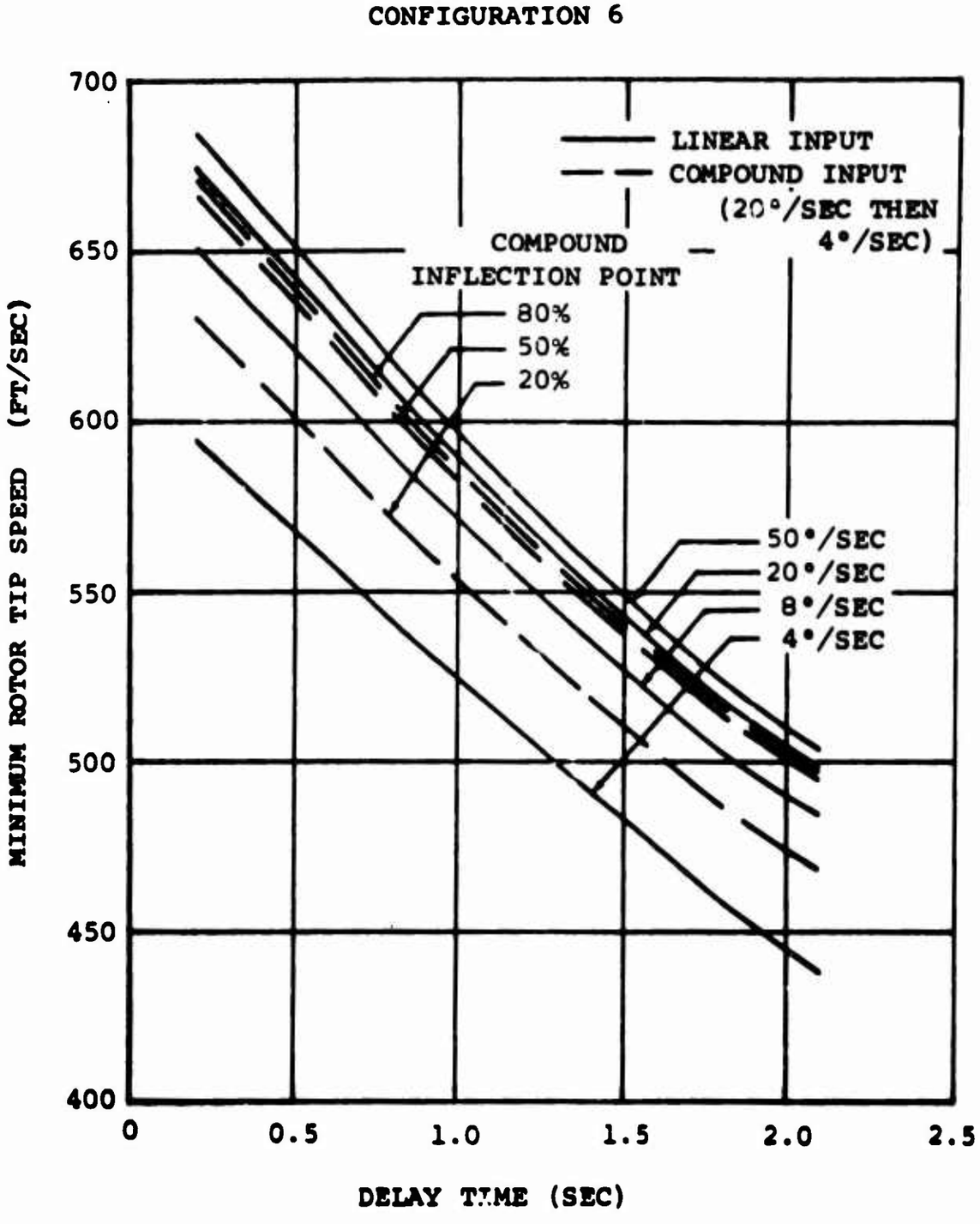

Figure 8. Effect of Collective Reduction on Minimum Rotor Tip Speed.

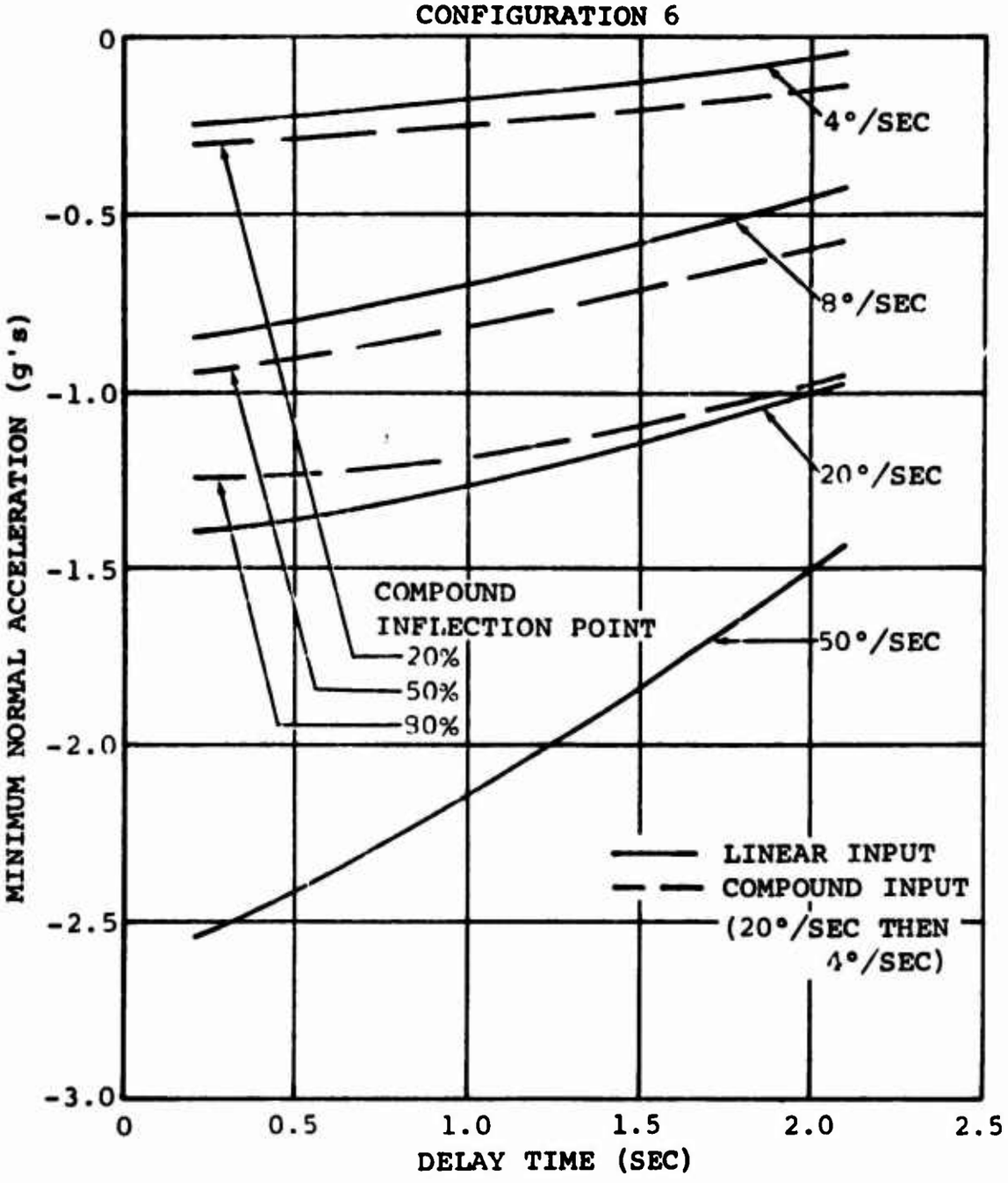

Figure 9. Effect of Collective Reduction on Minimum Normal Acceleration.

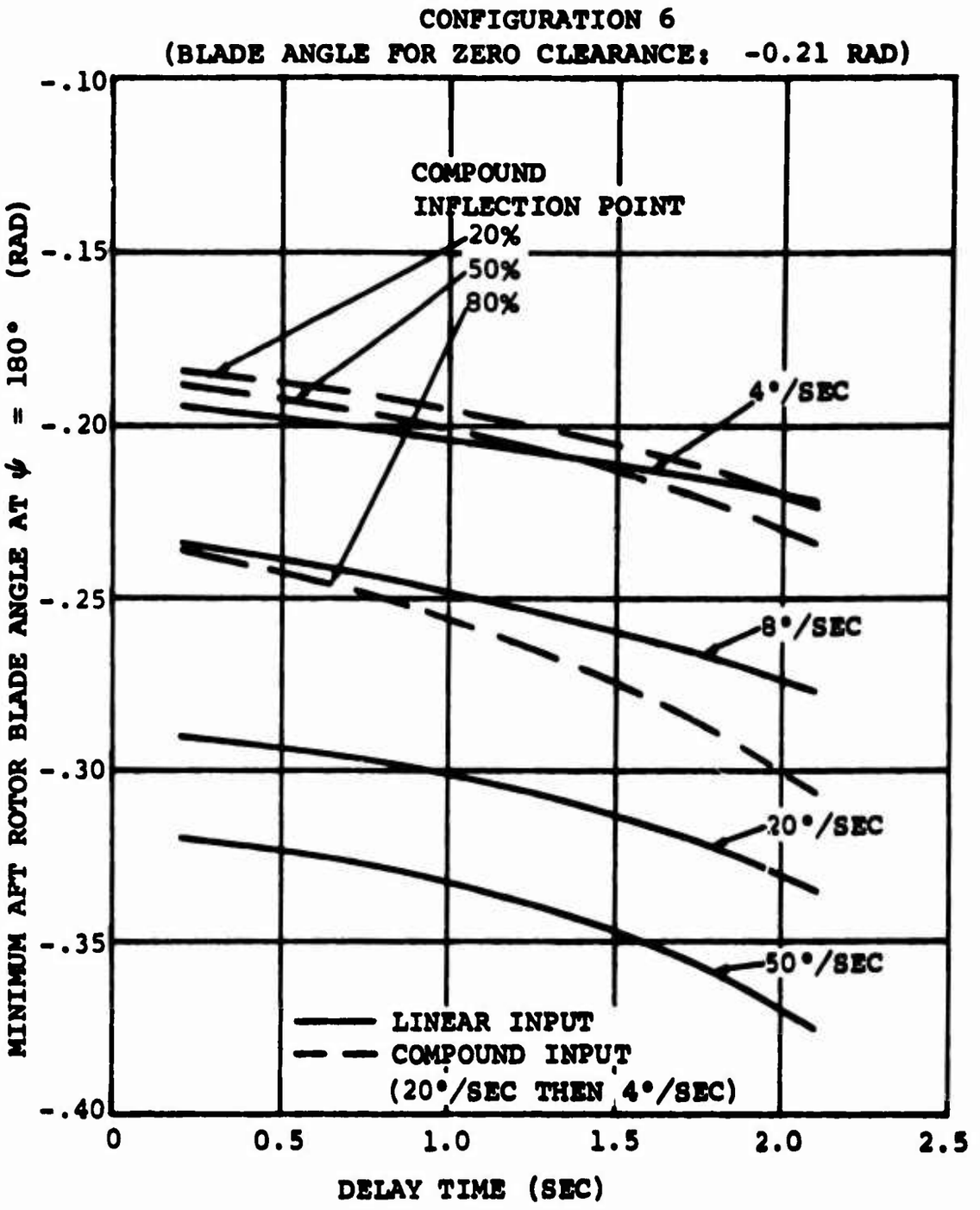

Figure 10. Effect of Collective Reduction on Minimum Aft Rotor Height Over Fuselage.

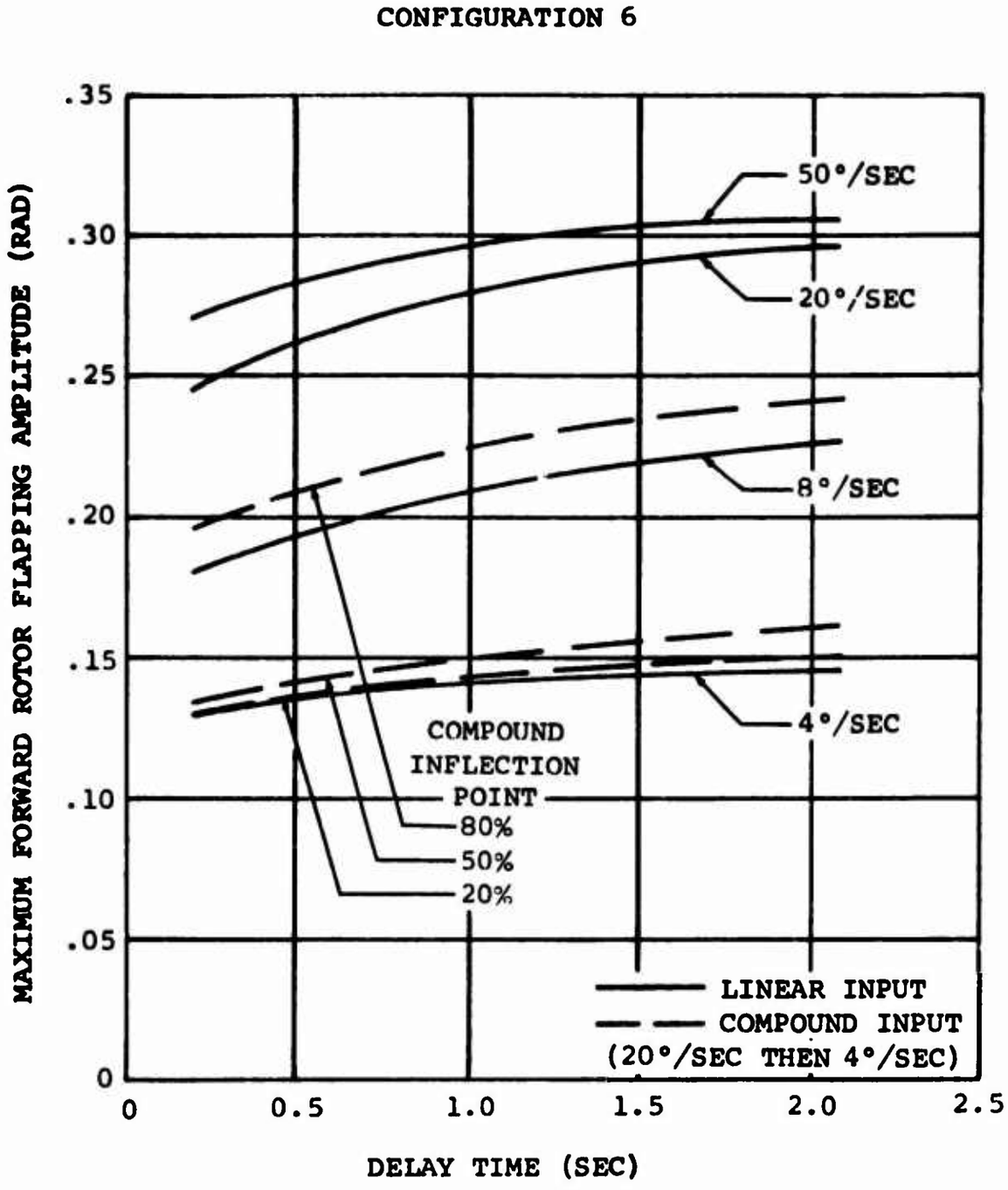

Figure 11. Effect of Collective Reduction on Maximum Forward Rotor Flapping Amplitude.

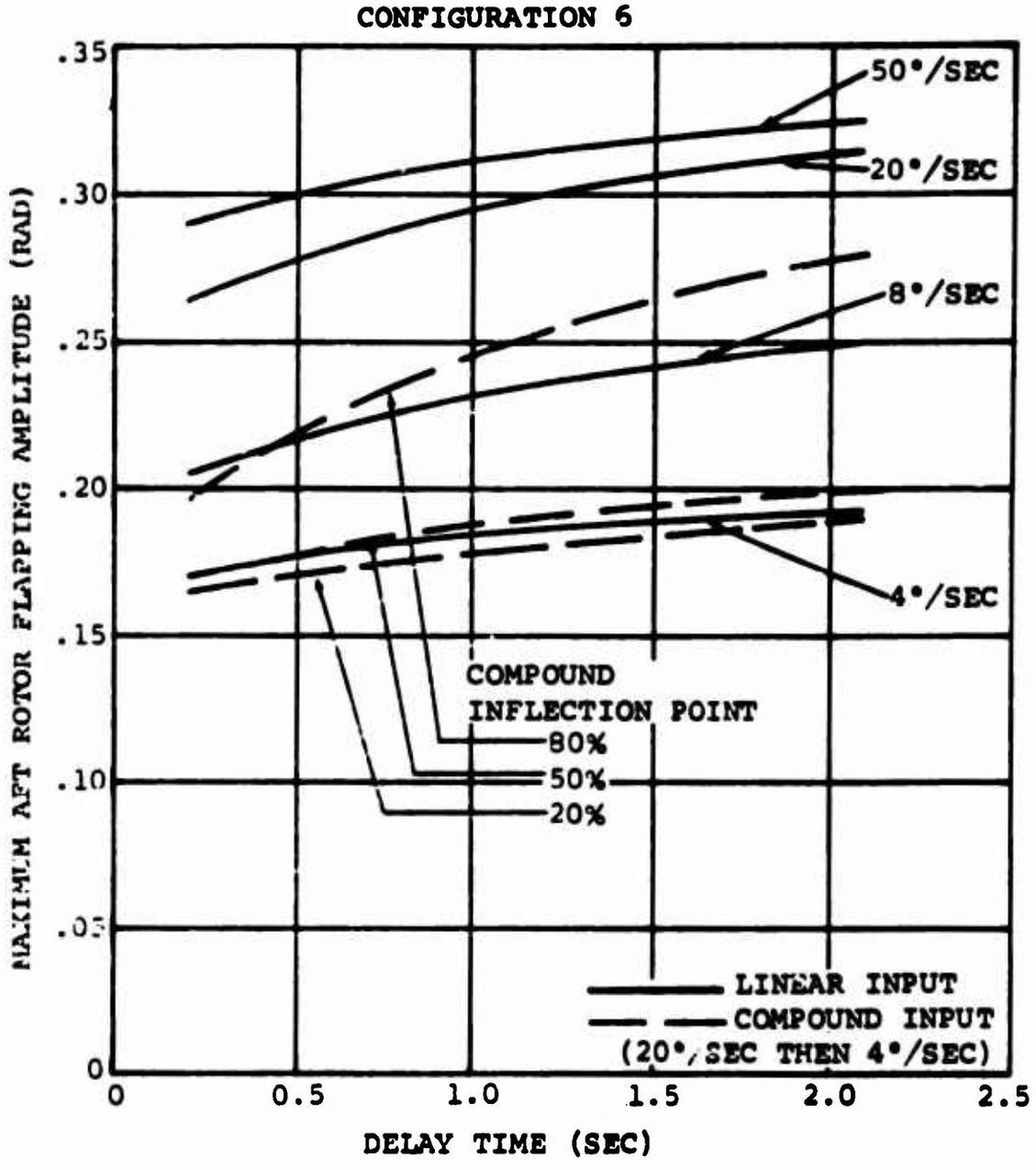

Figure 12. Effect of Collective Reduction on Maximum Aft Rotor Flapping Amplitude.

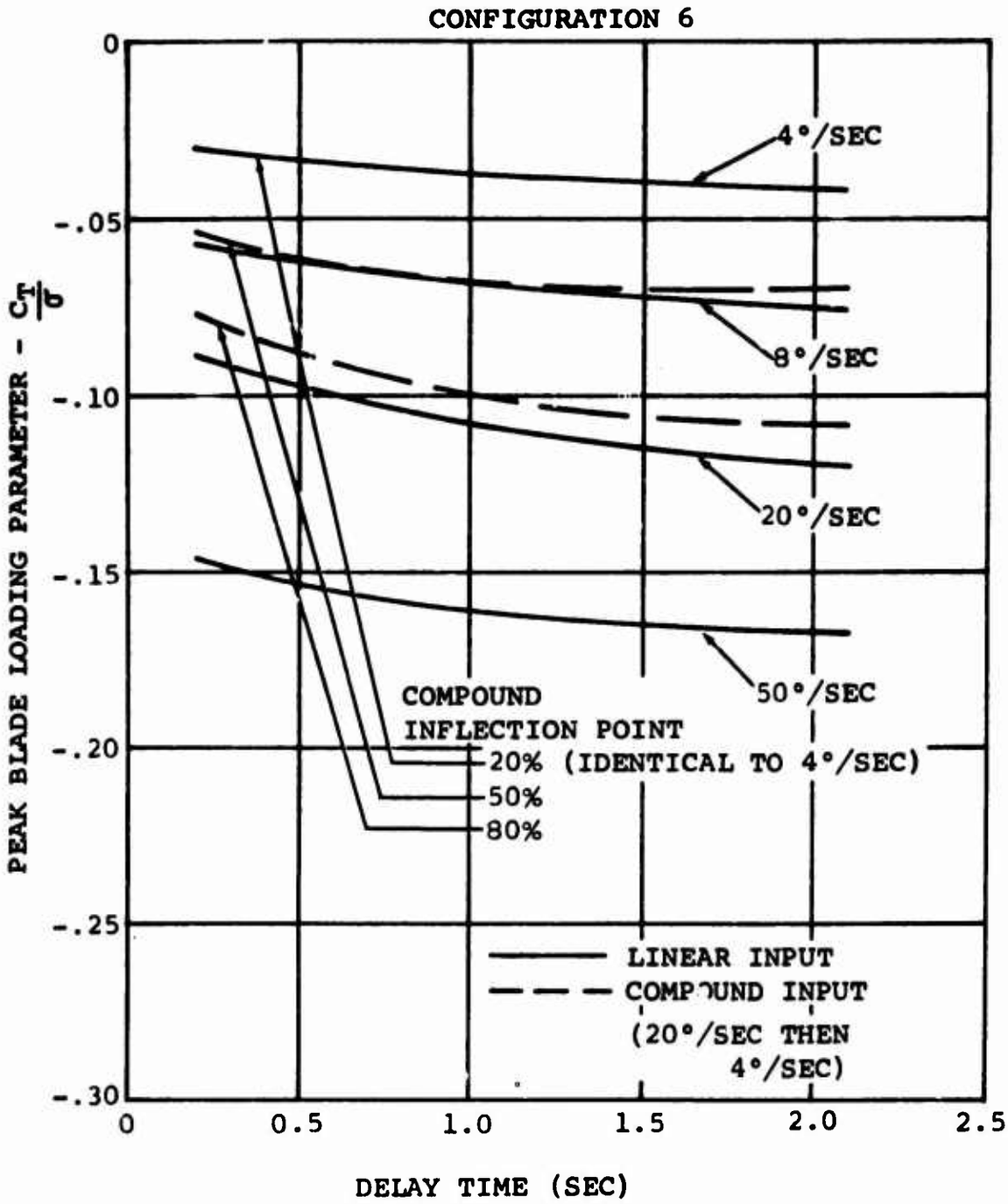

Figure 13. Effect of Collective Reduction on Peak Forward Rotor Blade Loading.

TABLE 6

SCHEDULE OF LINEAR COLLECTIVE REDUCTIONS

Collective Reduction Rate	4°/Sec	8°/Sec	20°/Sec	50°/Sec
Delay Time (Sec)	0.2	0.2	0.2	0.2
	0.6	-	0.6	-
	1.0	-	1.0	-
	2.0	2.0	2.0	2.0

The minimum rotor tip speed is read at the lowest value attained before, during, or within 0.5 second after the collective reduction. In Figure 78 this is shown as being at approximately 1.25 seconds. The maximum flapping amplitudes are taken as one-half of the greatest peak-to-peak values obtained before, during or within 0.5 second after the collective reduction. In Figure 78 the peak is obviously at about 1.75 seconds. In cases with slower collective reductions, the flapping at 5.0 seconds is sometimes greater, but such peaks are neglected in favor of the earlier peak. The blade loading (C_T/σ) data are presented for the forward rotor only, since the loads on both rotors are very similar.

Figure 8 shows the serious effect of delay time on the minimum rotor speed reached during recovery. If a certain minimum tip speed limit is not to be violated throughout the recovery, longer delay times will necessitate higher collective reduction rates. Conversely, higher reduction rates allow longer delay times, but very little is gained by rates higher than 20 degrees per second.

On the other hand, Figures 9 through 13 show that high collective rates have a very undesirable effect on the peak values of normal acceleration, blade-fuselage clearance, rotor flapping

amplitude, and blade load. These factors may place severe limitations on the allowable collective reduction rates. If, for example, the blade angle for zero clearance between the aft rotor and the fuselage is -0.21 radian, Figure 10 shows that, regardless of delay time, collective rates much greater than 4 degrees per second will cause the aft rotor blades to strike the fuselage. With this collective rate, and a minimum allowable tip speed of 550 feet per second, Figure 8 shows that the available delay time is 0.7 second, which is probably less than would normally be required by a pilot to positively identify and react to a sudden and unexpected complete power failure.

Therefore, if only linear collective rates and normal pilot reaction times (1.0 second or more) are considered, a complete failure at 200 knots on Configuration 6 will result in either a violation of the minimum tip speed criterion, if a low rate is used, or a collision of the aft rotor with the fuselage, if a high rate is used. The flapping amplitude criterion and the normal acceleration limit may also be exceeded with high collective rates.

COMPOUND COLLECTIVE REDUCTIONS

From an examination of the responses to the 12 linear collective inputs discussed above, it is evident that peak normal acceleration and flapping, minimum blade-fuselage clearance, and maximum blade loading occur simultaneously with, or slightly after, the end of the collective reduction (see Figure 78). For collective reductions of equal magnitude, therefore, these peak values must depend mainly on the immediately preceding final collective rate, and be largely independent of the initial rate. Consequently, a high initial rate of collective reduction might be tolerated in order to reduce rotor speed loss and increase delay time, provided a low final rate is used to reduce the severity of the normal acceleration, blade clearance, flapping amplitude, and blade load peaks.

Accordingly, a series of 18 compound collective reductions of 10-degree amplitude was applied to Configuration 6. Since Figure 8 indicates there is no advantage in using collective rates greater than 20 degrees per second, these compound inputs consisted of an initial rate of 20 degrees per second and final rates of 8 degrees per second or 4 degrees per second, with the inflection point (point of rate change) at 20 percent,

50 percent, or 80 percent of the total 10-degree collective reduction. Table 7 defines the 18 inputs.

TABLE 7

SCHEDULE OF COMPOUND COLLECTIVE REDUCTIONS

Initial Rate (Deg/Sec)	Final Rate (Deg/Sec)	Inflection Point (% Input)	Delay Times (Seconds)
20	8	20	0.2, 1.0, and 2.0
20	4	20	0.2, 1.0, and 2.0
20	8	50	0.2, 1.0, and 2.0
20	4	50	0.2, 1.0, and 2.0
20	8	80	0.2, 1.0, and 2.0
20	4	80	0.2, 1.0, and 2.0

A typical example of the resulting time histories is given in Figure 79, which deals with an initial collective reduction rate of 20 degrees per second and a final rate of 4 degrees per second, with inflection point at 50 percent, and with 1-second delay time. The results of the 18 compound inputs are summarized in Figures 8 through 13, for those inputs having an initial rate of 20 degrees per second and a final rate of 4 degrees per second. The results for inputs with a final rate of 8 degrees per second are significantly more severe in terms of normal acceleration, blade clearance, flapping and blade load, and are not, therefore, considered further in this report.

Acceptably precise compound collective reduction rates can be readily obtained in practice by incorporating a rate limiter in the collective control linkage. The pilot would be instructed

to lower collective pitch rapidly, following engine failure, to attain a high initial rate of reduction.

The limiter would be set to engage at the appropriate inflection point and would then limit the remainder of the collective reduction to the desired final rate.

From Figure 8 it is evident that compound rates having the inflection point at 50 percent and 80 percent of the collective reduction will provide rotor speed losses (or delay times) virtually the same as a linear 20-degree-per-second input, and not significantly worse than for a 50-degree-per-second input. At the same time, Figures 10, 11 and 12 show that compound inputs with inflection points at 20 percent and 50 percent have blade-fuselage clearance and rotor flapping amplitudes very similar to the 4-degree-per-second linear inputs. Hence, the compound inputs with the 50-percent inflection point will provide rotor speed losses close to the minimum attainable (or delay times close to the maximum), without incurring significant penalties in blade clearance or rotor flapping compared to the mild 4-degree-per-second linear collective input. The resultant normal acceleration and blade loading peaks will be approximately the same as for an 8-degree-per-second linear input, as shown in Figures 9 and 13.

The effectiveness of compound collective inputs in improving the rotor and helicopter responses to collective reduction may be assessed from Figures 8 and 10. These figures show that the compound input with inflection point at 50 percent will allow delay times up to 1.4 seconds without violating either the rotor tip speed criterion or the minimum blade height limit. All other responses remain within limits, except normal acceleration, which attains -0.73g. This improved delay time is considered sufficient for an alert pilot to identify and react to a complete power failure, as discussed in Section 3.

In order to convey some idea of how rapidly the situation deteriorates as delay time increases, Figures 80 and 81 are included. These show the responses of Configuration 6 to the same collective input as in Figure 79, except that the delay times are 2.0 seconds and 3.0 seconds, respectively. Although the 2-second delay results in a minimum tip speed of less than 550 feet per second and an aft rotor blade angle below -0.21 radian over the fuselage, the situation is not so bad that it could not be remedied by reduced Lock number, a higher aft rotor,

and/or a more favorable longitudinal cyclic pitch setting on the aft rotor. The situation which develops with a 3-second delay, however, is beyond hope of recovery for any configuration having D/L = 0.15.

LONGITUDINAL AND SIMULTANEOUS LONGITUDINAL-COLLECTIVE INPUTS

In order to assess the effects of various longitudinal stick inputs on helicopter behavior following complete power failure, a number of aft longitudinal stick pulses and steps were applied to Configuration 6, some alone and some in combination with a simultaneous collective reduction.

Longitudinal Stick Pulses

Eight aft longitudinal stick pulses yielding a differential collective pitch change of 1 degree per rotor were applied to Configuration 6 in accordance with the schedule of Table 8.

TABLE 8

SCHEDULE OF LONGITUDINAL PULSE INPUTS

Pulse Duration (Sec)	Collective Rate (Deg/Sec)	Delay Time (Sec)
0.5	0	0.2 and 2.0
1.0	0	0.2 and 2.0
2.0	0	0.2 and 2.0
1.0	20	0.2 and 2.0

The pulses are applied and taken out at the rate of 5 degrees per second per rotor, and the simultaneous linear collective input is of 10-degree magnitude.

A typical response is presented in Figure 82 for the 1.0-second pulse with 0.2-second delay time. Comparison with Figure 57 shows that, in the absence of collective reduction, aft longitudinal stick pulses cause higher rates of divergence in rotor flapping and tip speed, and in helicopter attitudes and airspeed. The increased divergences are due primarily to the larger angle of attack, which increases the thrust and hence the power requirements of the rotors. The increased power requirements cause a greater power deficiency and, hence, faster rotor deceleration and higher μ. As angle of attack and μ both increase, the aft flapping motion of the rotors diverges very quickly.

The effects of applying the same longitudinal pulse simultaneously with a linear collective reduction of 20 degrees per second at 0.2-second delay time is shown in Figure 83. Comparison with Figure 84, which shows the same collective reduction without the longitudinal pulse, indicates that the pulse has a negligible effect on maximum flapping amplitude and minimum aft rotor blade height. A slight increase in rotor deceleration occurs for the reasons discussed above. A noticeable relief in peak negative normal acceleration is evident, as a result of the sharp pitch-up which causes positive increments in rotor inflow and thrust. These effects are also evident in the blade loading data. Ultimate attitudes are not significantly different, however, since the SAS quickly damps out the momentary increase in pitch rate.

Longitudinal Stick Steps

If longitudinal stick steps are applied instead of pulses, a marked difference in response appears. Two such responses were examined for Configuration 6 with simultaneous aft longitudinal step inputs and compound collective reductions. Figure 85 shows one of these, in which the longitudinal stick step produces a differential collective pitch change of 2 degrees per rotor, applied at 5 degrees per second per rotor. The compound collective reduction is the same as in Figure 79.

Comparison of Figures 79 and 85 shows that the most important response difference (caused by the longitudinal stick step) occurs in rotor tip speed, which shows a distinct recovery after 3 seconds, instead of continuing to decay. This is because of the large angle of attack and strong positive inflow, which mark the entry into autorotation. Simultaneously, forward speed falls

as the aircraft pitches up, normal accelerations greater than 1.0g are encountered, and rate of descent is greatly reduced. The negative normal acceleration peak is not noticeably affected, however, becuase it occurs before the angle of attack and rotor inflow have changed by an appreciable amount. If the longitudinal input were completed sooner, the normal acceleration peak would be reduced, as shown in the above comparison of Figures 83 and 84. The peak flapping of the forward rotor at 1.5 seconds is greatly reduced, since the net rate of collective pitch change immediately before the peak is decreased by the longitudinal stick input to this rotor. Conversely, aft rotor peak flapping at 1.5 seconds is increased, due to the higher net rate of collective change prior to the peak. For the same reasons, the peak negative blade loading is reduced on the forward rotor and increased on the aft rotor.

The flapping amplitude of both rotors is decreased after the peaks because of the increased angle of attack. The angle of attack acts through the positive rotor derivative a_{1_α} to produce an aft flapping tendency. This offsets the forward flapping tendency caused by the collective reduction acting through the positive derivative $a_{1_{\theta_c}}$, and consequently, reduces the net flapping amplitudes.

3. CONTROLLED RECOVERY FROM POWER FAILURE

From the large array of control inputs studied in the previous section, the optimum collective schedule following a complete power failure on Configuration 6 was found to consist of an initial reduction rate of 20 degrees per second and a final rate of 4 degrees per second, with the inflection point at 50 percent of the total reduction. This compound input, with a total magnitude of 10 degrees, was then applied to all configurations with D/L = 0.15, in order to compare the responses of these configurations to a standard optimum collective reduction. The selection of an appropriate delay time to be used with this input was based on pilot comments. The results of the investigation are discussed later in this section, under the appropriate configuration headings.

It was the unanimous opinion of the four test pilots interviewed, that, in the event of a complete engine failure on existing tandem rotor helicopters, any rotor speed loss greater than about

10 rpm would be clearly discernable to the pilot because of the change in forward transmission and rotor noise. Assuming that noise levels in a 200-knot aircraft will be comparable to those in current production helicopters, complete power failure should be evident to the pilot when the rotor tip speed falls to 690 feet per second. For all configurations with D/L = 0.15, this occurs at 1/4 second after engine failure, except for Configuration 28 (reduced Lock number) where 1/2 second is required. Allowing a further 1/2 to 3/4 second for the pilot to evaluate and react to the situation, a delay time of 1 second is selected as standard. This approaches the best reaction time that can reasonably be expected of a pilot, considering that the power failure will normally be totally unexpected. Additional clues which help to identify the failure are the rapid decrease in normal acceleration and the beginning of rotor stall due to rotor speed decay.

The pilots observed, however, that partial power failure is not so clearly indicated, even if rotor speed falls more than 10 rpm, since the character of the forward transmission noise is not drastically altered, as in a complete power failure. This may be explained by the fact that a large driving torque is still being applied by the remaining engine. Because of this, and in view of the fairly rapid rotor speed decay involved, it is considered advisable to install a warning horn to indicate partial power failure. Since rotor speed decay and rotor divergence rates for a complete power failure at D/L = 0 are representative of partial failure at D/L = 0.15, the response of the latter to linear collective reductions after power failure may be estimated from the zero-drag, complete-failure cases discussed below.

Two linear collective inputs, one of 8 degrees per second and the other of 4 degrees per second, were selected as standard for the study of recovery from complete power failure on the low-drag (D/L = 0) configurations. The magnitude of each input was 5 degrees, and the delay time was set at 1 second, as for the standard compound input discussed above. These mild collective rates were chosen to take advantage of the slower rotor speed decay associated with zero drag, and thereby avoid the high peaks in rotor flapping, normal acceleration, and blade load, and the low blade-fuselage clearance, caused by high rates of collective reduction. The responses to both the 8-degree-per-second and the 4-degree-per-second inputs are discussed later in this section.

TYPICAL BEHAVIOR OF THE TANDEM HELICOPTER IN RECOVERY FROM POWER FAILURE

The following characteristics are typical of the behavior of a tandem rotor helicopter during recovery from a complete power failure at 200 knots. The pilot is assumed to make no lateral stick or rudder pedal inputs. Reference is made to Figures 79 and 86, which describe the behavior of Configurations 6 and 4, respectively, during and after collective pitch reductions initiated 1 second after engine failure.

As collective pitch is reduced, both rotors acquire forward longitudinal flapping angles, under the influence of the strongly positive derivative $a_{1_{\theta_c}}$. If the collective change is large, the forward flapping will be large, as in Figure 79. With sufficiently large collective reductions, rotor speed loss is halted and a slight recovery follows, leading to a fairly steady value of μ during and after the reduction. Rotor flapping due to increasing μ is thereby virtually eliminated. If the collective reduction is small, as in Figure 86, rotor decay will continue at a reduced rate.

At the high speeds involved in this study, rates of collective reduction as small as 4 degrees per second will produce negative thrust. If preceeded by a higher rate, as in the compound reduction of Figure 79, an appreciable negative thrust will be maintained until the reduction is completed. These negative thrust values cause negative normal accelerations, and may produce rates of descent up to 10,000 feet per minute during recovery. As soon as the collective reduction is completed, positive rotor thrust is reestablished.

As collective is reduced, the positive control derivative M_{θ_c} produces a nose-down moment and a negative pitch rate. This would normally produce a negative angle-of-attack change. However, sink rate is increasing rapidly, and the resultant increase in angle of attack is greater than the decrease caused by pitching over. Hence, the negative pitch rate and positive angle-of-attack change proceed simultaneously.

With the few exceptions discussed below, no significant lateral or directional disturbances occur during the power failure recoveries studied in this report. In cases where such disturbances do occur, they may usually be ascribed to the fact that,

during periods of negative normal acceleration, the rolling and yawing moments produced by the negative rotor thrust are reversed from their usual sense. The effectiveness of the SAS inputs is thereby reduced or even reversed.

ANALYSIS OF RECOVERY FROM POWER FAILURE

The standard compound collective input discussed at the beginning of this section was applied to a large number of configurations with D/L = 0.15. The peak responses from the resultant time histories are compiled in Table 15. Similarly, the 8-degree-per-second and 4-degree-per-second linear collective reductions discussed above were applied to a number of zero-drag configurations. The peak responses are presented in Table 16 for the more favorable 4-degree-per-second inputs only.

The influence of configuration variations on the behavior of the helicopter and rotors following application of these standard collective inputs is discussed in the paragraphs which follow.

Flapping Hinge Offset

The effects of hinge offset are presented in Figures 87 and 88, together with the standard case in Figure 79, for the high-drag configurations. The large forward flap angle resulting from the collective reduction creates a nose-down pitching rate roughly proportional to hinge offset, due to the longitudinal hub moment. Fuselage roll rates are also initiated by lateral hub moments or thrust changes. The SAS is effective in controlling these roll divergences for the configuration with e/R = 0.05 by means of hub moment, in spite of the negative thrust conditions. However, the configurations with e/R = 0 have no hub moments, and therefore diverge in roll under the influence of the destabilizing SAS control inputs when thrust is negative.

A large initial pitch rate augmented by the unstable SAS inputs together with large-amplitude aft rotor flapping leads to rapidly deteriorating conditions in the high hinge offset configuration. No thrust recovery was achieved, because of negative inflow conditions, and blade-fuselage contact is indicated for the aft rotor. An attempt to reduce the aft rotor flapping peak by changing the cyclic pitch to 4 degrees forward met with little success, as shown in Figure 89. The initial minimum rotor speed, normal acceleration, and flap angle, which are due entirely to

the collective dump and not to the ensuing fuselage motions, are unaffected by hinge offset. In all cases, normal acceleration exceeds the limit of -0.5g.

Similar initial trends also exist in the low-drag configurations for both the linear rates of collective dump. However, the extreme fuselage divergences occurring in the high hinge offset configurations do not exist at zero drag.

Drag/Lift Ratio

The principal effect of drag/lift ratio is to reduce rotor deceleration, thereby allowing a longer delay time before the start of corrective action by the pilot. This is evident in Figure 86, in which the 4-degree-per-second standard input is applied to Configuration 4 (D/L = 0). In addition to the comparative mildness of the responses, it is noted that, contrary to the high-drag cases, rotor tip speed continues to decay after the collective input, while forward speed actually increases as the helicopter pitches over. In a more realistic case, the pilot would apply some aft longitudinal stick to counteract the pitch-over and help conserve rotor speed.

In order to estimate roughly the increase in delay time available with D/L = 0, it is noted that the allowable delay time of 1.4 seconds on Configuration 6 (D/L = 0.15) is associated with a time of 1.5 seconds, given in Table 11, to attain the rotor speed criterion of 550 feet per second. On the same basis, the tabulated time of 4.4 seconds for Configuration 4 to attain this criterion indicates an allowable delay time of approximately 4.0 seconds.

Tip Path Plane Controllers and Delta-Three

Pitch-Cone Coupling - As a result of the reduced forward rotor thrust and coning response caused by pitch-cone feedback (Figure 90) the minimum normal acceleration and the forward flapping angle on this high-drag configuration are not so severe as for the standard high-drag case (Figure 79), when collective input is applied. The normal acceleration returns to a positive level much more quickly and does not exceed the limit. The decreased forward rotor thrust response also results in a nose-up pitch change which overcomes the nose-down effect of longitudinal hub moment. Aft rotor blade clearance is improved,

but a greater secondary drop in rotor speed is noted. The slower descent rate results from higher rotor thrust levels. The initial minimum rotor speed value is unaffected by the pitch-cone coupling.

The above trends are also evident in the low-drag configurations except that coupling leads to slightly improved tip speed decay rates through a higher initial angle of attack variation, resulting from pitch-up. This increased angle of attack variation also exists in the high-drag configuration but is not effective in checking the rotor speed secondary decay caused by the decreased forward velocity that results from the pitch-up.

Delta-Three - The effect of delta-three coupling is identical in most respects to the pitch-cone feedback (see Figure 91). The tendency toward fuselage lateral or directional divergences is increased with delta-three because of pitch-flap in-phase effects.

Pitch-Flap Out-of-Phase Coupling - The major effect of the pitch-flap out-of-phase feedback (Figure 92) on the forward rotor is to reduce the cyclic flapping change resulting from collective dump to a minimum. This increased forward rotor stability results in a quicker restabilizing of the forward rotor thrust to a positive value, which in turn leads eventually to increased pitch attitudes, reduced rates of descent, and increased rotor speed decay. The initial minimum normal acceleration and rotor speed are unaffected by the device. No significant improvement over the pitch-cone coupling feedback is evident, contrary to the case with no corrective action. Figure 93 shows the effect of including pitch-flap out-of-phase coupling on both rotors. This results in reduced aft rotor flap excursions and a nose-down pitch rate tendency due, again, to longitudinal hub moment. No improvement in rotor speed decay results, and a greater altitude loss is experienced. Similar trends appear in the low-drag configurations with some improvement in rotor speed decay, for the same reasons presented in the pitch-cone discussion.

Lock Number

Lower blade Lock number (that is, increased blade inertia) reduces the rate of flapping amplitude increase considerably over the standard case, but the peak amplitude and minimum flap

angle are the same (see Figure 94). A marked reduction in rotor speed decay results from the increased polar inertia of the rotating system, with little additional decay after the collective reduction. The normal acceleration peak reached was more severe because of the higher rotor speed at the corrective input.

On account of the small rate of tip speed decay and the quick recovery, an additional case (Figure 95) with a 2-second delay was run. The flapping response was unaffected, but the minimum normal acceleration reached was not so severe because of the reduced rotor speed at time of collective dump. Based on Figures 94 and 95, a time delay of about 2.5 seconds could be tolerated for this configuration without exceeding the minimum tip speed criterion of 550 feet per second. An alternative way of taking advantage of the slow rotor speed decay associated with reduced Lock number is demonstrated in Figure 96, in which the collective rates are one-half of the standard input rates. Maximum rotor flapping amplitudes are significantly reduced, aft rotor blade clearance is improved, and peak normal acceleration and blade loading are much less severe. All these advantages are obtained with only a slightly increased loss of rotor speed.

The low-drag configurations with increased inertia show similar trends to those above. The maximum delay time available is estimated, on the basis of rotor speed decay, to be well in excess of 5.0 seconds.

Longitudinal Cyclic Pitch

The effects of cyclic pitch variation obtained from Figures 97 and 98 together with the standard case (Figure 79) are presented in Figure 14 for the high-drag configuration. Contrary to the case with no collective input, forward cyclic pitch is not beneficial. The maximum peak-to-peak flapping and minimum aft rotor blade height become worse as a result of the increased forward trim flap angle, in addition to the always-present forward flapping with collective reduction. It is also noted that the minimum forward cyclic pitch (4 degrees) used on the configuration shown on Figure 97 leads to high aft trim flapping. The initial minimum normal acceleration and tip speed following input appear slightly worse with cyclic variations on either side of 8 degrees.

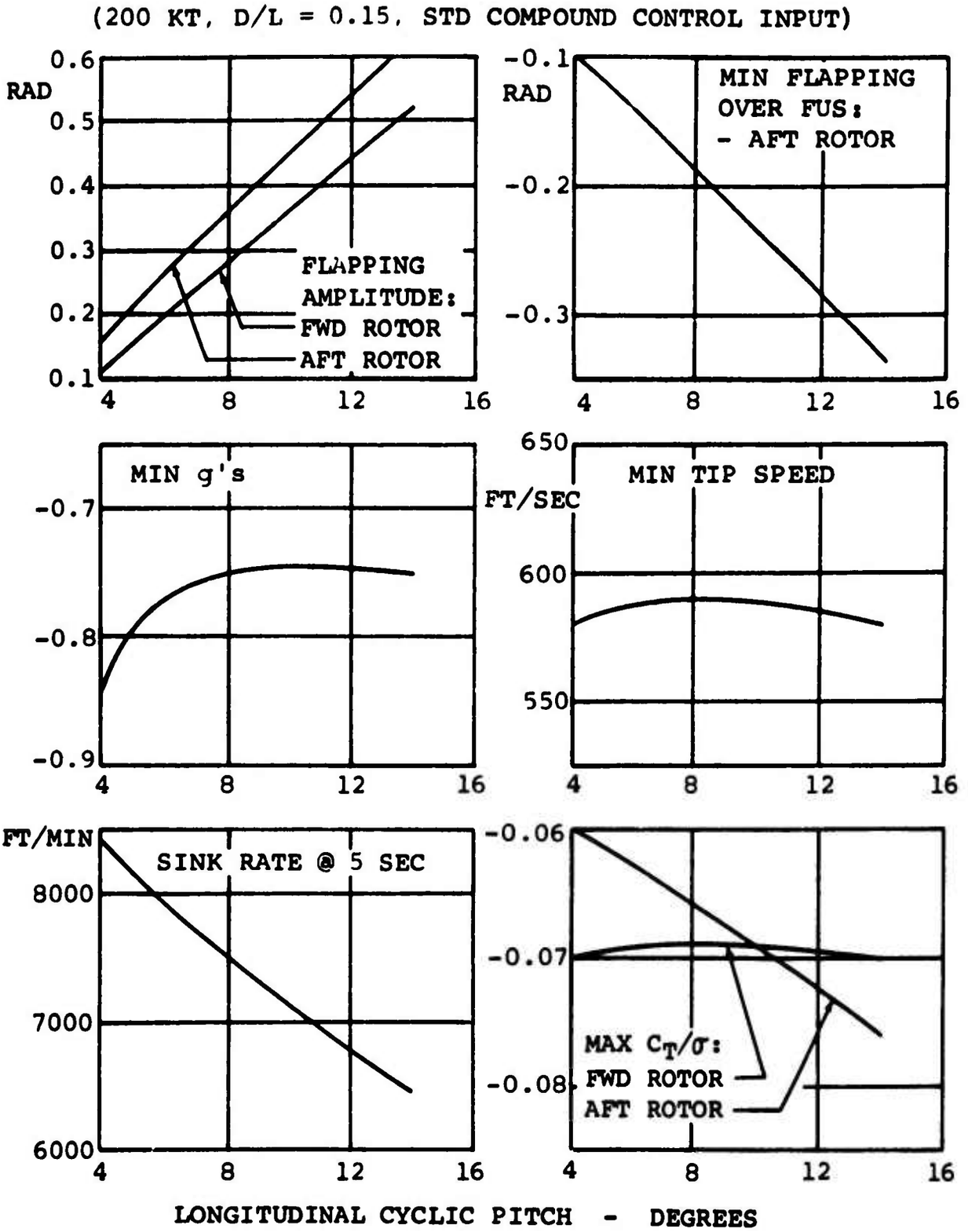

Figure 14. Effect of Longitudinal Cyclic Pitch On Helicopter Response to Collective Reduction (D/L=0.15).

Normal acceleration exceeds its limit of -0.5g regardless of cyclic pitch. The sink rate at 5 seconds becomes somewhat less with increasing cyclic because of the higher initial nose-up pitch attitude, leading to a reduced tendency to nose over along the flight path.

In an attempt to improve the aft rotor-fuselage clearance and equalize the rotor flapping behavior, an additional case was run with cyclic pitch values (7 degrees on the forward head and 6 degrees on the aft) obtained through interpolation of the above results. The responses are given in Figure 99, which shows a noticeable improvement over the standard configuration (Figure 79) in rotor flapping amplitude and aft rotor blade height, without any appreciable deterioration in rotor speed, normal acceleration, blade loading, or fuselage attitude.

Swashplate Dihedral

By varying the longitudinal cyclic pitch in opposite directions on each rotor, the effects of swashplate dihedral have been obtained. The results from Figures 100 and 101 and from the standard case (Figure 79), are summarized in Table 15, and presented in Figure 15.

Considering the rotors individually, the initial blade flapping variation for each rotor shows the same general effects with cyclic pitch as above. It is evident that, contrary to the zero-input cases considered previously, negative swashplate dihedral has a generally undesirable effect on rotor and helicopter responses to the standard collective input. Rotor flapping amplitudes are considerably worse, as are the normal acceleration and rotor blade loading peaks. The greater longitudinal flapping causes the helicopter to pitch over somewhat more rapidly. Lateral and directional divergences are more severe because of the longer time spent at a slightly more negative normal acceleration, which results in SAS control reversal as explained in previous sections. However, some improvement in aft rotor blade clearance and in rotor speed recovery are evident for negative dihedral.

The cyclic and dihedral effects, summarized in Table 16, for the low-drag cases, are presented as a function of longitudinal cyclic pitch and swashplate dihedral in Figures 16 and 17. Trends similar to the high-drag cases exist; these include large

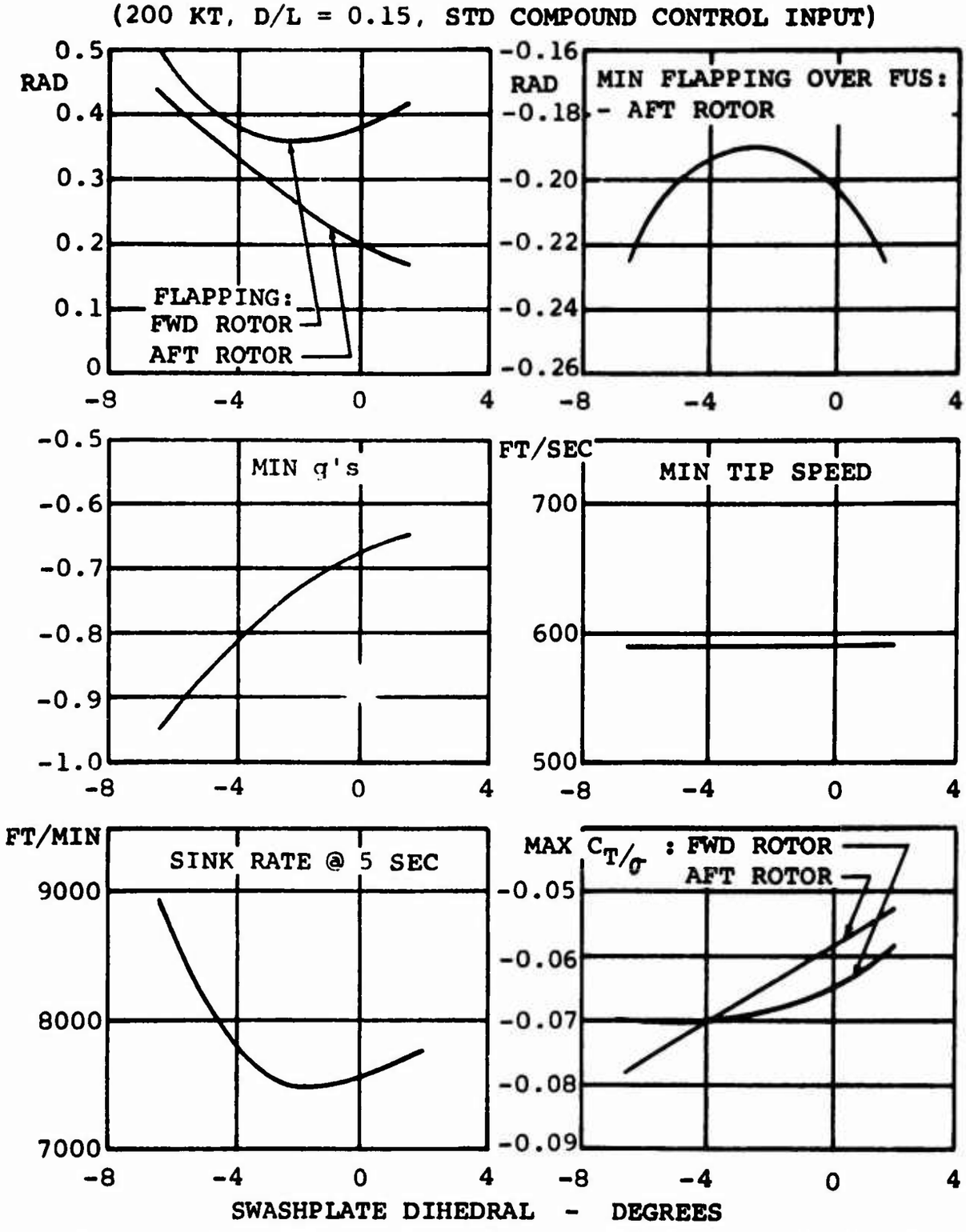

Figure 15. Effect of Swashplate Dihedral on Helicopter Response to Collective Reduction (D/L=0.15).

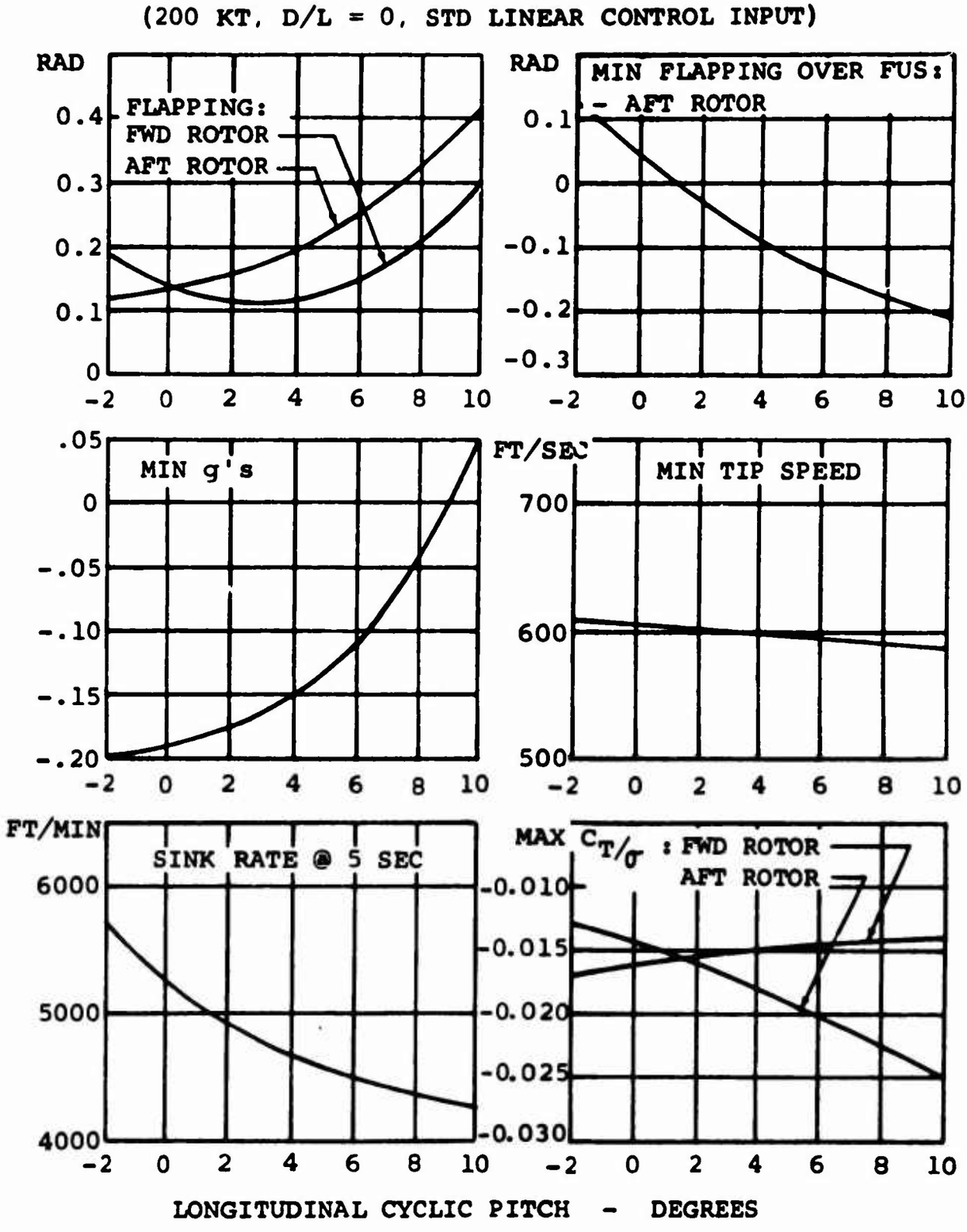

Figure 16. Effect of Longitudinal Cyclic Pitch on Helicopter Response to Collective Reduction (D/L=0).

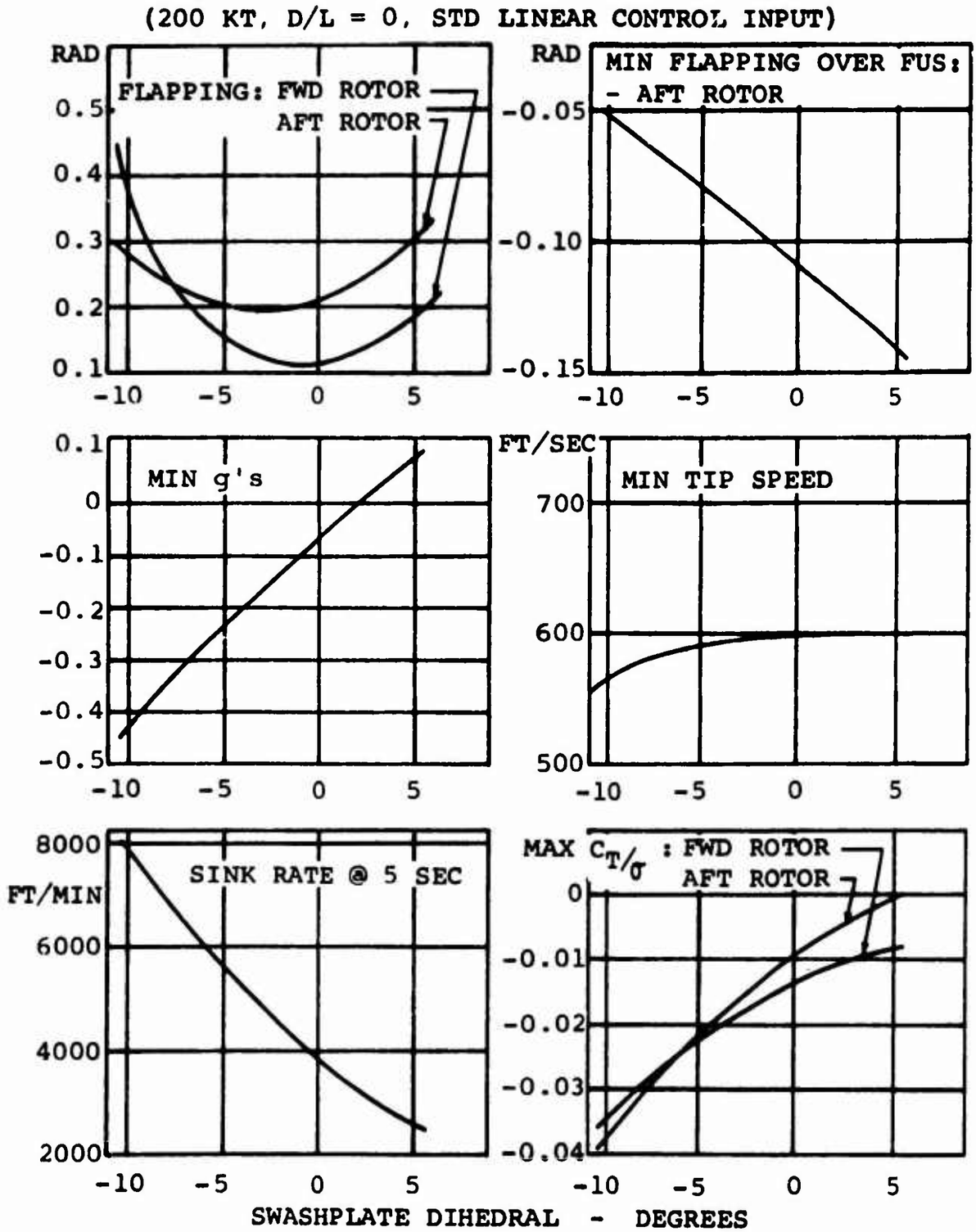

Figure 17. Effect of Swashplate Dihedral on Helicopter Response to Collective Reduction (D/L=0).

flapping amplitudes with application of too much or too little cyclic pitch.

Rotor Overlap and Relative Rotor Height

A comparison of Figures 102 (20-percent overlap), 103 (zero overlap), 104 (20-percent aft rotor height) and 105 (30-percent rotor height) with the basic case (35-percent overlap and 8-percent aft rotor height) shows that variations in these parameters have little effect on the plotted parameters, except, of course, that greater aft rotor height increases the minimum allowable aft rotor blade angle over the fuselage to -0.47 radian (20-percent aft rotor height) and -0.72 radian (30-percent aft rotor height).

Blade Twist

The effect of twist is presented in Figures 106 and 107. The rotor speed rise occurring after the initial minimum and before the secondary decay is greater with increasing negative twist. This would make for easier complete recovery through additional corrections applied subsequent to the standard collective input.

Teetering Rotors

The response to the standard collective input for a high-drag (D/L = 0.15) tandem helicopter with two-bladed teetering rotors is presented in Figure 108. Comparison with Figure 79 shows that the peak rotor flapping amplitudes are considerable reduced, and aft rotor blade clearance is greater than for any other high-drag configuration investigated. Rotor speed decay is not significantly affected.

The motions of the helicopter itself are very similar to the standard configuration, except that the peak normal acceleration is a little less severe, and a roll divergence is initiated at about 2.5 seconds. This roll disturbance is due to the negative thrust level together with the zero hinge offset of the teetering rotors, which combine to produce SAS control reversal, as explained previously. As soon as positive rotor thrust is reestablished, the roll divergence is halted. The severe vibrations caused by alternating blade loads are evident in the normal acceleration trace. These vibrations are much less severe when the rotor approaches the zero thrust condition, but appear again as positive thrust builds up.

4. ANALYSIS AT 250 KNOTS

The investigation at 250 knots consisted of a total of 10 time histories describing the responses of Configurations 45 to 48 (see Table 1) to complete power failure with and without corrective control inputs. These cases were arranged as follows:

1. Four runs with no control inputs.
2. Four runs with a standard collective reduction.
3. Two runs with modified collective reductions.

The configurations investigated at 250 knots all had auxiliary propulsion (D/L = 0), and differed from the corresponding 200-knot configurations in having 12 degrees of blade twist, 25-percent blade root cutout, a trim tip speed of 668 feet per second, and trim tip Mach number of 0.975.

COMPLETE POWER FAILURE WITH NO CORRECTIVE INPUTS

The divergence criteria used in the analysis of power failure at 250 knots with no control inputs are the same as for the analysis at 200 knots, except that the rotor tip speed criterion is 500 feet per second (75 percent of 668 feet per second) instead of 550 feet per second. Four time histories of complete power failure with no corrective control inputs were investigated, and the results are summarized in Table 17. A typical response is shown in Figure 109 for Configuration 45.

From a comparison of Table 17 with the data in Tables 11 through 14 it is evident that, except for rotor speed and sink rate, the responses at 250 knots are similar to those obtained for the corresponding configurations at 200 knots with D/L = 0.15. The large improvement in rotor speed decay is due to the lower trim power requirements and the consequent lower torque deficiency after power failure. This, in turn, results in a slower loss of rotor thrust and hence a lower rate of sink.

By an extension of this similarity to the other configurations not analyzed at 250 knots, forward cyclic pitch, negative swashplate dihedral, pitch-flap out-of-phase feedback, and reduced Lock number should all provide large improvements in helicopter and rotor response at 250 knots with no control input.

COMPLETE POWER FAILURE WITH STANDARD COLLECTIVE REDUCTION

The effect of a standard collective reduction on the four configurations considered above was investigated. The resultant peak responses are presented in Table 18. The collective input used was the same as the standard compound collective reduction applied in the previous section to all configurations having D/L = 0.15. The data show that Configurations 46 and 47 have well-behaved responses, while the responses of Configurations 45 and 48 would result in destruction of the helicopter. Typical examples are presented in Figures 110 and 111 for Configurations 45 and 46, respectively.

The principal difference between the well-behaved configurations and the unacceptable ones lies in the forward rotor responses to collective inputs. The good behavior typified by Figure 111 is associated with forward rotors incorporating either delta-three or pitch-cone feedback. Both of these mechanisms reduce the thrust and flapping response of the forward rotor to collective inputs. Consequently, when collective pitch is lowered, the total thrust lost by these configurations is less than on the two configurations which do not incorporate these devices. This alleviates the negative peak in normal acceleration and the prolonged negative values after the peak. Furthermore, since the thrust loss on the forward rotor is less than on the aft, the helicopter will pitch up and the angle of attack will increase, providing further relief of the negative normal acceleration. The sharply reduced peak flapping on the forward rotor arises mainly from the lower sensitivity of that rotor to collective reduction, $a_{1_{\theta_c}}$ being about one-half of the value for a rotor having no delta-three or pitch-cone feedback. The flapping of both rotors at and after the peaks is further reduced by the large angle of attack which acts through the positive rotor derivative a_{1_α} to offset the forward flapping due to $a_{1_{\theta_c}}$.

For the opposite reasons, large-amplitude forward flapping occurs on both rotors of Configurations 45 and 48, which have no delta-three or pitch-cone feedback. This causes the helicopter to pitch over sharply, bottoming the SAS. Rapid pitch divergence then follows. At the same time, the prolonged state of negative normal acceleration and the resulting reversal of the SAS control inputs destabilize the helicopter in roll and yaw.

COMPLETE POWER FAILURE WITH MODIFIED COLLECTIVE REDUCTION

From the above discussion, and from a consideration of Figures 9, 11, and 12, it is evident that if the rate of collective input is reduced, the rotor flapping and normal acceleration shown in Figure 110 can be greatly relieved. This is verified in Figure 112, in which the collective rates applied to Configuration 45 are one-half of the rates applied in Figure 110.

Although blade-fuselage contact is still indicated, the beneficial effect of the lower collective rate is clear. The reduced pitch rates are not severe enough to bottom the SAS, and the helicopter remains approximately level. The roll and yaw divergences are eliminated because the severity and extent of negative normal acceleration are not great enough to cause reversal of the roll and yaw SAS control inputs.

5. AEROELASTIC CONSIDERATIONS

A theoretical aeroelastic study of rotor dynamics during recovery from complete power failure at high speed has been carried out, using the Leone-Myklestad method of structural vibration analysis described in References 3 and 4. The analysis was applied to a number of the transient responses considered in the preceding sections of this report.

The Leone-Myklestad method calculates the free and forced aeroelastic responses of the rotor blades under specified conditions of rotor inflow, advance ratio, coning and flapping angles, collective and cyclic pitch settings, and rotor thrust. The method incorporates a free vibration analysis to provide the solutions for the normal modes of uncoupled flapwise and chordwise bending for both the stationary and rotating conditions, and a forced vibration analysis to provide the solutions for the forced modes of uncoupled flapwise and chordwise bending for the forward flight condition. Torsional freedom of the blade is not accounted for in the analysis; uniform rotor inflow and a linear section lift slope are assumed.

The cases analyzed were selected from 20 of the time histories discussed in previous sections of this report. Sixteen of these cases involve the application of a standard collective reduction to a variety of configurations having D/L = 0.15 at 200 knots. The remainder involve application of modified inputs to the standard configuration (Configuration 6), or to configurations having D/L = 0 at 250 knots. The cases selected are listed in Table 19, which correlates them with the appropriate configuration number and time history figure number. For each of these time histories, the conditions yielding the maximum absolute value of the blade loading parameter, $(C_{T/\sigma})_{max}$, were chosen for aeroelastic analysis. In all cases, the forward rotor only was analyzed, since the peak transient values of $C_{T/\sigma}$ were virtually identical for both rotors on all configurations except those involving some modification to the forward rotor (e.g., delta-three or tip path controller).

The physical characteristics of the rotors studied are presented in Appendix III, and the mass and stiffness properties

of the blades are defined in Figures 18, 19, and 20. These rotor blades were structurally designed to operate at high advance ratios, but were not specifically tailored to withstand the power failure cases investigated herein.

The results of the aeroelastic analysis are presented in Figures 21 through 40 as plots of the radial distribution of the maximum oscillatory flapwise and chordwise bending moments occurring during one rotor revolution (i.e. one-half of the peak-to-peak bending moment amplitude in one cycle). Since the analysis assumes quasi-steady flight conditions, the rotor conditions at the chosen point on each time history are assumed to persist throughout one rotor cycle.

Using these results, the maximum oscillatory bending moments of all cases investigated are compared with the standard case (Configuration 6, complete power failure, standard compound collective reduction) presented in Figure 22. The standard case had the following characteristics.

Configuration 6:

Aircraft speed at trim	200 knots
Rotor tip speed at trim	723 feet per second
Drag/lift ratio	0.15
Blade root cutout ratio	0.195
Flap or horizontal hinge offset ratio	0.05
Blade twist	-4 degrees
Longitudinal cyclic pitch	8 degrees
Swashplate dihedral	-2.5 degrees
Delta-three coupling ratio	0
Pitch-flap coupling ratio	0
Lock number	4.38
Rotor overlap	35 percent
Relative aft rotor height	8 percent

Standard Compound Collective Reduction:

Delay time	1 second
Magnitude	10 degrees
Initial rate	20 degrees per second
Final rate	4 degrees per second
Inflection point	50 percent

In order to demonstrate the changes in maximum oscillatory bending moments caused by variations from the standard characteristics given above, the following comparisons are provided. For each of the indicated variations in characteristics, the bending moment changes are given as percentage increases or reductions of the moments for the standard case.

1. Flap hinge offset ratio = 0 (Figure 21):

   Flapwise bending moment - 5-percent reduction.
   Chordwise bending moment - 25-percent reduction.

2. Delta-three coupling ratio = 0.5774 (Figure 23):

   Flapwise bending moment - 15-percent reduction.
   Chordwise bending moment - 40-percent reduction.

3. Lock number = 2.19 (Figure 24):

   Flapwise bending moment - 20-percent reduction.
   Chordwise bending moment - 40-percent reduction.

4. Longitudinal cyclic pitch = 4 degrees (Figure 25):

   Flapwise bending moment - 35-percent increase.
   Chordwise bending moment - 70-percent increase.

5. Longitudinal cyclic pitch = 14 degrees (Figure 26):

   Flapwise bending moment - 20-percent reduction.
   Chordwise bending moment - 40-percent reduction.

6. Swashplate dihedral = 1.5 degrees (Figure 27):

   Flapwise bending moment - 5-percent reduction.
   Chordwise bending moment - negligible change.

7. Swashplate dihedral = 6.5 degrees (Figure 28):

   Flapwise bending moment - 10-percent increase.
   Chordwise bending moment - 30-percent increase.

8. Rotor overlap = 20 and 0 percent (Figures 29 and 30)

   Flapwise bending moment - negligible change.
   Chordwise bending moment - negligible change.

9. Aft rotor height = 20 and 30 percent (Figures 31 and 32):

   Flapwise bending moment - negligible change.
   Chordwise bending moment - negligible change.

10. Blade twist = -8 degrees (Figure 33):

   Flapwise bending moment - 10-percent increase.
   Chordwise bending moment - 5-percent increase.

11. Blade twist = -12 degrees (Figure 34):

   Flapwise bending moment - 30-percent increase.
   Chordwise bending moment - 15-percent increase.

12. Forward speed = 250 knots, drag/lift ratio = 0, blade root cutout ratio = 0.25, blade twist = -12 degrees, rotor tip speed at trim = 668 feet per second (Figure 35):

   Flapwise bending moment - 30-percent increase.
   Chordwise bending moment - 5-percent increase.

13. Pitch-flap coupling ratio = -0.5774 (Figure 36):

   Flapwise bending moment - 5-percent increase.
   Chordwise bending moment - 20-percent reduction.

14. Smoothed input*, Configuration 6 (Figure 37):

   Flapwise bending moment - 5-percent increase.
   Chordwise bending moment - 20-percent reduction.

*Smoothed input: Gradual change from initial to final collective reduction rates.

15. Optimum longitudinal cyclic pitch* (Figure 38):

Flapwise bending moment - 30-percent increase.
Chordwise bending moment - 15-percent increase.

16. Longitudinal stick step** (Figure 39):

Flapwise bending moment - 10-percent increase.
Chordwise bending moment - 10-percent reduction.

17. Forward speed = 250 knots, drag/lift ratio = 0, blade root cutout ratio = 0.25, blade twist = -12 degrees, rotor tip speed at trim = 668 feet per second (Figure 40):

Flapwise bending moment - 45-percent increase.
Chordwise bending moment - 20-percent increase.

For all configurations subjected to the standard compound collective reduction described above, the comparable maximum oscillatory flapwise and chordwise bending moments in steady level flight were approximately one third of those determined herein for the transient peak blade loading conditions.

From the results, it is evident that cyclic blade stresses on the forward rotor during recovery from complete power failure at high speed are adversely affected by aft longitudinal cyclic pitch, blade twist, and forward speed, and are favorably affected by delta-three coupling on the forward rotor, reduced Lock number, and forward longitudinal cyclic pitch.

In addition to the maximum cyclic bending moment distributions presented herein, the mean bending moment distributions at the instant of maximum $(C_{T/\sigma})$ have also been determined for all

---

*Optimum longitudinal cyclic pitch: Forward rotor cyclic = 7 degrees forward, aft rotor cyclic = 6 degrees forward.
**Longitudinal stick step: Aft longitudinal stick input of 2 degrees per rotor, 1-second delay time.

the cases considered. The combination of the maximum cyclic bending moment superimposed upon the mean bending moment yields the peak transient bending moment that the rotor blades will experience, for each case investigated. None of the peak transient bending moments so computed for any of the cases considered is sufficiently large to cause failure of the blades in question. Since the blades were conventional in design and were not specially adapted to withstand the stresses imposed by conditions in this investigation, it is evident that recovery from complete power failure will generate no special problems in blade design for a high-speed tandem helicopter with articulated rotors.

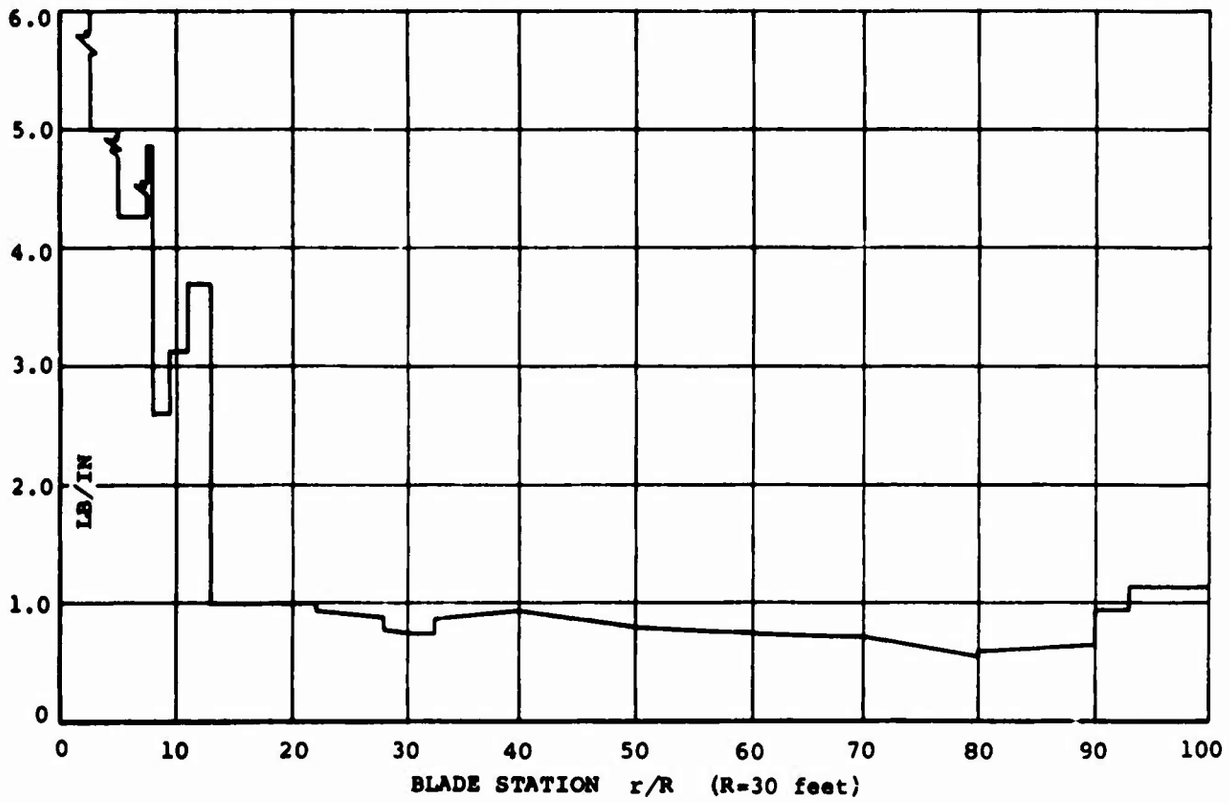

Figure 18. Blade Spanwise Weight Distribution.

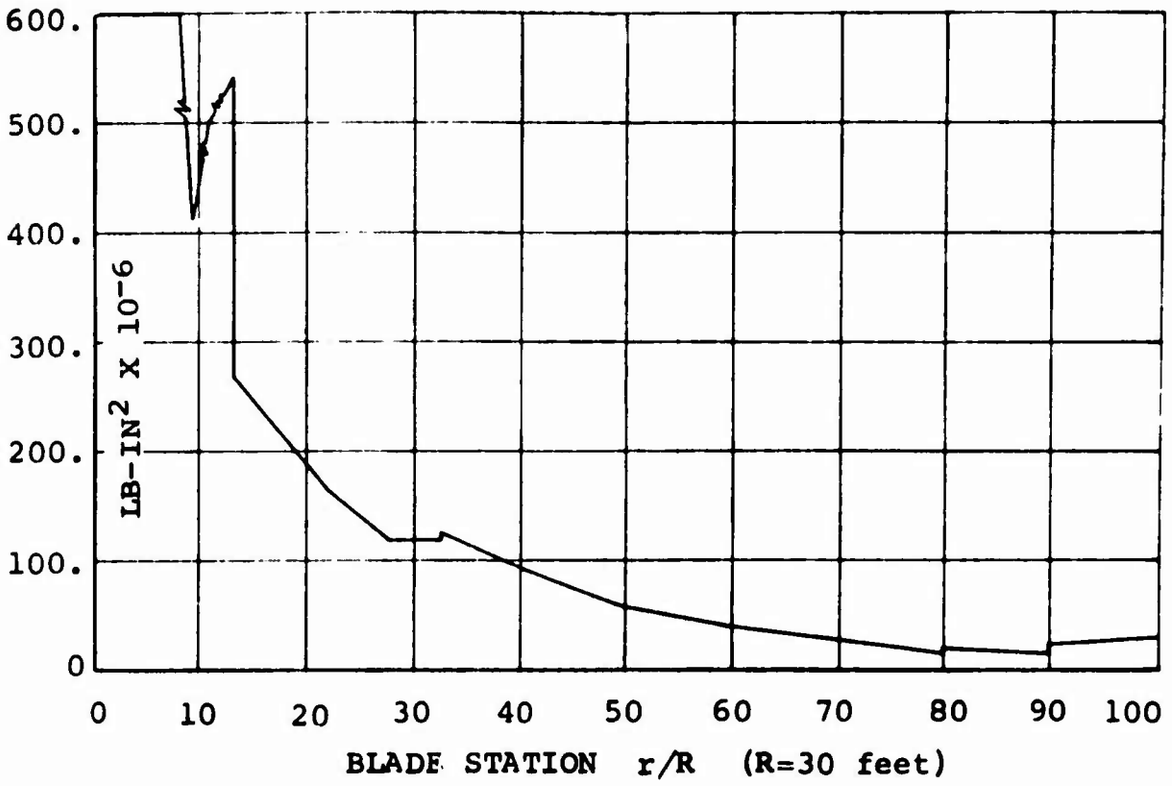

Figure 19. Blade Flapwise Stiffness Distribution.

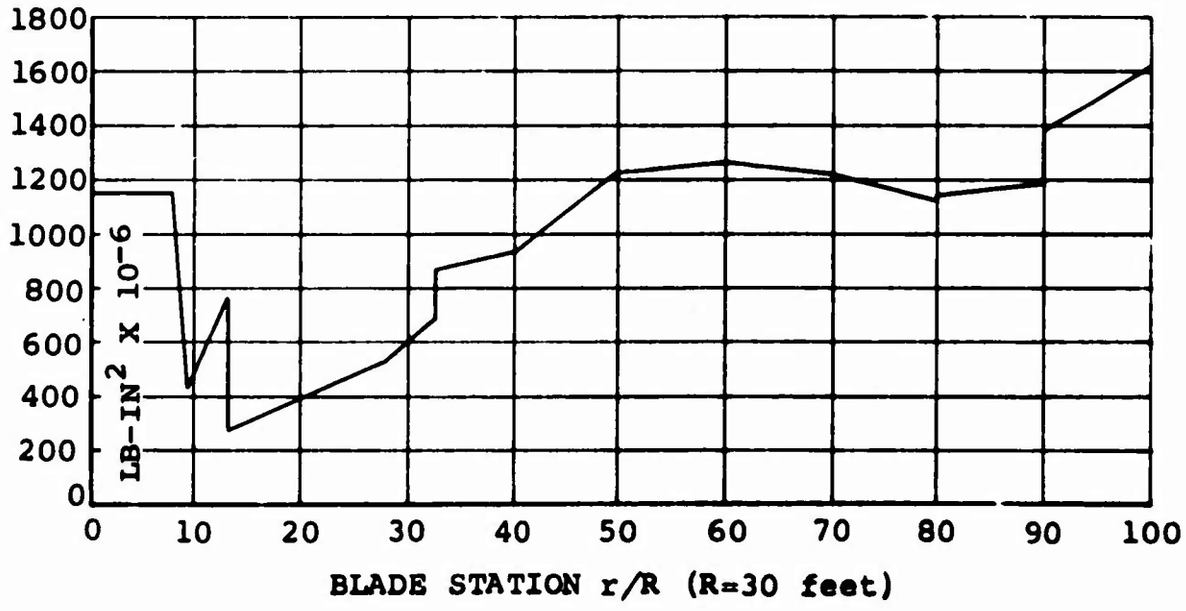

Figure 20. Blade Chordwise Stiffness Distribution.

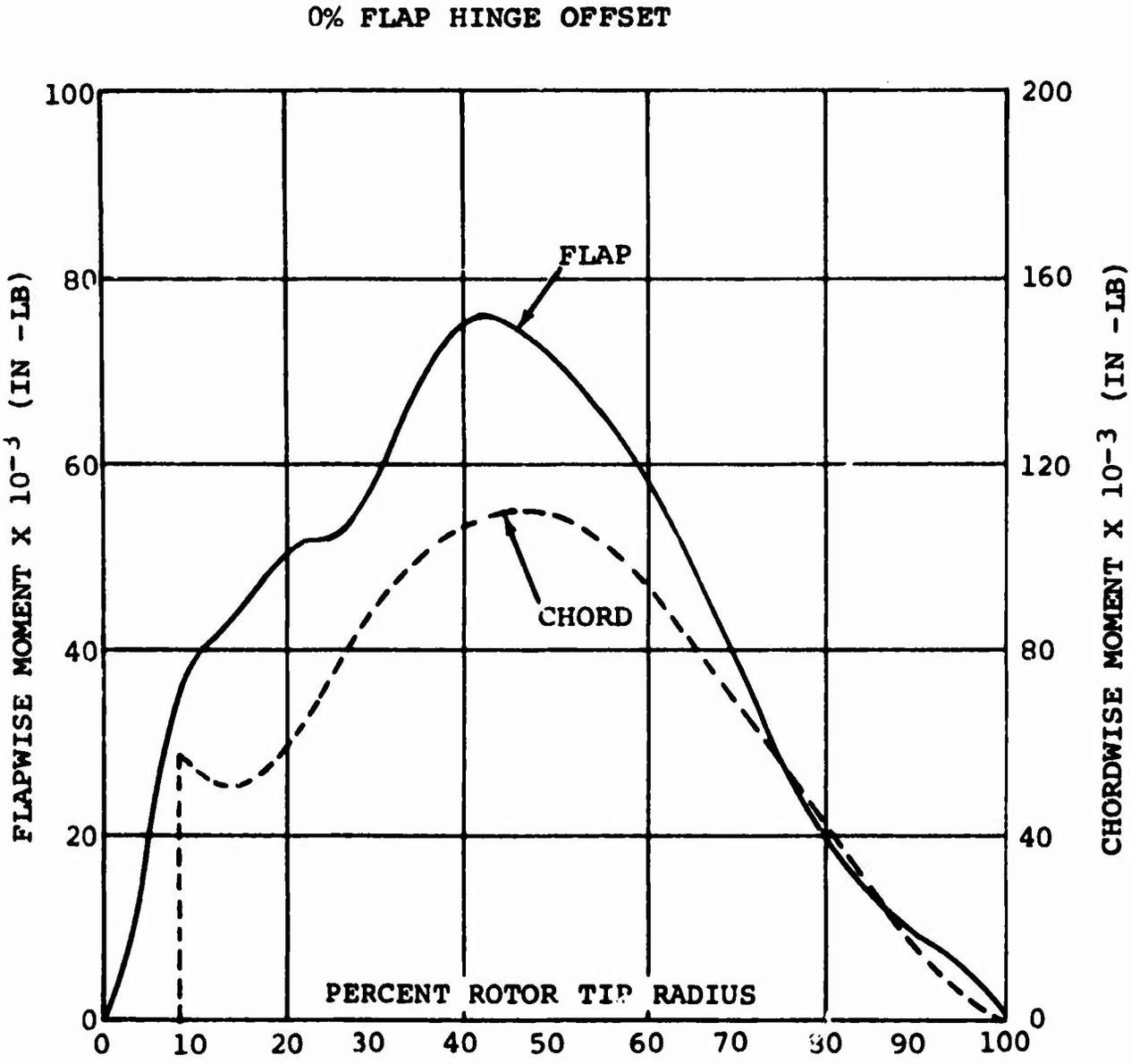

Figure 21. Rotor Blade Chordwise and Flapwise Moments versus Percent Rotor Tip Radius for 0-Percent Flap Hinge Offset.

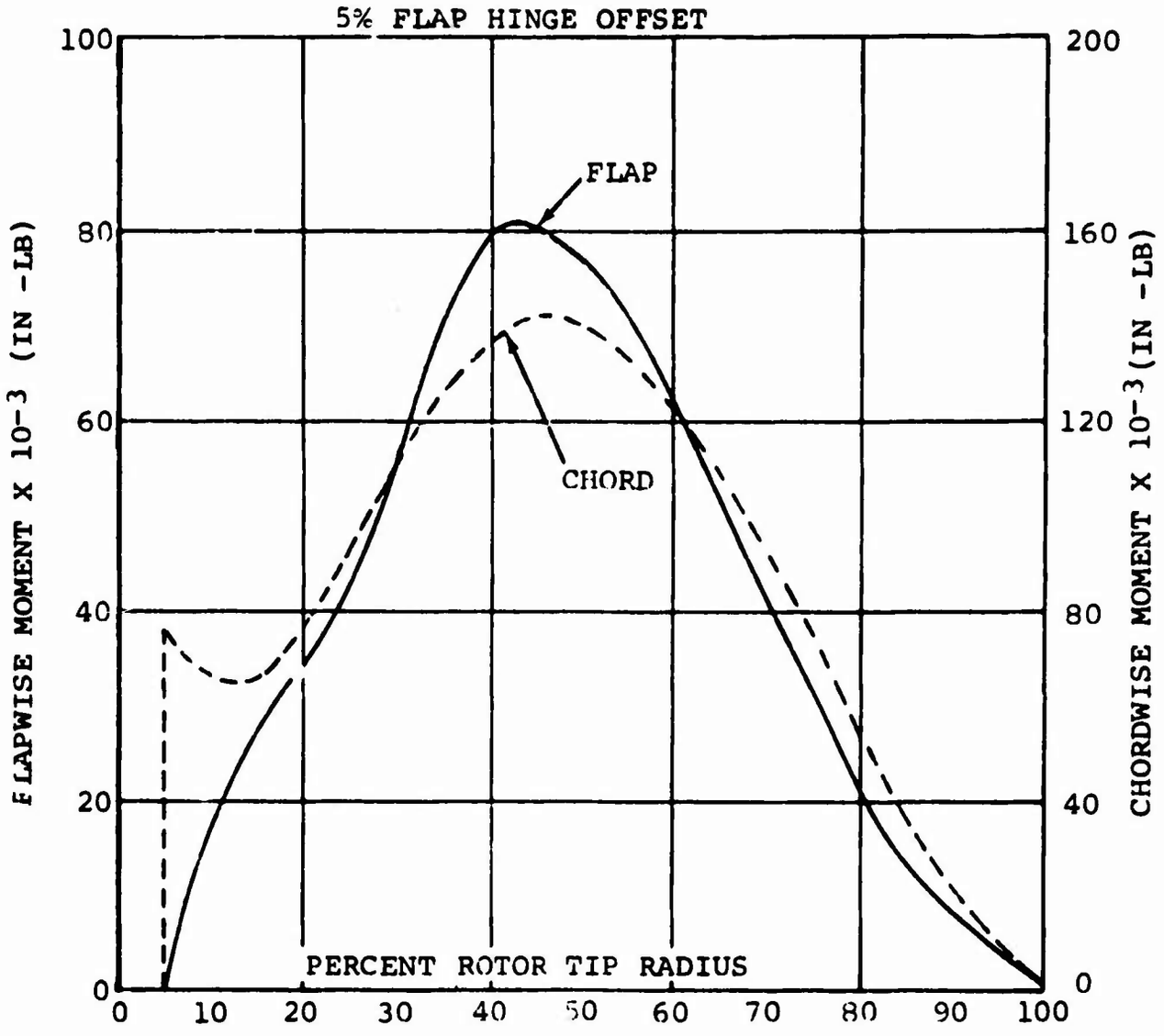

Figure 22. Rotor Blade Chordwise and Flapwise Moments versus Percent Rotor Tip Radius for 5-Percent Flap Hinge Offset.

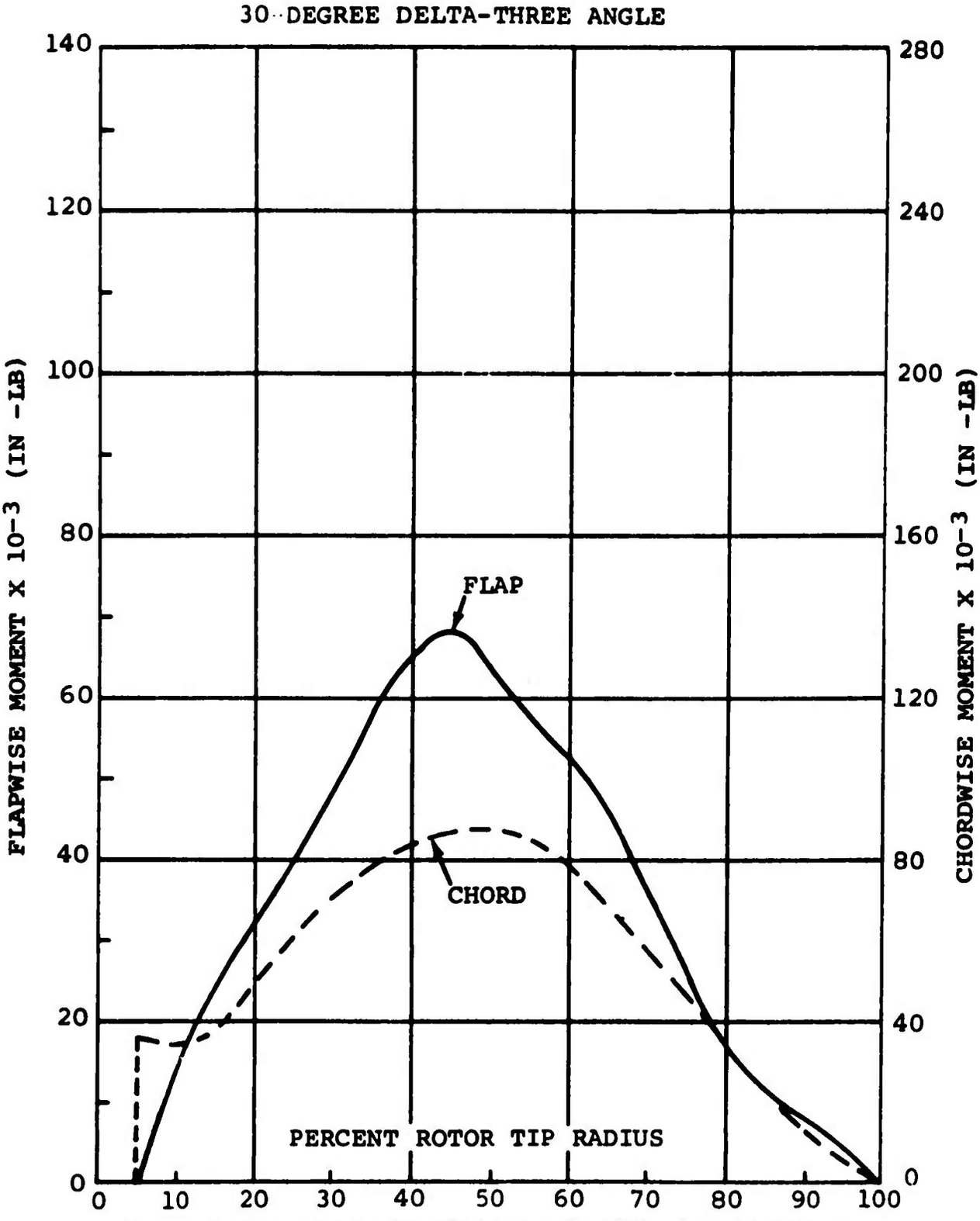

Figure 23. Rotor Blade Chordwise and Flapwise Moments versus Percent Rotor Tip Radius for 30-Degree Delta-Three Angle.

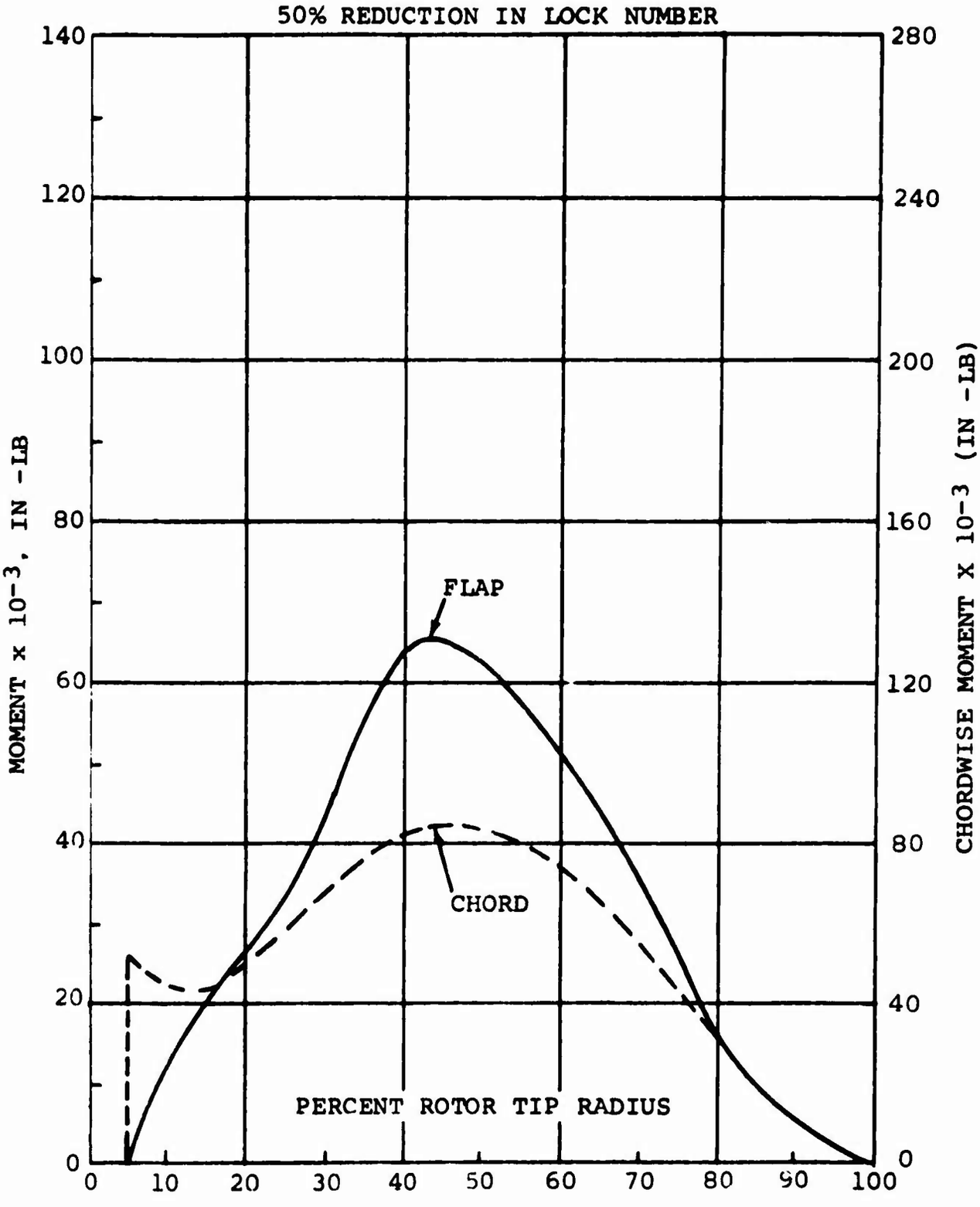

Figure 24. Rotor Blade Chordwise and Flapwise Moments versus Percent Rotor Tip Radius for 50-Percent Reduction in Lock Number.

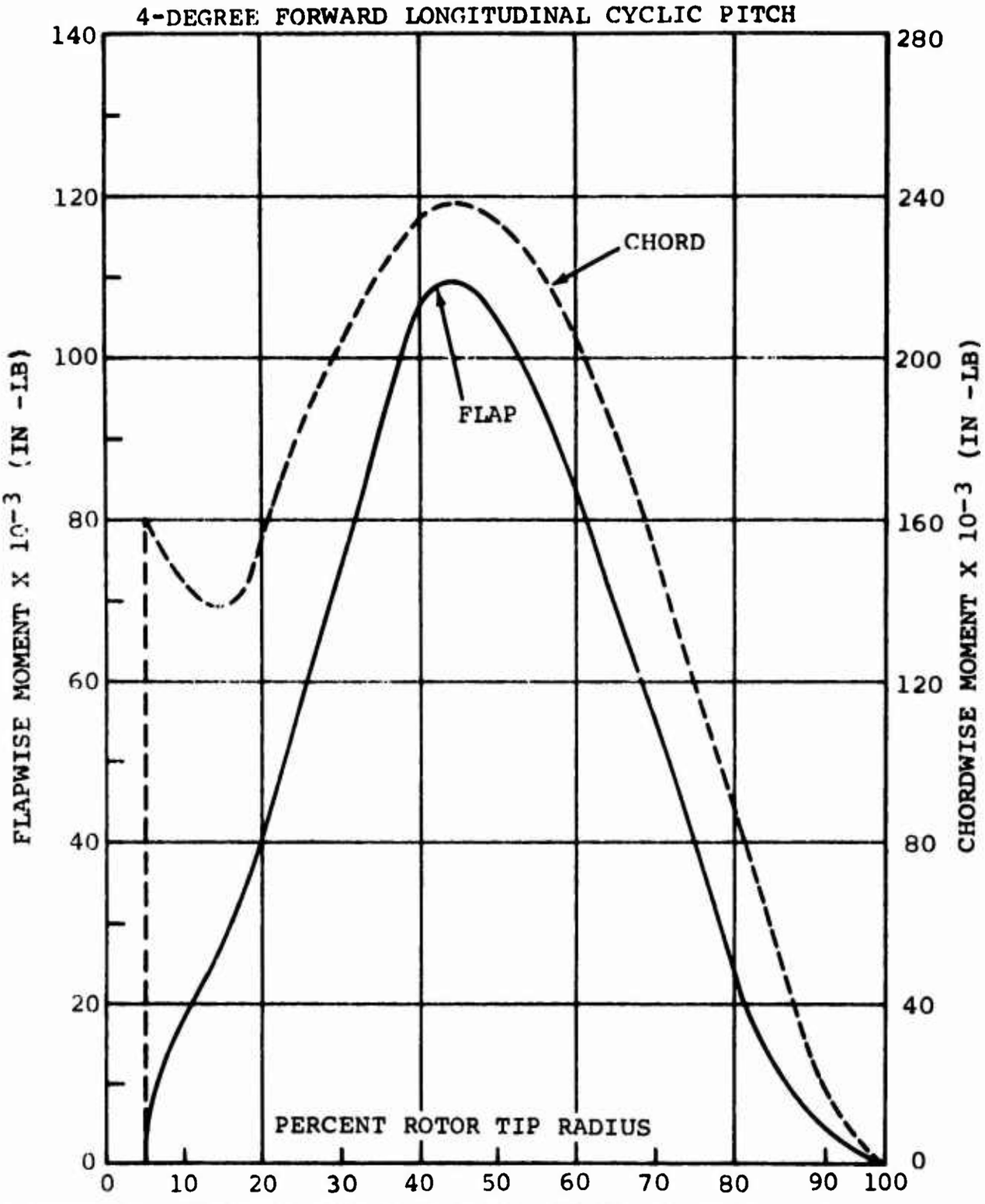

Figure 25. Rotor Blade Chordwise and Flapwise Moments versus Percent Rotor Tip Radius for 4-Degree Forward Longitudinal Cyclic Pitch.

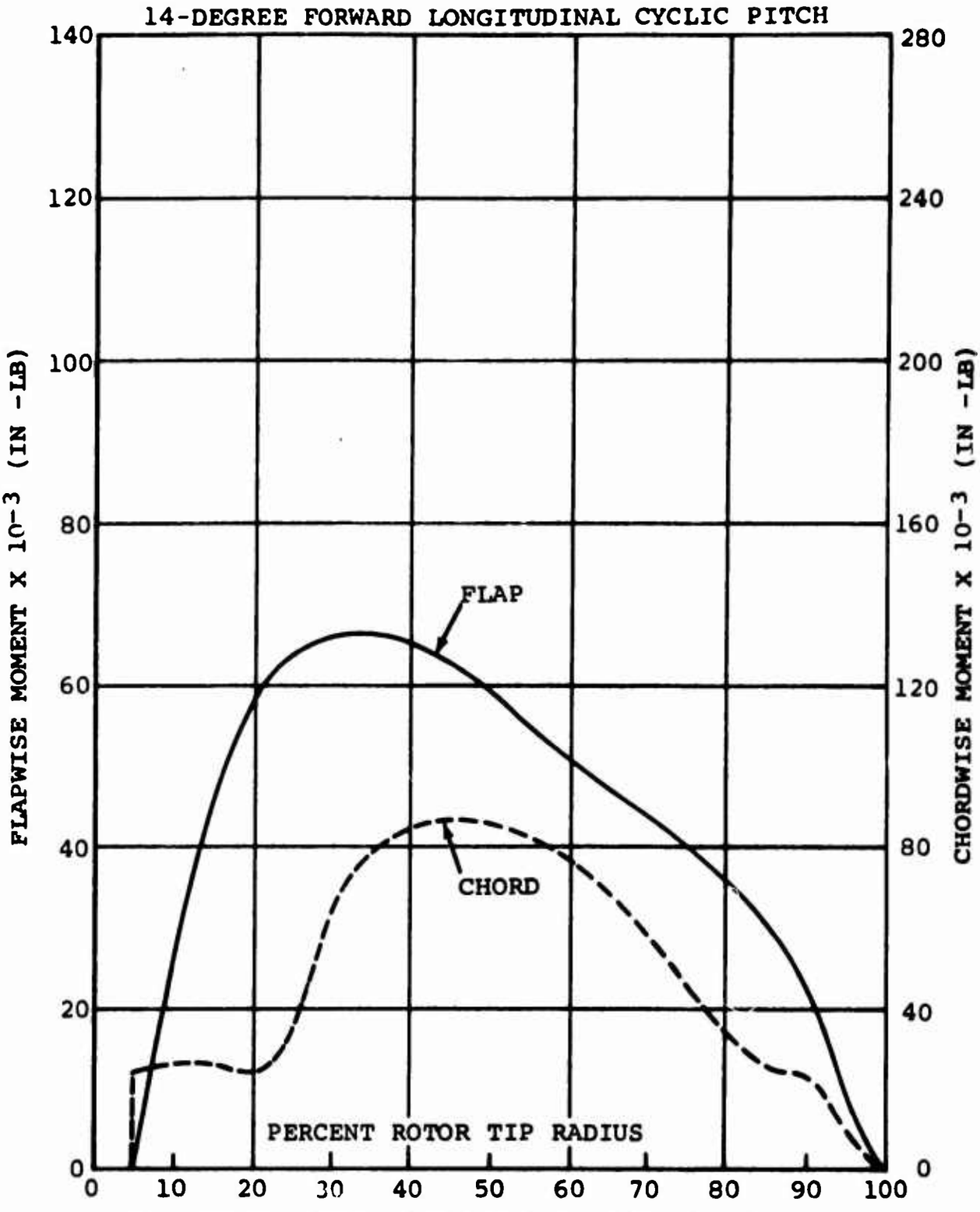

Figure 26. Rotor Blade Chordwise and Flapwise Moments versus Percent Rotor Tip Radius for 14-Degree Forward Longitudinal Cyclic Pitch.

1.5-DEGREE SWASHPLATE DIHEDRAL

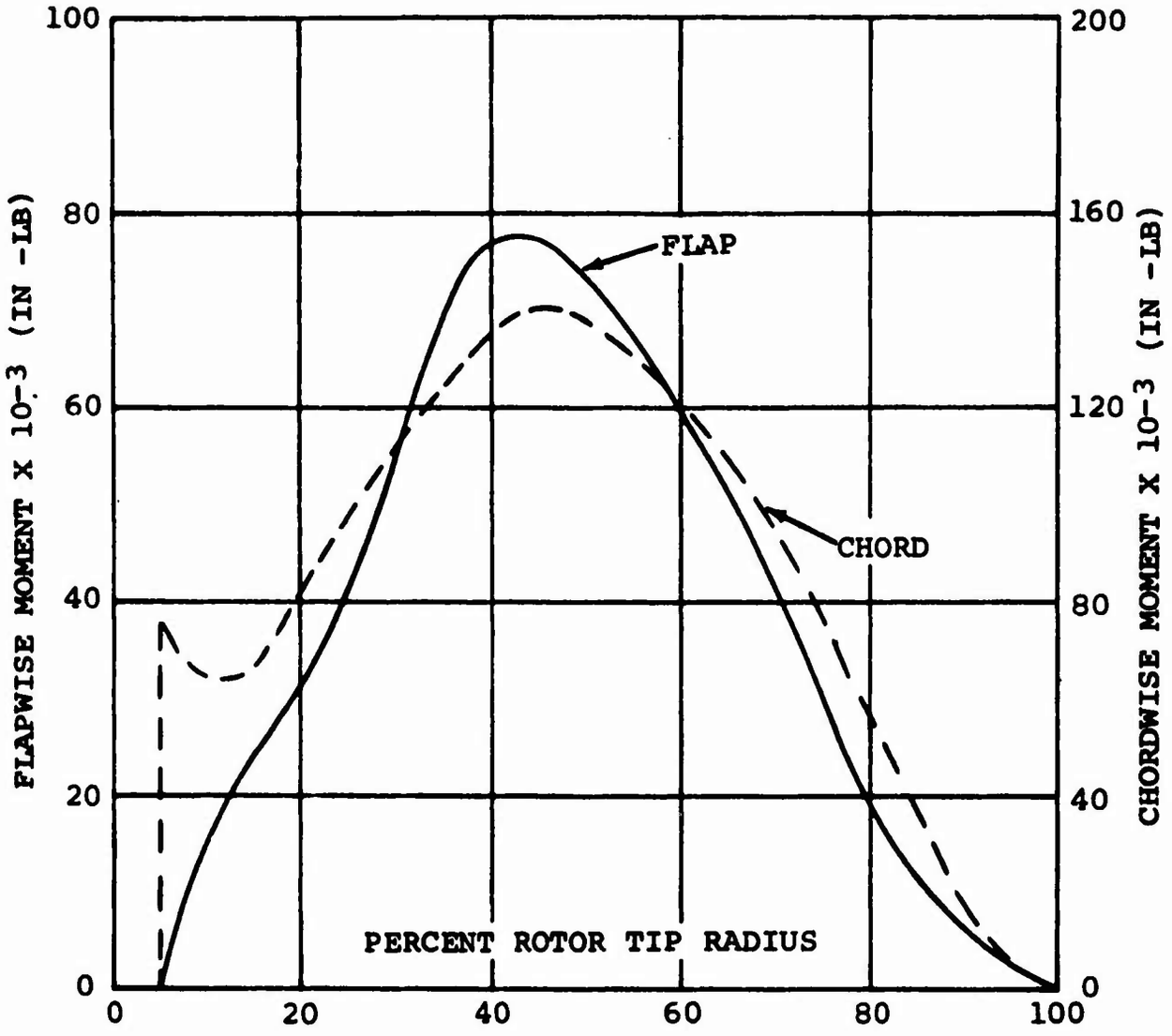

Figure 27. Rotor Blade Chordwise and Flapwise Moments versus Percent Rotor Tip Radius for 1.5-Degree Swashplate Dihedral.

6.5-DEGREE SWASHPLATE CATHEDRAL

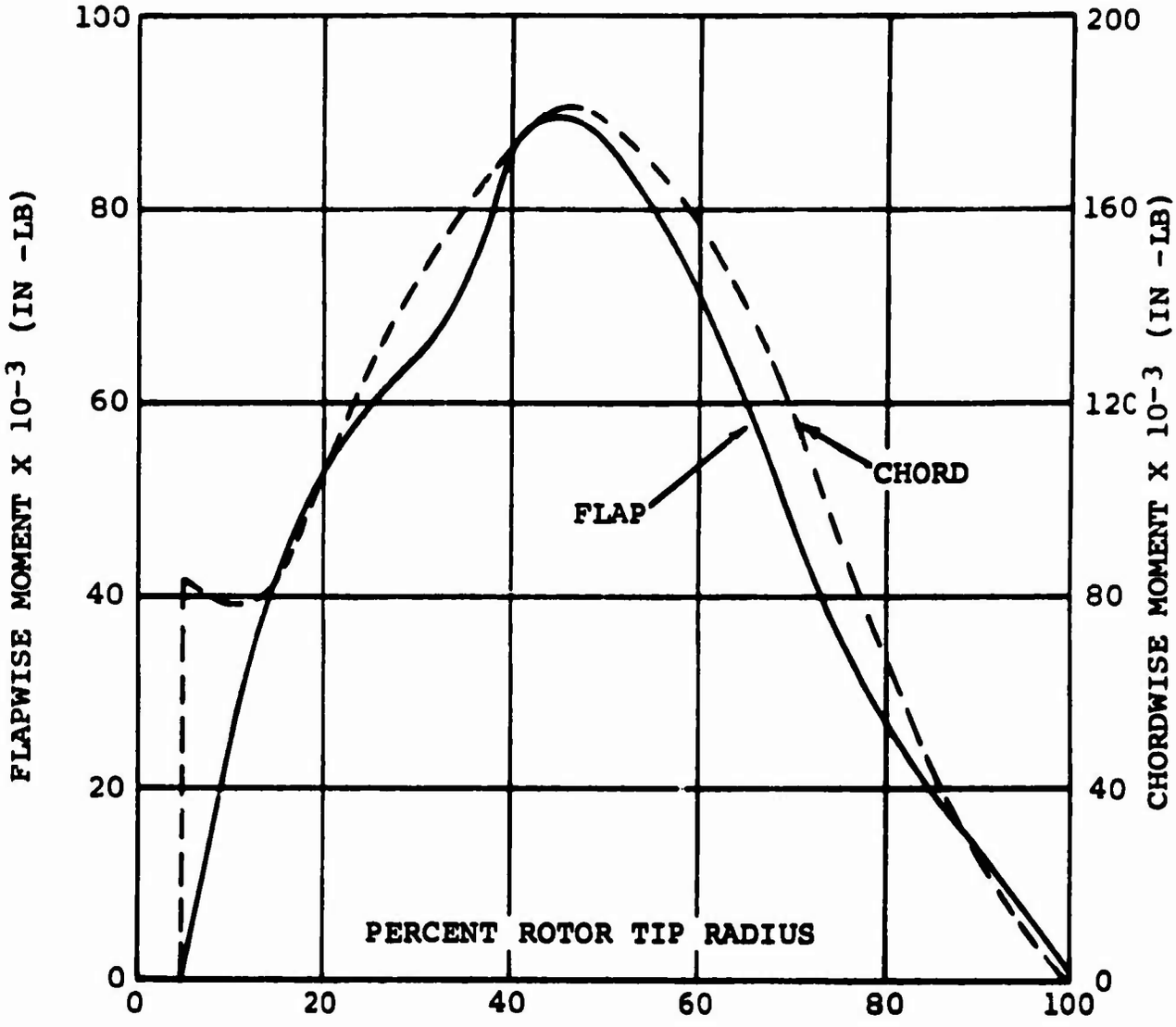

Figure 28. Rotor Blade Chordwise and Flapwise Moments versus Percent Rotor Tip Radius for 6.5-Degree Swashplate Cathedral.

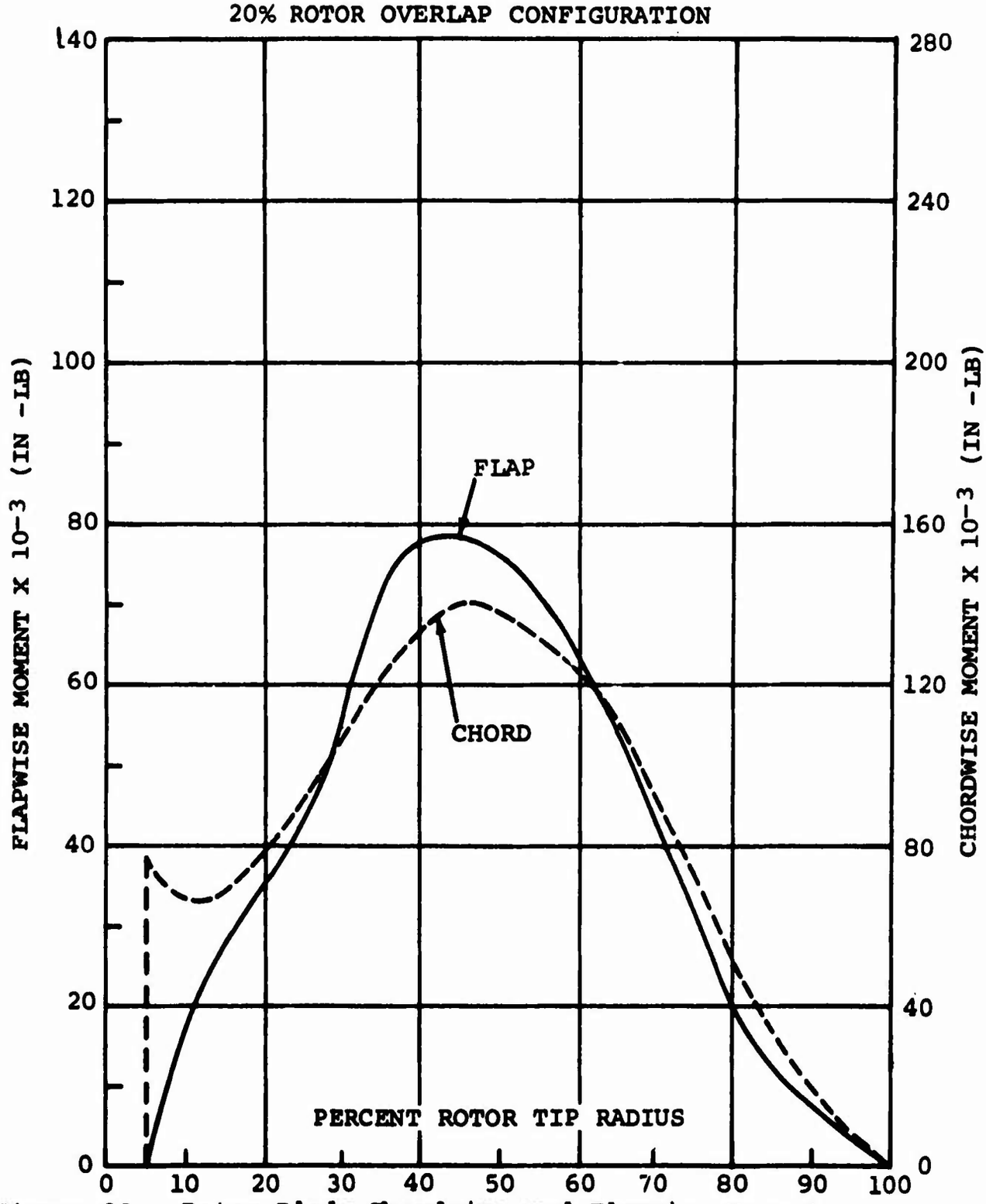

Figure 29. Rotor Blade Chordwise and Flapwise Moments versus Percent Rotor Tip Radius for 20-Percent Rotor Overlap.

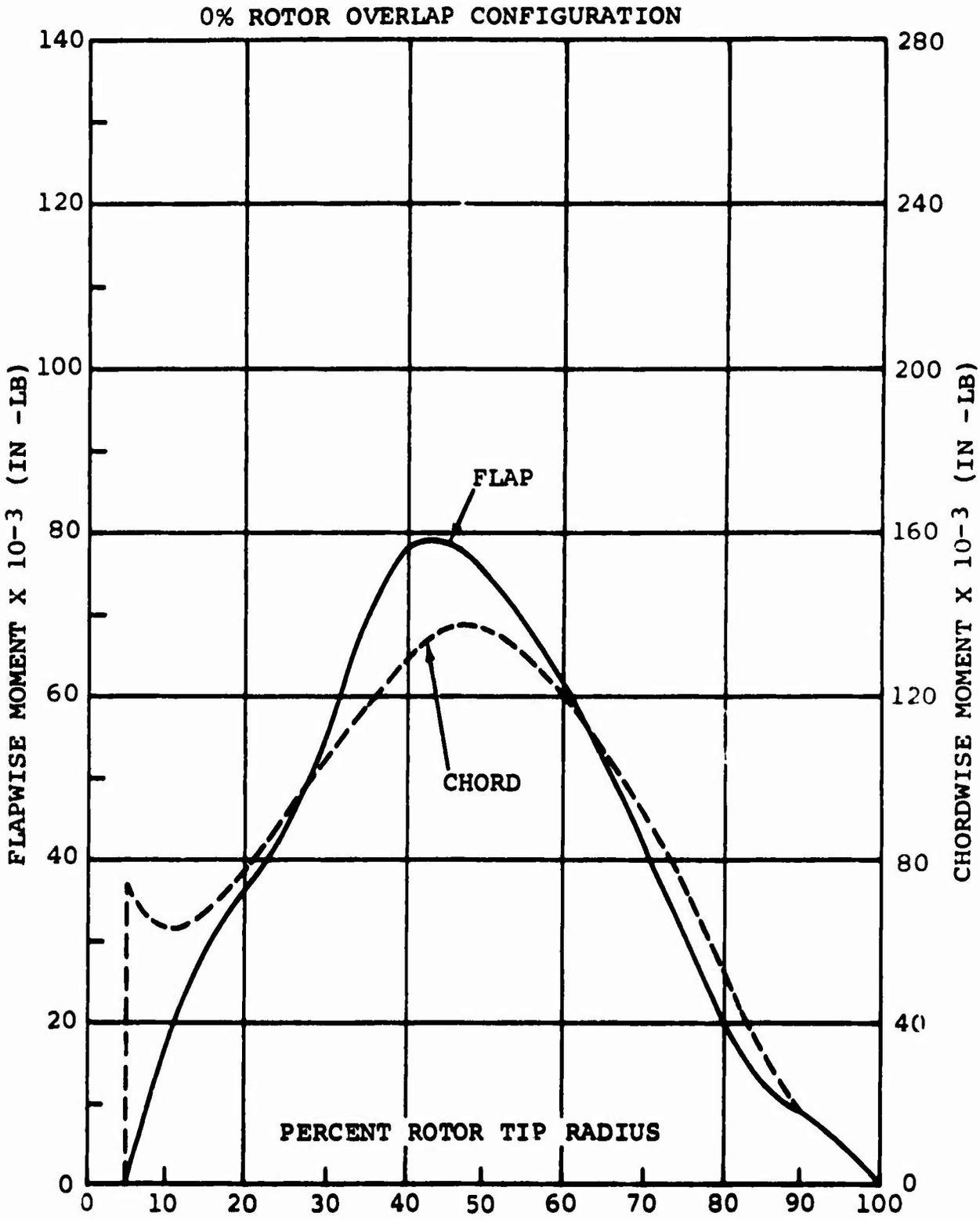

Figure 30. Rotor Blade Chordwise and Flapwise Moments versus Percent Rotor Tip Radius for 0-Percent Rotor Overlap.

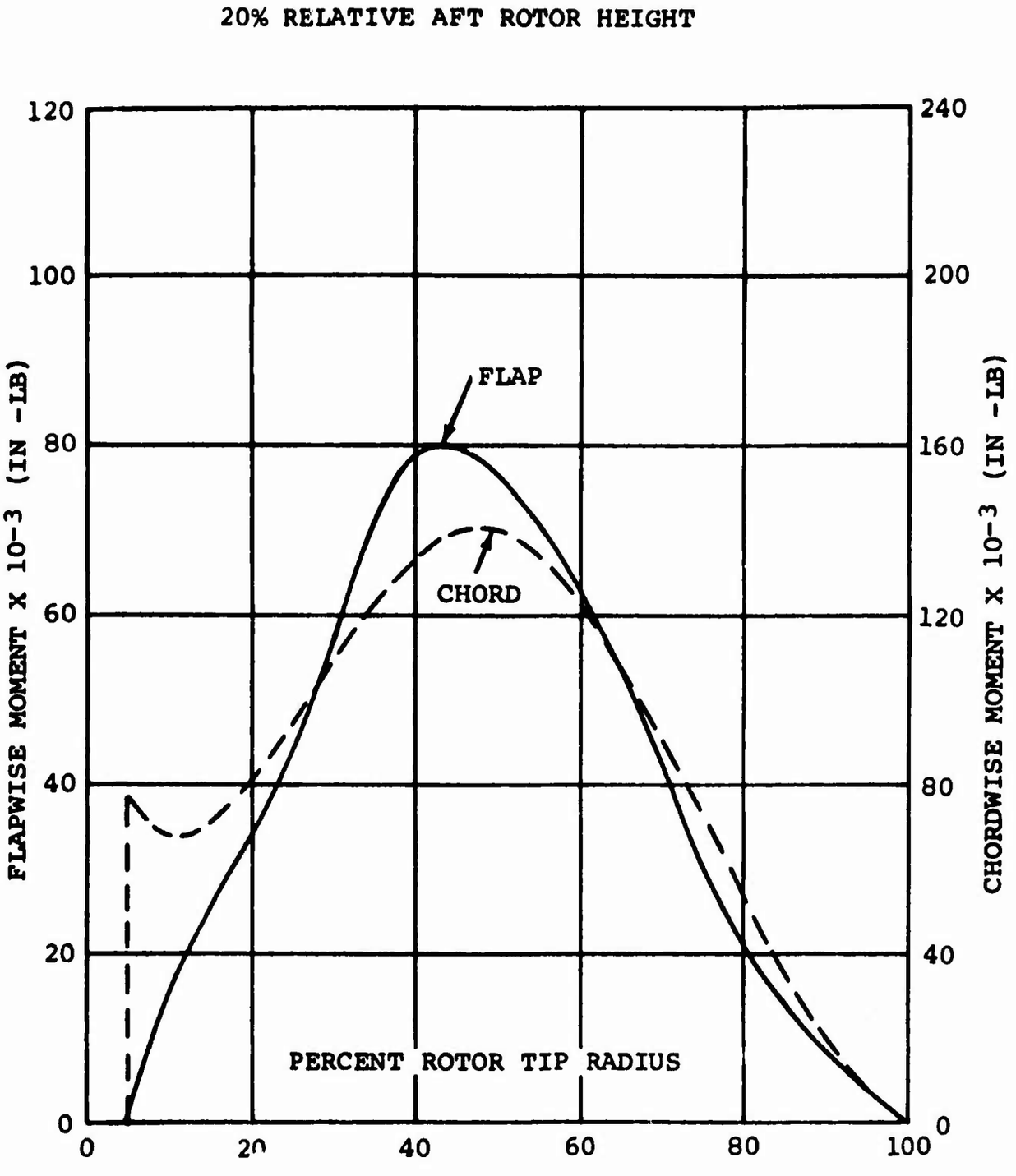

Figure 31. Rotor Blade Chordwise and Flapwise Moments versus Percent Rotor Tip Radius for 20-Percent Relative Aft Rotor Height.

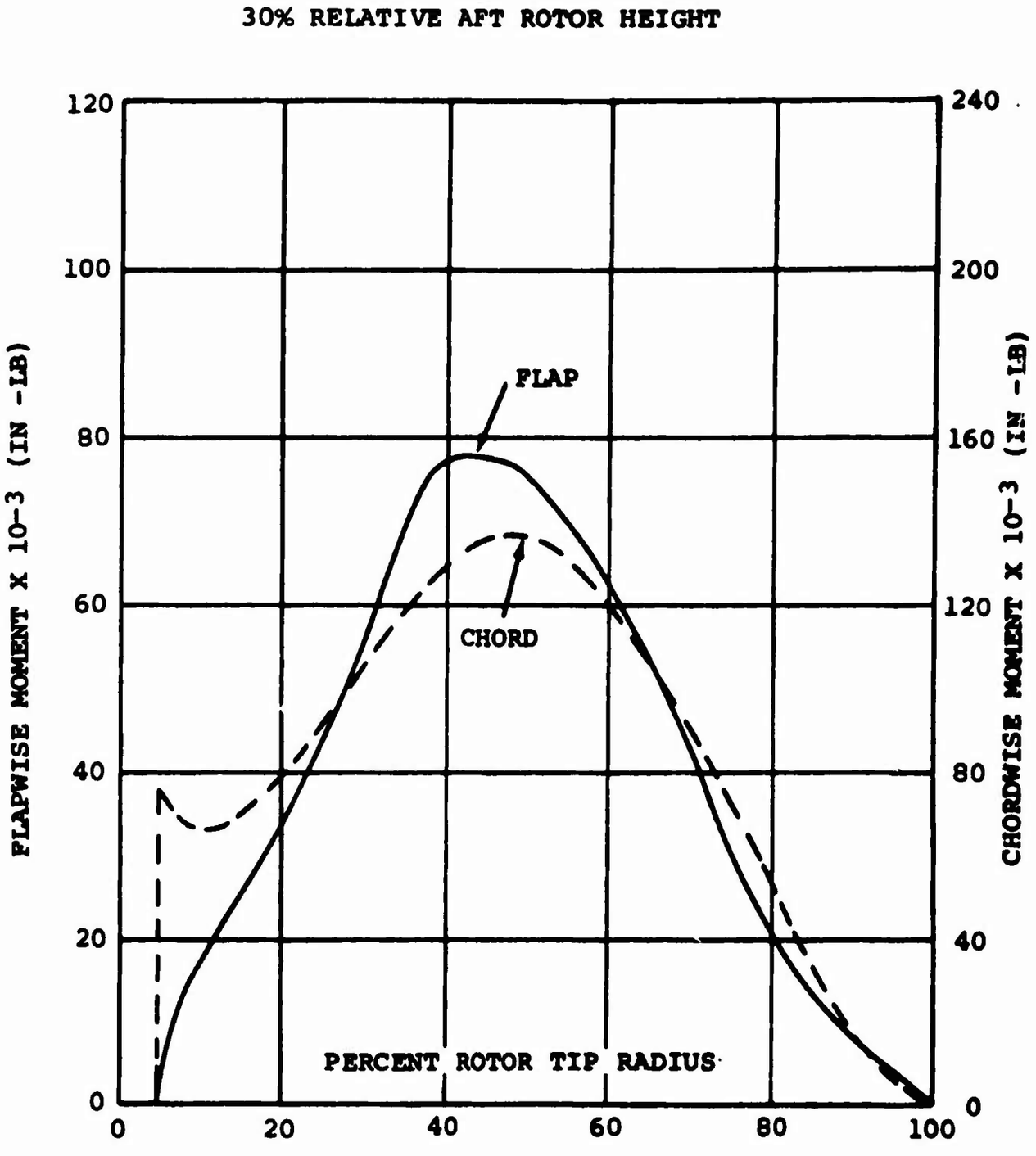

Figure 32. Rotor Blade Chordwise and Flapwise Moments versus Percent Rotor Tip Radius for 30-Percent Relative Aft Rotor Height.

-8-DEGREE STATIC TWIST ANGLE

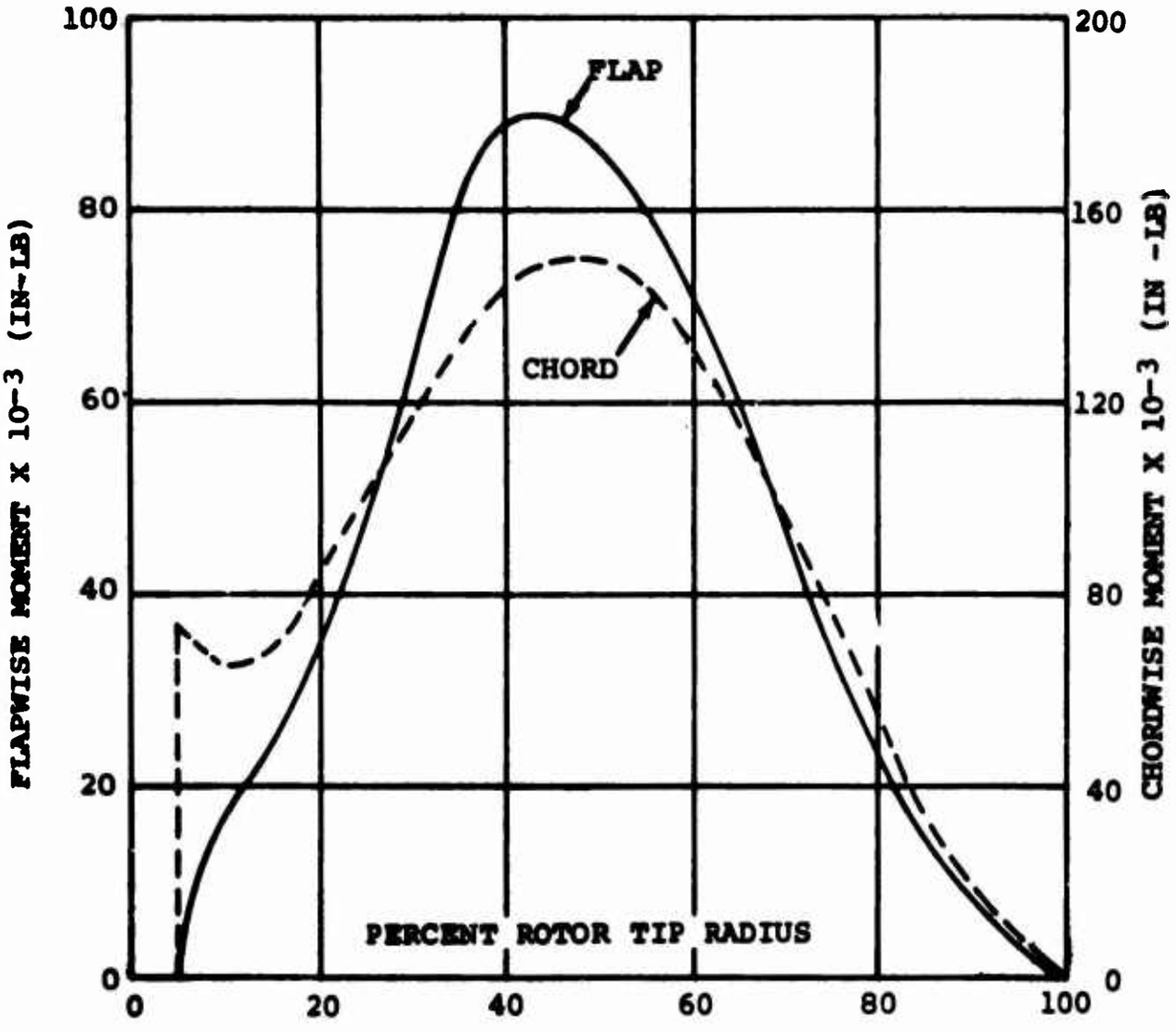

Figure 33. Rotor Blade Chordwise and Flapwise Moments versus Percent Rotor Tip Radius for -8-Degree Static Twist Angle.

-12-DEGREE STATIC TWIST ANGLE

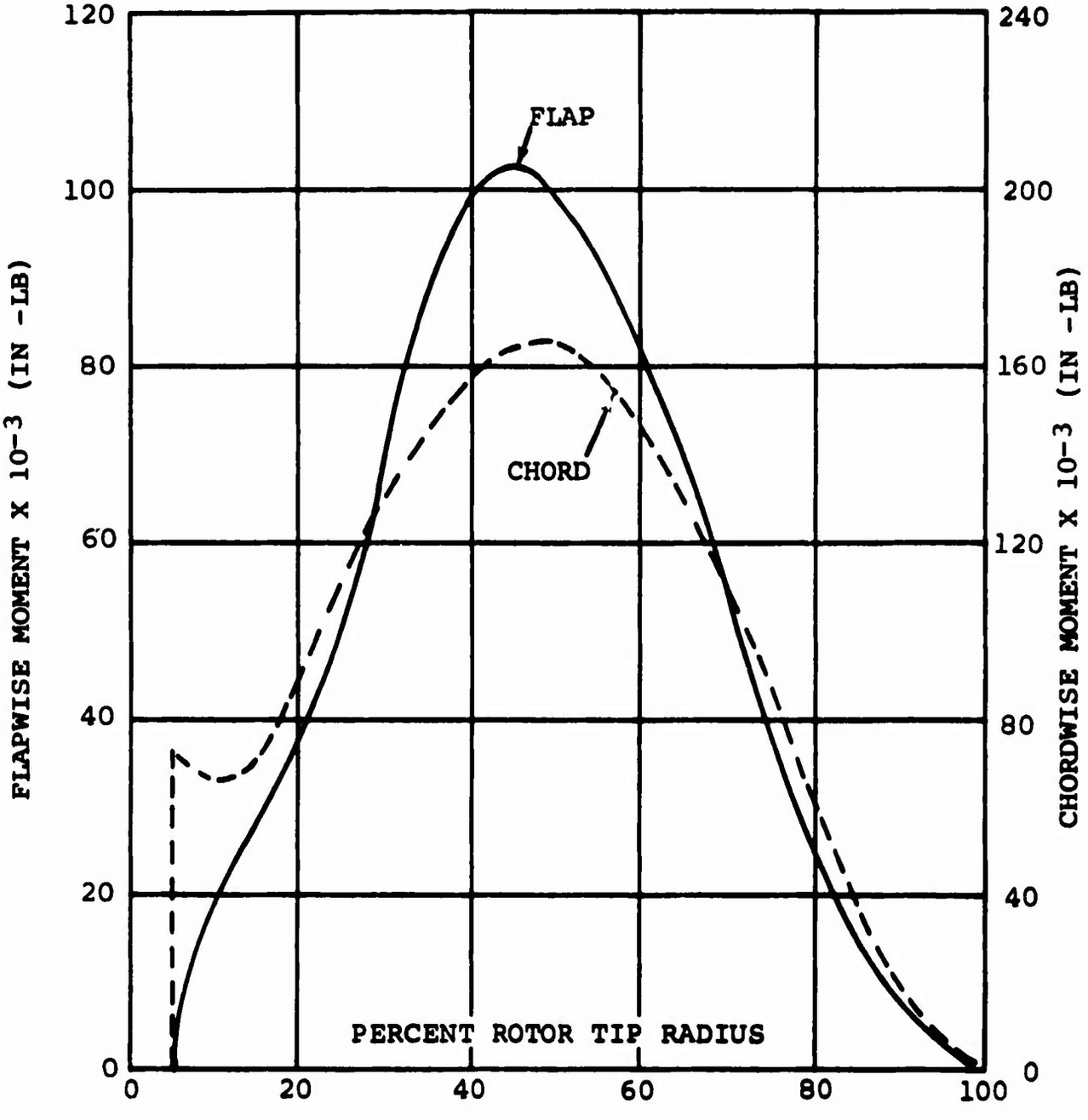

Figure 34. Rotor Blade Chordwise and Flapwise Moments versus Percent Rotor Tip Radius for -12-Degree Static Twist Angle.

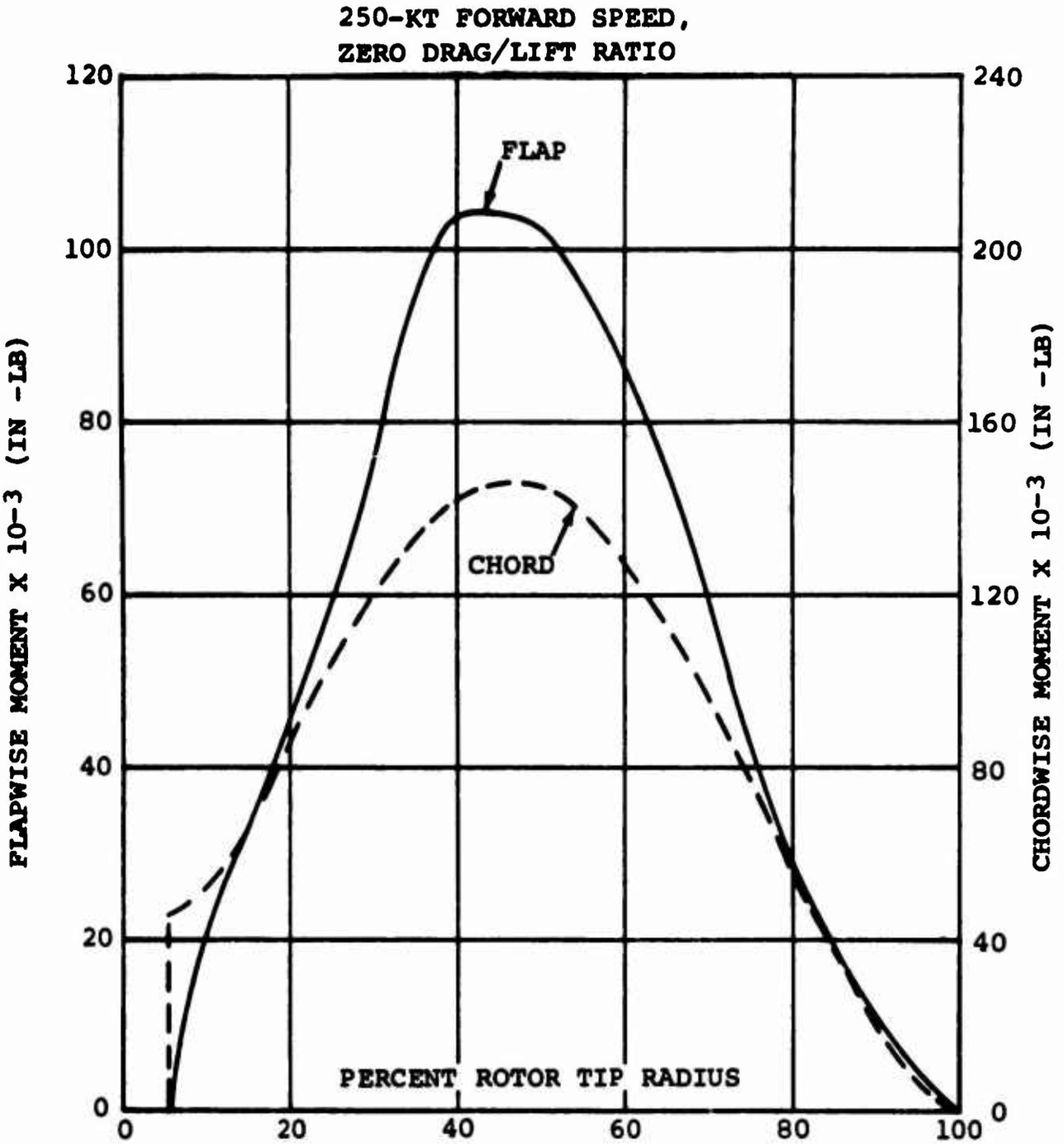

Figure 35. Rotor Blade Chordwise and Flapwise Moments versus Percent Rotor Tip Radius for 250-Knot Forward Speed, Zero Drag/Lift Ratio. Collective Pitch Initially Reduced at 20 Degrees per Second, Followed by 4 Degrees per Second.

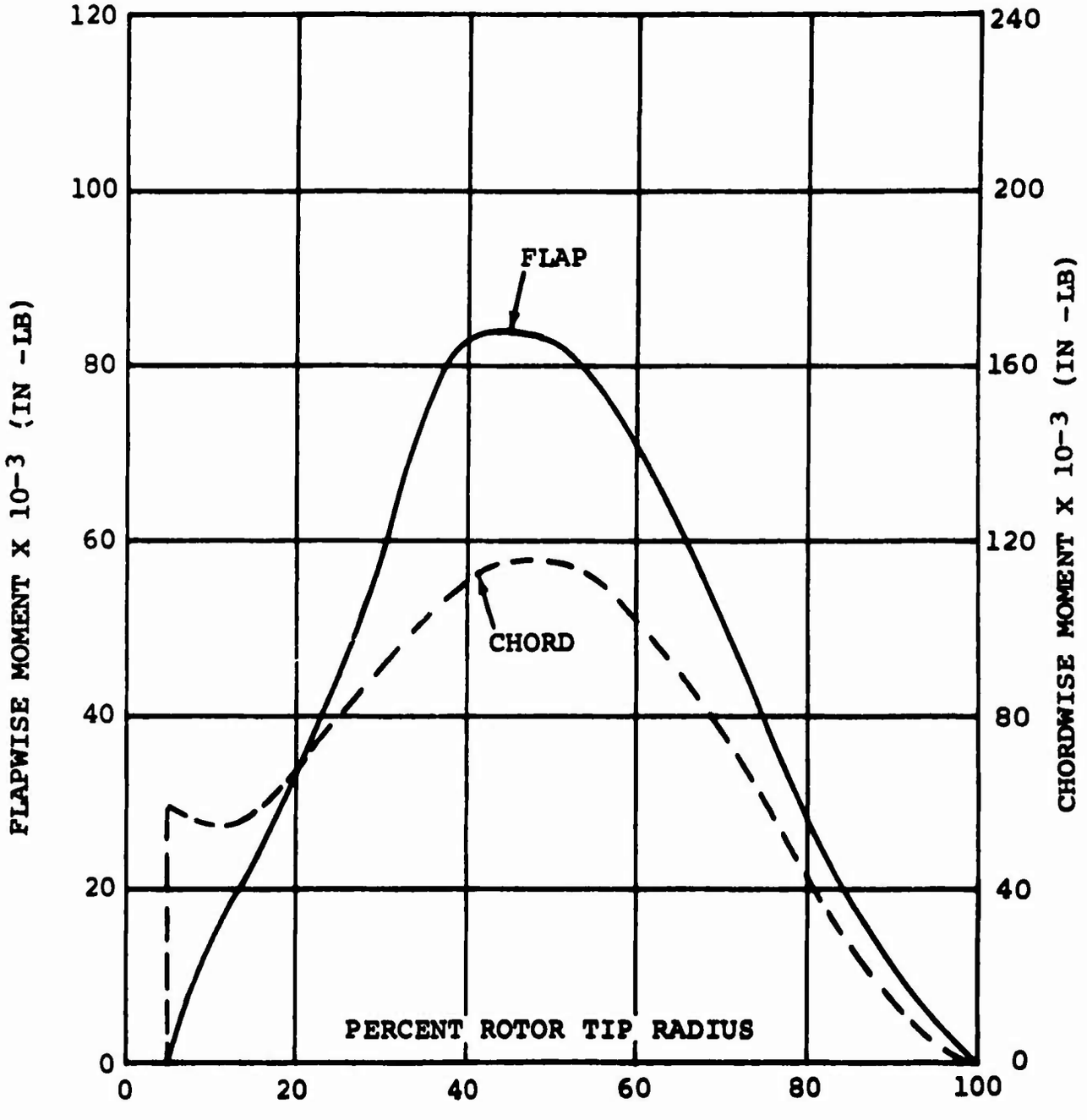

Figure 36. Rotor Blade Chordwise and Flapwise Moments versus Percent Rotor Tip Radius for Tip Path Plane Controller, 90 Degrees Out of Phase.

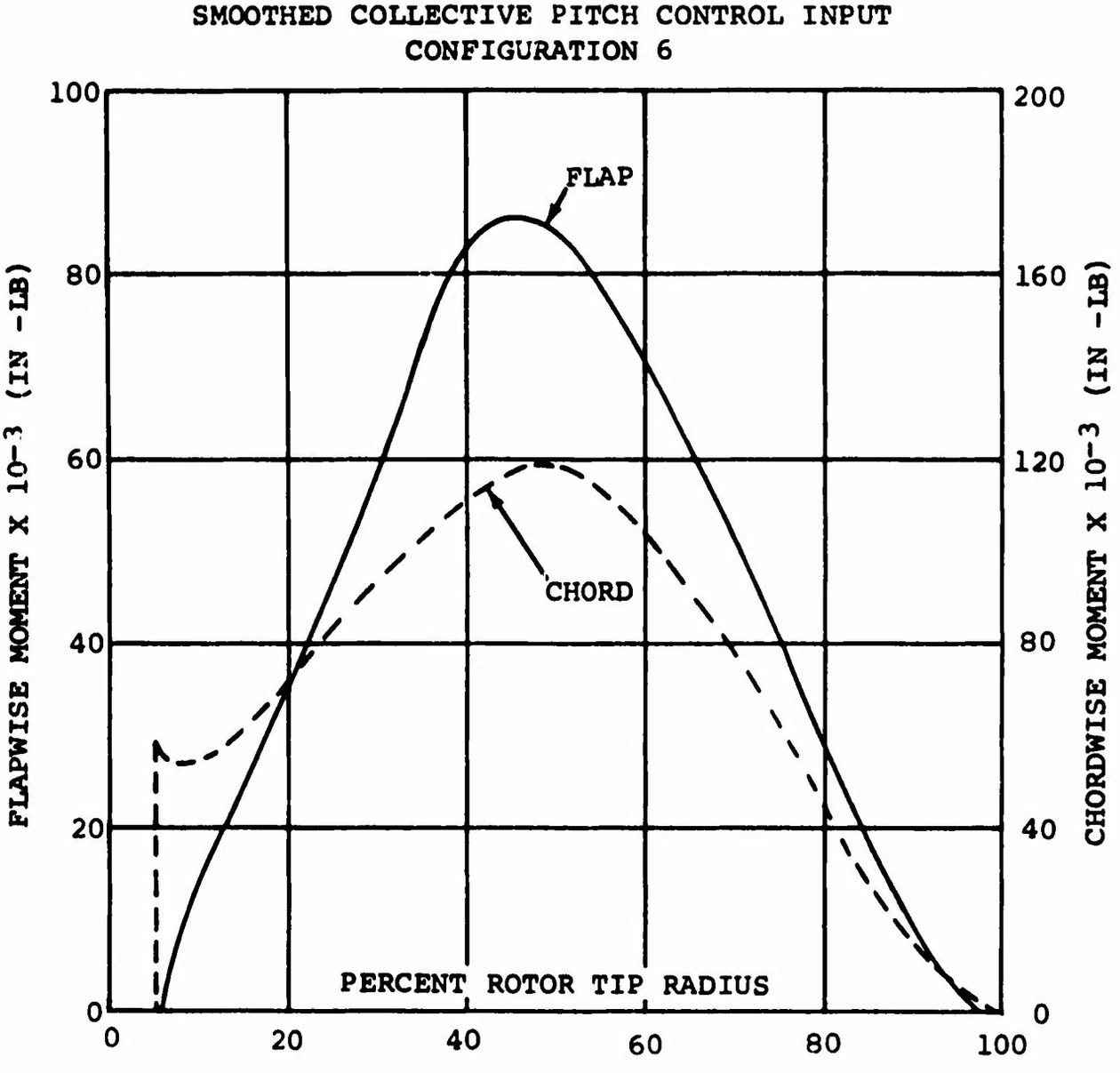

Figure 37. Rotor Blade Chordwise and Flapwise Moments versus Percent Rotor Tip Radius for Smoothed Collective Pitch Control Input.

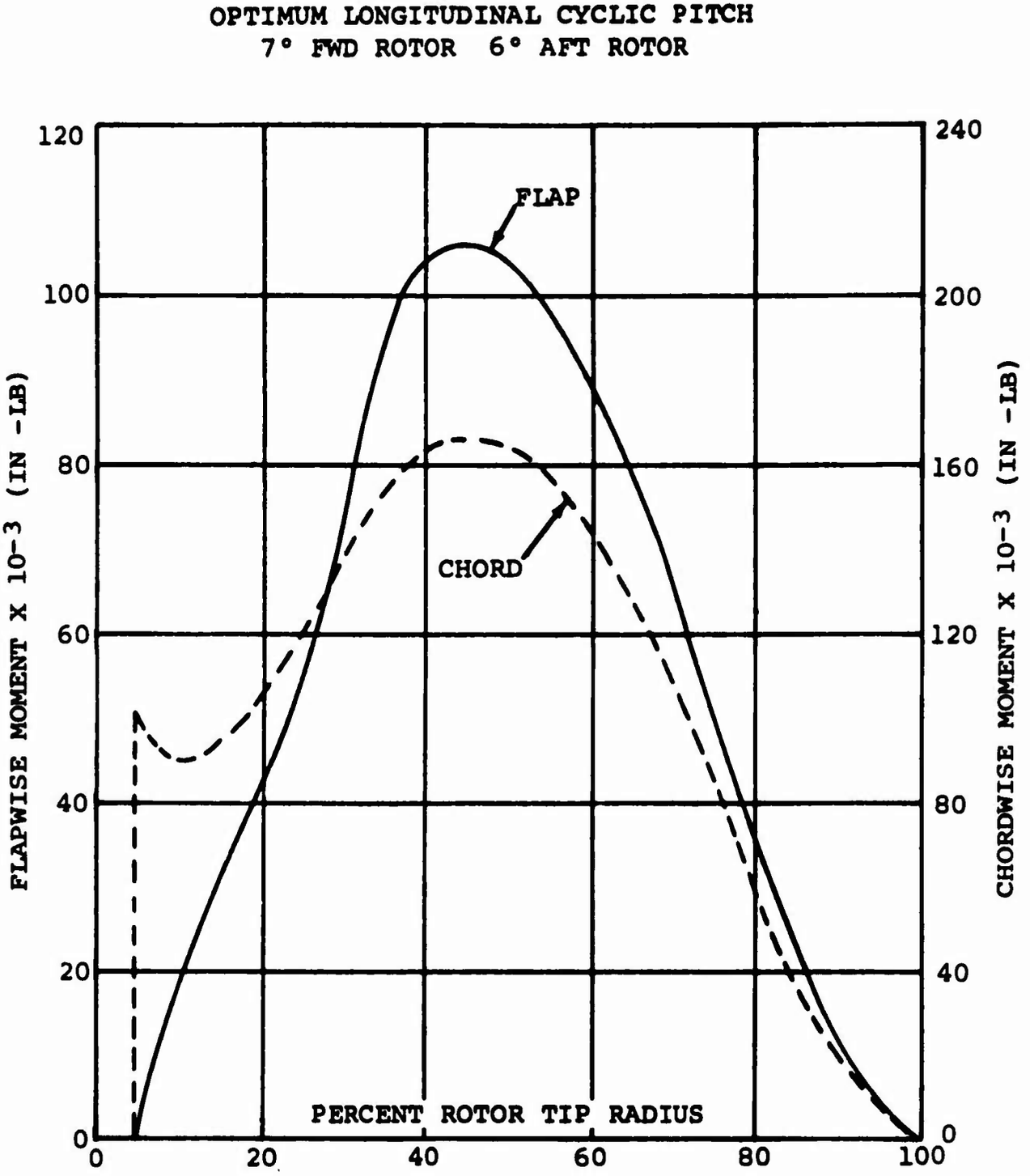

Figure 38. Rotor Blade Chordwise and Flapwise Moments versus Percent Rotor Tip Radius for Optimum Longitudinal Cyclic Pitch.

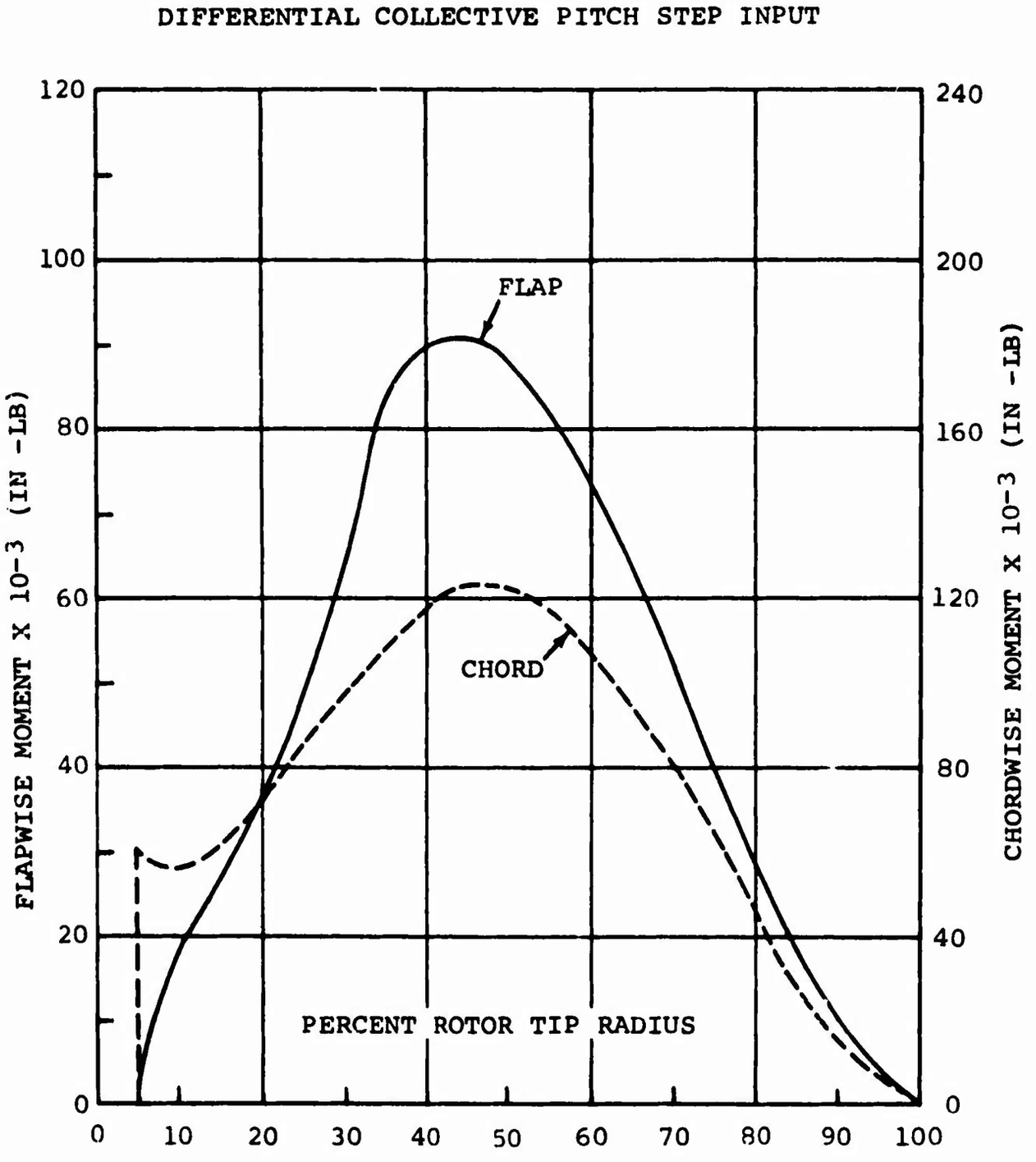

Figure 39. Rotor Blade Chordwise and Flapwise Moments versus Percent Rotor Tip Radius for Differential Collective Pitch Step Input.

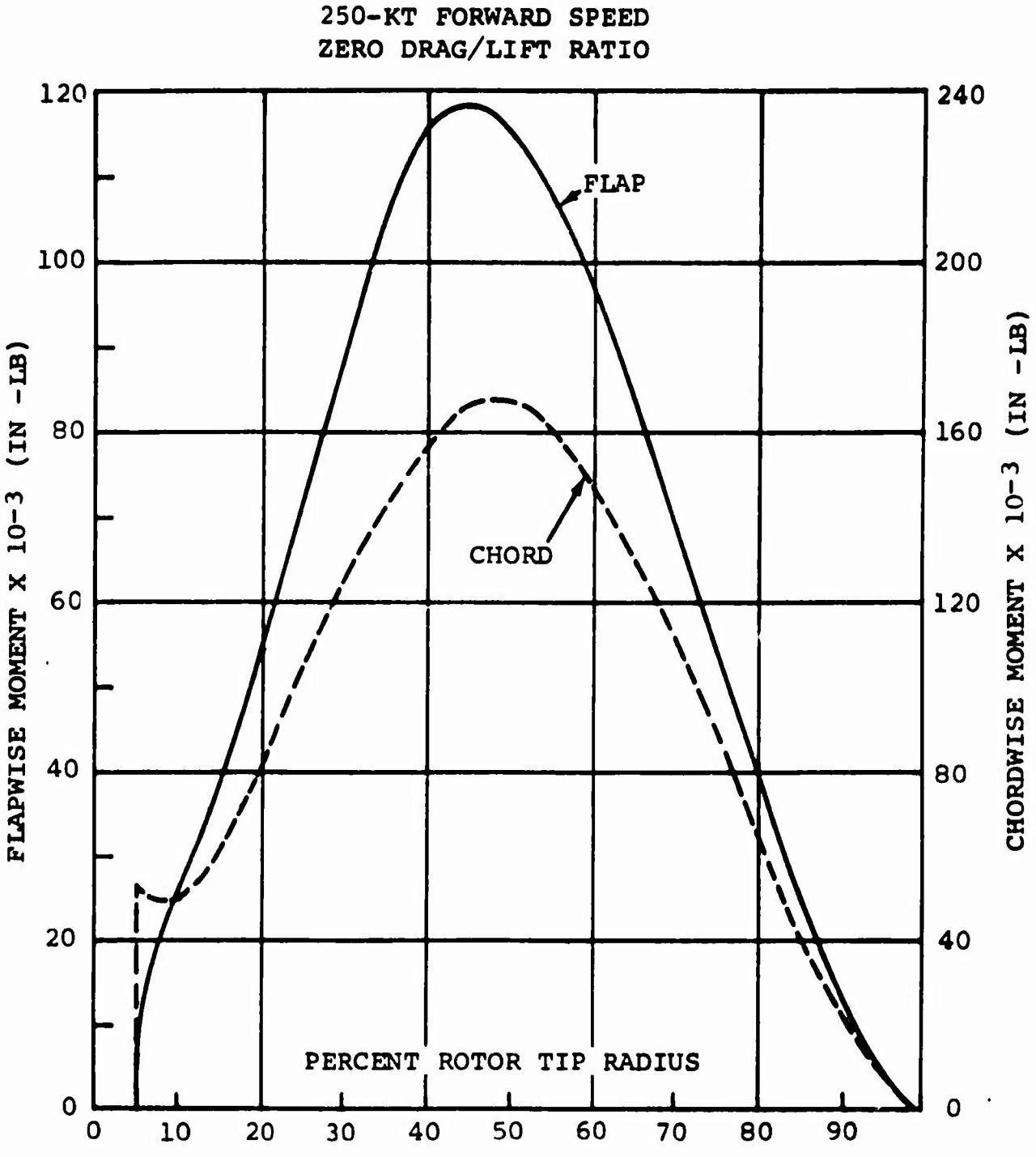

Figure 40. Rotor Blade Chordwise and Flapwise Moments versus Percent Rotor Tip Radius for 250-Knot Forward Speed, Zero Drag/Lift Ratio. Collective Pitch Reduced at 10 Degrees per Second Initially Followed by 2 Degrees per Second.

REFERENCES

1. Military Specification, Helicopter Flying and Ground Handling Qualities, General Requirements For MIL-H-8501A.

2. Model Specification, T55-L-5, Shaft Turbine Engine (Lycoming Model LTC4B-7), Specification No. 124.18-C, 15 October 1960.

3. Leone, P.F., Theory of Rotor Blade Uncoupled Flap Bending Aeroelastic Vibrations, Proceedings of the 10th Annual Forum of The American Helicopter Society, May 1954.

4. Leone, P.F., Theory of Rotor Blade Uncoupled Lag Bending Aeroelastic Vibrations, Proceedings of the 11th Annual Forum of The American Helicopter Society, April 1955.

5. Etkin, Bernard, Dynamics of Flight, John Wiley and Sons, 1959.

6. Gessow, Alfred, Equations and Procedures for Numerically Calculating the Aerodynamic Characteristics of Lifting Rotors, NACA TN3747, 1956.

7. Jewel, Joseph W.; Heyson, Harry H., Charts of the Induced Velocities Near a Lifting Rotor, NASA Memo 4-15-59L, 1959.

APPENDIX I - TRANSIENT ANALYSIS

INTRODUCTION

The transient response of the helicopter fuselage and rotary wing to arbitrary forcing functions is obtained through a digital solution of the helicopter equations of motion. The method presented in this appendix has been programmed for use on the IBM 7040/44 computer. It consists of a numerical simultaneous solution of the complete six-degree-of-freedom rigid-airframe equations of motion and the three-degree-of-freedom rotor equations of motion (flap, lag, and rotational speed). The forcing functions considered in the present study include:

1. Control inputs
2. Rotor-delivered power

The airframe equations are developed by resolving the various helicopter component forces and moments along and about a fixed-body axis system and equating these to their inertia counterparts. The force and moment components contain both rotor and fuselage terms.

The nonlinear fuselage aerodynamic characteristics (lift, drag, and side forces, roll, pitch, and yaw moments) are programmed as functions of angle of attack and sideslip in table look-up form.

The rotor equations of motion are developed by equating the net force moments about the flap and lag hinge to zero. A rotor speed equation has been incorporated, based on rotor unbalanced torque. In order to account for the effects of stall, compressibility, and reverse flow, a numerical blade element approach is used to compute the rotor blade aerodynamic parameters. The two-dimensional airfoil characteristics are programmed as functions of angle of attack and Mach number. The major assumptions

included in the rotor analysis are:

1. Lag motion is not coupled into flap motion, but flap motion is coupled into lag.
2. Induced velocity is uniform.
3. The rotor blades are rigid.
4. The rotor aerodynamic forces and moments do not include lag motion.
5. Nonsteady aerodynamic and spanwise flow effects are ignored.
6. Gravity effects are neglected in lag motions.

Equations to investigate either a three-bladed articulated, or a two-bladed teetering rotor system have been included.

Two additional items have been included in the simulation for purposes of helicopter and rotor stabilization:

1. A limited-authority stability augmentation system.
2. Rotor tip path plane control device.

The initial steady-state or time-zero conditions of the helicopter (control positions, attitudes, power required, etc.) are first determined through an iterative solution of the equations of motion with the inertia terms set to zero.

Upon completion of trim, the transient response of the helicopter (airframe and rotors) to specified time variations in the desired forcing functions is computed by a numerical integration of the complete set of equations. The output includes time variations of the following parameters:

1. Airframe angular and linear accelerations, rates, and displacements
2. Stability augmentation system inputs
3. Rotor blade flap and lead-lag motion (all blades)
4. Rotor speed variation
5. Altitude
6. Fuselage angle of attack and sideslip
7. Aircraft pitch, roll, and yaw attitude

LIST OF SYMBOLS USED IN APPENDIX I

Symbol	Definition	Units
$A = I_{xx}$	Moment of inertia about X axis	slug-ft^2
A_p, A_q, A_r	Shaping function coefficients	
A_R	Coefficient in blade gravity moment (cos i cos θ cos ϕ + sin i sin θ)	
A_{1C}	Lateral cyclic pitch angle	rad
$B = I_{yy}$	Moment of inertia about Y axis	slug-ft^2
$B_p, B_q, B_r, B_{pr}, B_\beta$	Shaping function coefficients	
B_R	Coefficient in blade gravity moment (sin i cos ϕ cos θ - cos i sin θ)	
$C = I_{zz}$	Moment of inertia about the Z axis	slug-ft^2
C_p, C_q, C_r	Shaping function coefficients	
C_o	Lag damper preload	ft-lb
C_1	Lag damper viscous damping	ft-lb/rad/sec
C_H	Rotor H force coefficient ($H \div \rho\pi R^2(\Omega R)^2$)	
C_p	Rotor power coefficient ($RHP \times 550 \div \rho\pi R^2(\Omega R)^3$)	
C_R	Coefficient in blade gravity moment (in ϕ cos θ)	
C_T	Rotor thrust coefficient ($T \div \rho\pi R^2(\Omega R)^2$)	
C_Y	Rotor Y force coefficient ($Y \div \rho\pi R^2(\Omega R)^2$)	
$D = I_{YZ}$	Product of inertia in Y-Z plane	slug-ft^2

$E = I_{XZ}$	Product of inertia in X-Z plane	slug-ft^2
$F = I_{XY}$	Product of inertia in X-Y plane	slug-ft^2
$\vec{F}$	Total force vector	lb
$F_{X_R}, F_{Y_R}, F_{Z_R}$	Scalar components of $\vec{F}$ due to rotors	lb
$F_{X_f}, F_{Y_f}, F_{Z_f}$	Scalar components of $\vec{F}$ due to fuselage	lb
$\vec{G}$	Total moment vector	ft-lb
G_p, G_q, G_r, G_{pr}	Stability augmentation system gains	in/rad/sec
G_β	Stability augmentation system gain	in/rad
H	Rotor drag force	lb
I_β	Mass moment of inertia about flap hinge	slug-ft^2
I_ρ	Mass moment of inertia about lag hinge	slug-ft^2
I_{TOT}	Total polar inertia of rotating system	slug-ft^2
K_p, K_q, K_r	Stability augmentation system authorities	inches
$\mathcal{L}_f$	Fuselage aerodynamic rolling moment about X axis (Scalar component of $\vec{G}$)	ft-lb
$\mathcal{L}_H$	Rotor hub rolling moment	ft-lb
$\mathcal{L}_R$	Scalar component of $\vec{G}$ due to rotors	ft-lb
M	Mach number	
M_f	Fuselage aerodynamic pitching moment about Y axis (Scalar component of $\vec{G}$ due to fuselage)	
M_H	Rotor hub pitching moment	ft-lb
M_R	Scalar component of $\vec{G}$ due to rotors about helicopter Y axis.	ft-lb

M_β	Mass moment of inertia of rotor blade about flap hinge	slug-ft
M_ρ	Mass moment of inertia of rotor blade about the lag hinge	slug-ft
N_f	Fuselage aerodynamic yawing moment about Z axis (Scalar component of $\vec{G}$ due to fuselage)	ft-lb
N_R	Scalar component of $\vec{G}$ due to rotors about helicopter Z axis	ft-lb
Q	Rotor torque	ft-lb
Q_A	Rotor torque available	ft-lb
Q_R	Rotor torque required at operating RPM	ft-lb
R	Rotor blade radius measured from center of rotation	ft
RHP	Rotor horsepower	HP
SHP_{TOT}	Total required shaft horsepower	HP
T	Rotor aerodynamic thrust force	lb
T_H	Vertical shear force at hub	lb
T_{DSD}	Thrust force to be matched in rotor routine	lb
V	Free stream velocity vector in XYZ	ft/sec
W	Gross weight of helicopter	lb
XYZ	Coordinate system fixed to body	
$X_1Y_1Z_1$	Inertial fixed coordinate system	
$X_{TPC}, Y_{TPC}, Z_{TPC}$	Rotating axis system used in tip path plane analysis	
Y	Rotor aerodynamic side force	lb
Y_{DSD}	Y force to be matched in rotor routine	lb
a_p, a_q, a_r	Shaping function coefficients	
b	Number of blades	

b_p, b_q, b_r	Shaping function coefficients	
c	Rotor blade chord projected to center of rotation	ft
c_l, c_d	Airfoil section lift and drag coefficients	
c_p, c_q, c_r	Shaping function coefficients	
c_1, c_2, c_3	Pitch-flap coupling terms	
e_β	Flap hinge offset	ft
e_ρ	Lag hinge offset	ft
g	Acceleration due to gravity (32.174)	ft/sec^2
h	Distance from the helicopter center of gravity to the projection of the rotor hub on the Z axis	ft ft
$\vec{h}$	Angular momentum vector of helicopter	$sl\text{-}ft^2/sec$
i	Angle of incidence of the rotor shaft in the helicopter X-Z plane	deg
k_1, k_2, k_3	Pitch-flap feedback kinematics	
ℓ	Distance from the helicopter center of gravity to the projection of the rotor hub on the X axis	ft
m	Helicopter mass	slugs
m_β, m_ρ	Blade mass outboard of the flap or lag hinge	slugs
n	Cycle number in numerical iteration	
n_x	Number of radial stations at which the rotor calculations are performed (9)	
n_ψ	Number of azimuth stations at which the rotor calculations are performed (20)	
p	Scalar component of $\vec{\omega}$ about helicopter X axis (helicopter roll rate)	rad/sec

p_r	Scalar component of $\vec{\omega}$ about rotor X axis	rad/sec
q	Scalar component of $\vec{\omega}$ about helicopter Y axis (helicopter pitch rate)	rad/sec
q_r	Scalar component of $\vec{\omega}$ about rotor Y axis	rad/sec
r	Scalar component of $\vec{\omega}$ about helicopter Z axis (helicopter yaw rate)	rad/sec
r_r	Scalar component of $\vec{\omega}$ about rotor Z axis	rad/sec
s	Laplace operator	
u	Nondimensional resultant velocity perpendicular to blade span axis at blade element	
u	Scalar component of $\vec{v}_c$	ft/sec
u_p	Nondimensional blade element velocity component perpendicular to blade span axis and u_T	
u_T	Nondimensional blade element velocity component perpendicular to blade span axis and to rotor shaft axis	
v	Scalar component of $\vec{v}_c$	ft/sec
$\vec{v}_c$	Velocity vector of center of gravity	ft/sec
v_i	Induced velocity of rotor at rotor disc plane	ft/sec
w	Scalar component of $\vec{v}_c$	ft/sec
x	Ratio of the blade element radius to rotor blade radius	
x_B	Radial station for tip loss	
x_c	Radial station for blade cutout	
Δe	$e_p - e_\beta$	ft
Ω	Rotor rotational speed	rad/sec

α_f	Local fuselage angle of attack	deg
β	Total blade flap angle with respect to the rotor shaft normal plane at a particular azimuth position	rad
β_f	Fuselage angle of sideslip	deg
β_o	Pre-cone angle of teetering rotor	rad
β_o	Mean cone angle for tip path plane control analysis	deg
β_x, β_y	Tip path plane tilt about X_{TPC} and Y_{TPC} axes	deg
γ_s	Rotor wake angle = $\tan^{-1}\left(\frac{\mu}{-\lambda}\right)$	deg
δ_B	Longitudinal cockpit control deflection	in
δ_{BS}	Equivalent longitudinal input from SAS	in
δ_C	Collective control input	in
δ_L	Lateral cockpit control deflection	in
δ_{LS}	Equivalent lateral input from SAS	in
δ_R	Directional cockpit control deflection	in
δ_{RS}	Equivalent directional input from yaw rate feedback	in
δ_{RP}	Equivalent directional input from roll rate feedback	in
$\delta_{R\beta}$	Equivalent directional input from sideslip feedback	in
δ_{RSt}	Equivalent total directional input from SAS	in
η	Transmission efficiency of rotor drive system	
θ	Euler angle (pitch)	deg

$\theta_{.75}$	Collective pitch at 3/4 radius	rad
λ	Rotor inflow ratio with respect to rotor disc plane	
μ	Rotor advance ratio with respect to rotor disc plane	
ξ_β	Radius ratio of flap hinge offset	
ξ_ρ	Radius ratio of lag hinge offset	
ρ	Lag angle	rad
ρ	Air density	$slug/ft^3$
σ_X	Local solidity at blade station X	
ϕ	Euler angle (roll)	deg
ϕ	Inflow angle	deg
ψ	Euler angle (yaw)	deg
$\vec{\omega}$	Helicopter angular rate vector	rad/sec

Subscripts

F	**Front rotor**
R	**Rear rotor**
f	**Fuselage**

HELICOPTER RIGID-BODY EQUATIONS OF MOTION

The equations of motion of the helicopter rigid body are presented with respect to a body-fixed axis system (X, Y, Z) whose origin is located at the center of gravity:

X points forward and is aligned to the waterline reference;
Y points right and is aligned to the buttline reference; and
Z points down and is aligned to the station line reference.

From Reference 5, the equations are:

$$\vec{F} = m\left(\frac{\vec{\delta} v_c}{\delta t} + \vec{\omega} \times \vec{v}_c\right)$$

$$\vec{G} = \frac{\delta \vec{h}}{\delta t} + \vec{\omega} \times \vec{h} \qquad (4)$$

or

$$F_{X_R} + F_{X_f} - W \sin\theta = m(\dot{u} + qw - rv)$$

$$F_{Y_R} + F_{Y_f} + W \cos\theta \sin\phi = m(\dot{v} + ru - pw)$$

$$F_{Z_R} + F_{Z_f} + W \cos\theta \cos\phi = m(\dot{w} + pv - qu)$$

$$\mathcal{L}_R + \mathcal{L}_f = A\dot{p} - F\dot{q} - E\dot{r} - Epq + D(r^2 - q^2) + (C - B)qr + Fpr$$

$$M_R + M_f = -F\dot{p} + B\dot{q} - D\dot{r} + (A - C)rp + E(p^2 - r^2) - Fqr + Dqp$$

$$N_R + N_f = -E\dot{p} - D\dot{q} + C\dot{r} + F(q^2 - p^2) + (B - A)pq - Dpr + Eqr \qquad (5)$$

The orientation and position of the helicopter are given with respect to a fixed inertial frame of reference X_1, Y_1, Z_1 by standard Euler angles ψ, θ, ϕ, and displacements X_1, Y_1 and Z_1. The time derivatives of the displacements and attitudes are related to the body-fixed linear and angular velocities by:

$$\begin{vmatrix} \dot{X}_1 \\ \dot{Y}_1 \\ \dot{Z}_1 \end{vmatrix} = \begin{vmatrix} \cos\theta\cos\psi & \cos\psi\sin\theta\sin\phi - \sin\psi\cos\phi & \cos\psi\sin\theta\cos\phi + \sin\psi\sin\phi \\ \sin\psi\cos\theta & \sin\psi\sin\theta\sin\phi + \cos\psi\cos\phi & \sin\psi\sin\theta\cos\phi - \cos\psi\sin\phi \\ -\sin\theta & \cos\theta\sin\phi & \cos\theta\cos\phi \end{vmatrix} \begin{vmatrix} u \\ v \\ w \end{vmatrix} \tag{6}$$

and

$$\dot{\psi} = \frac{r\cos\phi + q\sin\phi}{\cos\theta}$$

$$\dot{\theta} = q\cos\phi - r\sin\phi$$

$$\dot{\phi} = p + q\tan\theta\sin\phi + r\tan\theta\cos\phi \tag{7}$$

ARTICULATED ROTOR SYSTEM EQUATIONS

Rotor Blade Flap and Lag Equations of Motion

The equations describing blade flap and lag motion of an articulated rotor with respect to the rotor disc plane are presented in this section. The solution of this motion is a prerequisite to obtaining the rotor force and moment contributions to the helicopter rigid-body equations. The major assumptions included in the rotor analysis are listed in the introduction.

The flap and lag moments from isolated rotor considerations along with the Coriolis effects due to helicopter angular rates are included in the blade motion equations. Aerodynamic moments have been developed in a similar manner as in Reference 6. In addition, a preloaded lag damper is included. The complete equations used in the simulation follow.

Lead-Lag:

$$I_\rho \ddot{\rho} + M_\rho \Omega^2 \sin\rho\cos\beta(\Delta e\cos\beta + e_\beta) + 2\dot{\beta}\Omega\sin\beta(I_\rho + M_\rho \Delta_e \cos\rho) - \dot{\Omega}[I_\rho\cos\beta + M_\rho\cos\rho(\Delta e\cos\beta + e_\beta)] + \left(\frac{C_o}{|\dot{\rho}|} + C_1\right)\dot{\rho} - 2(I_\rho + \Delta e M_\rho)\dot{\beta}[p_r\cos\beta\cos\psi - q_r\cos\beta\sin\psi + r_r\sin\beta]$$

$$= \frac{\rho\pi R^3(\Omega R)^2}{2b}\left[\int_{x_c}^{1.0}\sigma_x u(x-\xi_\rho)(c_d u_T - c_\ell u_p)dx + \int_B^1 \sigma_x u(x-\xi_\rho)\, c_\ell u_p dx\right] \quad (8)$$

Flap:

$$I_\beta \ddot{\beta} + \Omega^2 \sin\beta[I_\beta \cos\beta + M_\beta e_\beta] +$$

$$gM_\beta[A_R \cos\beta - (B_R \cos\psi + C_R \sin\psi)\sin\beta] -$$

$$2(I_\beta \cos\beta + e_\beta M_\beta)[p_r\Omega \cos\beta \cos\psi -$$

$$q_r\Omega \cos\beta \sin\psi + r_r\Omega \sin\beta]$$

$$= \frac{\rho\pi R^3(\Omega R)^2}{2b}\left[\int_{x_C}^{1.0} \sigma_x u(x - \xi_\rho)(c_\ell u_T + c_d u_p)dx - \right.$$

$$\left. \int_B^{1.0} \sigma_x u(x - \xi_\beta) c_\ell u_T dx \right] \qquad (9)$$

The blade element velocity components include the effect of the helicopter angular motion.

The solution of the above equations is discussed in Steady-State Equations, page 115.

Rotor Speed

The time rate of change of angular velocity is obtained by equating the net torque unbalance to its inertia counterpart.

$$\dot{\Omega} = \frac{Q_A - Q_R}{I_{TOT}} \qquad (10)$$

The rotors are constrained to operate at the same rotational speed; hence, Q_A, Q_R, and I_{TOT} represent total system values.

Rotor Force and Moment Equations

Lag motion has not been included in the rotor force and moment calculations. The rotor force contributions are obtained by computing three mutually perpendicular components of the rotor resultant force:

1. Thrust force
2. Drag force
3. Side force

The force components due to a single blade at azimuth ψ are presented below in coefficient form:

$$C_{T_\psi} = \frac{1}{2b}\int_{x_c}^{1.0}\sigma_x u(c_\ell u_T + c_d u_p)\cos\beta_\psi dx - \frac{1}{2b}\int_{B}^{1.0}\sigma_x u(c_\ell u_T)\cos\beta_\psi dx \tag{11}$$

$$C_{H_\psi} = \frac{1}{2b}\left\{\int_{x_c}^{1.0}\sigma_x u[c_d(u_T\sin\psi - u_p\cos\psi\sin\beta - c_\ell(u_p\sin\psi + u_T\sin\beta\cos\psi]dx + \int_{B}^{1.0}\sigma_x u c_\ell(u_p\sin\psi + u_T\cos\psi\sin\beta)dx\right\} \tag{12}$$

$$C_Y = \frac{1}{2b}\left\{\int_{x_c}^{1.0} \sigma_x u[c_\ell(u_p \cos\psi - u_T \sin\beta \sin\psi) - c_d(u_T \cos\psi + u_p \sin\beta \sin\psi)]dx - \int_B^{1.0} \sigma_x u c_\ell (u_p \cos\psi - u_T \sin\beta \sin\psi)dx\right\} \quad (13)$$

The vertical force acting at the flapping hinge, T_H, is not, in general, equal to the aerodynamic component, T, due to flapping effects.

$$T_{H_\psi} = T_\psi - M_\beta \ddot{\beta} \cos\beta \quad (14)$$

The rotor moment computations result in components directed about the three axes; they are:

1. Torque
2. Rolling moment
3. Pitching hub moment

The rotor power is obtained directly from the torque computation.

The expressions for the rotor torque coefficient and the hub moments due to a single blade at azimuth ψ are:

$$C_{Q_\psi} = C_{P_\psi} = \frac{1}{2b}\left\{\int_{x_c}^{1.0} \sigma_x ux \, ccs\, \beta(c_d u_T - c_\ell u_p)dx + \int_B^{1.0} \sigma_x uxc_\ell u_p \cos\beta dx\right\} \quad (15)$$

$$\mathcal{L}_{H_\psi} = -T_{H_\psi} e_\beta \sin \psi$$

$$M_{H_\psi} = -T_{H_\psi} e_\beta \cos \psi \qquad (16)$$

The net forces and moments at the rotor are obtained by summing the contributions of each blade. For steady state computations, the mean values of the forces and moments are required. These are obtained by averaging the parameters over the rotor cycle.

Numerical Evaluation of Integrals

The expressions for the quantities C_{T_ψ}, C_{H_ψ}, C_{Y_ψ}, C_{P_ψ} and the aerodynamic moments involve radial integrations of functions containing σ, U, c_ℓ, c_d, U_p, U_T. In order to retain the effects of stall, compressibility and reverse flow, it is necessary to numerically evaluate these integrals. This consists of computing individual force and moment contributions of a specific number of blade sections, and radially integrating these values, using Simpson's Rule and the Trapezoidal Rule. For this analysis, the computations are performed at 9 points, equally spaced from the cutout to the tip, and at the tip loss factor location (X = 0.97). The approach is similar to that presented in Reference 6.

If mean values are required, the radially integrated values obtained at specific azimuth locations around the disc are averaged. Twenty equally spaced azimuth locations ($\Delta\psi$ = 18°) are used in this analysis.

TEETERING (SEESAW) ROTOR EQUATIONS

Blade Flap Equations of Motion

The equations describing the blade flap motion of the teetering system are developed in the same manner as those for the articulated system. A rigid two-bladed rotor, free to flap about a hinge at the hub, is considered. The boundary condition is that the sum of the moments from each blade about the seesaw hinge is zero.

The complete flap equation is as follows:

$$2I_\beta\ddot{\beta} + I_\beta\Omega^2 \cos 2\beta_0 \sin 2\beta - 2gM_\beta \sin \beta_0 [A_R \sin \beta + \cos \beta (B_R \cos \psi - C_R \sin \psi) -$$

$$2I_\beta\Omega\Big| + p_r \cos \psi[\cos^2(\beta_0 + \beta) + \cos^2 (\beta_0 - \beta)] -$$

$$q_r \sin \psi[\cos^2 (\beta_0 + \beta) + \cos^2 (\beta_0 - \beta)] + r_r \cos 2\beta_0 \sin 2\beta\Big|$$

$$= \frac{\rho\pi R^3(\Omega R)^2}{2b}\left[\left(\int \sigma_x u x (c_\ell u_T + c_d u_p)dx\right)_\psi - \left(\int \sigma_x u x (c_\ell u_T + c_d u_p)dx\right)_{\psi+\pi}\right] \quad (17)$$

Rotor Force and Moment Equations

The individual blade force and moment contributions are obtained in the same manner as those of the articulated system. Since the seesaw hinge is at the center of rotation, no hub moments are present; also, the vertical shear force is equal to the thrust force. The net rotor contributions are obtained by summing the effects of each blade.

TIP PATH PLANE CONTROLLER (ARTICULATED ROTOR)

The tip path plane controller is a device which provides a means of incorporating various types of pitch-flap feedback. The three basic types considered in this analysis are:

1. Pitch-cone feedback (C_1) -- blade pitch changes proportional to coning angle.

2. Pitch-flap out-of-phase feedback (C_2) -- blade pitch changes proportional to tip path plane tilt about an axis in the rotor disc plane perpendicular to blade flapping axis.

3. Pitch flap in-phase feedback (C_3) -- blade pitch changes proportional to tip path plane tilt about an axis in the rotor disc parallel to the blade flapping axis.

The kinematic ratios (k_1, k_2, k_3) used in the aerodynamic analysis are derived below.

Consider a rotating axis system in the rotor disc plane with X_{TPC} under blade 1. Defining β_0 as the coning angle, β_x as the tilt about the X_{TPC} axis of the tip path relative to the rotor disc plane, and β_y analogously, the equations relating these to the flapping angles of blades β_1 β_2, and β_3 are, from Figure 41:

$$\begin{aligned} \beta_1 &= \beta_0 + \beta_y \\ \beta_2 &= \beta_0 - \beta_y \sin 30° - \beta_x \cos 30° \\ \beta_3 &= \beta_0 - \beta_y \sin 30° + \beta_x \cos 30° \end{aligned} \qquad (18)$$

Substituting for sin 30° and cos 30°, and solving for β_0, β_x, β_y

$$\begin{aligned} \beta_0 &= \frac{\beta_1 + \beta_2 + \beta_3}{3} \\ \beta_x &= \frac{\beta_3 - \beta_2}{\sqrt{3}} \\ \beta_y &= \frac{2\beta_1 - \beta_2 - \beta_3}{3} \end{aligned} \qquad (19)$$

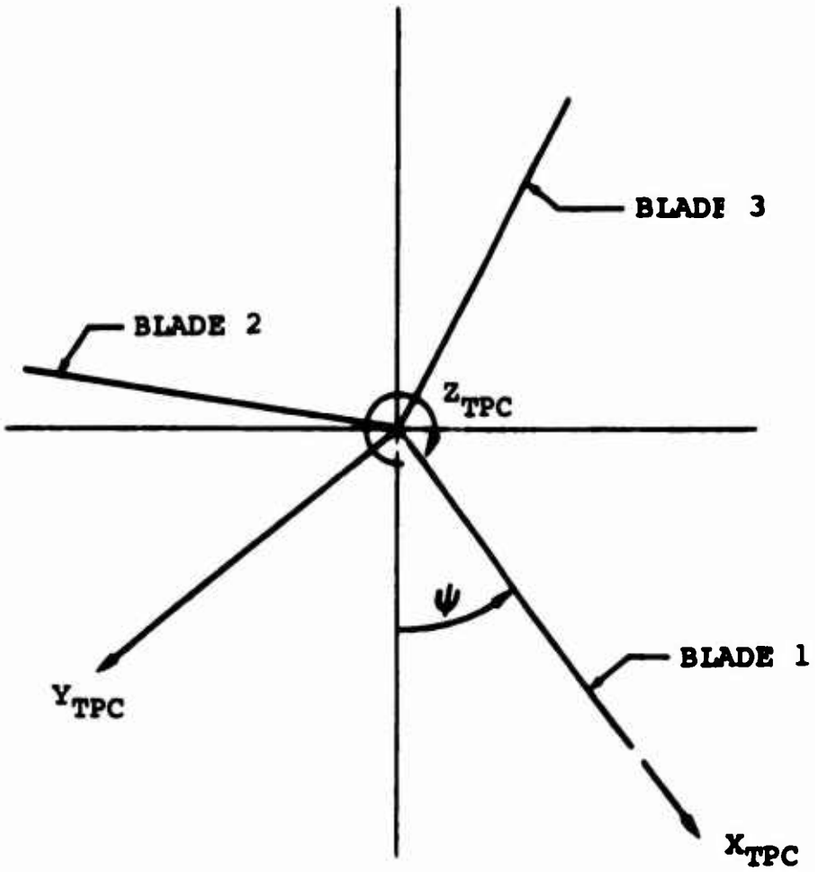

Figure 41. Tip Path Plane Controller Axis System.

Defining C_1, C_2, C_3 as the kinematic ratios between blade pitch change and blade flap for pitch-cone, pitch-flap out-of-phase and pitch-flap in-phase feedback respectively, the relationships between pitch and flap for the coupling mechanism at each blade are:

$$\theta_{C_1} = C_1\beta_0 + C_2\beta_x + C_3\beta_y$$

$$\theta_{C_2} = C_1\beta_0 + C_2(\beta_y \cos 30° - \beta_x \sin 30°) + C_3(-\beta_y \sin 30° - \beta_x \cos 30°)$$

$$\theta_{C_3} = C_1\beta_0 + C_2(-\beta_y \cos 30° - \beta_x \sin 30°) + C_3(-\beta_y \sin 30° + \beta_x \cos 30°) \quad (20)$$

Substituting Equation 19 into 20 and rearranging:

$$\theta_{C_1} = k_1\beta_1 + k_2\beta_2 + k_3\beta_3$$

$$\theta_{C_2} = k_3\beta_1 + k_1\beta_2 + k_2\beta_3$$

$$\theta_{C_3} = k_2\beta_1 + k_3\beta_2 + k_1\beta_3 \quad (21)$$

where

$$k_1 = (C_1 + 2C_3) \div 3$$

$$k_2 = (C_1 - \sqrt{3}C_2 - C_3) \div 3$$

$$k_3 = (C_1 + \sqrt{3}C_2 - C_3) \div 3 \quad (22)$$

The kinematic ratios used in the analysis are equated in Equation 22 to the type of pitch-flap feedback desired. The effect consists of both pitch-cone (C_1) and pitch-flap in-phase (C_3) coupling. It can be seen from Equation 21 that the k_1 kinematic ratio changes only the blade pitch of a given blade in response to its flapping and is, therefore, the kinematic.

STABILITY AUGMENTATION SYSTEM

A limited-authority stability augmentation system (SAS) has been included in the simulation. A block diagram of the system is shown in Figure 42. Its effect is to modify the control inputs at the rotor head, based on the magnitude of the feedback variable and its shaping function. The general characteristics of the system are listed below:

1. Pitch Axis:
   Pitch rate feedback
2. Roll Axis:
   Roll rate feedback
3. Yaw Axis:
   Yaw rate feedback
   Sideslip angle feedback
   Roll rate feedback

INTERFERENCE EFFECTS

Rotor on Rotor

The induced velocity at the rear rotor produced by the front rotor and vice versa are treated in terms of v_i, the self-induced downwash for an isolated rotor.

This interference velocity (as shown in Reference 7) can be considered to be of a function of rotor wake angle (γ_s) and rotor location. For computation purposes, the mean value of interference velocity over the longitudinal axis of the rotor is assumed to act normal to the disc plane. Its effect is to modify the free stream velocity and disc plane angle of attack. The induced velocity charts of Reference 7 were used to evaluate the velocity magnitudes.

Rotor on Fuselage

The induced velocity at the fuselage due to rotor downwash has also been evaluated using Reference 7. For computation, the mean value of rotor downwash over the fuselage is used to alter

the free stream velocity and angle of attack.

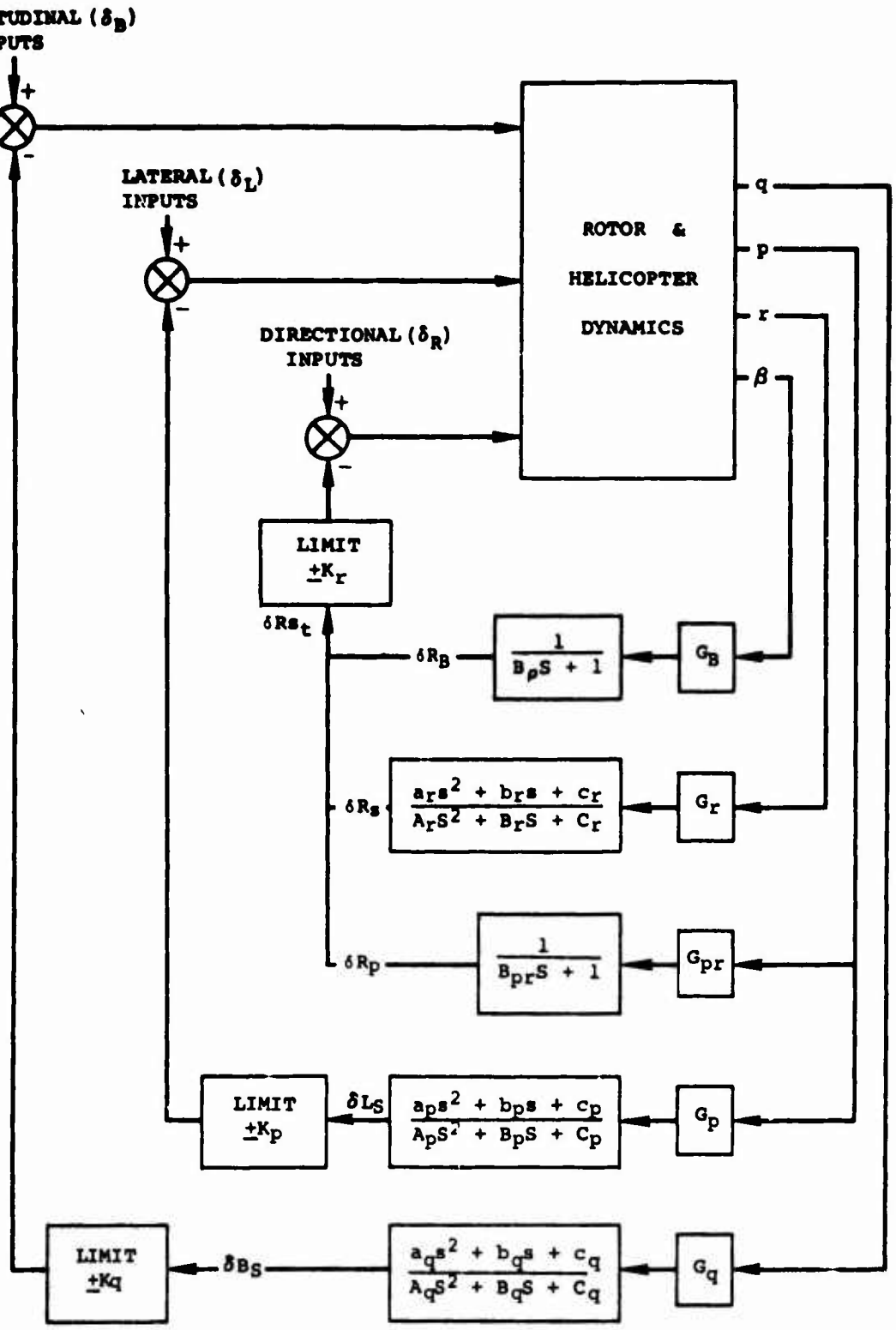

Figure 42. Schematic of Stability Augmentation System.

SOLUTION OF EQUATIONS OF MOTION

Steady-State Equations

Prior to initiating the transient response calculations, the initial steady-state conditions of the helicopter rigid body and rotors are obtained. An iterative solution to trim is required, due to the complexity of the rotor equations.

The longitudinal rigid-body equations written in matrix form are

$$\begin{vmatrix} \sin i_F & \sin i_R & -W \\ -\cos i_F & -\cos i_R & 0 \\ -h_F \sin i_F + \ell_F \cos i_F & -h_R \sin i_R - \ell_R \cos i_R & 0 \end{vmatrix} \begin{vmatrix} T_F \\ T_R \\ \sin \theta \end{vmatrix} = \begin{vmatrix} \bar{X} \\ \bar{Z} \\ \bar{M} \end{vmatrix}$$

where

$$\bar{X} = H_F \cos i_F + H_R \cos i_R - F_{X_f}$$

$$\bar{Z} = H_F \sin i_F + H_R \sin i_R - F_{Z_f} - W \cos \theta \cos \phi$$

$$\bar{M} = H_F(-h_F \cos i_F - \ell_F \sin i_F) + H_R(-h_R \cos i_R + \ell_R \sin i_R) - M_{H_F} - M_{H_R} - M_f \qquad (23)$$

The rotor components of Equation 5 have been expanded using Figure 43. These equations are solved for the rotor thrusts and pitch attitude, assuming the fuselage and rotor

forces and moments in the constant column are those from the previous iteration.

Similarly, the lateral-directional set of equations is

$$\begin{vmatrix} h_F & -h_R & 0 \\ 1 & -1 & W \cos\theta \\ \ell_F & \ell_R & 0 \end{vmatrix} \begin{vmatrix} Y_F \\ Y_R \\ \sin\phi \end{vmatrix} = \begin{vmatrix} \bar{L} \\ \bar{Y} \\ \bar{N} \end{vmatrix}$$

where

$$\bar{L} = \mathcal{L}_{H_F} \cos i_F - \mathcal{L}_{H_R} \cos i_R + Q_F \sin i_F - Q_R \sin i_R - \mathcal{L}_f$$

$$\bar{Y} = -F_{Y_f}$$

$$\bar{N} = -\mathcal{L}_{H_F} \sin i_F + \mathcal{L}_{H_R} \sin i_R - Q_F \cos i_F + Q_R \cos i_R - N_f$$

(24)

These are solved for the rotor side forces and helicopter bank angle, assuming the forces and moments in the constant column are those from the previous iteration or the solution of the longitudinal set.

The fuselage terms are contained as functions of α_f and β_f in table look-up form. The independent variables (α_f, β_f) are obtained from a consideration of the free stream and rotor-induced velocity effects.

The required rotor characteristics are obtained through a solution of the equations presented in sections titled ARTICULATED ROTOR SYSTEM EQUATIONS and TEETERING (SEESAW) ROTOR EQUATIONS, pages 104 through 109 . These equations are used to obtain the following parameters consistent with the rotor thrust and side forces required for trim, as determined from the solutions of the helicopter rigid-body equations.

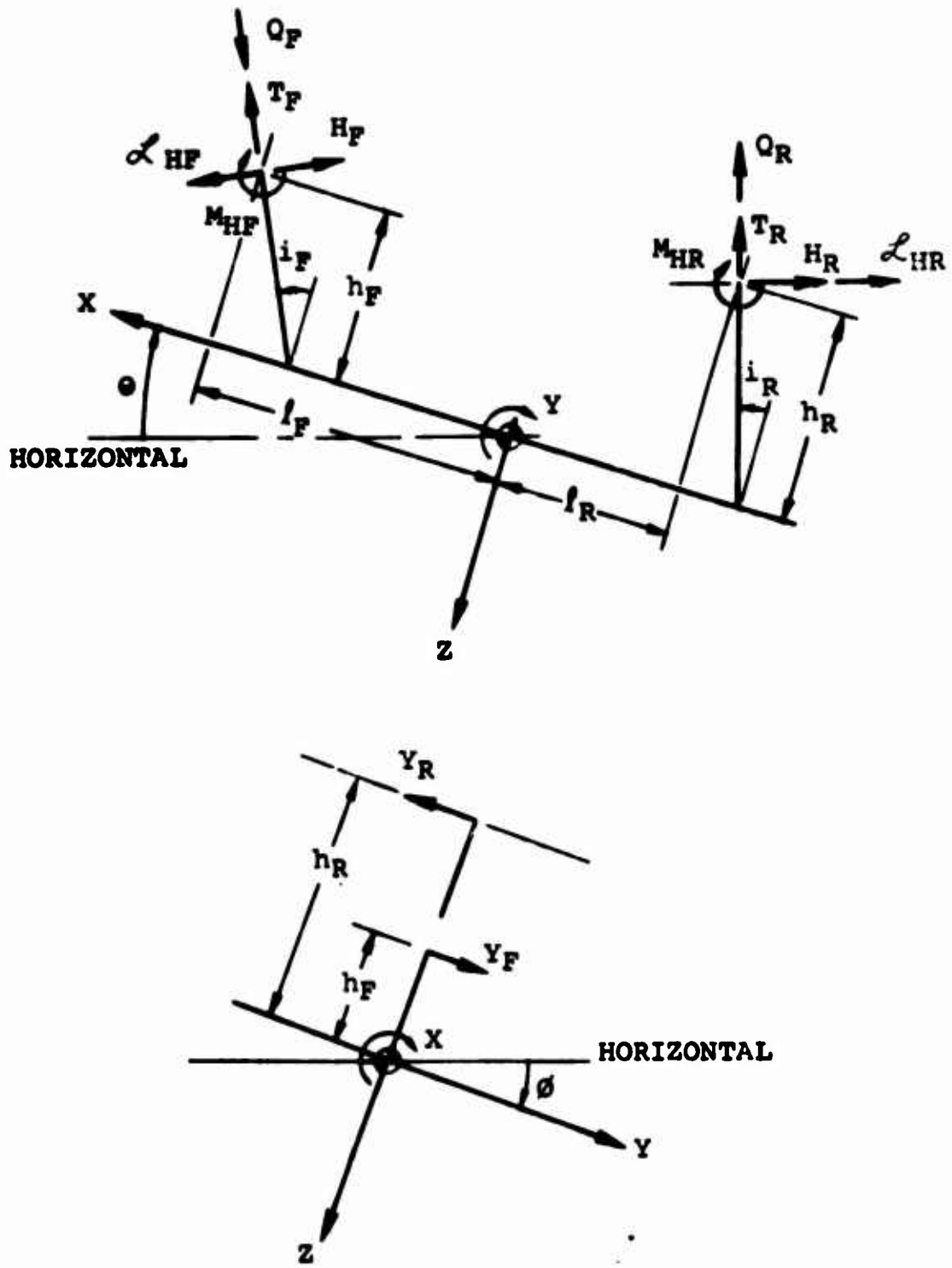

Figure 43. Helicopter Force and Moment Schematic.

1. Blade flapping and lead-lag motion
2. Collective and lateral cyclic pitches
3. H force
4. Hub moments
5. Torque and power required
6. Induced velocities

The same set of equations is used for both the forward and aft rotors with the appropriate input-output relationships.

An iteration procedure on collective pitch and lateral cyclic pitch is required as a result of the conditions set on the magnitude of the thrust and side forces. As mentioned earlier, the solution of the flapping motion is a prerequisite to the force and moment computations.

Solution of Flapping Differential Equation:

The differential equation for flapping has the form

$$\ddot{\beta} = f(\psi, \beta, \dot{\beta}) \qquad (25)$$

where β is a function of azimuth rather than time and f is a complicated function of $\psi, \beta, \dot{\beta}$, the rotor geometry, the section characteristics and the flight conditions. The parameters ψ, β and $\dot{\beta}$ are the only variables. The numerical solution of this equation is obtained through the use of finite difference equations and a step-by-step procedure. The function β which represents a steady-state flapping has the property $\beta(\psi) = \beta(\psi + 2\pi)$.

The finite difference equations are obtained by assuming a first harmonic Fourier series for the known β, $\dot{\beta}$ and $\ddot{\beta}$ at some azimuth station ψ

$$\beta = A_0 - A_1 \cos\psi - B_1 \sin\psi$$

$$\dot{\beta} = A_1 \sin\psi - B_1 \cos\psi = \frac{\dot{\beta}}{\Omega}$$

$$\ddot{\beta} = A_1 \cos\psi + B_1 \sin\psi = \frac{\ddot{\beta}}{\Omega^2} \qquad (26)$$

Using a step-by-step method where $\psi_{n+1} = \psi_n + \Delta\psi$ and substituting in the above equations

$$\beta_{n+1} = A_o - \cos \Delta\psi(A_1 \cos \psi_n + B_1 \sin \psi_n) + \sin \Delta\psi(A_1 \sin \psi_n - B_1 \cos \psi_n)$$

$$\bar{\beta}_{n+1} = \cos \Delta\psi(A_1 \sin \psi_n - B_1 \cos \psi_n) + \sin \Delta\psi(A_1 \cos \psi_n + B_1 \sin \psi_n) \quad (27)$$

Solving now for the three unknowns A_o, $(A_1 \cos \psi_n + B_1 \sin \psi_n)$ and $(A_1 \sin \psi_n - B_1 \cos \psi_n)$

$$\beta_{n+1} = \beta_n + \bar{\beta}_n \sin \Delta\psi + (1 - \cos \Delta\psi)\bar{\bar{\beta}}$$

$$\bar{\beta}_{n+1} = \bar{\beta}_n \cos \Delta\psi + \bar{\bar{\beta}}_n \sin \Delta\psi \quad (28)$$

Starting out with a given β_n and $\bar{\beta}_n$ (assumed or approximated) the next β_{n+1} and $\bar{\beta}_{n+1}$ are calculated by assuming $\bar{\bar{\beta}}_n$ is constant over the interval. Notice that for small $\Delta\psi$ the trigonometric functions can be expanded to give

$$\beta_{n+1} = \beta_n + \Delta\psi\bar{\beta}_n + 1/2(\Delta\psi)^2\bar{\bar{\beta}}_n$$

$$\bar{\beta}_{n+1} = \bar{\beta}_n + \Delta\psi\bar{\bar{\beta}}_n \quad (29)$$

which are the first terms of an ordinary Taylor series. Therefore, for sufficiently small values of $\Delta\psi$ one can get an exact solution for the differential equation. A $\Delta\psi$ increment of 18° ($n_\psi = 20$) is used in this analysis.

The steps involved in the solution of the rotor equations are outlined in detail below. Note the flow chart on Figure 44.

1. The input quantities are computed or set equal to the respective rotor mass or geometric parameters. The required thrust (vertical force) and side force are obtained from the solution of trim equations.

2. The values of μ and λ are computed from the input values of V, α, T_{DSD}, Ω and rotor geometric parameters.

3. Approximate values of the control inputs ($\theta_{.75}$, A_{1C}) required to match the desired force inputs, and the initial flap angle and flap rate are estimated.

4. The initial flap acceleration $\ddot{\beta}_o$ is computed. Subsequent values of β_n, $\dot{\beta}_n$ and $\ddot{\beta}_n$ are obtained. The same procedure is carried out simultaneously on all blades of the articulated rotor for pitch-flap feedback. The numerical scheme is repeated until β_o and β_{360} repeat within prescribed tolerances. Usually, two or three rotor revolutions are required.

5. The mean vertical and side forces, computed by averaging the azimithal variations, are compared with the desired input values. If the desired closure is not attained, steps 4 and 5 are repeated following an adjustment to $\theta_{.75}$ and A_{1C}.

6. The mean values of H force, hub moments, rotor torque and power are then obtained.

These rigid-body and rotor equations are solved by the iterative technique shown on Figures 44 and 45 until the desired closure on subsequent values of T_F, T_R, Y_F, Y_R and ϕ is attained. Upon closure of these parameters, additional trim output is computed as follows.

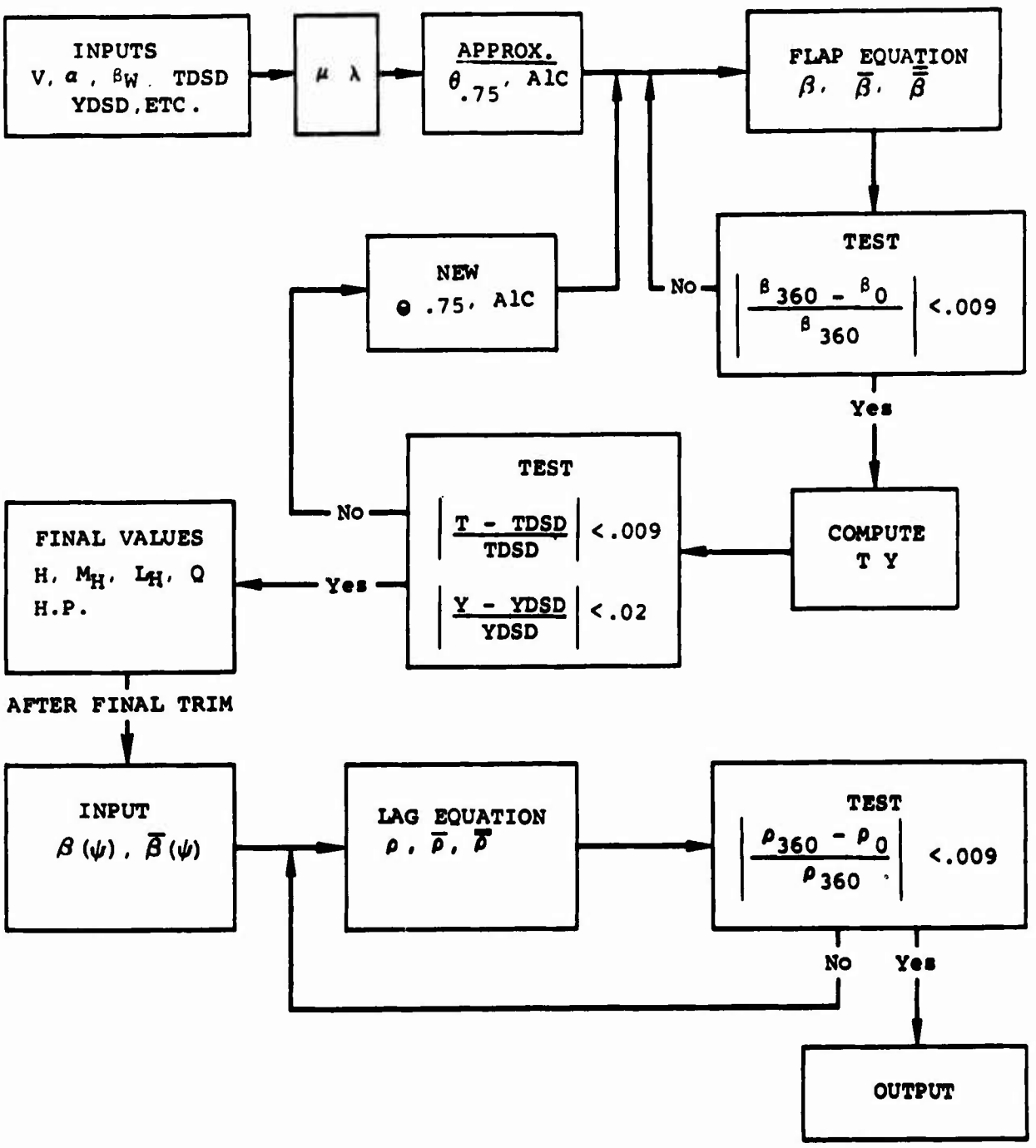

Figure 44. Block Diagram - Rotor Solutions, Trim.

1. Lead-lag motion: The lag equation of motion for the articulated rotor is solved in an identical manner to the flap. The final azimithal variation of β and $\bar{\beta}$ is retained for use in the solution.

2. Control positions: The trim control positions are obtained from previously determined collective and cyclic pitch inputs.

3. Performance data: The total shaft horsepower required is obtained from the final rotor power calculations.

Transient Response Analysis

Solution Scheme: Following determination of the initial steady-state trim conditions, the responses of the helicopter rigid body and rotor blades to arbitrary time variations in control positions and delivered power are computed. The response characteristics are obtained by the simultaneous solutions of the helicopter six-degree-of-freedom equations, the forward and aft rotor flap and lag equations, rotor speed equations, and the stability augmentation system equations.

Since an explicit solution of these equations is impossible, a numerical integration procedure is employed. During any time interval of the solution, the computed values of the highest order derivative of any of the major variables ($\dot{u}$, $\dot{v}$, $\dot{w}$, $\dot{p}$, $\dot{q}$, $\dot{r}$, $\dot{\bar{\beta}}$, $\dot{\bar{\rho}}$ $\dot{\Omega}$) are assumed to be constant. Letting X_n represent a typical variable at time t, the following equations are used for the calculation of $\dot{X}_{n+1}$ and X_{n+1} at time $t + \Delta t$ [basic Euler-Cauchy Method].

$$X_{n+1} = X_n + \dot{X}_n \Delta t + 1/2\ \ddot{X}_n (\Delta t)^2$$

$$\dot{X}_{n+1} = \dot{X}_n + \ddot{X}_n \Delta t \qquad (30)$$

The time derivatives of the secondary variables (θ, ψ, ϕ, X_1, Y_1, Z_1) which are functions of the major variables, are assumed constant over the interval at the half interval value.

The rotor flap and lag equations are computed by using the Fourier method presented in the section titled SOLUTIONS OF EQUATIONS OF MOTION, Steady-State Equations, page 115.

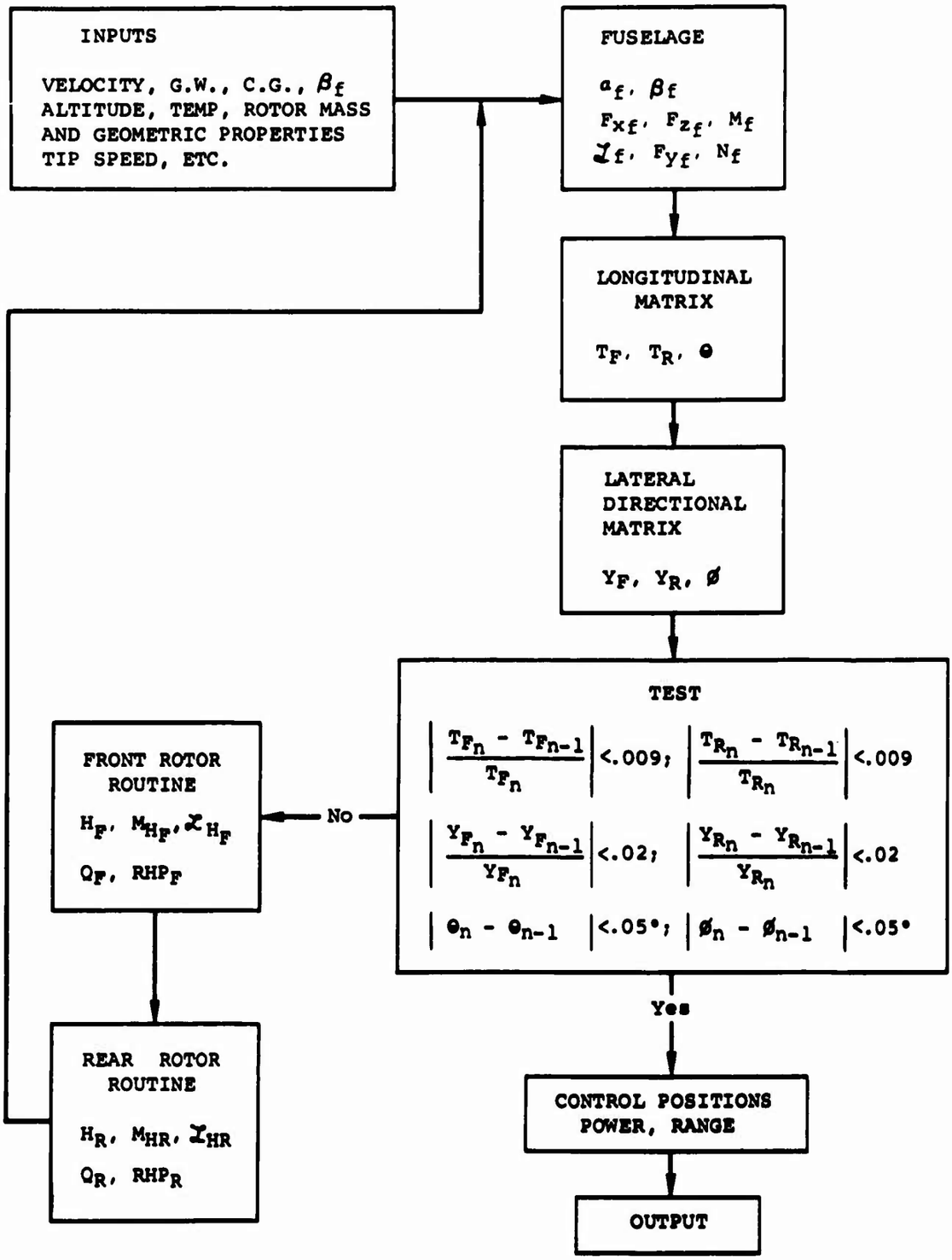

Figure 45. Block Diagram - Steady-State Solution.

Time Increment: The time increment used in the numerical integration is based on rotor speed. As specified in the above-noted section, the rotor flap and lag equations are integrated by assuming the accelerations ($\ddot{\beta}$,$\ddot{\rho}$) remain constant for $\Delta\psi$ degrees of azimuthal motion. In order to retain a constant $\Delta\psi$ increment in the rotor solution, a variable time increment based on the time required for the rotor blades to traverse $\Delta\psi$ degrees is used. For typical rotor speed variations, this results in approximately 50 to 100 solutions per second.

Induced Velocity Considerations: No attempt has been made to incorporate equations to describe the time rate of change of induced velocity. At the end of each complete rotor revolution, a new value of induced velocity is computed, based on the mean value of the rotor aerodynamic thrust for the revolution. This essentially has the effect of introducing a time lag into the induced velocity equal to the time required for a rotor revolution. The effects of velocity and angle-of-attack changes in the inflow expression are accounted for instantaneously.

Initial Conditions: The time-zero or steady-state values of the parameters are set from the trim computations.

Blade Flap and Lag Condition: The initial azimuth positions of the blades are assumed for both rotors of the articulated system as follows:

Blade 1 - $\psi_1 = 0$

Blade 2 - $\psi_2 = -120°$

Blade 3 - $\psi_3 = 120°$

The initial values of flap and lag angle and rate, for all blades, are set to their respective trim values.

For the teetering system, the front rotor blade azimuth positions are:

Blade 1 - $\psi_1 = 0$

Blade 2 - $\psi_2 = 180°$

and the equivalent rear rotor positions are:

Blade 1 - $\psi_1 = 90°$

Blade 2 - $\psi_2 = 270°$

A typical solution cycle illustrated in Figure 46 is outlined below:

1. The forcing functions are obtained from the input by linearly interpolating between two input time values surrounding the computation time.

2. The forward rotor inputs are then set up.

3. The flap and lag accelerations are computed for the 3 blades of the articulated rotor system at their respective n^{th} azimuth positions and integrated for the $(n+1)^{th}$ values of β, $\bar{\beta}$, ρ, $\bar{\rho}$. The (n+1) azimuth locations are $\psi_{n+1} = \psi_n + \Delta\psi$.

   For the teetering rotor system the flap acceleration is computed for the blade at n^{th} azimuth station and integrated for the $(n+1)^{th}$ values of β, $\bar{\beta}$.

4. The radially integrated value of T_n, T_{Hn}, H_n, Y_n R.H.P_n, Q_n, obtained for each blade are summed for net rotor values.

5. The aft rotor parameters are obtained in a manner similar to the forward rotor parameters.

6. Rotor acceleration is determined.

7. The fuselage forces and moments are determined.

8. Gravity forces are determined.

9. The net rotor forces and moments are then computed.

10. The linear accelerations are obtained by solving the force equations.

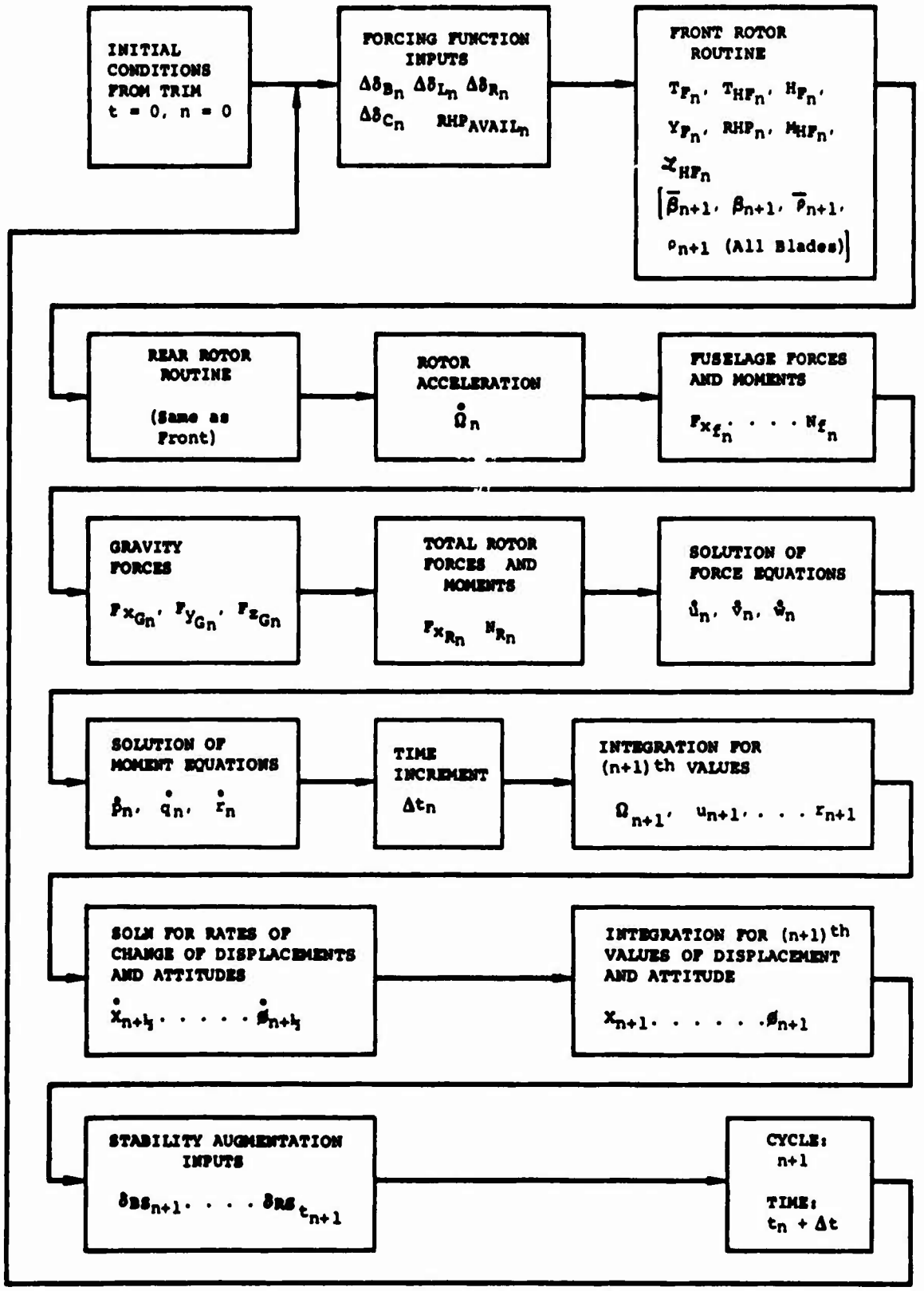

Figure 46. Block Diagram - Transient Solution.

11. The angular accelerations are obtained from a solution of the moment equations.

12. The time increment for this cycle is then computed.

13. Integration - The (n+1) values of the linear and angular velocities and rotor speed are obtained by numerically integrating the n^{th} acceleration quantities.

    The values at n + 1/2 are also computed for use in the linear and angular displacement equations.

14. The helicopter attitudes are obtained by numerically integrating the n + 1/2 values of $\dot{\psi}$, $\dot{\theta}$, $\dot{\phi}$ over the time interval. An iteration is required to obtain $\psi_{n+1/2}$, etc., since $\dot{\psi}_{n+1/2}$, etc., are functions of $\psi_{n+1/2}$.

15. The displacements with respect to the inertial axis system are computed by integrating the half increment values of $\dot{X}_I$, $\dot{Y}_I$, $\dot{Z}_I$ over the time interval.

16. The stability augmentation system inputs are obtained by integrating the system equations.

17. This completes one integration cycle or time increment. The cycle number is set to n+1 and real time to $t_n + \Delta t$, and the process is repeated.

APPENDIX II - CORRELATION WITH FLIGHT TEST DATA

CORRELATION OF ANALYSIS

The analysis used in the study is outlined in Appendix I. This section has been included to substantiate the predicted parameter variations through correlation with results obtained from tandem rotor helicopter flight tests. Those parameters requiring substantiation include:

1. Rotor thrust and blade motion response to collective control inputs.

2. Rotor speed variation with delivered power.

3. Helicopter rigid-body response to control variations.

Since most of the testing has been performed with only those parameters vital to the particular test being recorded, the correlation discussed below is presented for a variety of conditions. The forcing functions (that is, control input and delivered power) used in the theoretical predictions were identical to those recorded in the tests. Figures 47 through 49 show correlation of estimated rotor decay, blade motion envelope, and normal acceleration (Figure 49) with results from simulated power failures at airspeeds to 142 knots on the CH-47A (Chinook) helicopter. The predictions are for the most part quite adequate, with the minimum aft rotor blade flap angle estimations somewhat optimistic for the cases shown in Figures 47 and 48.

The change and rates of change of collective required to check the decay in the above tests are not as large as those required in the 200-knot regime for the high-drag configuration. Figures 50 to 52 show additional correlation of rotor thrust response (through normal acceleration) and blade motion to rapid collective input rates (approximately 60 degrees per second). Figure 50 presents the minimum aft blade flap envelope

over the fuselage, and normal acceleration variation obtained during a collective dump test on the CH-46A helicopter. Figures 51 and 52 show similar data obtained on the CH-47A for both a collective dump and a collective pullup. Excellent agreement was achieved. Body motions were not available on the above tests for correlation. Since a requirement of the study was to investigate the effects of longitudinal control inputs on rotor speed decay, Figure 53 is included to show correlation with the response of the CH-47A to a longitudinal step input.

TRANSIENT ANALYSIS CORRELATION

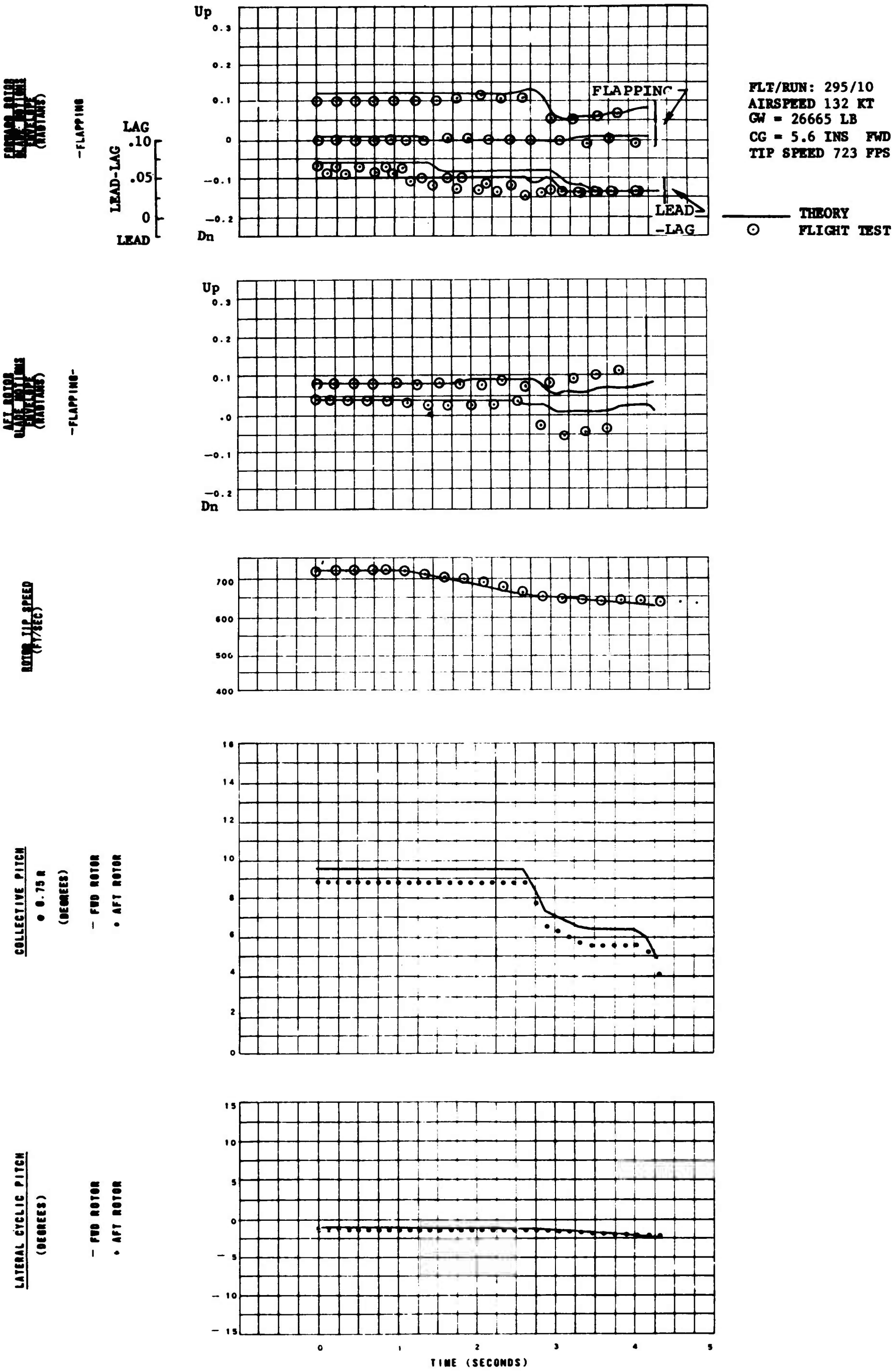

Figure 47. Transient Analysis Correlation - Simulated Power Failure at 132 Knots.

TRANSIENT ANALYSIS CORRELATION

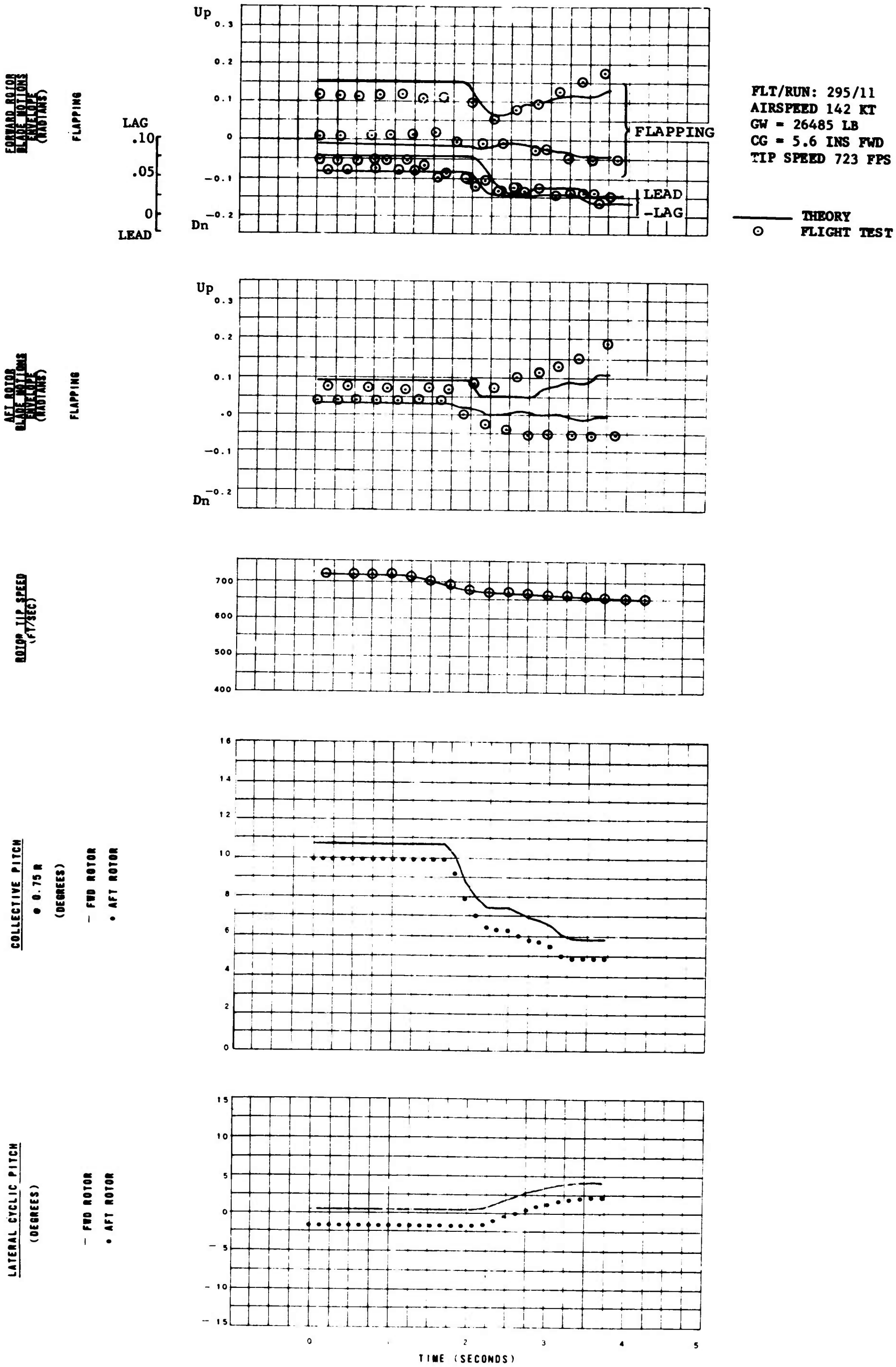

Figure 48. Transient Analysis Correlation - Simulated Power Failure at 142 Knots.

TRANSIENT ANALYSIS CORRELATION

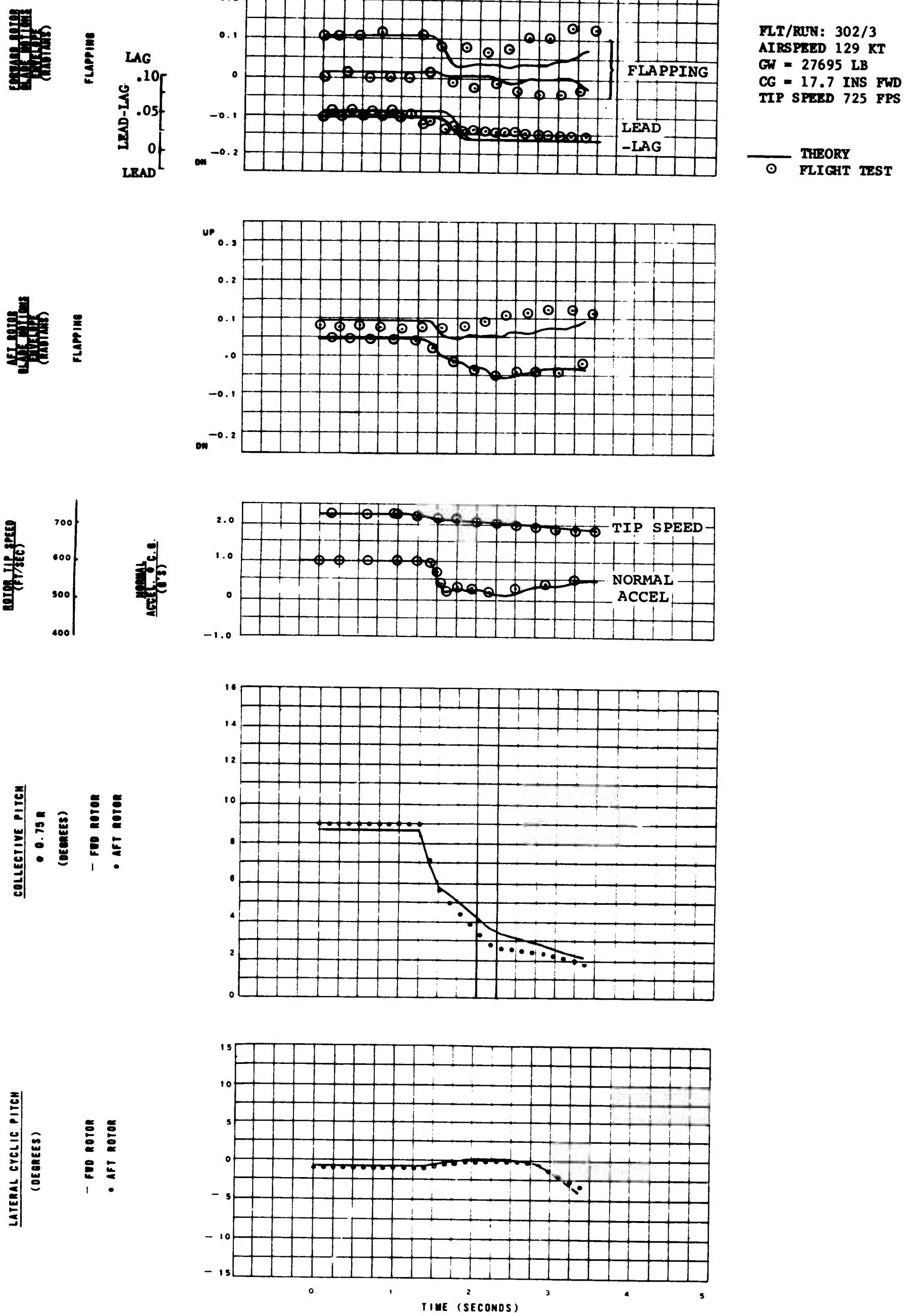

Figure 49. Transient Analysis Correlation - Simulated Power Failure at 129 Knots.

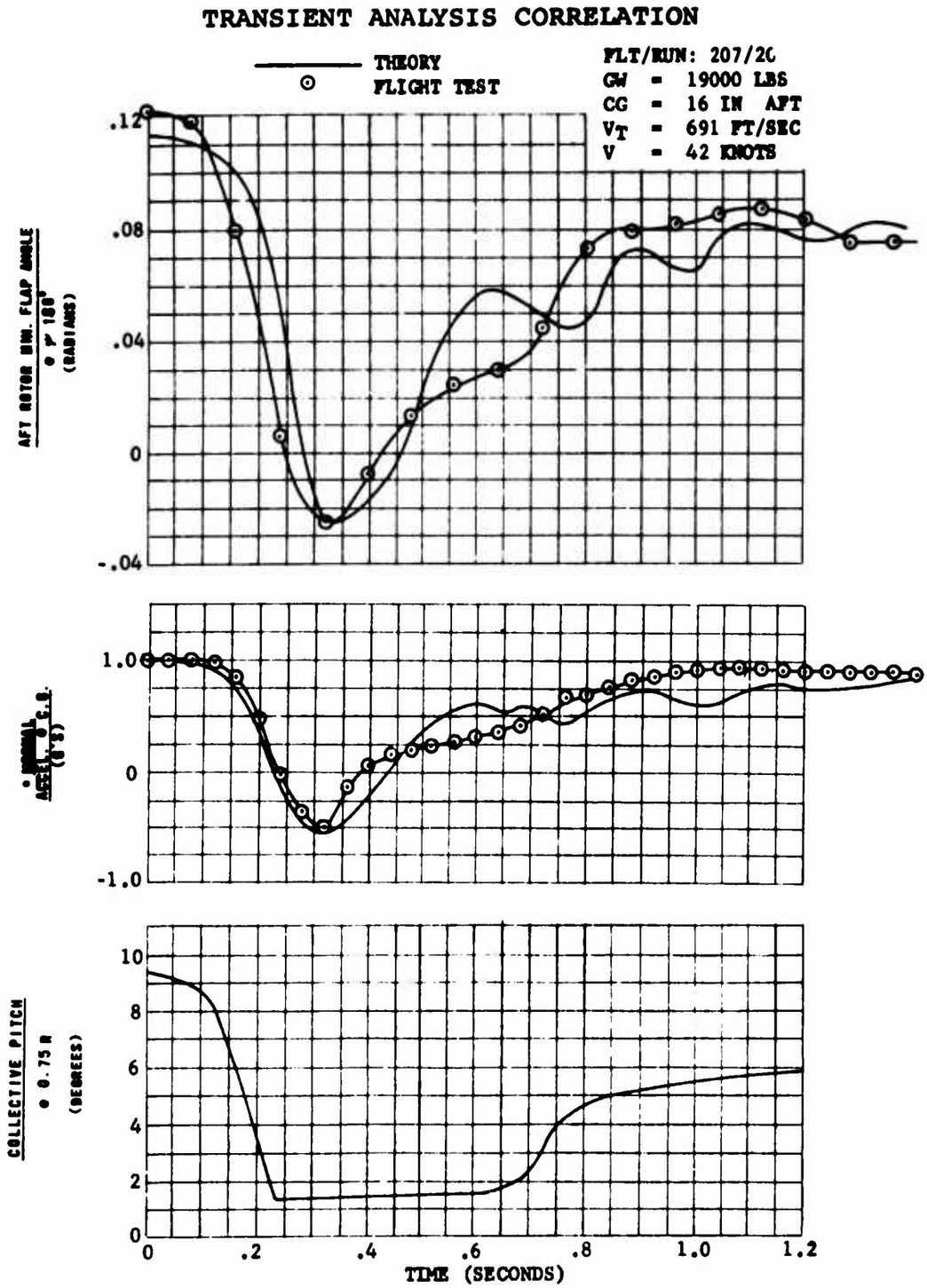

Figure 50. Transient Analysis Correlation - Response to a Collective Dump, CH-46A Helicopter.

TRANSIENT ANALYSIS CORRELATION

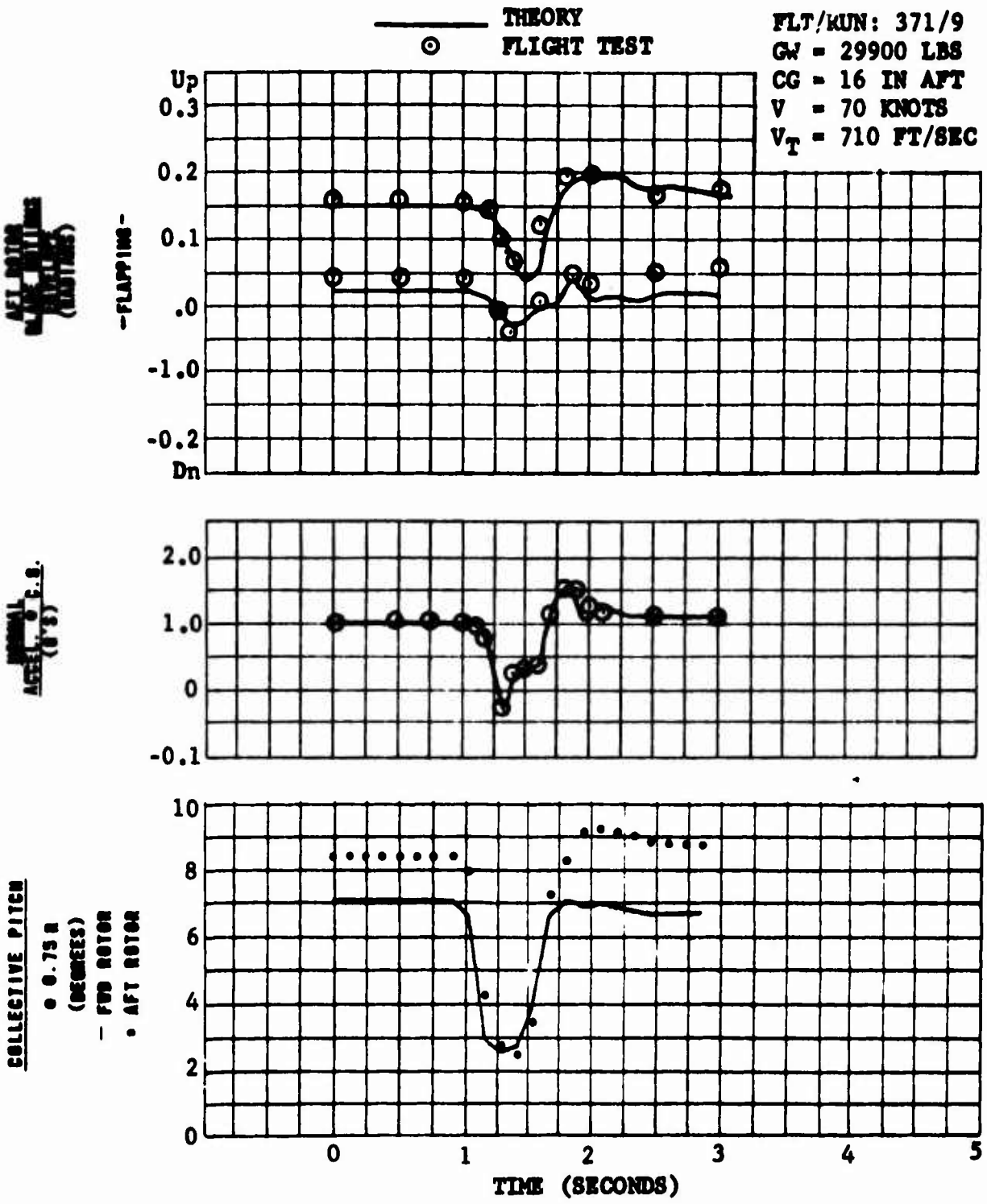

Figure 51. Transient Analysis Correlation - Response to a Collective Dump, CH-47A Helicopter.

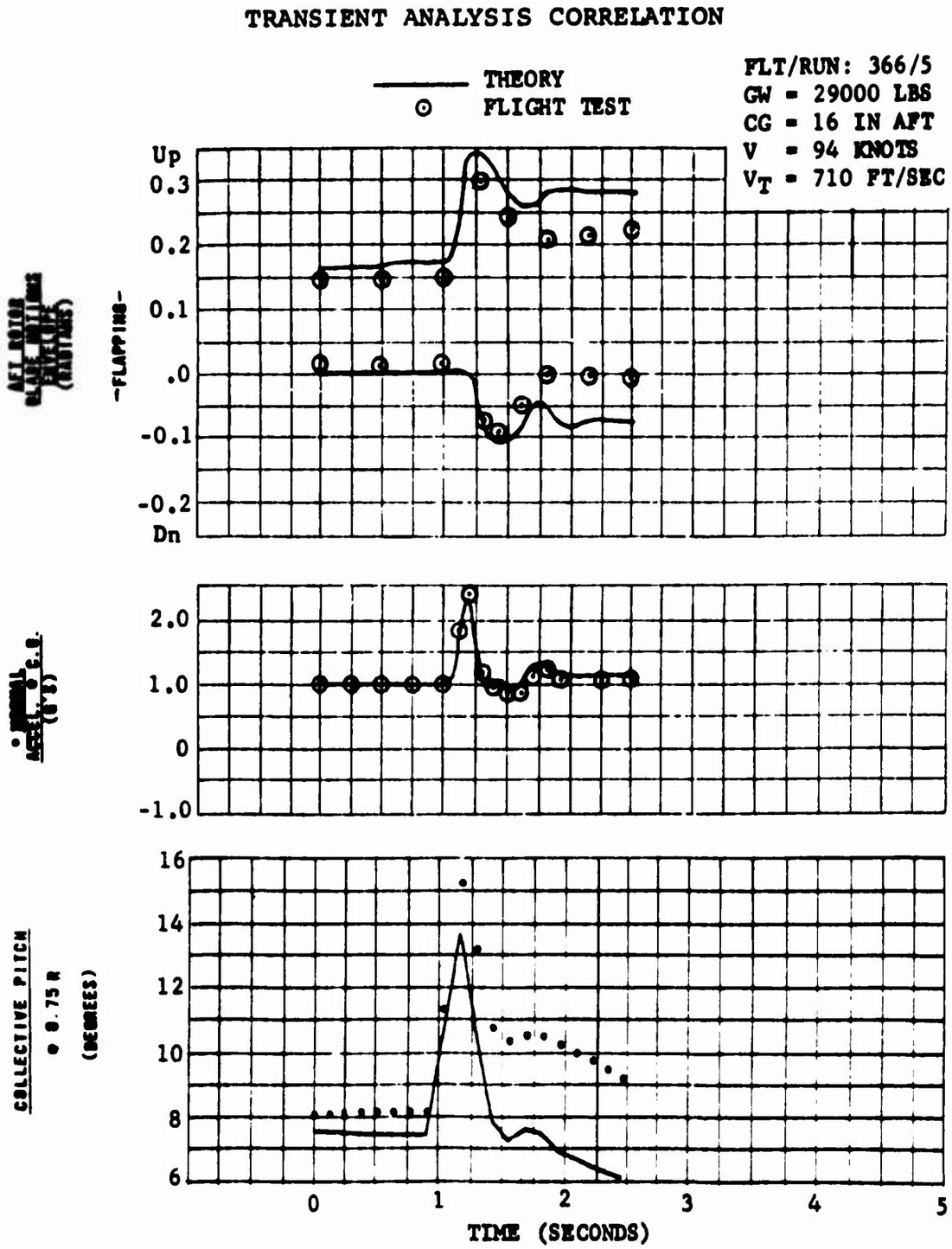

Figure 52. Transient Analysis Correlation - Response to a Collective Pullup, CH-47A Helicopter.

TRANSIENT ANALYSIS CORRELATION

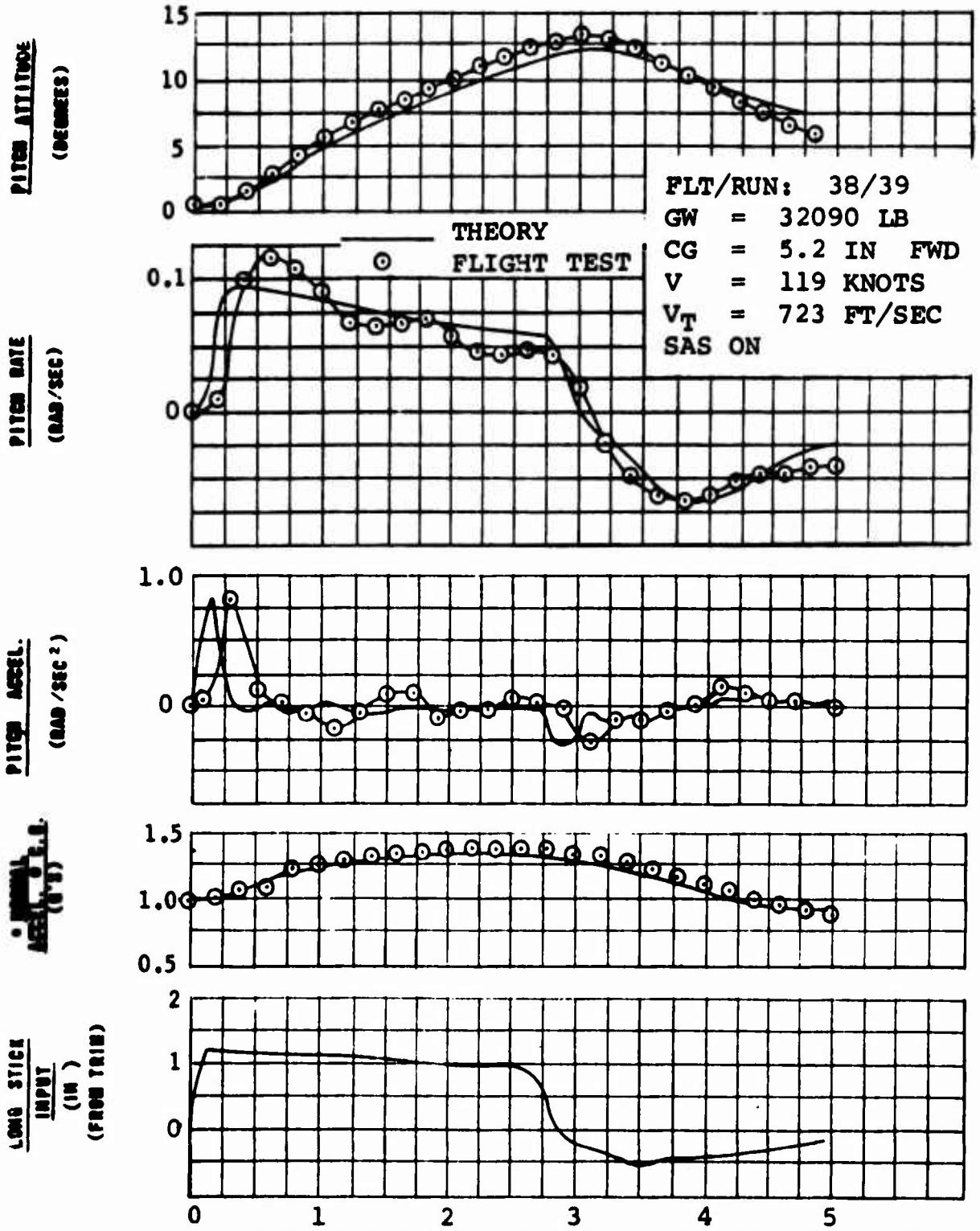

Figure 53. Transient Analysis Correlation - Response to an Aft Longitudinal Step, CH-47A Helicopter.

APPENDIX III - AIRCRAFT CHARACTERISTICS

DESCRIPTION OF CONFIGURATIONS

The aircraft configurations analyzed in this investigation are listed in Table 1, which identifies each by a configuration number. A baseline case (Configuration 6) was selected, and systematic variations thereto were made to obtain the other configurations. Unless otherwise noted in Table 10, all configurations conform to the following baseline characteristics:

Rotor radius	30.0 ft
Blade chord	2.67 ft
Number of blades/rotor	3
Rotor solidity	0.085
Flap hinge offset ratio	0.05
Blade twist	-4.0 deg
Blade root cutout ratio	0.195
Longitudinal cyclic pitch	8.0 deg
Blade flapping moment of inertia	3364 sl-ft^2
Blade flapping static moment	5580 lb-ft
Lock number	4.38
Lag hinge offset	2.46 ft
Blade lag pre-load	1065 lb-ft
Blade lag damping	689 lb-ft/rad/sec
Blade lag moment of inertia	2845 sl-ft^2
Blade lag static moment	4750 lb-ft
Aircraft weight	30,000 lb
Fuselage flat plate drag area	32.0 ft^2
Fuselage drag/total lift	0.15
Forward shaft inclination	9.0 deg
Aft shaft inclination	4.0 deg
Length from cg to forward rotor	19.57 ft
Length from cg to aft rotor	19.33 ft
Height from cg to forward rotor	6.30 ft
Height from cg to aft rotor	10.97 ft
Aircraft moments of inertia: I_x	23,000 sl-ft^2
I_y	165,000 sl-ft^2
I_z	153,000 sl-ft^2

Aircraft product of inertia	12,900 sl-ft^2
Moment of inertia of rotating parts	20,600 sl-ft^2
Rotor tip speed at trim	723 ft/sec
Advancing tip Mach No. at trim	0.950
Aircraft speed at trim	200 knots
Pressure altitude	0 ft
Ambient temperature	59 deg F
Rate of climb at trim	0 ft/min
Trim sideslip angle	0 deg

Fuselage characteristics: The aerodynamic lift, drag and sideforce of the Boeing-Vertol CH-47A Chinook are used to represent the fuselage characteristics of the typical 200-knot helicopter studied herein. In accordance with the minimum design objectives of Boeing-Vertol for 200-knot helicopters, neutral fuselage stability is assumed about all three axes. Hence, rolling, pitching, and yawing moments are zero.

Stability augmentation system: The effects of an artificial stability system are programmed into this analysis. The system provides rate damping about all three axes, and also provides static directional (sideslip) stability. The characteristics of the system are the same as those currently in use on production models of the CH-47A, except that the sideslip stability loop operates at reduced gain, to allow for the improved directional stability characteristics of the fuselage. The characteristics of the stability augmentation system (SAS) are given in Table 9.

No autopilot, q-sensed longitudinal cyclic trim, or differential collective speed trim are considered to be operative, as their effects would tend to obscure the significance of the results. The incorporation of the SAS, however, was found to be necessary in order to limit divergences to reasonable values throughout the five-second time histories.

Control kinematics: The control motion limits used in this investigation are substantially the same as for the CH-47A, and are defined in Table 9.

TABLE 9.

SAS CHARACTERISTICS AND CONTROL MOTION LIMITS

SAS Mode	Gain $\left(\frac{\text{in of control}}{\text{rad/sec}}\right)$	Lead Time Const (sec)	Lag Time Const (sec)	Washout Time Const (sec)
Pitch	23.85	0.40	1.60	-
Roll	12.00	0.60	0.37	-
Yaw	10.32	-	0.27	4.20
Sideslip	2.27*	-	0.27	-
Roll into Yaw	5.77	-	4.20	-

Cockpit Control Motion		Blade Angular Motion (at each Rotor Head)	
Coll. Stick	0 to 9.13 in	Coll. Pitch @ 0.75R	0° to 17°
Long. Stick	± 6.50 in	Diff. Coll.	± 5°
Lat. Stick	± 4.19 in	Lat. Cyclic	± 8°
Dir. Pedals	± 3.60°	Lat. Cyclic	± 11.4°

*Inches of control per radian

OTHER CONFIGURATIONS

A complete listing of all changes made to the baseline configuration in order to produce the desired array of configurations is presented in Table 10. Each such change is discussed below.

Articulated rotors with varying values of flap hinge offset ratio: Only the flap hinge location is changed.

Teetering rotors: With the number of blades reduced to two, the chord is increased to maintain the same solidity as the

baseline configuration. Blade inertias are increased as well, to maintain the same Lock number.

Delta-three and tip path plane controllers on forward rotor: Only the hub geometry is changed to incorporate these modifications. The delta-three hinge couples the pitch angle of each blade to its own flapping angle. The tip path plane controllers studied are of four types:

1. Pitch-cone feedback which couples the pitch angle of each blade to the mean coning angle of the rotor.

2. Pitch-flap out-of-phase which couples the pitch angle of each blade to the rotor flapping angle 90 degrees ahead of the blade position.

3. Pitch-flap in-phase which couples the pitch angle of each blade to the rotor flapping angle at the blade position.

4. A combination of all three of the above types of coupling.

Reduced Lock Number: The inertias about the flap hinge and the lag hinge are doubled, as are the lag preload and damping, and the rotating inertia.

Longitudinal cyclic pitch variations: Only cyclic pitch is changed.

Swashplate dihedral variations: Only cyclic pitch is changed.

Rotor overlap variations: The fuselage moments of inertia are changed commensurate with the fuselage elongation, as are the aerodynamic lift and sideforce characteristics.

Aft rotor height variations: The fuselage moments of inertia are changed commensurate with the aft pylon extension, as are the aerodynamic sideforce characteristics.

Configurations at 250 knots: These are identical to the corresponding 200-knot configurations, except that blade twist, blade root cutout and rotor speed are modified.

ROTOR AERODYNAMIC CHARACTERISTICS

The synthesized section characteristics ($c_\ell = f(M,\alpha)$, $c_d = f(M,\alpha)$) for the drooped-nose NACA 0006 airfoil are presented in Figures 54 through 56.

The data were assembled as outlined below, using test results from the Boeing Transonic Wind Tunnel (BTWT) together with those from full-scale rotor studies published in NACA TN-4357.

The NACA rotor test stand data, generally referred to as NACA 0012 synthesized, were used as a basis for correcting the Boeing two-dimensional 6-percent data for rotation effects. The basic 6-percent symmetric data were obtained through extrapolation (with regard to the Transonic Similarity Rule for c_d) of BTWT 12-percent and 9.5-percent symmetric test results. A further correction factor due to the drooped nose has been included, based on BTWT data for 9.5-percent symmetric and 9.5-percent drooped airfoils.

TABLE 10

PARAMETER VARIATIONS

Airspeed at Trim (KT)							200	200	200	200	200	250
Drag/Lift							0	0.075	0.15	0.15	0.15	0
Rotor Blade Twist (DEG)							0	-4	-4	-8	-12	-12
Longitudinal Cyclic Pitch, except as noted below (DEG)							4	8	8	8	8	8
Equivalent Flat Plate Drag Area (FT^2)							0	17	32	32	32	0
VARIATIONS TO BASELINE CONFIGURATION												
Articulated Rotors:	e/R = 0	e_F = 0					1	2	3	--	--	--
	e/R = 0.05	e_F = 1.5 ft					4	5	6*	7	8	45**
	e/R = 0.15	e_F = 4.5 ft					9	10	11	--	--	--
Teetering Rotors		e = 0	c = 4.0 ft	I_F = 5050 sl-ft^2	M_F = 8360 lb-ft	b = 2	12	13	14	--	--	--
				I_R = 20200 sl-ft^2								
Articulated Rotors with Delta -3 on Fwd Rotor		k_{1F} = -.5774					15	--	16	--	17	46**
Articulated Rotors with Tip Path Plane Controller on Fwd Rotor:	(a) Pitch-Cone	k_{1F} = -.193	k_{2F} = -.193	k_{3F} = -.193			18	--	19	--	20	47**
	(b) Pitch-Flap Out-of-Phase	k_{1F} = 0	k_{2F} = .333	k_{3F} = -.333			21	--	22	--	23	--
	(c) Pitch-Flap In-Phase	k_{1F} = -.385	k_{2F} = .193	k_{3F} = .193			--	--	24	--	--	--
	(d) All Three Combined	k_{1F} = -.5774	k_{2F} = .333	k_{3F} = -.333			--	--	25	--	--	--
Articulated Rotors with Reduced Lock Number: L.N. = 2.19		I_F = 6728 sl-ft^2	M_F = 11160 lb-ft	I_L = 5690 sl-ft^2	M_L = 9450 lb-ft	c_o = 2130 lb-ft	26	27	28	--	--	48**
		c_1 = 1378 lb-ft/rad/sec	I_R = 41200 sl-ft^2									
Articulated Rotors with Longitudinal Cyclic Pitch Variations	(a) 2° Aft Cyclic	B_{ITF} = -2°	B_{ITR} = -2°				29	--	--	--	--	--
	(b) 4° Fwd Cyclic	B_{ITF} = 4°	B_{ITR} = 4°				--	--	30	--	--	--
	(c) 10° Fwd Cyclic	B_{ITF} = 10°	B_{ITR} = 10°				31	--	--	--	--	--
	(d) 14° Fwd Cyclic	B_{ITF} = 14°	B_{ITR} = 14°				--	--	32	--	--	--
Articulated Rotors with Swashplate Dihedral Variations	(a) 5.5° Dihedral	B_{ITF} = -4°	B_{ITR} = 12°				33	--	--	--	--	--
	(b) 1.5° Dihedral	B_{ITF} = 4°	B_{ITR} = 12°				--	--	34	--	--	--
	(c) -6.5° Dihedral	B_{ITF} = 12°	B_{ITR} = 4°				--	--	35	--	--	--
	(d) -10.5° Dihedral	B_{ITF} = 12°	B_{ITR} = -4°				36	--	--	--	--	--
Articulated Rotors with Rotor Overlap Variations	(a) 20% Overlap	l_F = 24.12 ft	I_X = 19300 sl-ft^2	I_Z = 272000 sl-ft^2	FUSELAGE A		37	--	38	--	--	--
		l_R = 23.88 ft	I_Y = 284000 sl-ft^2	J_{ZX} = 18400 sl-ft^2								
	(b) 0% Overlap	l_F = 30.12 ft	I_X = 22400 sl-ft^2	I_Z = 423000 sl-ft^2	FUSELAGE B		39	--	40	--	--	--
		l_R = 29.88 ft	I_Y = 437000 sl-ft^2	J_{ZX} = 26000 sl-ft^2								
Articulated Rotors with Aft Rotor Height Variations	(a) 20% Relative Height	h_F = 5.10 ft	I_X = 41700 sl-ft^2	I_Z = 179000 sl-ft^2	FUSELAGE C		41	--	42	--	--	--
		h_R = 17.10 ft	I_Y = 214000 sl-ft^2	J_{ZX} = 34500 sl-ft^2								
	(b) 30% Relative Height	h_F = 4.10 ft	I_X = 62400 sl-ft^2	I_Z = 196000 sl-ft^2	FUSELAGE D		43	--	44	--	--	--
		h_R = 22.10 ft	I_Y = 251000 sl-ft^2	J_{ZX} = 52700 sl-ft^2								

* BASELINE CONFIGURATION

** FOR THESE CONFIGURATIONS - X_C = 0.250, V_T = 668 fps, M_T = 0.975

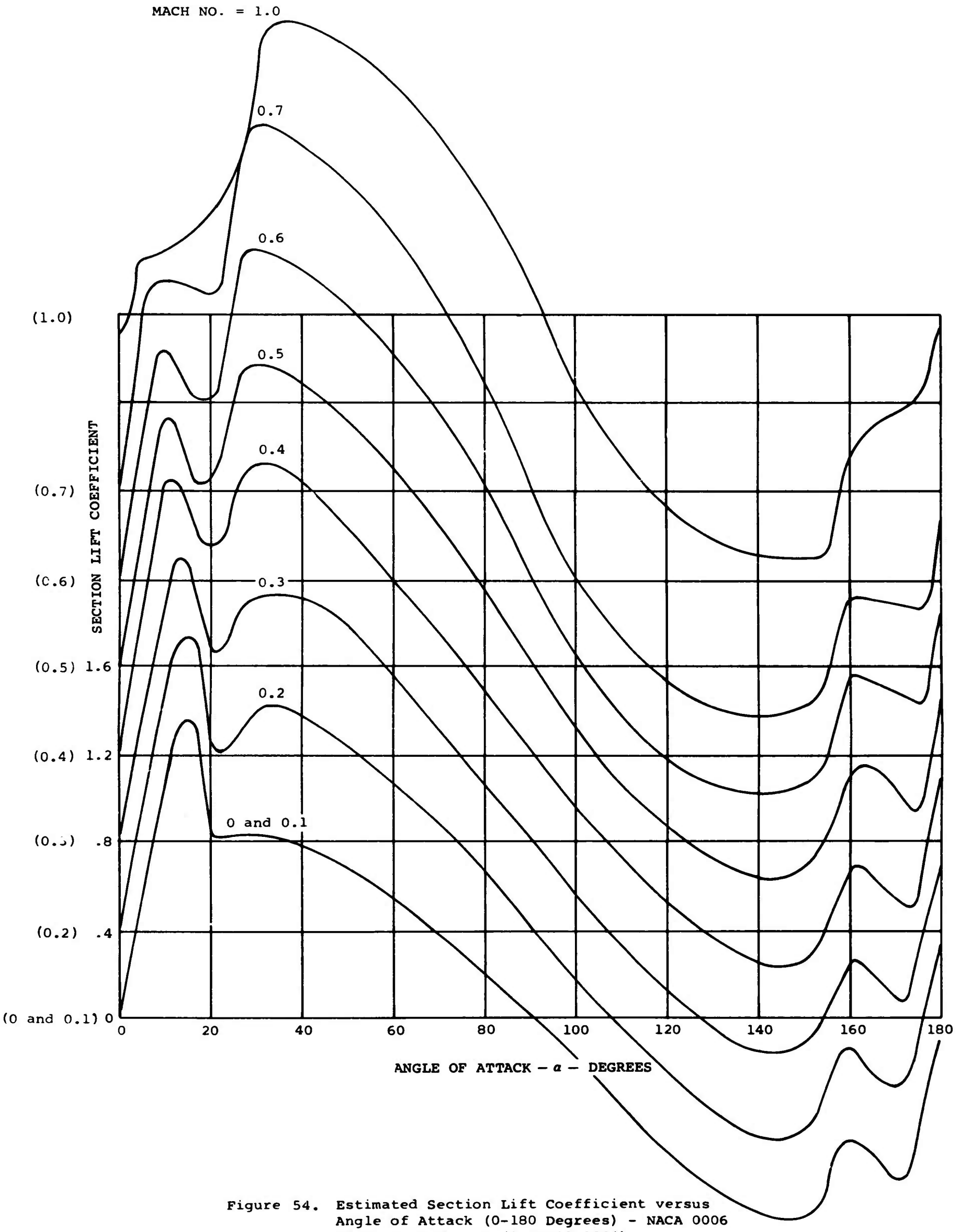

Figure 54. Estimated Section Lift Coefficient versus Angle of Attack (0-180 Degrees) - NACA 0006 with Drooped Nose (1 April 1964).

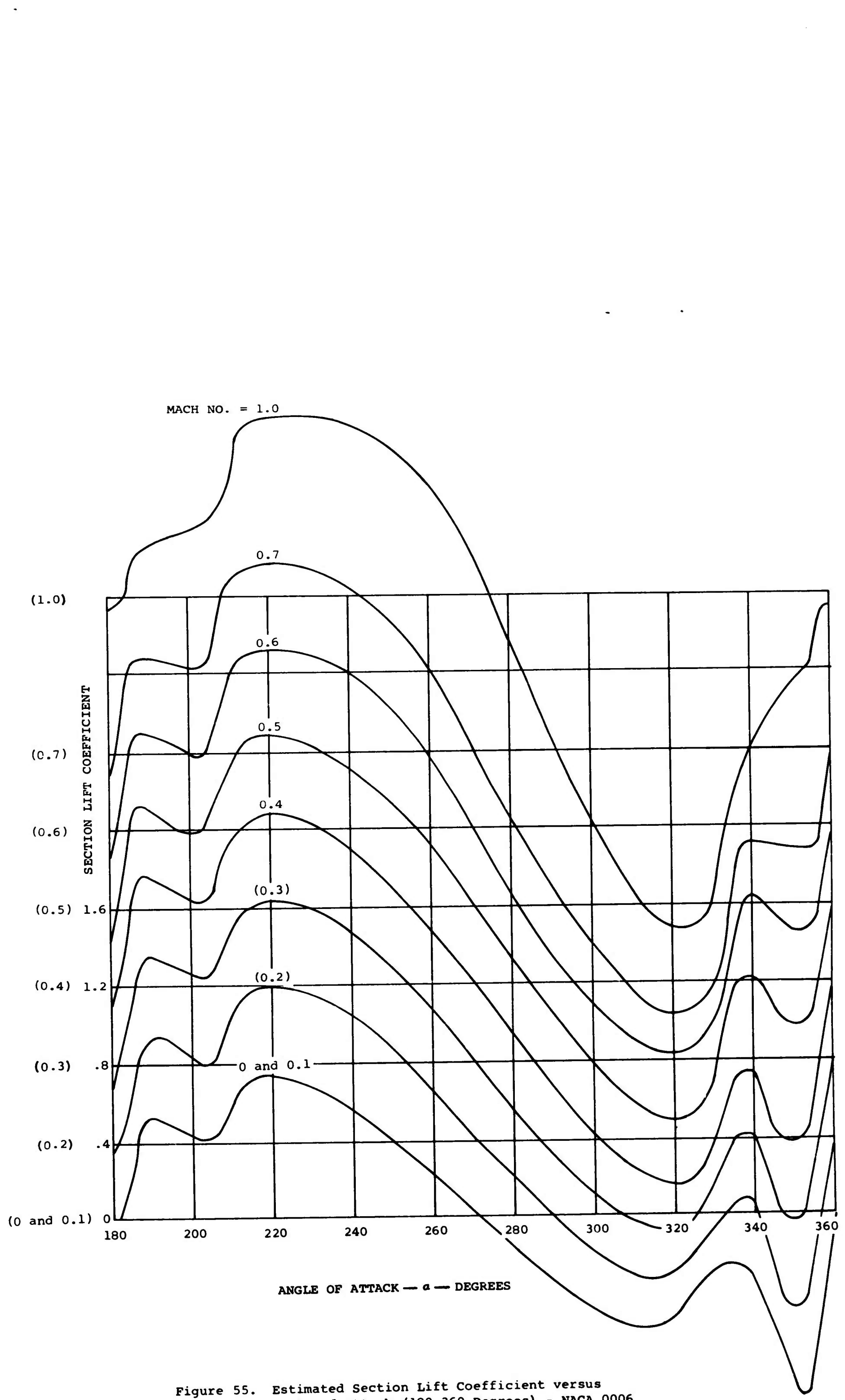

Figure 55. Estimated Section Lift Coefficient versus Angle of Attack (180-360 Degrees) - NACA 0006 with Drooped Nose (1 April 1964).

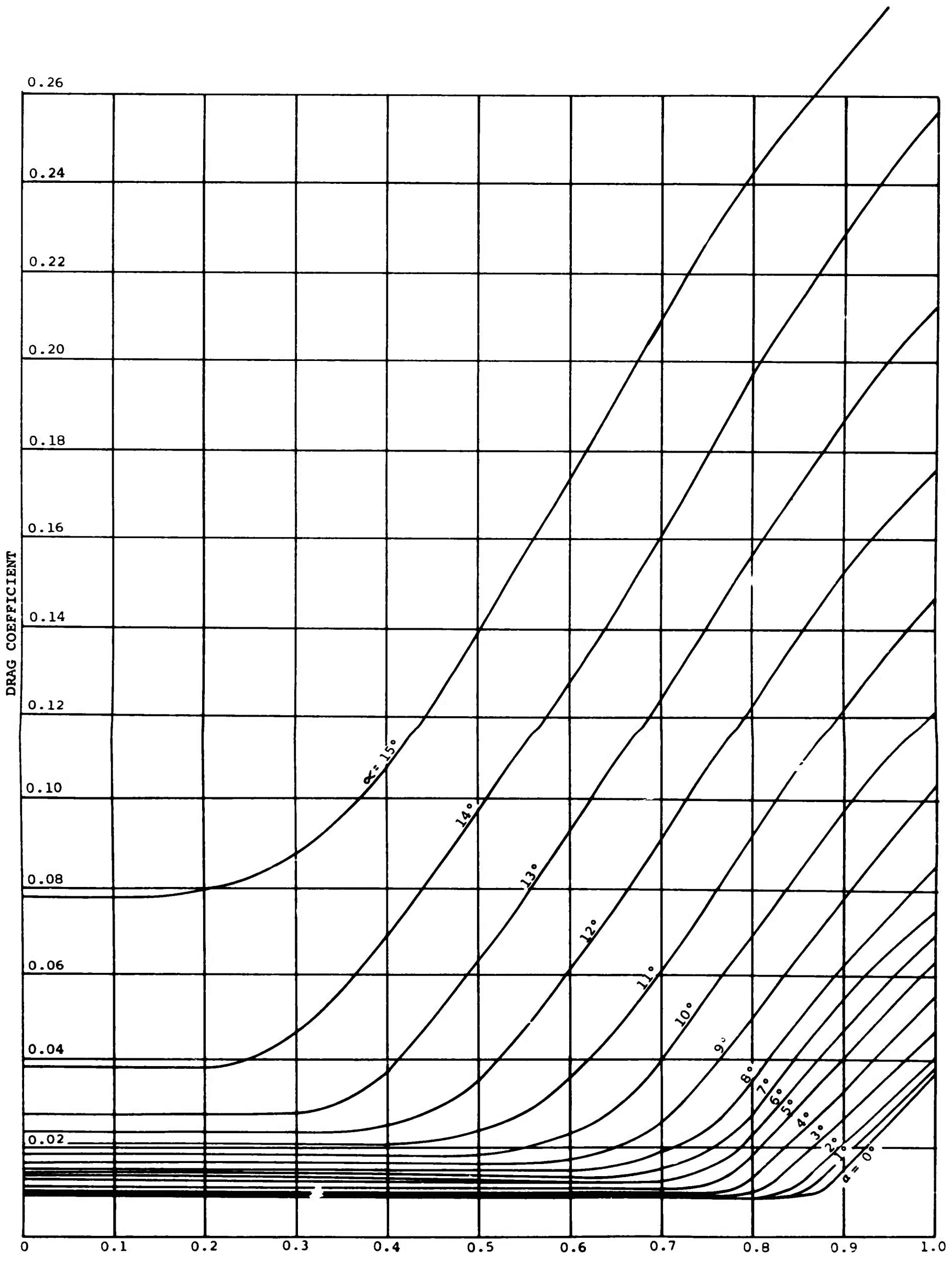

Figure 56. Estimated Section Drag Coefficient versus Mach Number - NACA 0006 with Drooped Nose (1 April 1964).

APPENDIX IV - RESULTS OF TRANSIENT ANALYSIS

This appendix presents a selection of significant time histories which form the basis of the Discussion and Conclusions. These time histories (Figures 57 to 112) were chosen from the 198 cases investigated in connection with this report. Tables 11 through 18 summarize the data gleaned from these time histories.

DATA PLOTTING DEFECTS

In some of the time histories, one or more of the following defects may be found.

Misalignment: The amount of misalignment may be easily determined by noting that the following parameters should have the initial values indicated:

Rotor tip speed	723 ft/sec(668 ft/sec)
Height loss	0 ft
Airspeed	200 kt(250 kt)
Normal acceleration	1.0 g
Sideslip angle	0 deg
Yaw angle	0 deg

Scalloping: Parameters which should have smooth variations (rotor tip speed, airspeed, angle of attack and pitch angle) or consist of straight lines (longitudinal and collective inputs) show wavy traces. This in no way indicates a faulty analysis, but is rather a consequence of the manner in which the data plotter pen may travel from point to point. The computed data points on such traces are accurate, but the pen follows an erroneous curved path between them, instead of a straight line.

Truncated Collective Input Corners: The corners of the collective input traces are often lopped off. This occurs because the data plotter pen travels in a straight line from data point to data point on the collective trace. Unless a data point occurs exactly at a given corner of the trace, the pen will bypass the corner, which will then appear truncated. The accuracy of the analysis is not affected, since the computer operates with the exact input, not the approximate plot thereof.

DESCRIPTION OF PARAMETERS

Cockpit Control Positions: The longitudinal and collective stick positions are presented in terms of percent of their total travel, 0 percent being full aft longitudinal stick or full down collective stick, and 100 percent being full forward longitudinal stick or full up collective stick. The control limits given in Table 9 are based on a current tandem-rotor-type helicopter, and should not be regarded as definitive for a 200-knot helicopter, since they can be readily changed to suit various requirements.

Forward Rotor Blade Motions Envelope: The envelope of forward rotor blade flapping motions is specified by the upper and lower flapping limit traces. The upper trace represents the combination of coning, longitudinal flapping, and lateral flapping at that azimuth where the three combine to produce the maximum blade flapping angle. The lower trace represents the same combination at the azimuth where the three combine to produce the minimum blade flapping angle. The specific azimuths at which maximum and minimum flapping occur are not identified by these traces.

The flapping angle of the rotor blades at azimuth station 0 degrees is also presented. This parameter represents the combination of coning and longitudinal flapping of the forward rotor directly over the fuselage, and therefore gives an indication of blade-fuselage clearance. In addition, comparison of this parameter with the blade flapping envelope indicates whether the blade flapping motion is mainly longitudinal or lateral. If longitudinal flapping predominates, the flapping at azimuth station 0 degrees will lie along the upper trace of the envelope for forward flapping, or along the lower trace for aft flapping. If lateral flapping predominates, the flapping at azimuth station 0 degrees will lie about midway between the upper and lower traces.

The envelope of forward rotor lead-lag motions is specified by the upper and lower lead-lag limit traces. The upper trace represents the maximum lag angle, and the lower trace, the minimum lag angle.

Aft Rotor Blade Motions Envelope: The above comments on the forward rotor blade motions also apply to the aft rotor, except that the flapping angle of the rotor blades is presented at azimuth station 180 degrees instead of 0 degrees. This parameter represents the combination of coning and longitudinal flapping of the aft rotor directly over the fuselage, and therefore gives an indication of blade-fuselage clearance. A further exception is that, if longitudinal flapping predominates, the flapping at azimuth station 180 degrees will lie along the lower (not upper) trace of the envelope for forward flapping, or along the upper (not lower) trace for aft flapping.

Rotor Tip Speed: Self-explanatory.

Height Loss: Self-explanatory.

Airspeed: Self-explanatory.

Normal Acceleration at CG: Self-explanatory.

Angle of Attack: Self-explanatory.

Sideslip Angle: Self-explanatory.

Fuselage Attitudes: Self-explanatory.

Collective Pitch: The collective pitch of each rotor is presented; this includes the effects of collective stick, longitudinal stick, and pitch SAS inputs. The effects of an autopilot and of any q-sensed differential collective pitch mechanism are not included.

Lateral Cyclic Pitch: The lateral cyclic pitch of each rotor is presented; this includes the effect of the trim-fixed lateral stick and rudder pedals combined with SAS inputs generated by roll and yaw rates and by sideslip angle.

Blade Loading Parameter: The ratio of thrust coefficient to rotor solidity is a nondimensional representation of average blade loading, which is essential to the blade loads analysis.

Advance Ratio: The ratio of aircraft velocity (along the flight path) to rotor tip speed.

Inflow Ratio: The ratio of air velocity through the rotor disc to rotor tip speed. The velocity through the rotor disc includes the normal component of aircraft velocity, induced velocity, and rotor hub velocity due to pitching rate.

TABLE 11 - TIME IN SECONDS TO ATTAIN ROTOR FLAPPING AMPLITUDE AND ROTOR TIP SPEED CRITERIA
(200 KNOTS, COMPLETE POWER FAILURE, NO INPUTS)

Drag/Lift	0			0.075			0.15			0.15			0.15		
Blade Linear Twist	0°			-4°			-4°			-8°			-12°		
Criteria / Configurations	Fwd Rotor Flap: ± .20 Rad	Aft Rotor Flap: ± .20 Rad	Rotor Tip Speed: 550 Fps	Fwd Rotor Flap: ± .20 Rad	Aft Rotor Flap: ± .20 Rad	Rotor Tip Speed: 550 Fps	Fwd Rotor Flap: ± .20 Rad	Aft Rotor Flap: ± .20 Rad	Rotor Tip Speed: 550 Fps	Fwd Rotor Flap: ± .20 Rad	Aft Rotor Flap: ± .20 Rad	Rotor Tip Speed: 550 Fps	Fwd Rotor Flap: ± .20 Rad	Aft Rotor Flap: ± .20 Rad	Rotor Tip Speed: 550 Fps
Articulated Rotor: e/R = 0	5.0+	5.0+	4.2	4.9	5.0+	2.2	3.2	3.6	1.5	--	--	--	--	--	--
e/R = 0.05	5.0+	5.0+	4.4	4.3	4.3	2.3	2.9	2.9	1.5	3.2	3.1	1.5	3.4	3.3	1.5
e/R = 0.15	4.3	3.5	4.0	3.8	3.4	2.2	2.6	2.2	1.5	--	--	--	--	--	--
Teetering Rotor	5.0+	5.0+	4.7	5.0+	5.0+	2.0	3.9	4.2	1.4	--	--	--	--	--	--
Delta Three on Fwd Rotor	5.0+	5.0+	4.5	--	--	--	2.9	2.8	1.4	--	--	--	3.3	3.2	1.4
Tip Path Controller on Fwd Rotor:															
Pitch-Cone	5.0+	5.0+	4.6	--	--	--	2.8	2.7	1.5	--	--	--	3.3	3.1	1.5
Pitch-Flap Out-of-Phase	5.0+	5.0+	4.5	--	--	--	5.0+	5.0+	1.5	--	--	--	5.0+	5.0+	1.5
Pitch-Flap In-Phase	--	--	--	--	--	--	3.1	3.0	1.5	--	--	--	--	--	--
All Three	--	--	--	--	--	--	5.0+	5.0+	1.5	--	--	--	--	--	--
Reduced Lock Number	5.0+	5.0+	5.0+	5.0+	5.0+	4.4	4.9	4.4	2.8	--	--	--	--	--	--
Cyclic Pitch: 2° Aft	2.2	1.5	2.5	--	--	--	--	--	--	--	--	--	--	--	--
4° Fwd	--	--	--	--	--	--	2.0	1.6	1.2	--	--	--	--	--	--
10° Fwd	5.0+	5.0+	3.6	--	--	--	--	--	--	--	--	--	--	--	--
14° Fwd	--	--	--	--	--	--	4.2	4.5	1.4	--	--	--	--	--	--
Swashplate Dihedral: 5.5°	1.8	2.7	2.9	--	--	--	--	--	--	--	--	--	--	--	--
1.5°	--	--	--	--	--	--	1.8	2.1	1.4	--	--	--	--	--	--
-6.5°	--	--	--	--	--	--	5.0+	5.0	1.5	--	--	--	--	--	--
-10.5°	5.0+	5.0+	3.5	--	--	--	--	--	--	--	--	--	--	--	--
Rotor Overlap: 20%	5.0+	5.0+	4.6	--	--	--	2.9	2.9	1.5	--	--	--	--	--	--
0%	5.0+	5.0+	4.7	--	--	--	2.9	3.0	1.5	--	--	--	--	--	--
Aft Rotor Height: 20%	5.0+	5.0+	4.5	--	--	--	2.9	2.8	1.4	--	--	--	--	--	--
30%	5.0+	5.0+	4.5	--	--	--	2.9	2.8	1.4	--	--	--	--	--	--

TABLE 12 - TIME IN SECONDS TO ATTAIN SINKING SPEED, ANGLE OF ATTACK, AND SIDESLIP CRITERIA
(200 KNOTS, COMPLETE POWER FAILURE, NO INPUTS)

Drag/Lift	0			0.075			0.15			0.15			0.15		
Blade Linear Twist	0°			-4°			-4°			-8°			-12°		
Criteria / Configurations	Sink Speed: 1500 Fpm	Angle of Attack: 20°	Side Slip Angle: 10°	Sink Speed: 1500 Fpm	Angle of Attack: 20°	Side Slip Angle: 10°	Sink Speed: 1500 Fpm	Angle of Attack: 20°	Side Slip Angle: 10°	Sink Speed: 1500 Fpm	Angle of Attack: 20°	Side Slip Angle: 10°	Sink Speed: 1500 Fpm	Angle of Attack: 20°	Side Slip Angle: 10°
Articulated Rotor: e/R = 0	4.7	5.0+	5.0+	2.8	5.0+	5.0+	2.2	5.0+	4.9	--	--	--	--	--	--
e/R = 0.05	5.0	5.0+	5.0+	3.3	5.0+	5.0+	2.4	5.0	4.0	2.3	5.0+	4.4	2.2	5.0+	4.8
e/R = 0.15	5.0+	4.6	4.2	5.0+	4.3	4.0	5.0+	3.3	3.0	--	--	--	--	--	--
Teetering Rotor	5.0	5.0+	5.0+	3.2	5.0+	5.0+	2.4	5.0+	5.0+	--	--	--	--	--	--
Delta Three on Fwd Rotor	4.2	5.0+	5.0+	--	--	--	2.4	4.2	3.6	--	--	--	2.3	4.7	4.1
Tip Path Controller on Fwd Rotor:															
Pitch-Cone	5.0+	5.0+	5.0+	--	--	--	2.3	5.0+	3.8	--	--	--	2.3	5.0+	4.5
Pitch-Flap Out-of-Phase	3.4	5.0+	5.0+	--	--	--	2.0	5.0+	5.0+	--	--	--	1.8	5.0+	5.0+
Pitch-Flap In-Phase	--	--	--	--	--	--	2.1	4.2	4.0	--	--	--	--	--	--
All Three	--	--	--	--	--	--	1.9	5.0+	5.0+	--	--	--	--	--	--
Reduced Lock Number	5.0+	5.0+	5.0+	5.0+	5.0+	5.0+	4.4	5.0+	5.0	--	--	--	--	--	--
Cyclic Pitch: 2° Aft	5.0+	4.7	3.2	--	--	--	--	--	--	--	--	--	--	--	--
4° Fwd	--	--	--	--	--	--	2.1	4.1	3.1	--	--	--	--	--	--
10° Fwd	4.3	5.0+	5.0+	--	--	--	--	--	--	--	--	--	--	--	--
14° Fwd	--	--	--	--	--	--	2.5	5.0+	5.0+	--	--	--	--	--	--
Swashplate Dihedral: 5.5°	5.0+	4.7	4.1	--	--	--	--	--	--	--	--	--	--	--	--
1.5°	--	--	--	--	--	--	5.0	3.8	3.4	--	--	--	--	--	--
-6.5°	--	--	--	--	--	--	1.9	5.0+	5.0+	--	--	--	--	--	--
-10.5°	2.7	5.0+	5.0+	--	--	--	--	--	--	--	--	--	--	--	--
Rotor Overlap: 20%	5.0	5.0+	5.0+	--	--	--	2.4	5.0+	4.6	--	--	--	--	--	--
0%	5.0	5.0+	5.0+	--	--	--	2.4	5.0+	4.9	--	--	--	--	--	--
Aft Rotor Height: 20%	5.0	5.0+	5.0+	--	--	--	2.4	5.0	4.1	--	--	--	--	--	--
30%	5.0	5.0+	5.0+	--	--	--	2.4	4.0	4.2	--	--	--	--	--	--

TABLE 13 - TIME IN SECONDS TO ATTAIN ROLL, PITCH, AND YAW RATE CRITERIA
(200 KNOTS, COMPLETE POWER FAILURE, NO INPUTS)

Drag/Lift	0			0.075			0.15			0.15			0.15		
Blade Linear Twist	0°			-4°			-4°			-8°			-12°		
Configurations \ Criteria	Roll Rate: 10°/Sec	Pitch Rate: 10°/Sec	Yaw Rate: 10°/Sec	Roll Rate: 10°/Sec	Pitch Rate: 10°/Sec	Yaw Rate: 10°/Sec	Roll Rate: 10°/Sec	Pitch Rate: 10°/Sec	Yaw Rate: 10°/Sec	Roll Rate: 10°/Sec	Pitch Rate: 10°/Sec	Yaw Rate: 10°/Sec	Roll Rate: 10°/Sec	Pitch Rate: 10°/Sec	Yaw Rate: 10°/Sec
Articulated Rotor: e/R = 0	5.0+	5.0+	5.0+	5.0+	5.0+	5.0+	5.0	5.0+	4.8	--	--	--	--	--	--
e/R = 0.05	5.0+	5.0+	5.0+	5.0+	5.0+	5.0+	3.8	5.0+	3.6	4.1	5.0+	4.0	4.2	5.0+	3.9
e/R = 0.15	4.3	3.8	3.7	3.9	3.6	3.5	2.9	2.5	2.4	--	--	--	--	--	--
Teetering Rotor	5.0+	5.0+	5.0+	--	--	--	5.0+	5.0+	5.0+	--	--	--	--	--	--
Delta Three on Fwd Rotor	5.0+	5.0+	5.0+	--	--	--	3.0	5.0+	2.8	--	--	--	3.6	5.0+	3.5
Tip Path Controller on Fwd Rotor:															
Pitch-Cone	5.0+	5.0+	5.0+	--	--	--	3.7	5.0+	3.5	--	--	--	4.2	5.0+	4.1
Pitch-Flap Out-of-Phase	5.0+	5.0+	5.0+	--	--	--	5.0+	5.0+	5.0+	--	--	--	5.0+	5.0+	5.0+
Pitch-Flap In-Phase	--	--	--	--	--	--	3.3	4.0	3.2	--	--	--	--	--	--
All Three	--	--	--	--	--	--	5.0+	5.0+	5.0+	--	--	--	--	--	--
Reduced Lock Number	5.0+	5.0+	5.0+	--	--	--	5.0+	5.0+	4.7	--	--	--	--	--	--
Cyclic Pitch: 2° Aft	3.1	4.6	2.7	--	--	--	--	--	--	--	--	--	--	--	--
4° Fwd	--	--	--	--	--	--	3.0	3.8	2.8	--	--	--	--	--	--
10° Fwd	5.0+	5.0+	5.0+	--	--	--	--	--	--	--	--	--	--	--	--
14° Fwd	--	--	--	--	--	--	5.0+	5.0+	5.0	--	--	--	--	--	--
Swashplate Dihedral: 5.5°	5.0	4.6	4.7	--	--	--	--	--	--	--	--	--	--	--	--
1.5°	--	--	--	--	--	--	2.9	3.3	2.9	--	--	--	--	--	--
-6.5°	--	--	--	--	--	--	5.0+	5.0+	5.0+	--	--	--	--	--	--
-10.5°	5.0+	5.0+	5.0+	--	--	--	--	--	--	--	--	--	--	--	--
Rotor Overlap: 20%	5.0+	5.0+	5.0+	--	--	--	4.0	5.0+	4.6	--	--	--	--	--	--
0%	5.0+	5.0+	5.0+	--	--	--	4.4	5.0+	4.0	--	--	--	--	--	--
Aft Rotor Height: 20%	5.0+	5.0+	5.0+	--	--	--	3.8	5.0+	3.6	--	--	--	--	--	--
30%	5.0+	5.0+	5.0+	--	--	--	3.8	5.0	3.6	--	--	--	--	--	--

TABLE 14 - TRIM HORSEPOWER AND TIME IN SECONDS TO ATTAIN BLADE LOADING CRITERIA
(200 KNOTS, COMPLETE POWER FAILURE, NO INPUTS)

Drag/Lift	0			0.075			0.15			0.15			0.15		
Blade Linear Twist	0°			-4°			-4°			-8°			-12°		
Criteria / Configurations	Trim Horse-Power	Fwd Blade Load C_T/σ = .12	Aft Blade Load C_T/σ = .12	Trim Horse-Power	Fwd Blade Load C_T/σ = .12	Aft Blade Load C_T/σ = .12	Trim Horse-Power	Fwd Blade Load C_T/σ = .12	Aft Blade Load C_T/σ = .12	Trim Horse-Power	Fwd Blade Load C_T/σ = .12	Aft Blade Load C_T/σ = .12	Trim Horse-Power	Fwd Blade Load C_T/σ = .12	Aft Blade Load C_T/σ = .12
Articulated Rotor: e/R = 0	2135	5.0+	5.0+	3651	5.0+	5.0+	5324	4.3	4.0	--	--	--	--	--	--
e/R = 0.05	2143	5.0+	5.0+	3652	5.0+	4.6	5320	3.7	3.2	5251	3.9	3.3	5374	3.9	3.4
e/R = 0.15	2181	4.3	3.7	3671	3.8	3.3	5300	2.7	2.2	--	--	--	--	--	--
Teetering Rotor	2219	2.1	2.7	3766	1.4	1.8	5359	1.0	1.0	--	--	--	--	--	--
Delta Three on Fwd Rotor	2130	5.0+	5.0+	--	--	--	5337	3.2	2.9	--	--	--	5364	3.6	3.3
Tip Path Controller on Fwd Rotor:															
Pitch-Cone	2147	5.0+	5.0+	--	--	--	5309	3.9	3.1	--	--	--	5363	4.1	3.3
Pitch-Flap Out-of-Phase	2130	5.0+	5.0+	--	--	--	5224	5.0+	5.0+	--	--	--	5361	5.0+	5.0+
Pitch-Flap In-Phase	--	--	--	--	--	--	5358	3.3	3.2	--	--	--	--	--	--
All Three	--	--	--	--	--	--	5199	5.0+	5.0+	--	--	--	--	--	--
Reduced Lock Number	2198	5.0+	5.0+	3710	5.0+	5.0+	5322	4.7	4.0	--	--	--	--	--	--
Cyclic Pitch: 2° Aft	2409	3.8	2.9	--	--	--	--	--	--	--	--	--	--	--	--
4° Fwd	--	--	--	--	--	--	5904	3.0	2.4	--	--	--	--	--	--
10° Fwd	2395	5.0+	5.0+	--	--	--	--	--	--	--	--	--	--	--	--
14° Fwd	--	--	--	--	--	--	5172	4.5	4.3	--	--	--	--	--	--
Swashplate Dihedral: 5.5°	2189	3.9	3.3	--	--	--	--	--	--	--	--	--	--	--	--
1.5°	--	--	--	--	--	--	5350	2.7	2.2	--	--	--	--	--	--
-6.5°	--	--	--	--	--	--	5428	5.0+	5.0+	--	--	--	--	--	--
-10.5°	2279	5.0+	5.0+	--	--	--	--	--	--	--	--	--	--	--	--
Rotor Overlap: 20%	2121	5.0+	5.0+	--	--	--	5346	3.8	3.3	--	--	--	--	--	--
0%	2076	5.0+	5.0+	--	--	--	5337	4.0	3.5	--	--	--	--	--	--
Aft Rotor Height: 20%	2130	5.0+	5.0+	--	--	--	5305	3.6	3.2	--	--	--	--	--	--
30%	2116	5.0+	5.0+	--	--	--	5279	3,6	3.2	--	--	--	--	--	--

TABLE 15 - COMPLETE POWER FAILURE AT 200 KNOTS WITH COMPOUND COLLECTIVE CONTROL INPUTS OF 5 DEGREES AT 20 DEGREES PER SECOND FOLLOWED BY 5 DEGREES AT 4 DEGREES PER SECOND

Drag/Lift 0.15

Blade Linear Twist -4° (except where indicated)

NOTE: All response peaks are read before during, or within ½ second after the collective input.

Rotor & Helicopter Responses / Configurations	Maximum Peak-to-Peak Flapping		Min Aft Rotor Blade Flapping Over Fus (Radians)	Minimum Normal Accel (g's)	Minimum Rotor Tip Speed (ft/sec)	Rate of Sink At 5 Seconds (ft/min)	Peak Blade Loading Parameter C_T/σ	
	Forward Rotor (Radians)	Aft Rotor (Radians)					Forward Rotor	Aft Rotor
Articulated Rotor: e/R = 0	0.27	0.40	-0.17	-0.75	585	7500	-0.068	-0.064
e/R = 0.05	0.28	0.36	-0.19	-0.75	590	7500	-0.069	-0.066
e/R = 0.15	0.26	0.56	-0.30	-1.40	585	13300	-0.069	-0.067
Teetering Rotor	0.26	0.30	-0.085	-0.75	585	7050	-0.091	-0.078
Delta Three on Fwd Rotor	0.15	0.30	-0.14	-0.50	545	5030	-0.024	-0.058
Tip Path Controller on Fwd Rotor								
Pitch-Cone	0.17	0.29	-0.15	-0.50	540	5000	-0.025	-0.058
Pitch-Flap Out-of-Phase	0.15	0.36	-0.175	-0.75	560	4880	-0.047	-0.072
Reduced Lock Number	0.23	0.33	-0.185	-1.00	640	7850	-0.062	-0.064
Cyclic Pitch: 2° Aft / 4° Fwd	0.11*	0.16*	-0.10	-0.85	580	8400	-0.070	-0.060
Cyclic Pitch: 10° Fwd / 14° Fwd	0.52	0.63	-0.335	-0.75	580	6460	-0.070	-0.076
Swashplate Dihedral: 5.5° / 1.5°	0.165*	0.42	-0.225	-0.65	580	7570	-0.060	-0.054
Swashplate Dihedral: -6.5° / -10.5°	0.495	0.44	-0.190	-0.95	590	8930	-0.080	-0.078
Articulated Rotor e/R = 0.05, Blade Linear Twist = -8°	0.28	0.35	-0.20	-0.90	590	7670	-0.068	-0.068
Articulated Rotor e/R = 0.05, Blade Linear Twist = -12°	0.27	0.34	-0.21	-0.95	590	8000	-0.069	-0.067

*For these cases, blade flapping envelope reduced by application of collective pitch.

TABLE 16 - COMPLETE POWER FAILURE AT 200 KNOTS WITH COLLECTIVE CONTROL INPUTS OF 5 DEGREES AT 4 DEGREES PER SECOND

Drag/Lift 0

Blade Linear Twist 0°

NOTE: All response peaks are read before, during, or within ½ second after the collective input.

Rotor & Helicopter Responses / Configurations	Maximum Peak-to-Peak Flapping		Min Aft Rotor Blade Flapping Over Fus (Radians)	Minimum Normal Accel (g's)	Minimum Rotor Tip Speed (ft/sec)	Rate of Sink At 5 Seconds (ft/min)	Peak Blade Loading Parameter C_T/σ	
	Forward Rotor (Radians)	Aft Rotor (Radians)					Forward Rotor	Aft Rotor
Articulated Rotor: e/R = 0	0.09	0.17	-0.065	0	600	4370	-0.012	-0.008
e/R = 0.05	0.115	0.195	-0.090	-0.15	595	4680	-0.015	-0.018
e/R = 0.15	0.095	0.225	-0.125	-0.35	600	5780	-0.019	-0.041
Teetering Rotor	0.085	0.120	-0.010	0	600	4370	-0.021	-0.014
Delta Three on Fwd Rotor	0.060*	0.130	-0.045	+0.30	595	3110	+0.010	+0.006
Tip Path Controller on Fwd Rotor								
Pitch-Cone	0.060*	0.125	-0.045	+0.30	600	2960	+0.022	+0.008
Pitch-Flap Out-of-Phase	0.065*	0.140	-0.065	+0.20	600	3480	+0.005	+0.001
Reduced Lock Number	0.085	0.150	-0.075	-0.10	650	4390	-0.014	-0.021
Cyclic Pitch: 2° Aft	0.185*	0.125	+0.055	-0.20	610	5710	-0.0170	-0.013
4° Fwd / 10° Fwd / 14° Fwd	0.300	0.415	-0.210	+0.05	590	4280	-0.014	-0.025
Swashplate Dihedral: 5.5°	0.200*	0.320	-0.140	+0.10	600	2490	0	-0.008
1.5° / -6.5° / -10.5°	0.430	0.290	-0.05	-0.45	550	8000	-0.039	-0.036
Articulated Rotor: e/R = 0.05 Drag Lift = 0.075 Blade Linear Twist = -4° 7.5 Deg Input at 4 Deg/Sec, 1 Sec Delay	0.260	0.345	-0.185	-0.10	550	5870	-0.026	-0.031
Drag Lift = 0.15 Blade Linear Twist = -4° 10 Deg Input at 4 Deg/Sec, 1 Sec Delay	0.275	0.360	-0.20	-0.20	525	7000	-0.036	-0.039

*For these cases, blade flapping envelope reduced by application of collective pitch.

TABLE 17

TIME IN SECONDS TO ATTAIN ROTOR AND HELICOPTER DIVERGENCE CRITERIA

(250 KNOTS, COMPLETE POWER FAILURE, NO INPUTS)

CRITERIA \ CONFIGURATION NUMBER	45	46	47	48
Fwd Rotor Flap: $\pm$ 0.20 Rad	2.9	2.7	2.7	5.0+
Aft Rotor Flap: $\pm$ 0.20 Rad	2.8	2.6	2.6	4.9
Rotor Tip Speed: 500 fps	2.7	2.4	2.6	5.0+
Sink Speed: 1500 fpm	5.0	5.0+	4.4	5.0+
Angle of Attack: 20 deg	5.0+	4.4	5.0+	5.0+
Sideslip Angle: 10 deg	3.9	3.3	3.7	5.0+
Roll Rate: 10 deg/sec	3.7	2.8	3.7	5.0+
Pitch Rate: 10 deg/sec	5.0+	5.0+	4.7	5.0+
Yaw Rate: 10 deg/sec	3.8	2.7	3.9	5.0+
Trim Horsepower	2716	2793	2735	2780
Fwd Blade Load: C_T/σ = 0.12	3.6	2.9	4.3	5.0+
Aft Blade Load: C_T/σ = 0.12	3.0	2.5	2.9	4.4

TABLE 18

COMPLETE POWER FAILURE AT 250 KNOTS WITH STANDARD COLLECTIVE CONTROL INPUTS

ROTOR AND HELICOPTER RESPONSES \ CONFIGUPATION NUMBER	45	46	47	48
Max. Peak-to-Peak Flapping:				
Fwd Rotor (Rad)	0.51	0.21	0.23	0.39
Aft Rotor (Rad)	0.60	0.37	0.37	0.58
Min. Blade Flapping Over Fuselage:				
Aft Rotor (Rad)	-0.34	-0.20	-0.19	-0.32
Min. Normal Accel. (g's)	-1.00	-0.52	-0.52	-1.70
Min. Rotor Tip Speed (ft/sec)	545	550	550	580
Sink Speed at 5 Sec. (ft/min)	11700	4200	4300	-
Peak Blade Loading Parameter:				
Fwd Rotor (C_T/σ)	-0.065	-0.030	-0.026	-0.170
Aft Rotor (C_T/σ)	-0.071	-0.060	-0.061	-0.155

All response peaks are read before, during, or within ½ second after collective reduction.

TABLE 19

CROSS-INDEX OF CASES SELECTED FOR AEROELASTIC ANALYSIS

Figure No. In Aeroelastic Analysis	Figure No. Of Corresponding Time History	Configuration Number
21	87	3
22	79	6
23	91	16
24	94	28
25	97	30
26	98	32
27	100	34
28	101	35
29	102	38
30	103	40
31	104	42
32	105	44
33	106	7
34	107	8
35	110	45
36	92	22
37	-	6
38	99	6 (optimum B_{1T})
39	85	6
40	112	45

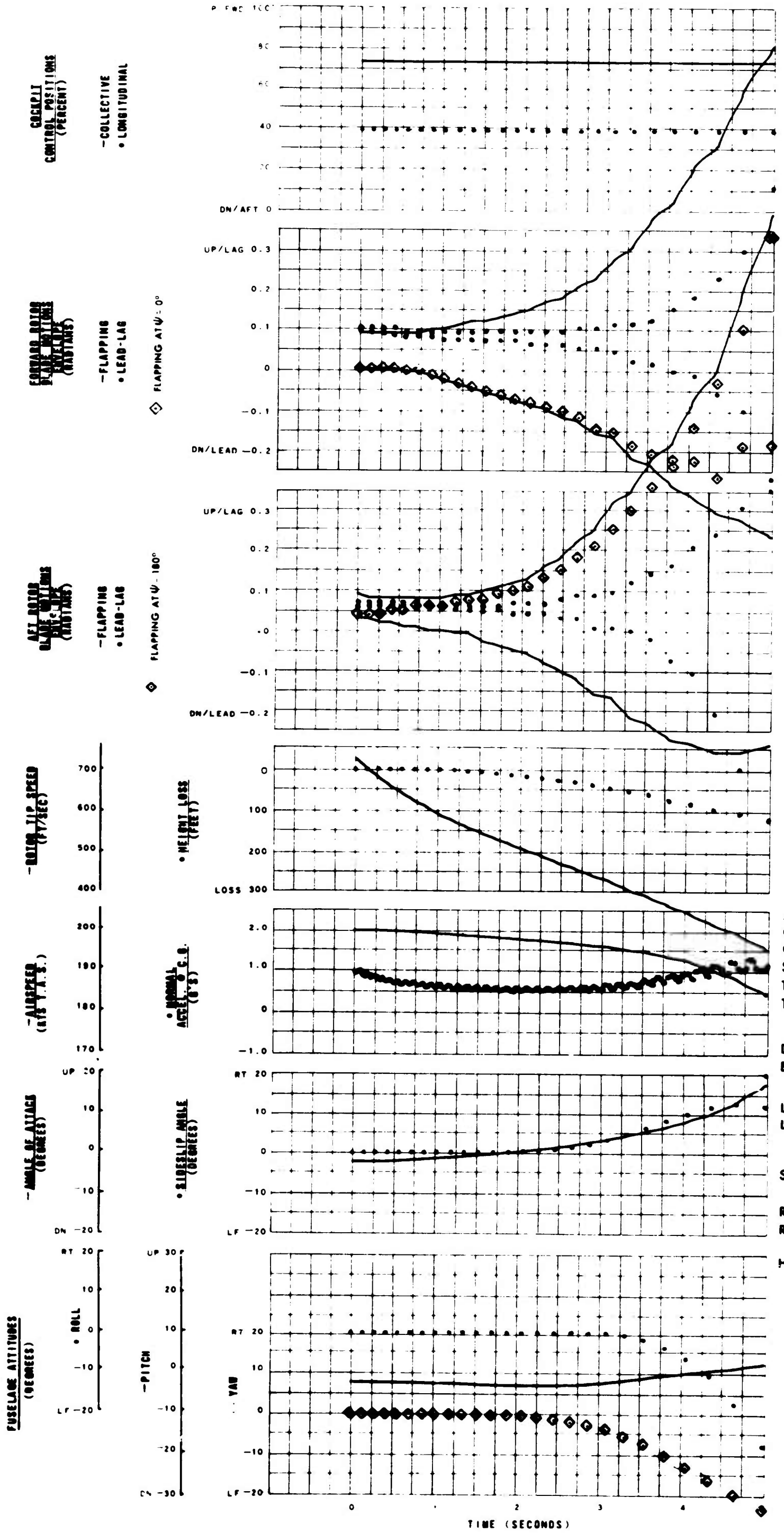

AIRSPEED	200 KT
GROSS WEIGHT	30,000 LB
C. G.	5 IN FWD
SEA LEVEL, STANDARD DAY	
TIP SPEED	723 FPS
TIP MACH NO	0.95
DRAG/LIFT	0.15
BLADE TWIST	-4 DEG
LOCK NO	4.38
LONG CYCLIC PITCH	
FWD ROTOR	8 DEG FWD
AFT ROTOR	8 DEG FWD
SWASHPLATE	
CATHEDRAL	2.5 DEG
ROTOR OVERLAP	35%
RELATIVE AFT ROTOR HEIGHT	8%
HINGE OFFSET	5%

Figure 57. Configuration 6.

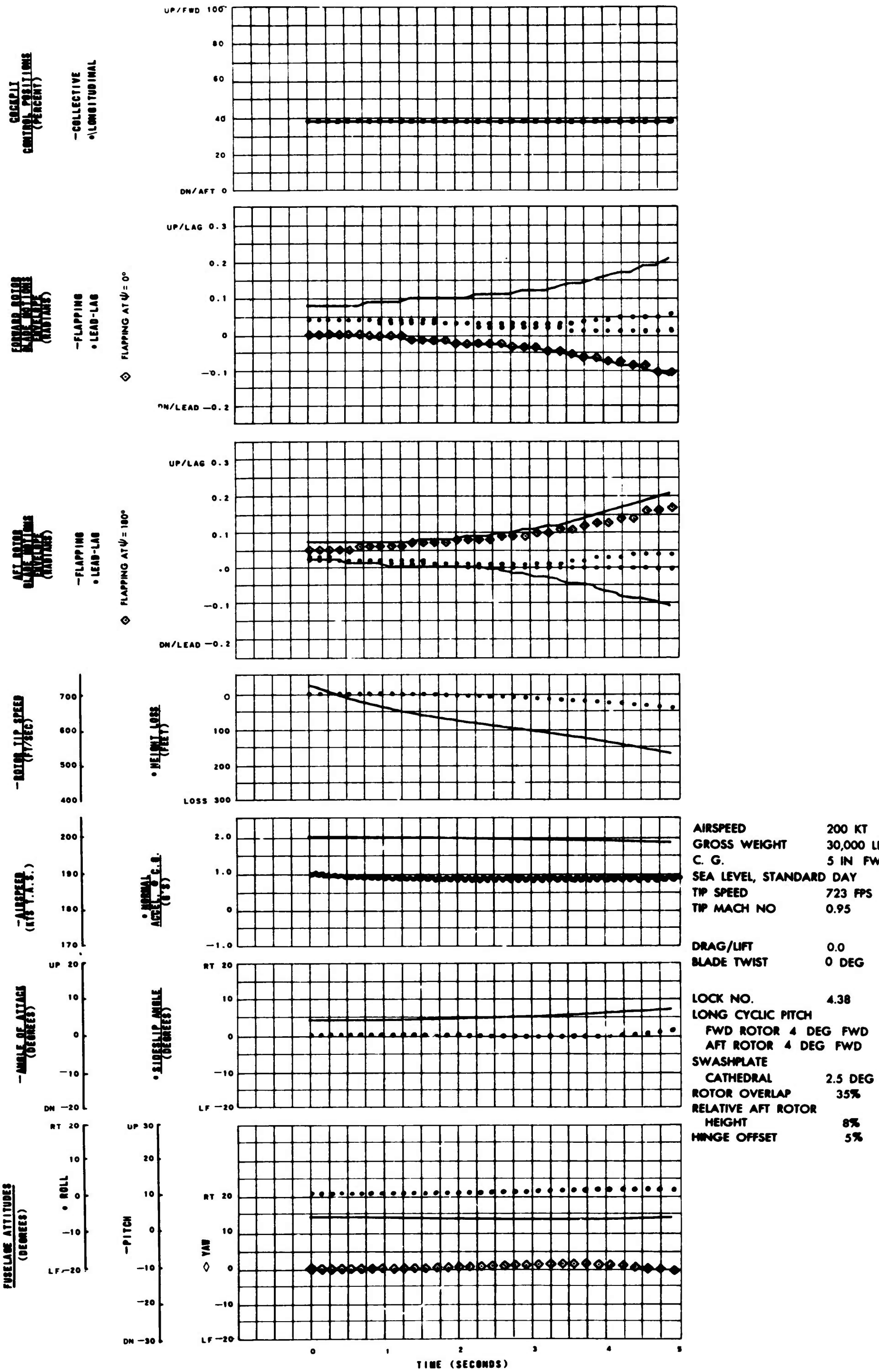

AIRSPEED	200 KT
GROSS WEIGHT	30,000 LB
C. G.	5 IN FWD
SEA LEVEL, STANDARD DAY	
TIP SPEED	723 FPS
TIP MACH NO	0.95
DRAG/LIFT	0.0
BLADE TWIST	0 DEG
LOCK NO.	4.38
LONG CYCLIC PITCH	
FWD ROTOR	4 DEG FWD
AFT ROTOR	4 DEG FWD
SWASHPLATE	
CATHEDRAL	2.5 DEG
ROTOR OVERLAP	35%
RELATIVE AFT ROTOR HEIGHT	8%
HINGE OFFSET	5%

Figure 58. Configuration 4.

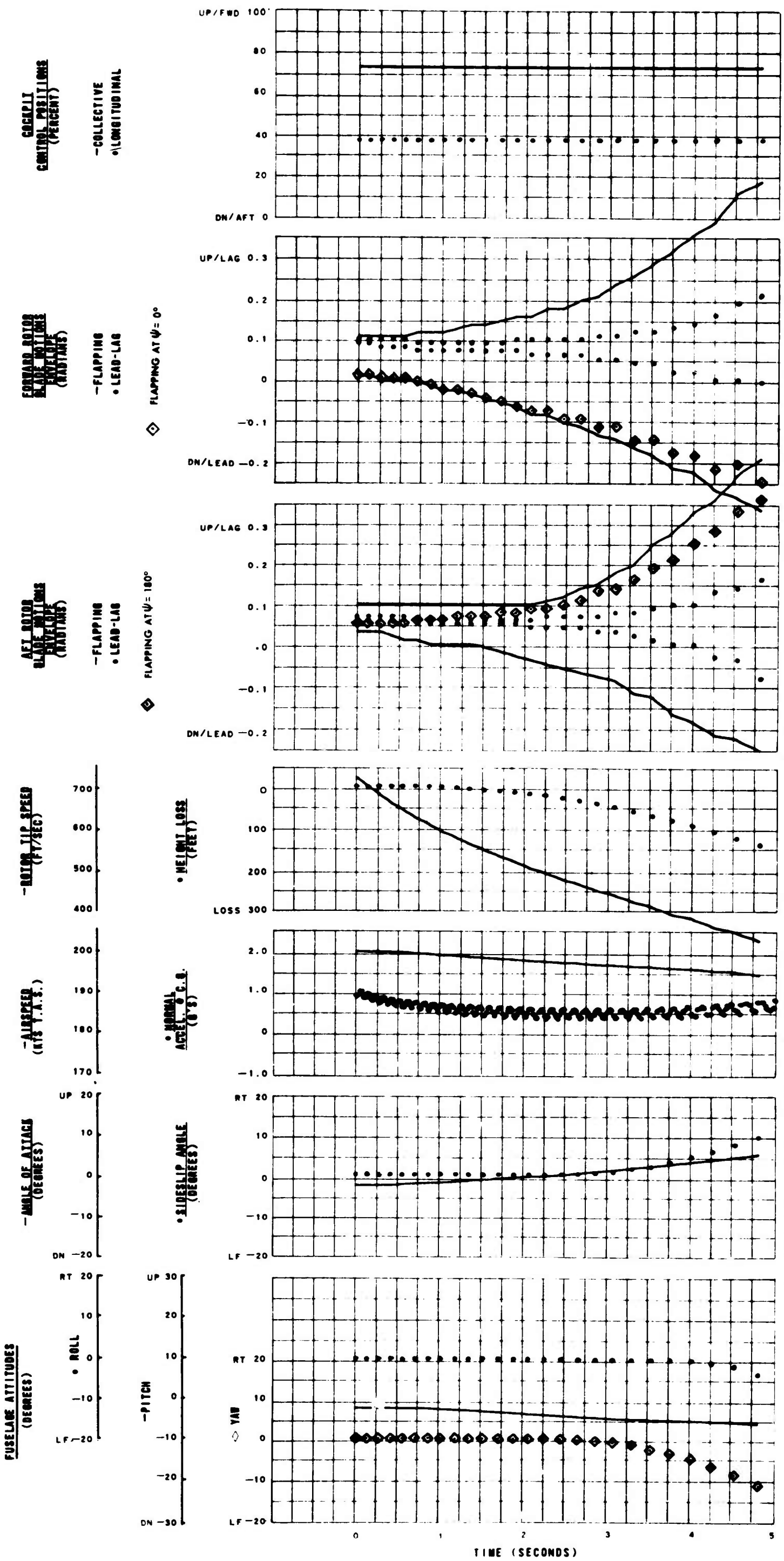

AIRSPEED	200 KT
GROSS WEIGHT	30,000 LB
C. G.	5 IN FWD
SEA LEVEL, STANDARD DAY	
TIP SPEED	723 FPS
TIP MACH NO	0.95
DRAG/LIFT	0.15
BLADE TWIST	-4 DEG
LOCK NO	4.38
LONG CYCLIC PITCH	
FWD ROTOR	8 DEG FWD
AFT ROTOR	8 DEG FWD
SWASHPLATE	
CATHEDRAL	2.5 DEG
ROTOR OVERLAP	35%
RELATIVE AFT ROTOR HEIGHT	8%
HINGE OFFSET	0%

Figure 59. Configuration 3.

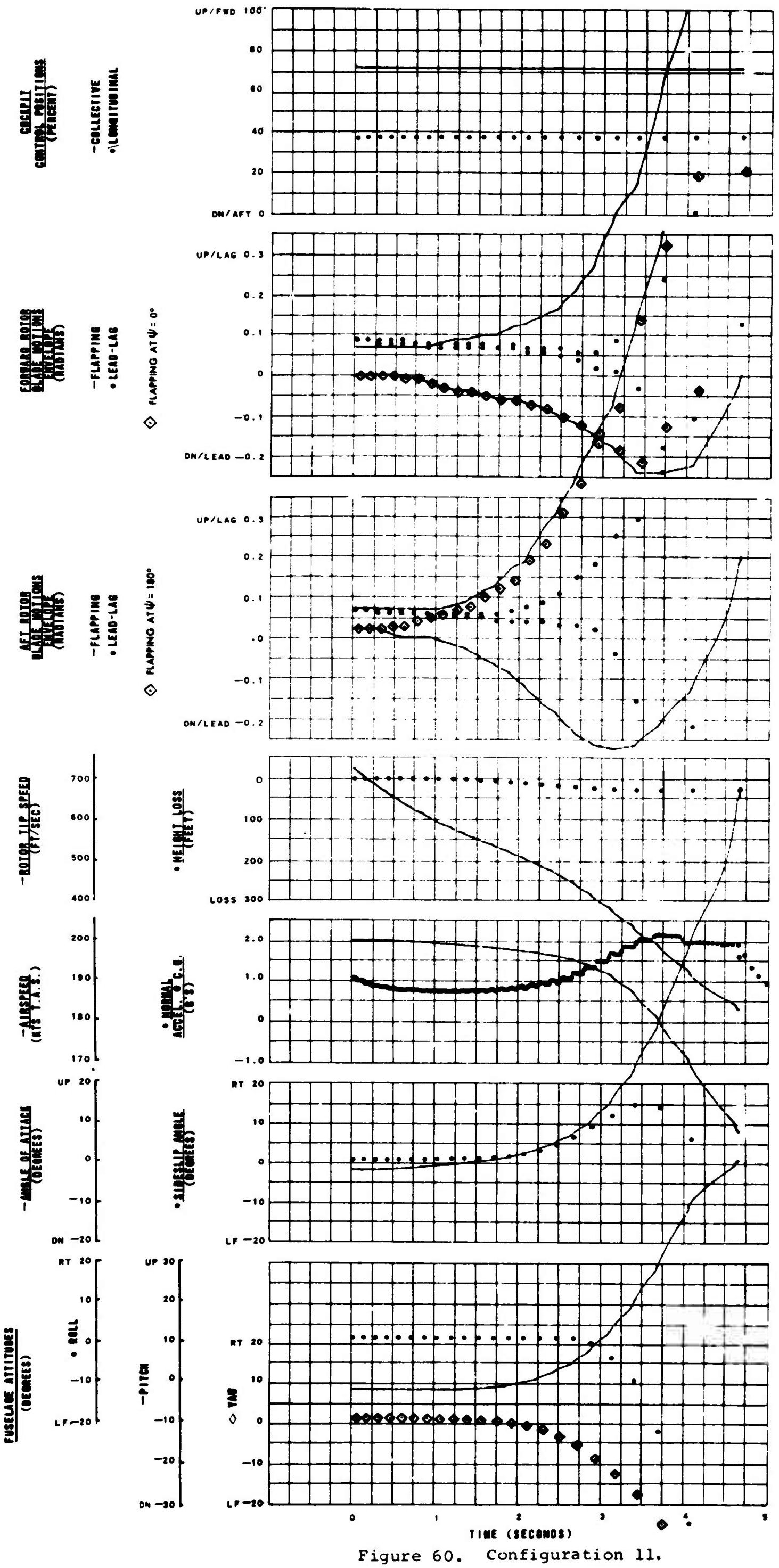

AIRSPEED	200 KT
GROSS WEIGHT	30,000 LB
C. G.	5 IN FWD
SEA LEVEL, STANDARD DAY	
TIP SPEED	723 FPS
TIP MACH NO	0.95
DRAG/LIFT	0.15
BLADE TWIST	—4 DEG
LOCK NO.	4.38
LONG CYCLIC PITCH	
FWD ROTOR	8 DEG FWD
AFT ROTOR	8 DEG FWD
SWASHPLATE CATHEDRAL	2.5 DEG
ROTOR OVERLAP	35%
RELATIVE AFT ROTOR HEIGHT	8%
HINGE OFFSET	15%

Figure 60. Configuration 11.

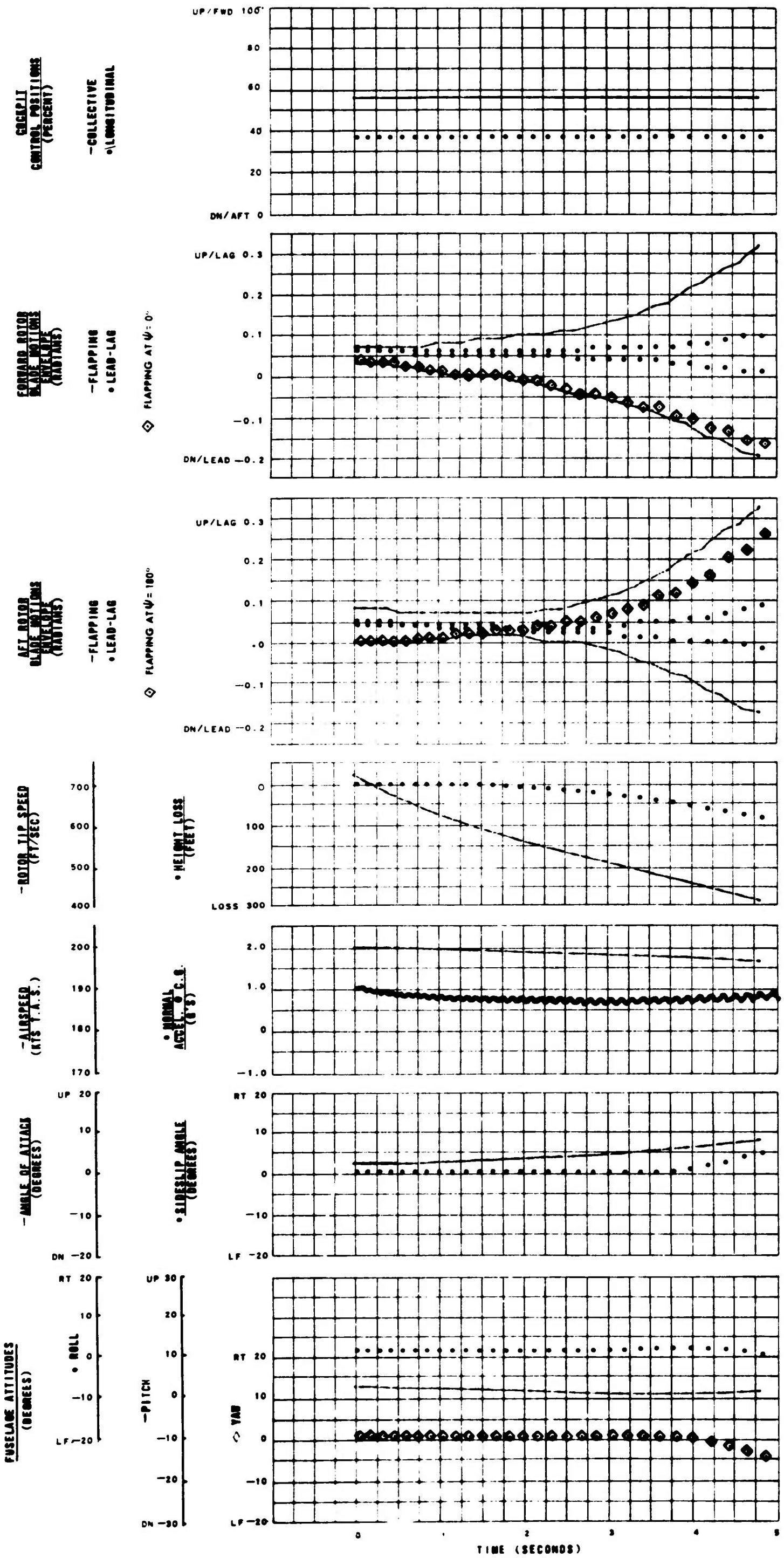

AIRSPEED	200 KT
GROSS WEIGHT	30,000 LB
C. G.	5 IN FWD
SEA LEVEL, STANDARD DAY	
TIP SPEED	723 FPS
TIP MACH NO	0.95
DRAG/LIFT	0.075
BLADE TWIST	—4 DEG
LOCK NO.	4.38
LONG CYCLIC PITCH	
FWD ROTOR	8 DEG FWD
AFT ROTOR	8 DEG FWD
SWASHPLATE CATHEDRAL	2.5 DEG
ROTOR OVERLAP	35%
RELATIVE AFT ROTOR HEIGHT	8%
HINGE OFFSET	5%

Figure 61. Configuration 5.

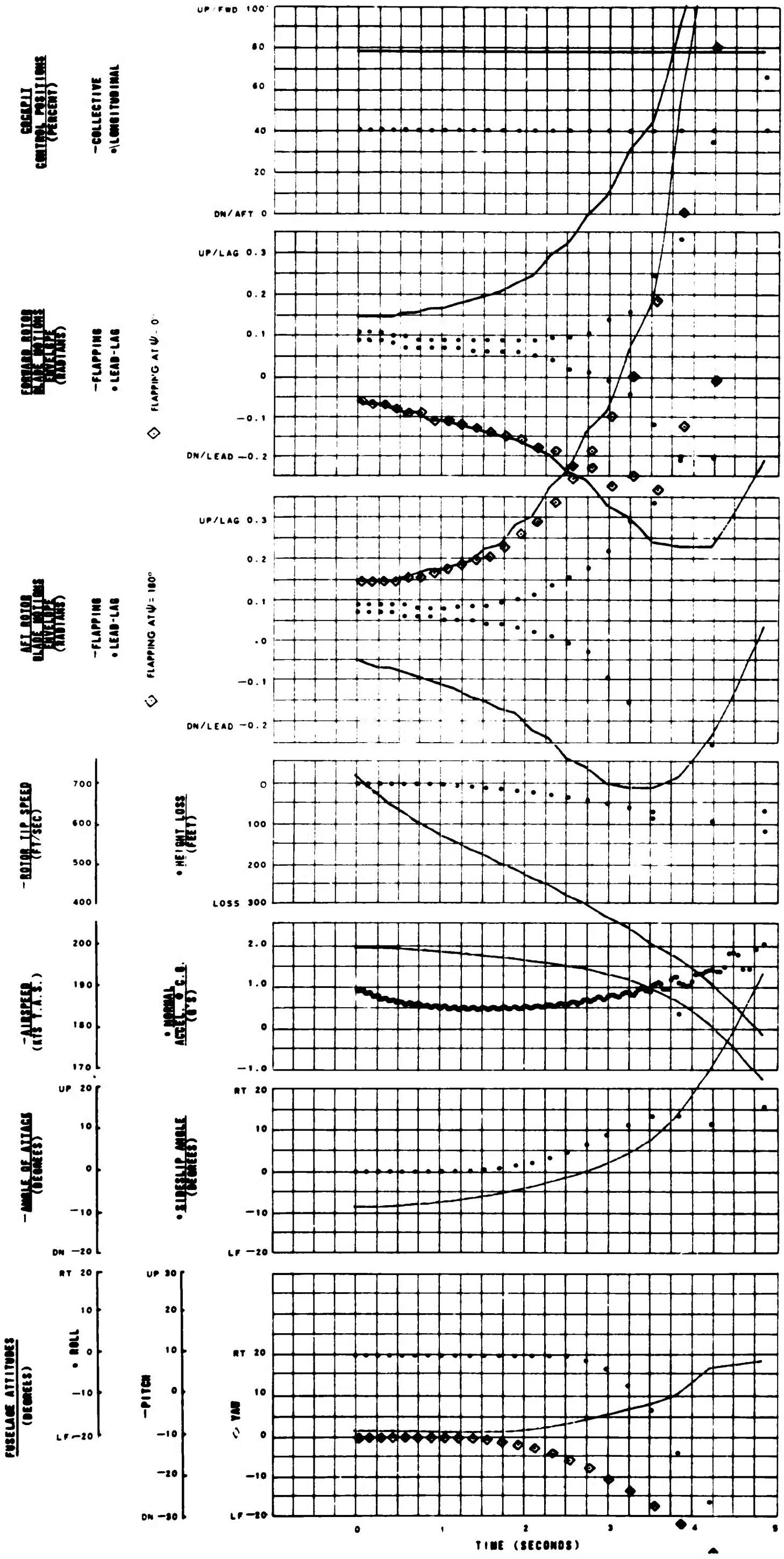

AIRSPEED	200 KT
GROSS WEIGHT	30,000 LB
C. G.	5 IN FWD
SEA LEVEL, STANDARD DAY	
TIP SPEED	723 FPS
TIP MACH NO	0.95
DRAG/LIFT	0.15
BLADE TWIST	—4 DEG
LOCK NO.	4.38
LONG CYCLIC PITCH	
FWD ROTOR 4 DEG FWD	
AFT ROTOR 4 DEG FWD	
SWASHPLATE	
CATHEDRAL	2.5 DEG
ROTOR OVERLAP	35%
RELATIVE AFT ROTOR	
HEIGHT	8%
HINGE OFFSET	5%

Figure 62. Configuration 30.

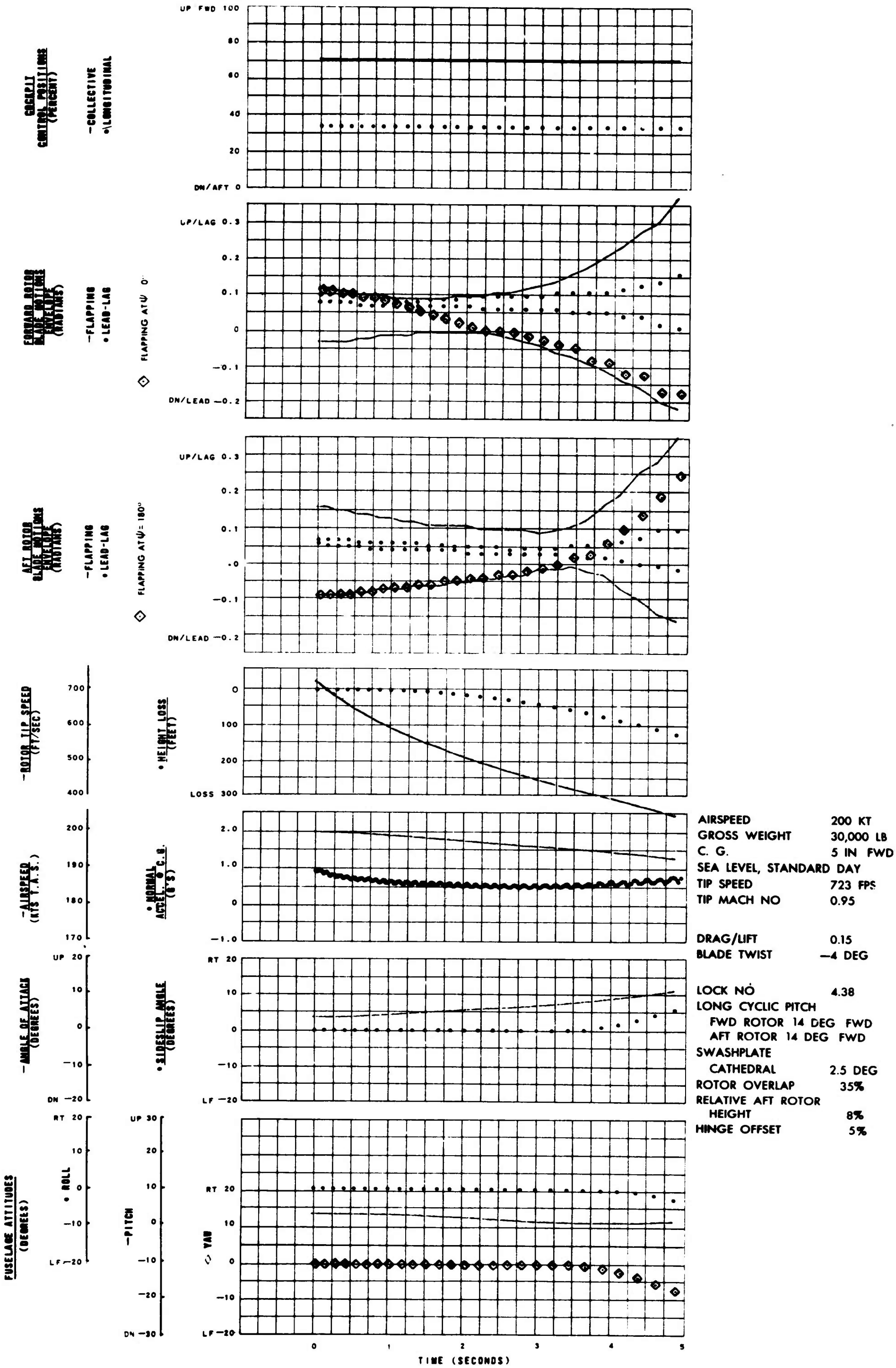

AIRSPEED	200 KT
GROSS WEIGHT	30,000 LB
C. G.	5 IN FWD
SEA LEVEL, STANDARD DAY	
TIP SPEED	723 FPS
TIP MACH NO	0.95
DRAG/LIFT	0.15
BLADE TWIST	—4 DEG
LOCK NO	4.38
LONG CYCLIC PITCH	
FWD ROTOR 14 DEG FWD	
AFT ROTOR 14 DEG FWD	
SWASHPLATE CATHEDRAL	2.5 DEG
ROTOR OVERLAP	35%
RELATIVE AFT ROTOR HEIGHT	8%
HINGE OFFSET	5%

Figure 63. Configuration 32$_4$

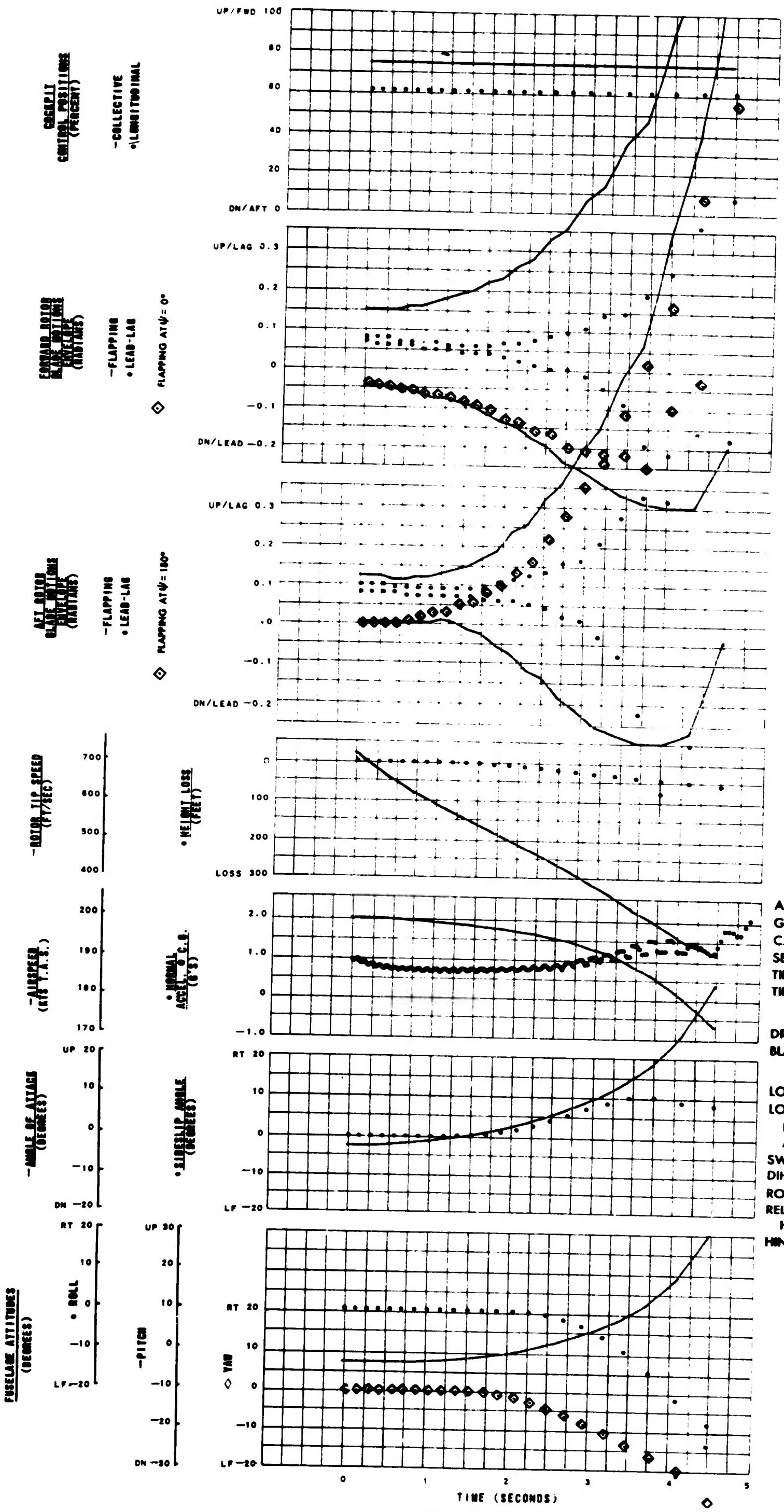

AIRSPEED	200 KT
GROSS WEIGHT	30,000 LB
C. G.	5 IN FWD
SEA LEVEL, STANDARD DAY	
TIP SPEED	723 FPS
TIP MACH NO	0.95
DRAG/LIFT	0.15
BLADE TWIST	—4 DEG
LOCK NO.	4.38
LONG CYCLIC PITCH	
FWD ROTOR	4 DEG FWD
AFT ROTOR	12 DEG FWD
SWASHPLATE	
DIHEDRAL	1.5 DEG
ROTOR OVERLAP	35%
RELATIVE AFT ROTOR HEIGHT	8%
HINGE OFFSET	5%

Figure 64. Configuration 34.

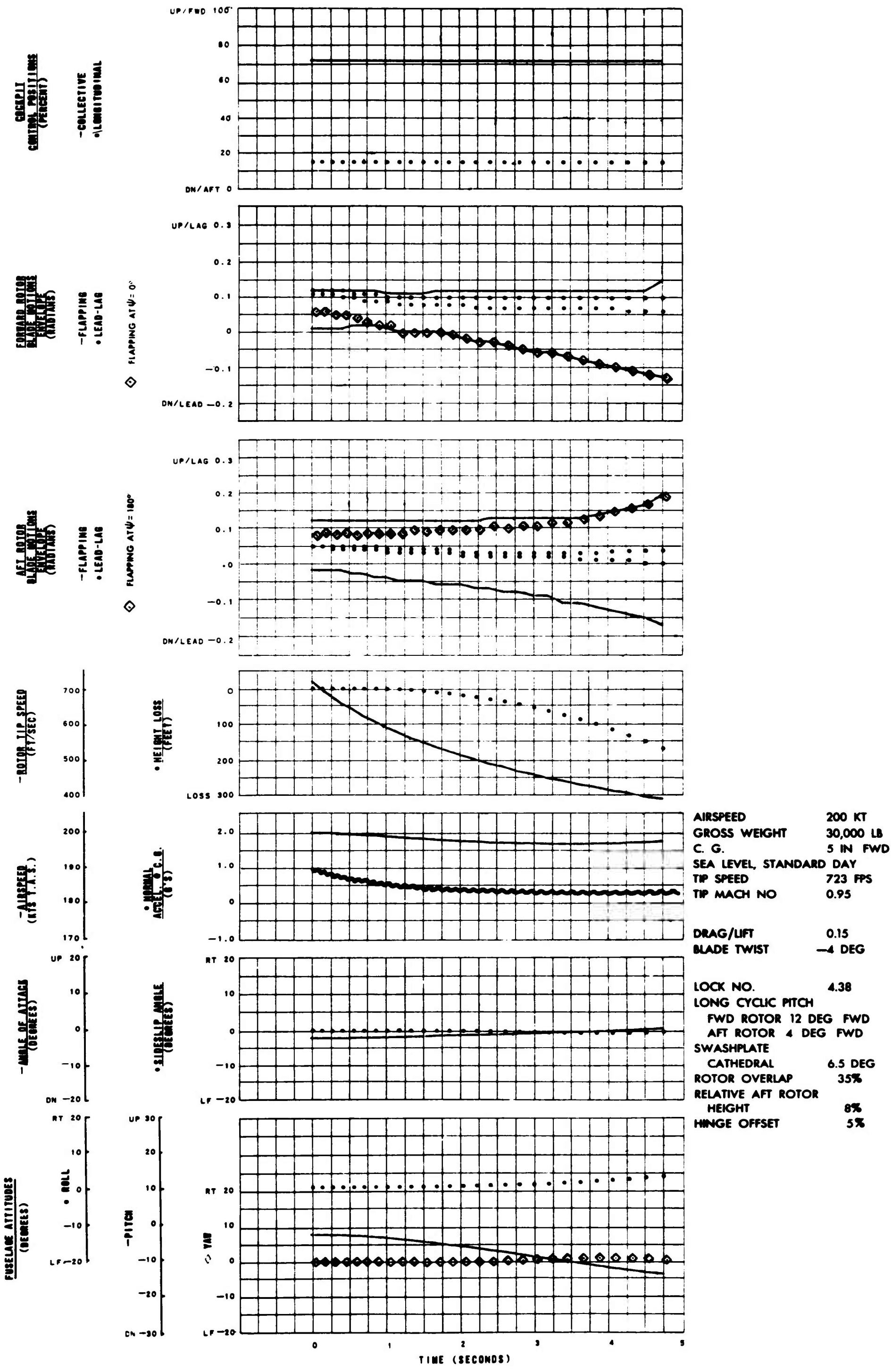

AIRSPEED	200 KT
GROSS WEIGHT	30,000 LB
C. G.	5 IN FWD
SEA LEVEL, STANDARD DAY	
TIP SPEED	723 FPS
TIP MACH NO	0.95
DRAG/LIFT	0.15
BLADE TWIST	–4 DEG
LOCK NO.	4.38
LONG CYCLIC PITCH	
FWD ROTOR	12 DEG FWD
AFT ROTOR	4 DEG FWD
SWASHPLATE	
CATHEDRAL	6.5 DEG
ROTOR OVERLAP	35%
RELATIVE AFT ROTOR HEIGHT	8%
HINGE OFFSET	5%

Figure 65. Configuration 35.

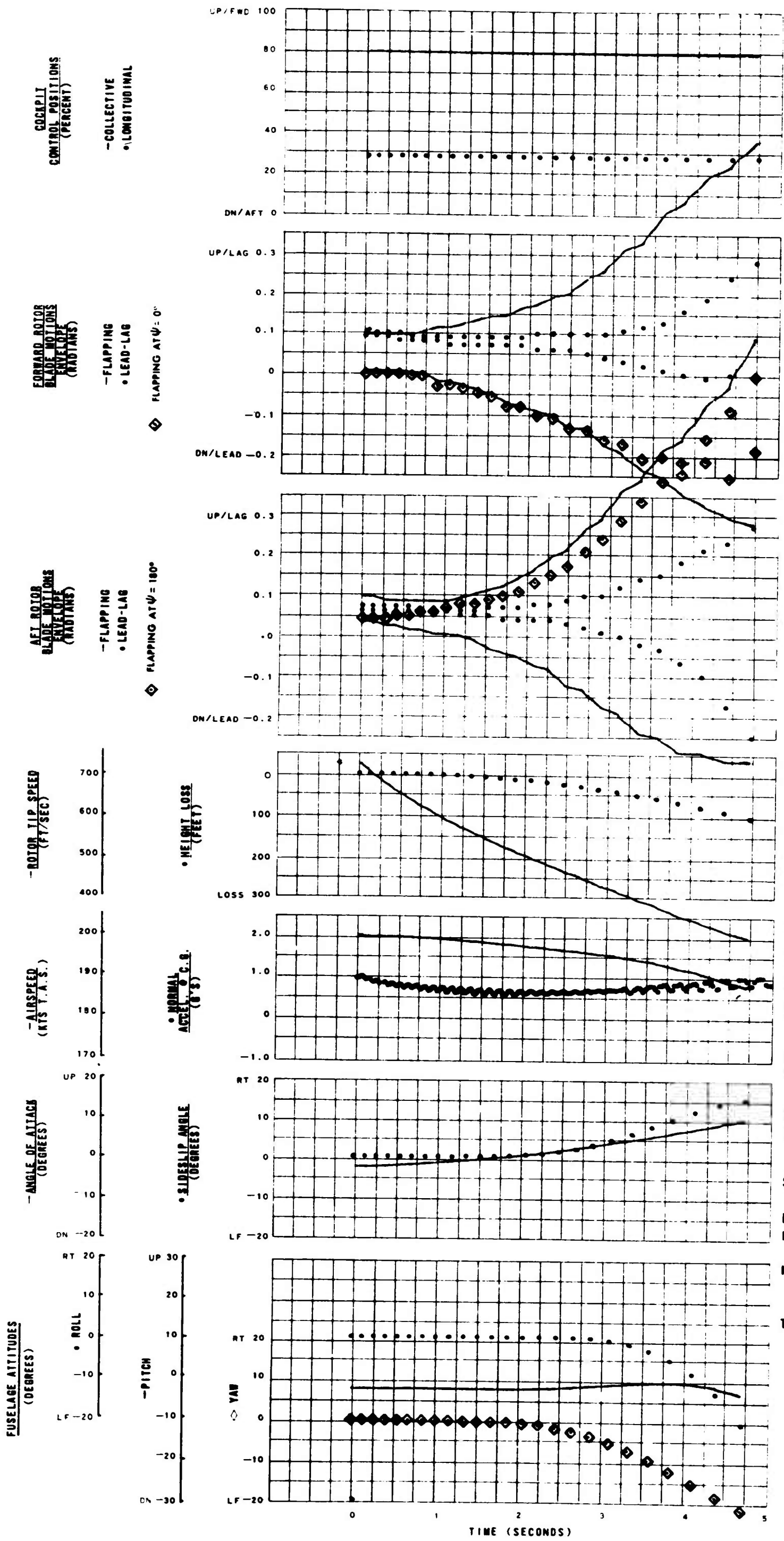

AIRSPEED	200 KT
GROSS WEIGHT	30,000 LB
C. G.	5 IN FWD
SEA LEVEL, STANDARD DAY	
TIP SPEED	723 FPS
TIP MACH NO	0.95
DRAG/LIFT	0.15
BLADE TWIST	—4 DEG
LOCK NO	4.38
LONG CYCLIC PITCH	
FWD ROTOR	8 DEG FWD
AFT ROTOR	8 DEG FWD
SWASHPLATE	
CATHEDRAL	2.5 DEG
ROTOR OVERLAP	35%
RELATIVE AFT ROTOR	
HEIGHT	8%
HINGE OFFSET	5%

TIP PATH PLANE CONTROLLER
30 DEG PITCH—CONE

Figure 66. Configuration 19.

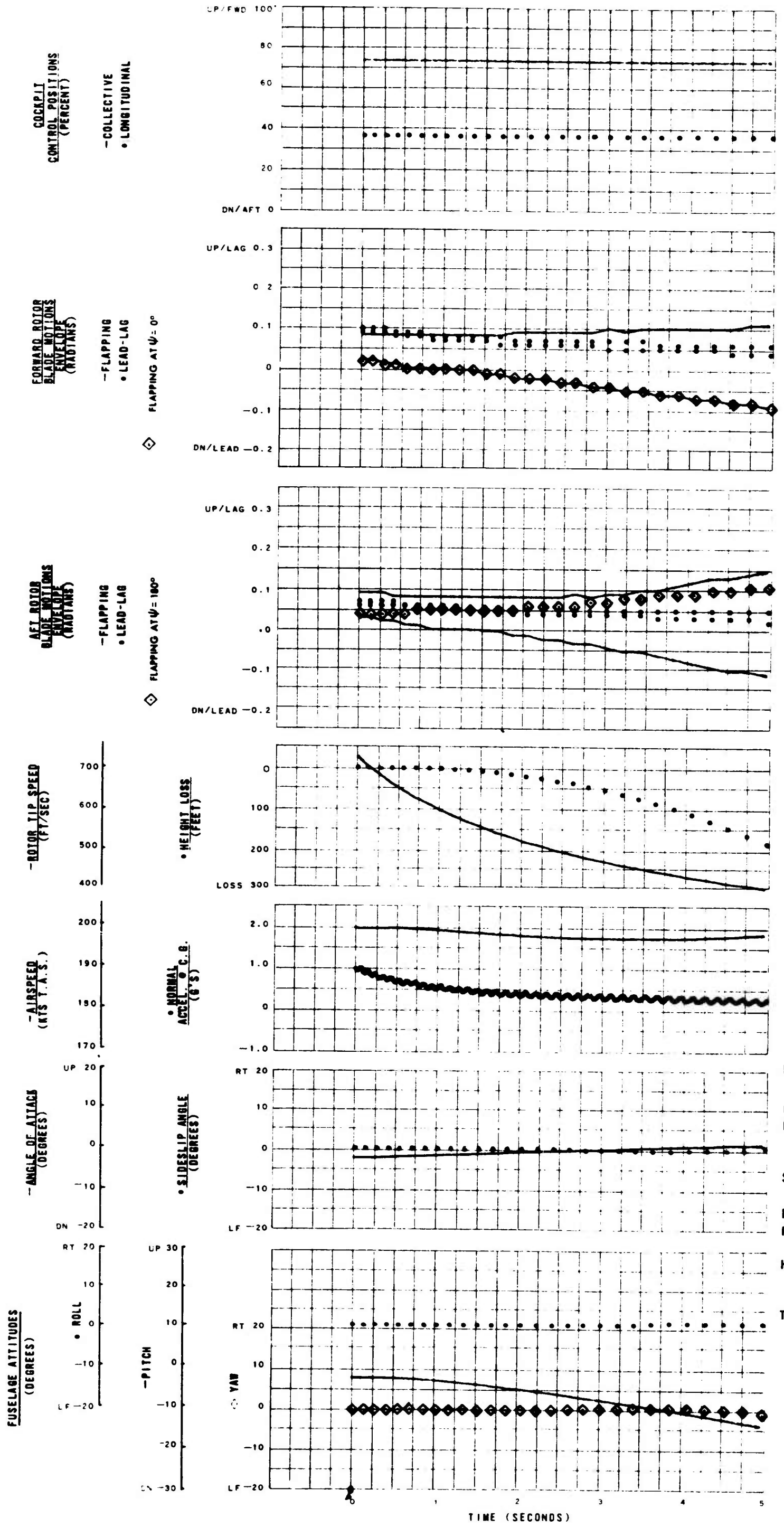

AIRSPEED	200 KT
GROSS WEIGHT	30,000 LB
C. G.	5 IN FWD
SEA LEVEL, STANDARD DAY	
TIP SPEED	723 FPS
TIP MACH NO	0.95
DRAG/LIFT	0.15
BLADE TWIST	—4 DEG
LOCK NO.	4.38
LONG CYCLIC PITCH	
FWD ROTOR	8 DEG FWD
AFT ROTOR	8 DEG FWD
SWASHPLATE CATHEDRAL	2.5 DEG
ROTOR OVERLAP	35%
RELATIVE AFT ROTOR HEIGHT	8%
HINGE OFFSET	5%

TIP PATH PLANE CONTROLLER

30 DEG PITCH—FLAP
(OUT OF PHASE)

Figure 67. Configuration 22.

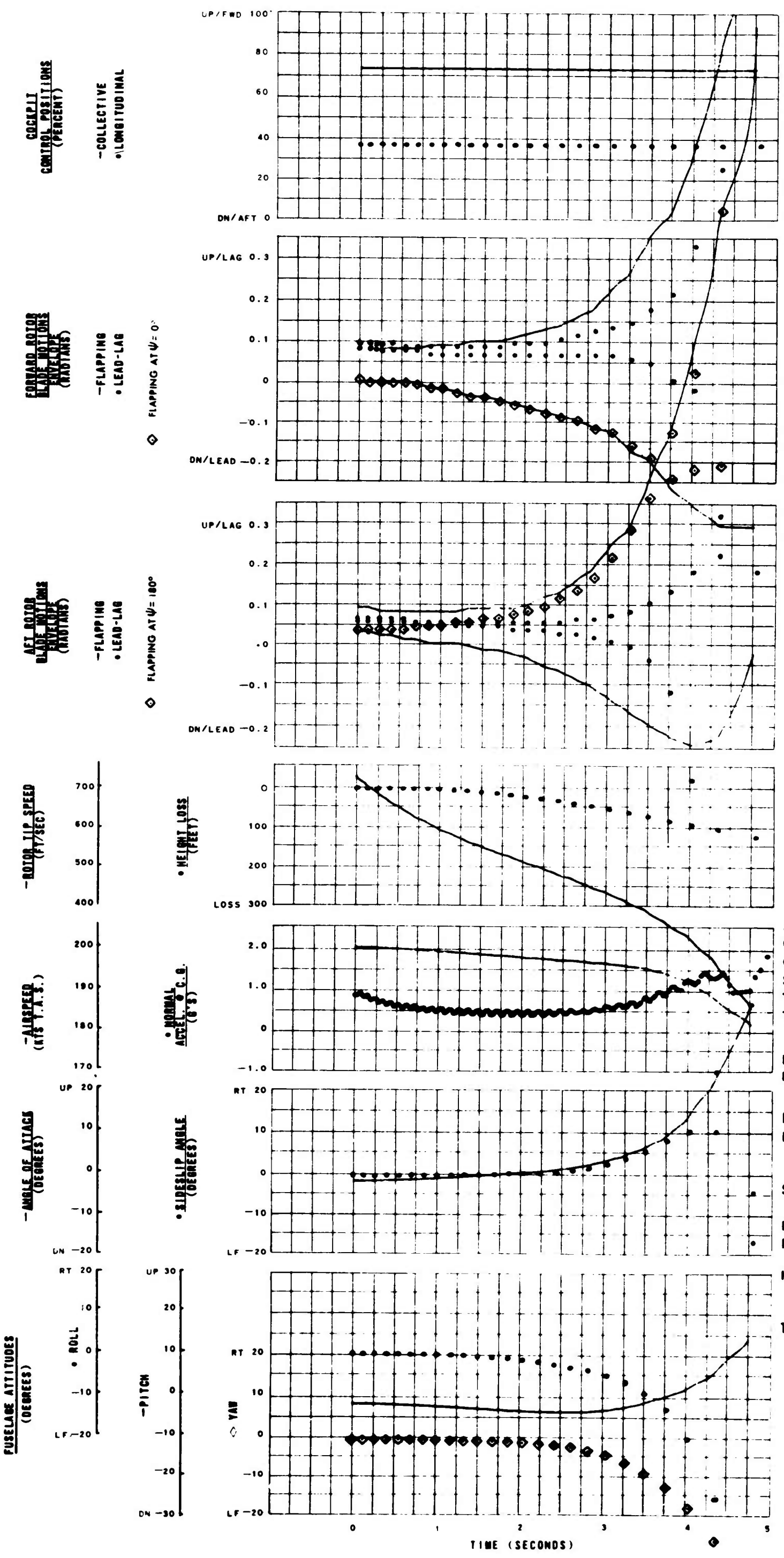

Figure 68. Configuration 24.

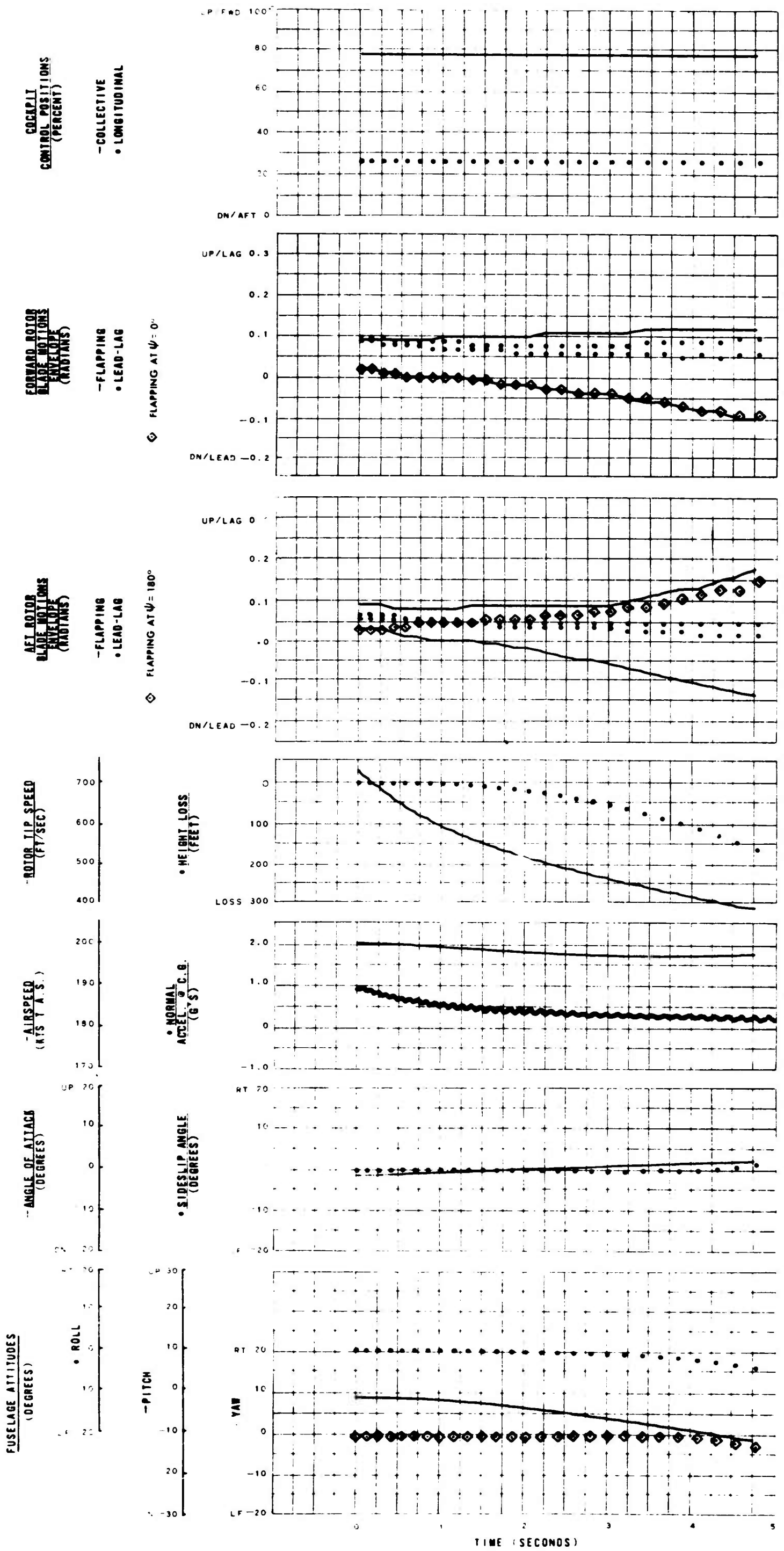

AIRSPEED	200 KT
GROSS WEIGHT	30,000 LB
C. G.	5 IN FWD
SEA LEVEL, STANDARD DAY	
TIP SPEED	723 FPS
TIP MACH NO	0.95
DRAG/LIFT	0.15
BLADE TWIST	−4 DEG
LOCK NO	4.38
LONG CYCLIC PITCH	
FWD ROTOR	8 DEG FWD
AFT ROTOR	8 DEG FWD
SWASHPLATE	
CATHEDRAL	2.5 DEG
ROTOR OVERLAP	35%
RELATIVE AFT ROTOR HEIGHT	8%
HINGE OFFSET	5%

TIP PATH PLANE CONTROLLER
30 DEG PITCH—CONE
30 DEG PITCH—FLAP
(OUT OF PHASE)

30 DEG PITCH - FLAP
(IN PHASE)

Figure 69. Configuration 25.

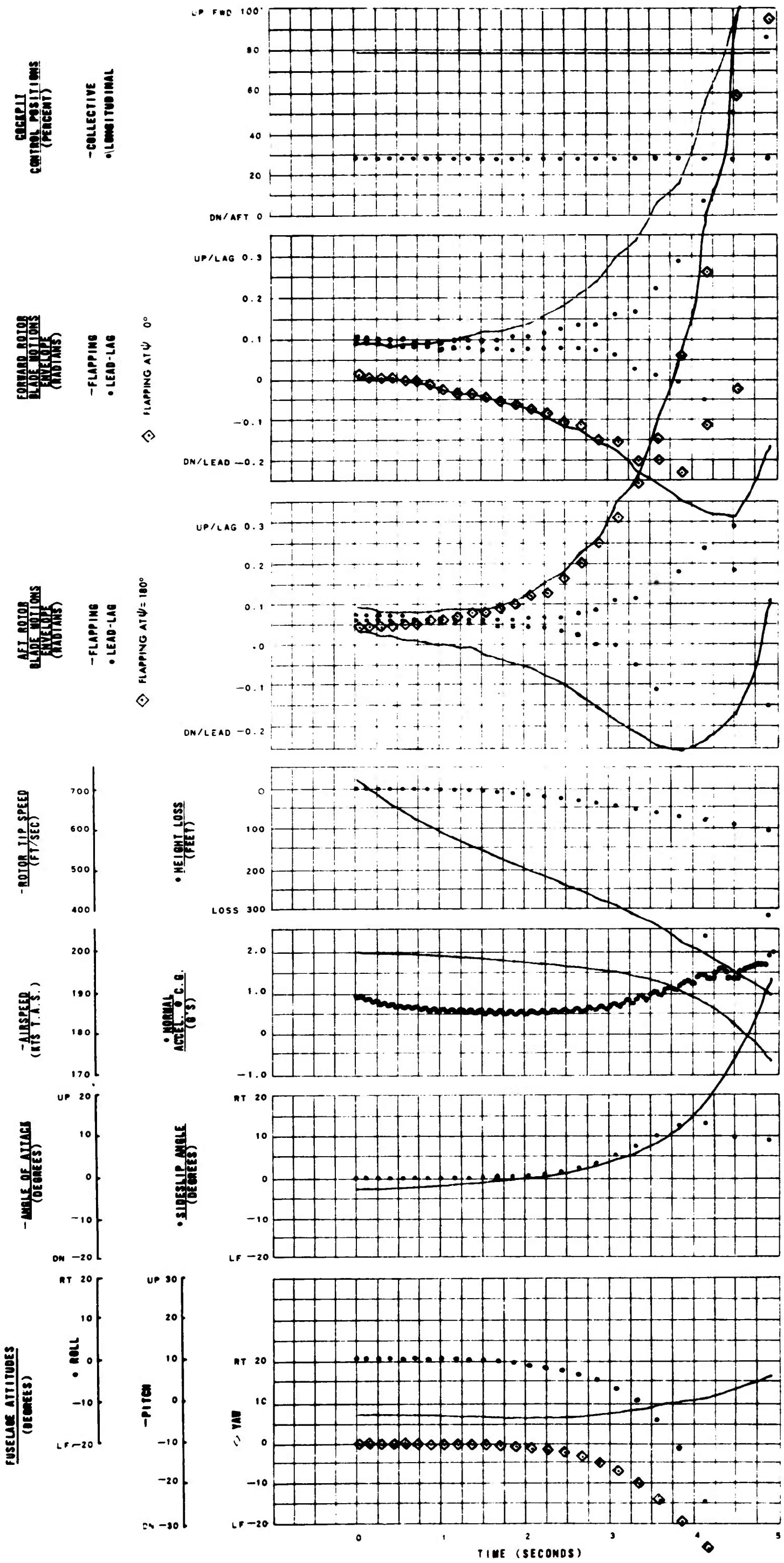

AIRSPEED	200 KT
GROSS WEIGHT	30,000 LB
C. G.	5 IN FWD
SEA LEVEL, STANDARD DAY	
TIP SPEED	723 FPS
TIP MACH NO	0.95
DRAG/LIFT	0.15
BLADE TWIST	−4 DEG
LOCK NO	4.38
LONG CYCLIC PITCH	
FWD ROTOR	8 DEG FWD
AFT ROTOR	8 DEG FWD
SWASHPLATE CATHEDRAL	2.5 DEG
ROTOR OVERLAP	35%
RELATIVE AFT ROTOR HEIGHT	8%
HINGE OFFSET	5%
DELTA THREE	30 DEG

Figure 70. Configuration 16.

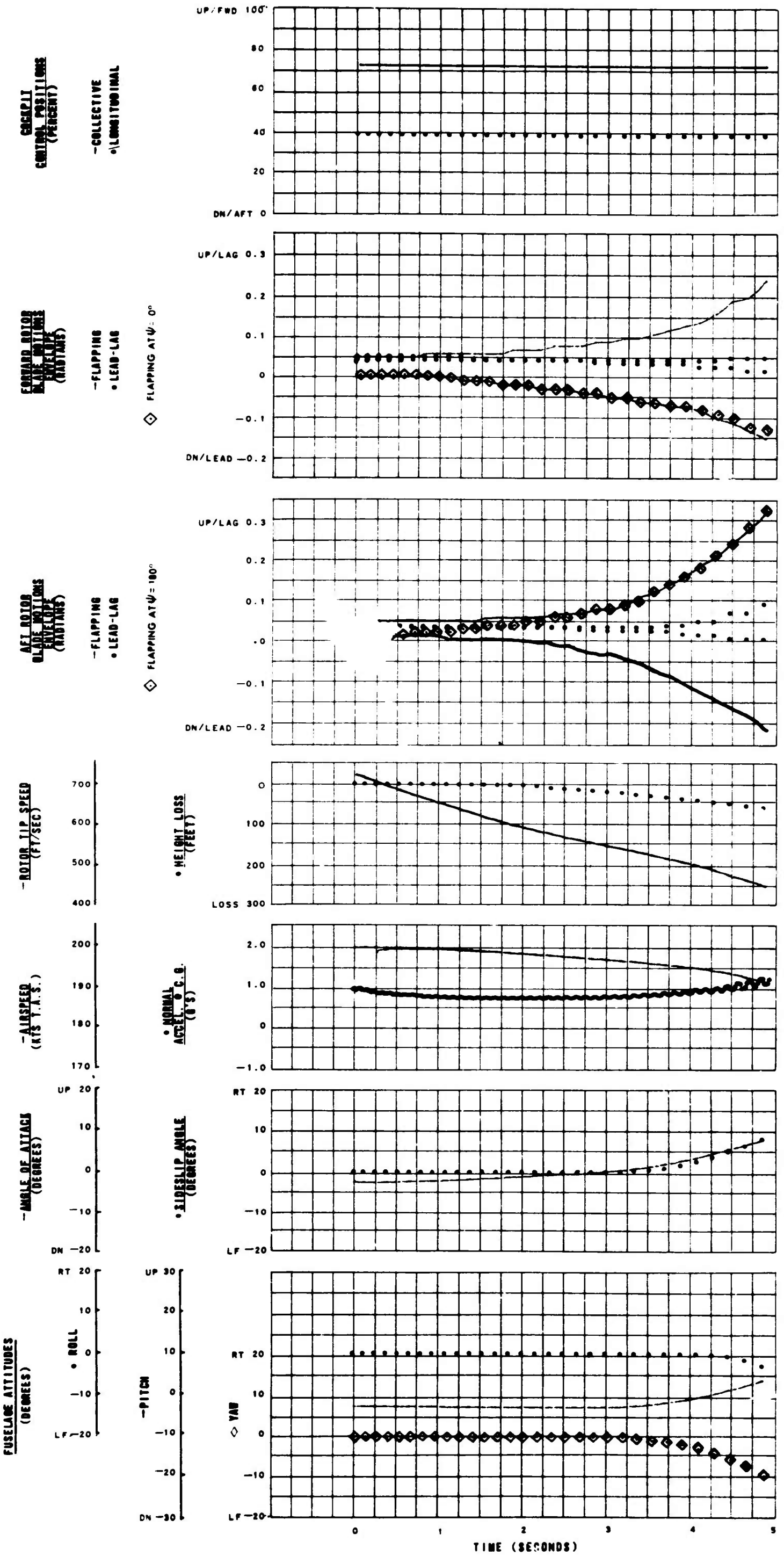

AIRSPEED	200 KT
GROSS WEIGHT	30,000 LB
C. G.	5 IN FWD
SEA LEVEL, STANDARD DAY	
TIP SPEED	723 FPS
TIP MACH NO	0.95
DRAG/LIFT	0.15
BLADE TWIST	−4 DEG
LOCK NO	2.19
LONG CYCLIC PITCH	
FWD ROTOR	8 DEG FWD
AFT ROTOR	8 DEG FWD
SWASHPLATE CATHEDRAL	2.5 DEG
ROTOR OVERLAP	35%
RELATIVE AFT ROTOR HEIGHT	8%
HINGE OFFSET	5%

Figure 71. Configuration 28.

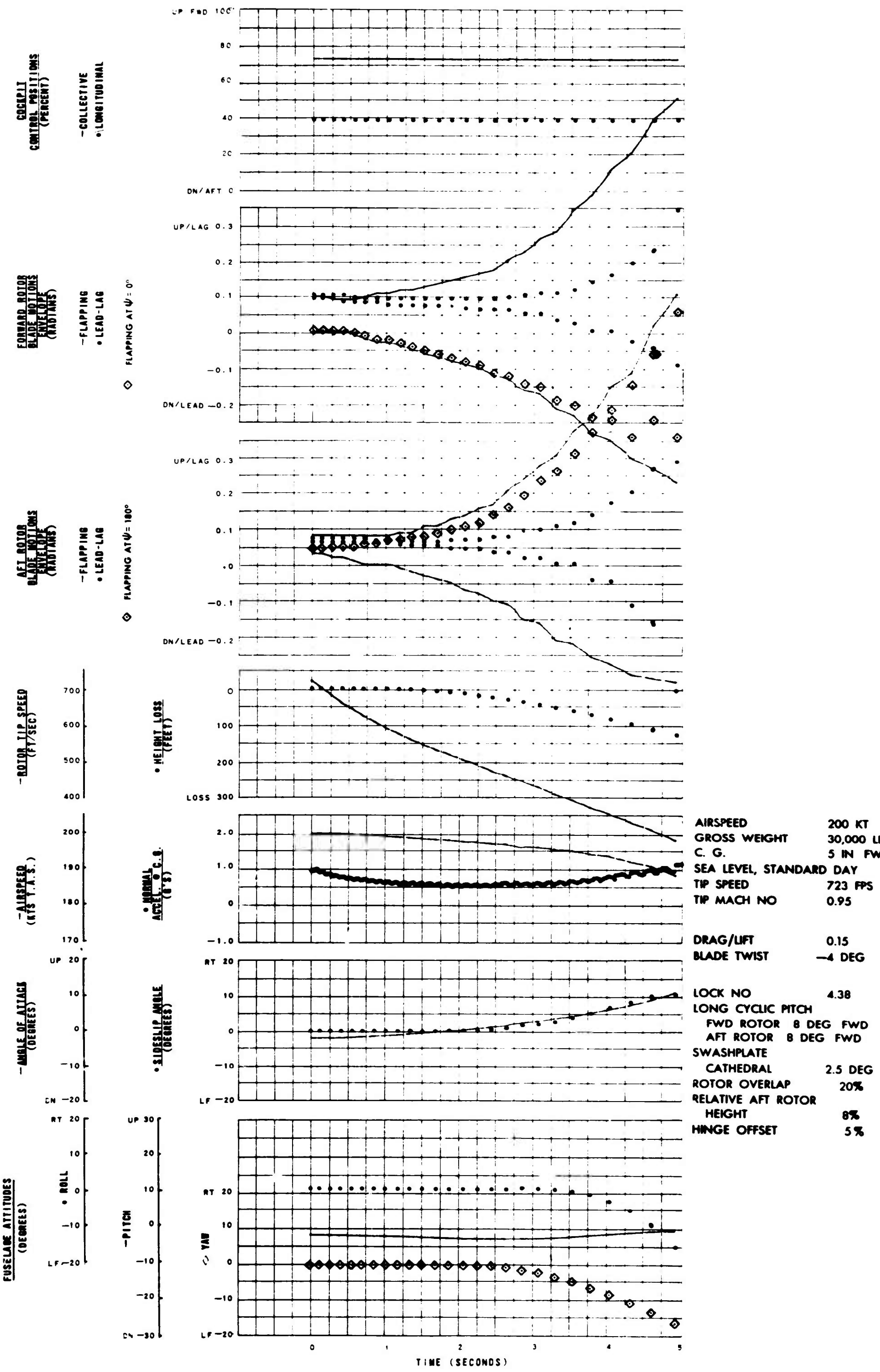

AIRSPEED	200 KT
GROSS WEIGHT	30,000 LB
C. G.	5 IN FWD
SEA LEVEL, STANDARD DAY	
TIP SPEED	723 FPS
TIP MACH NO	0.95
DRAG/LIFT	0.15
BLADE TWIST	–4 DEG
LOCK NO	4.38
LONG CYCLIC PITCH	
FWD ROTOR	8 DEG FWD
AFT ROTOR	8 DEG FWD
SWASHPLATE	
CATHEDRAL	2.5 DEG
ROTOR OVERLAP	20%
RELATIVE AFT ROTOR HEIGHT	8%
HINGE OFFSET	5%

Figure 72. Configuration 38.

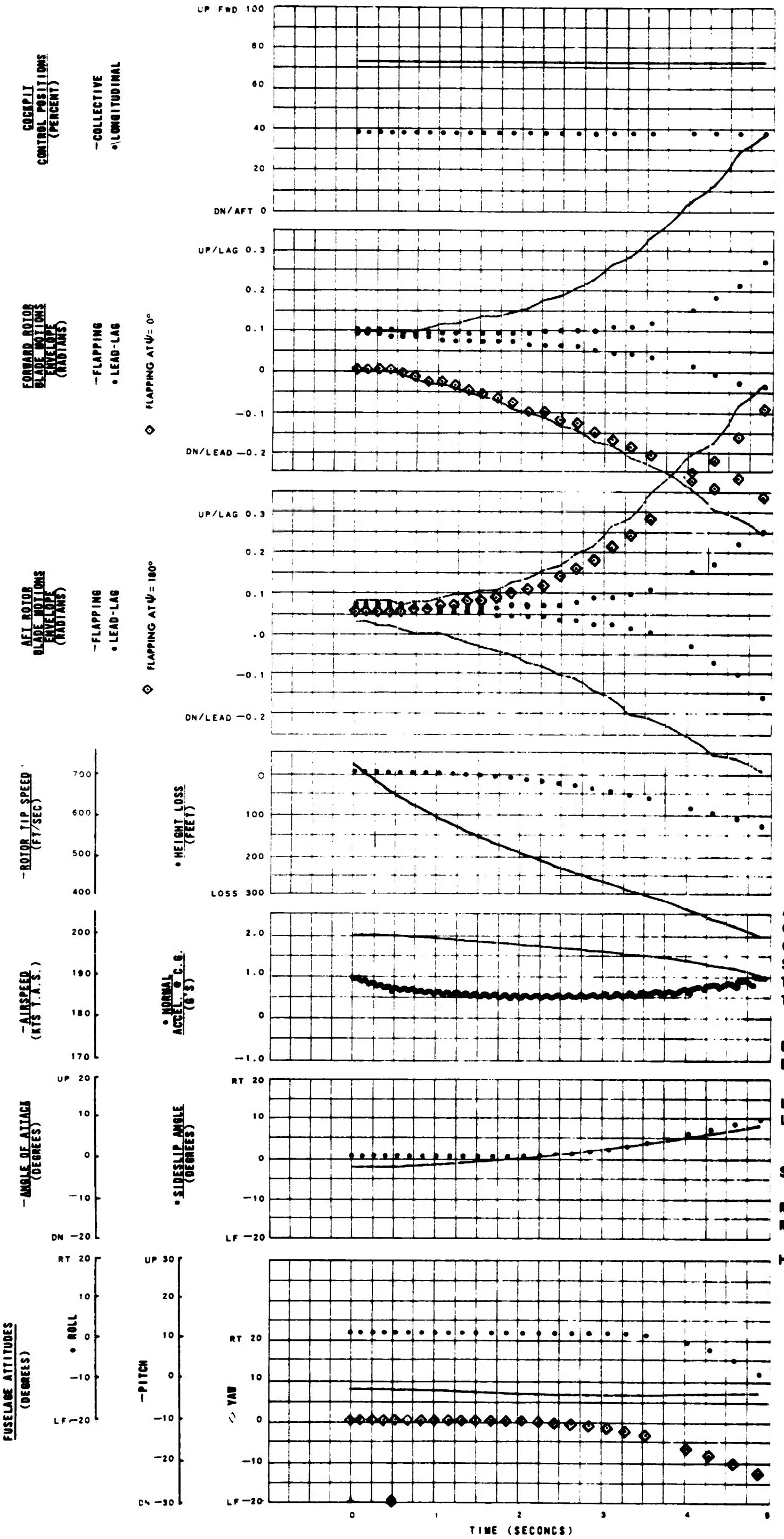

AIRSPEED	200 KT
GROSS WEIGHT	30,000 LB
C. G.	5 IN FWD
SEA LEVEL, STANDARD DAY	
TIP SPEED	723 FPS
TIP MACH NO	0.95
DRAG/LIFT	0.15
BLADE TWIST	—4 DEG
LOCK NO.	4.38
LONG CYCLIC PITCH	
FWD ROTOR	8 DEG FWD
AFT ROTOR	8 DEG FWD
SWASHPLATE CATHEDRAL	2.5 DEG.
ROTOR OVERLAP	0%
RELATIVE AFT ROTOR HEIGHT	8%
HINGE OFFSET	5%

Figure 73. Configuration 40.

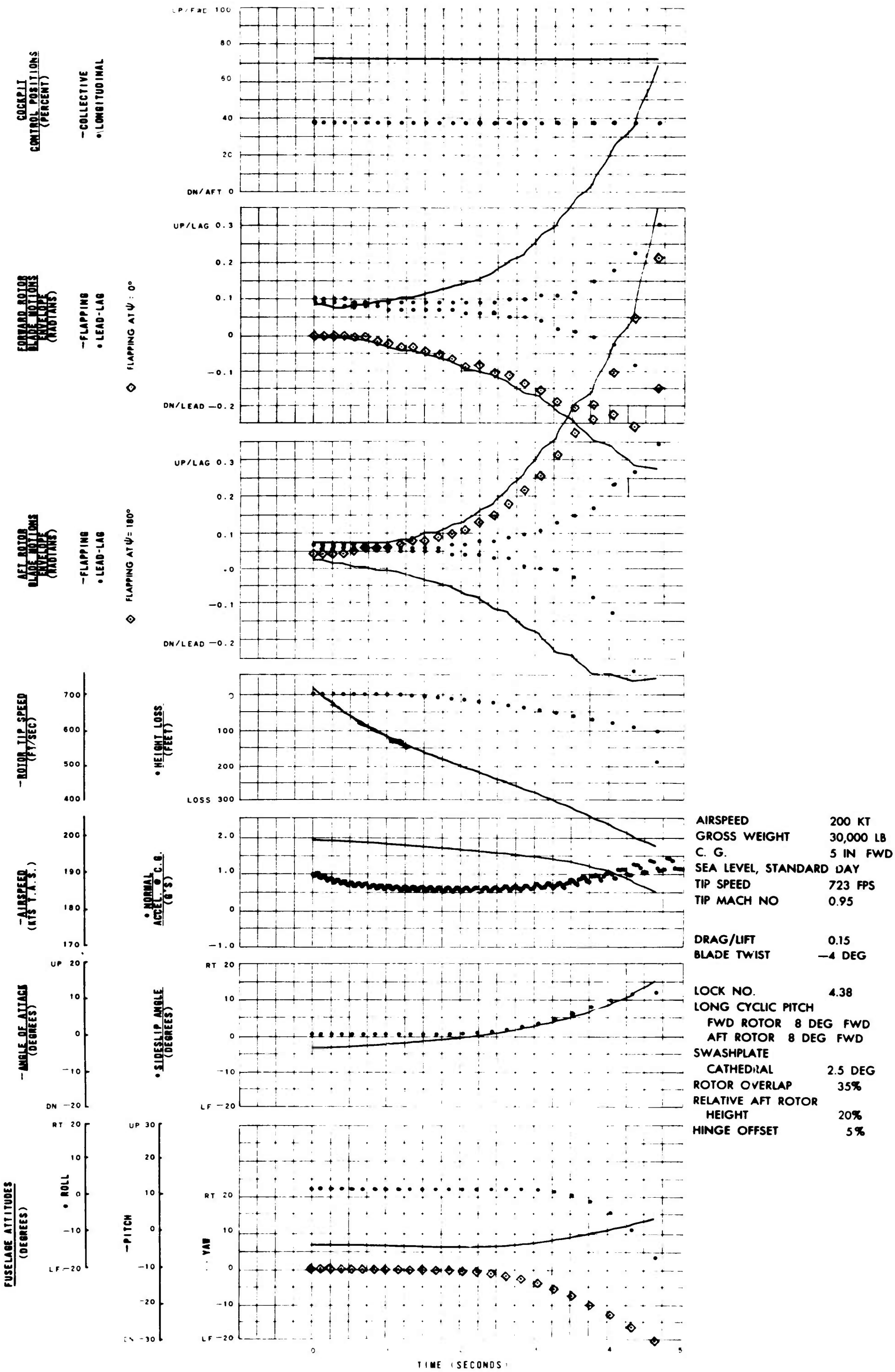

AIRSPEED	200 KT
GROSS WEIGHT	30,000 LB
C. G.	5 IN FWD
SEA LEVEL, STANDARD DAY	
TIP SPEED	723 FPS
TIP MACH NO	0.95
DRAG/LIFT	0.15
BLADE TWIST	-4 DEG
LOCK NO.	4.38
LONG CYCLIC PITCH	
FWD ROTOR	8 DEG FWD
AFT ROTOR	8 DEG FWD
SWASHPLATE CATHEDRAL	2.5 DEG
ROTOR OVERLAP	35%
RELATIVE AFT ROTOR HEIGHT	20%
HINGE OFFSET	5%

Figure 74. Configuration 42.

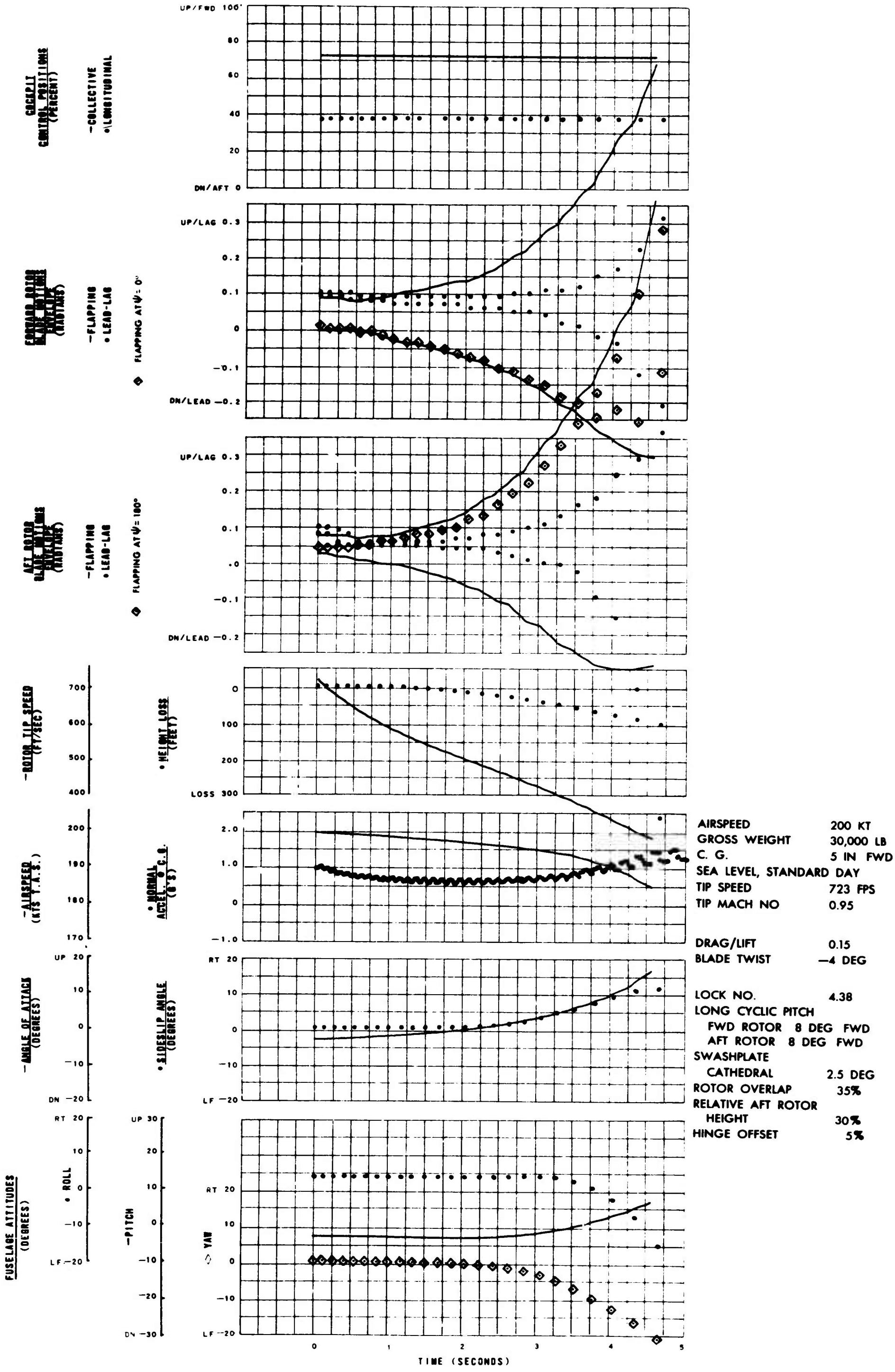

AIRSPEED	200 KT
GROSS WEIGHT	30,000 LB
C. G.	5 IN FWD
SEA LEVEL, STANDARD DAY	
TIP SPEED	723 FPS
TIP MACH NO	0.95
DRAG/LIFT	0.15
BLADE TWIST	-4 DEG
LOCK NO.	4.38
LONG CYCLIC PITCH	
FWD ROTOR	8 DEG FWD
AFT ROTOR	8 DEG FWD
SWASHPLATE	
CATHEDRAL	2.5 DEG
ROTOR OVERLAP	35%
RELATIVE AFT ROTOR HEIGHT	30%
HINGE OFFSET	5%

Figure 75. Configuration 44.

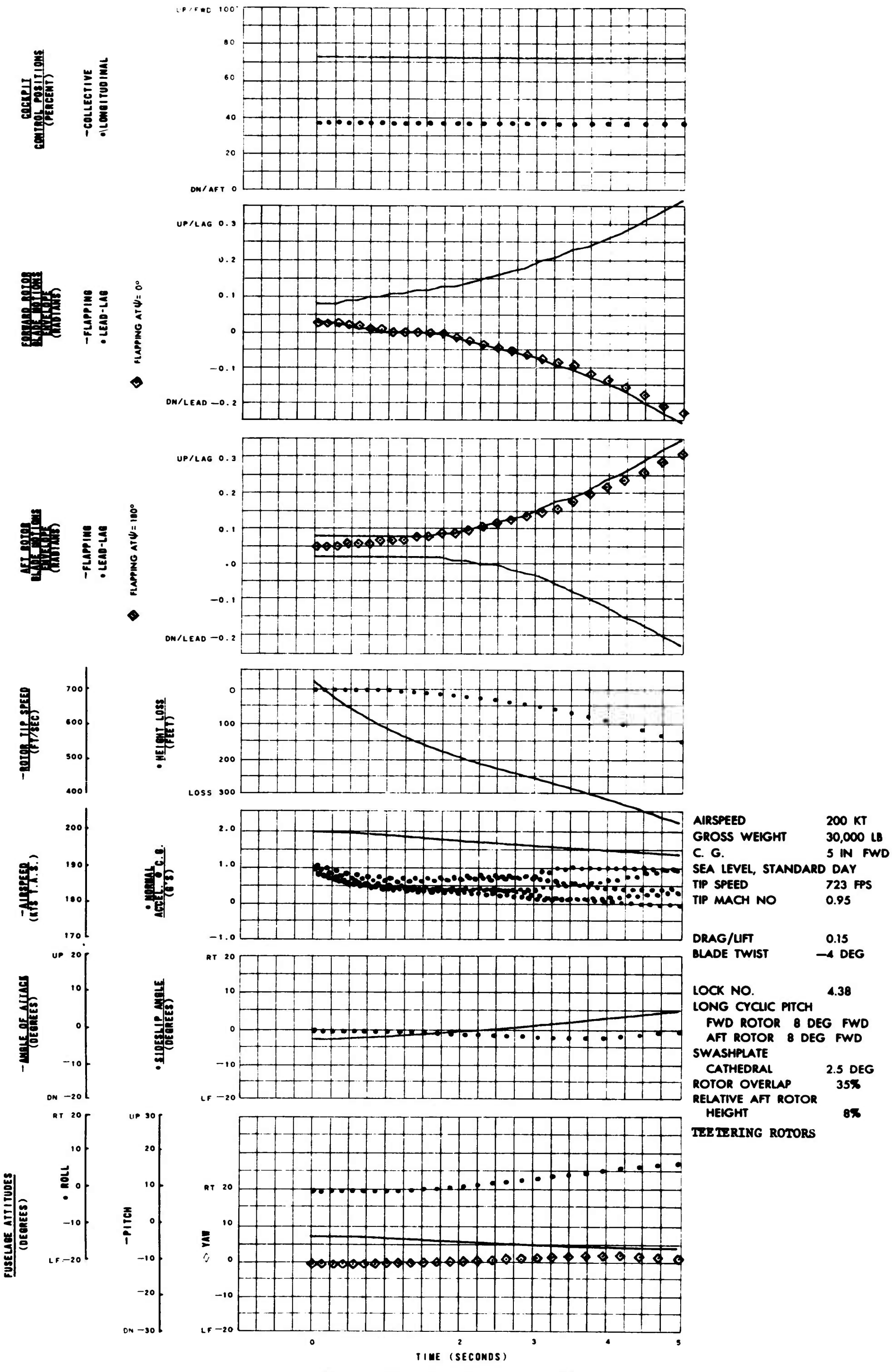

Figure 76. Configuration 14.

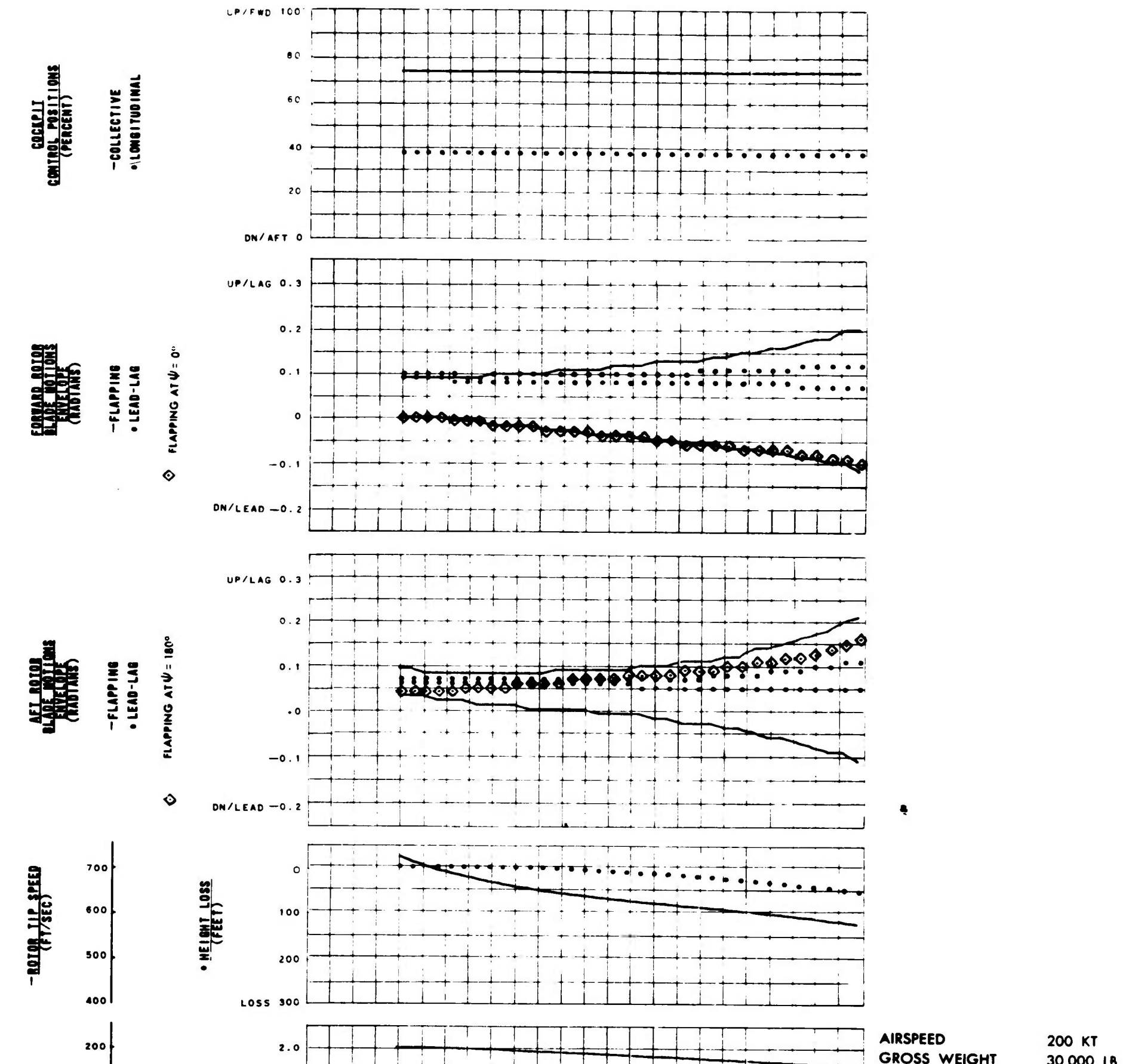

AIRSPEED	200 KT
GROSS WEIGHT	30,000 LB
C. G.	5 IN FWD
SEA LEVEL, STANDARD DAY	
TIP SPEED	723 FPS
TIP MACH NO	0.95
DRAG/LIFT	0.15
BLADE TWIST	—4 DEG
LOCK NO	4.38
LONG CYCLIC PITCH	
FWD ROTOR	8 DEG FWD
AFT ROTOR	8 DEG FWD
SWASHPLATE CATHEDRAL	2.5 DEG
ROTOR OVERLAP	35%
RELATIVE AFT ROTOR HEIGHT	8%
HINGE OFFSET	5%

Figure 77. Time History of Partial Power Failure at 200 Knots with No Corrective Control Input, Configuration 6.

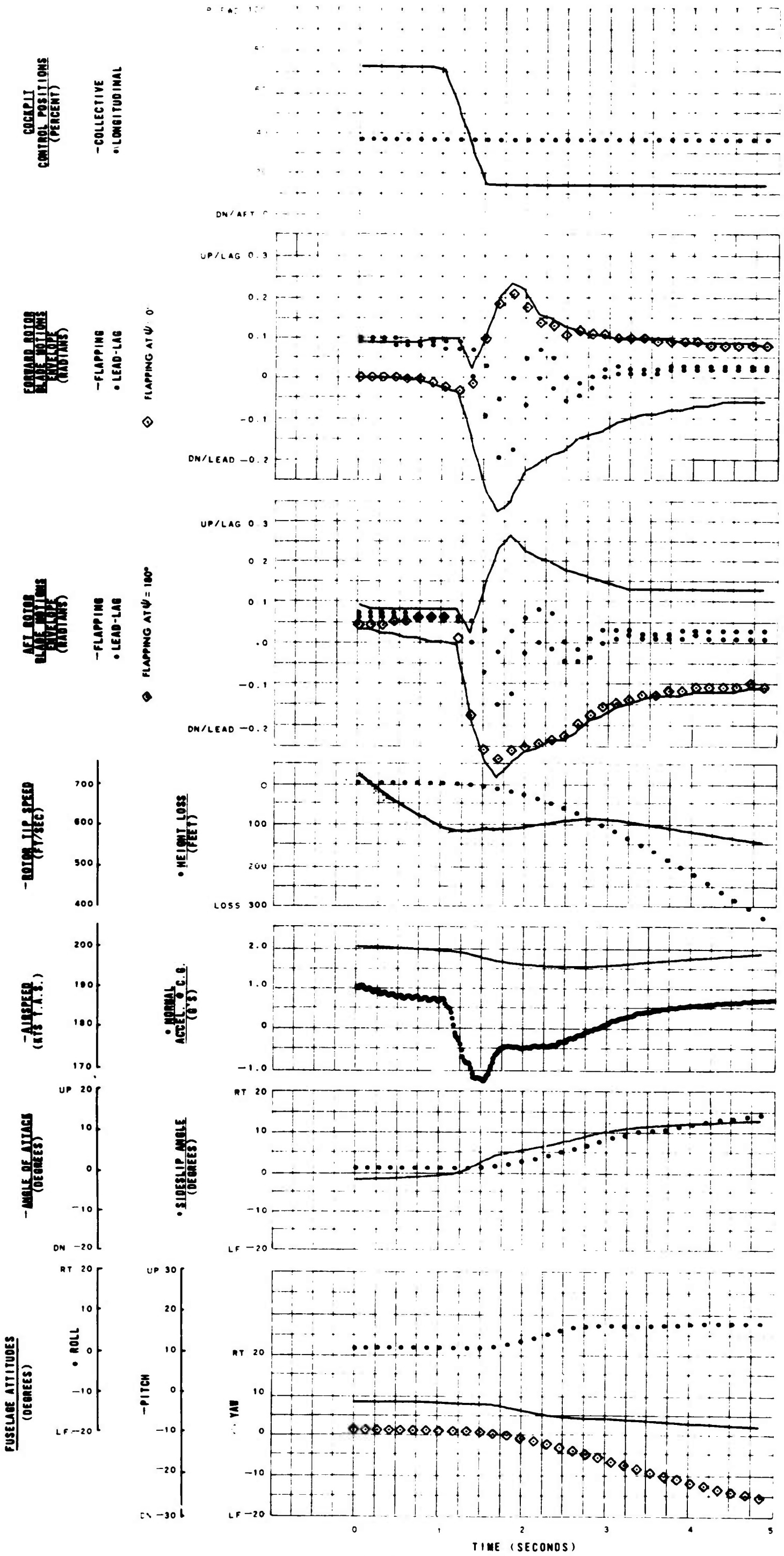

AIRSPEED	200 KT
GROSS WEIGHT	30,000 LB
C. G.	5 IN FWD
SEA LEVEL, STANDARD DAY	
TIP SPEED	723 FPS
TIP MACH NO	0.95
DRAG/LIFT	0.15
BLADE TWIST	-4 DEG
LOCK NO.	4.38
LONG CYCLIC PITCH	
FWD ROTOR	8 DEG FWD
AFT ROTOR	8 DEG FWD
SWASHPLATE	
CATHEDRAL	2.5 DEG
ROTOR OVERLAP	35%
RELATIVE AFT ROTOR	
HEIGHT	8%
HINGE OFFSET	5%

Figure 78. 10-Degree Collective Input at 20 Degrees per Second, 1.0-Second Delay.

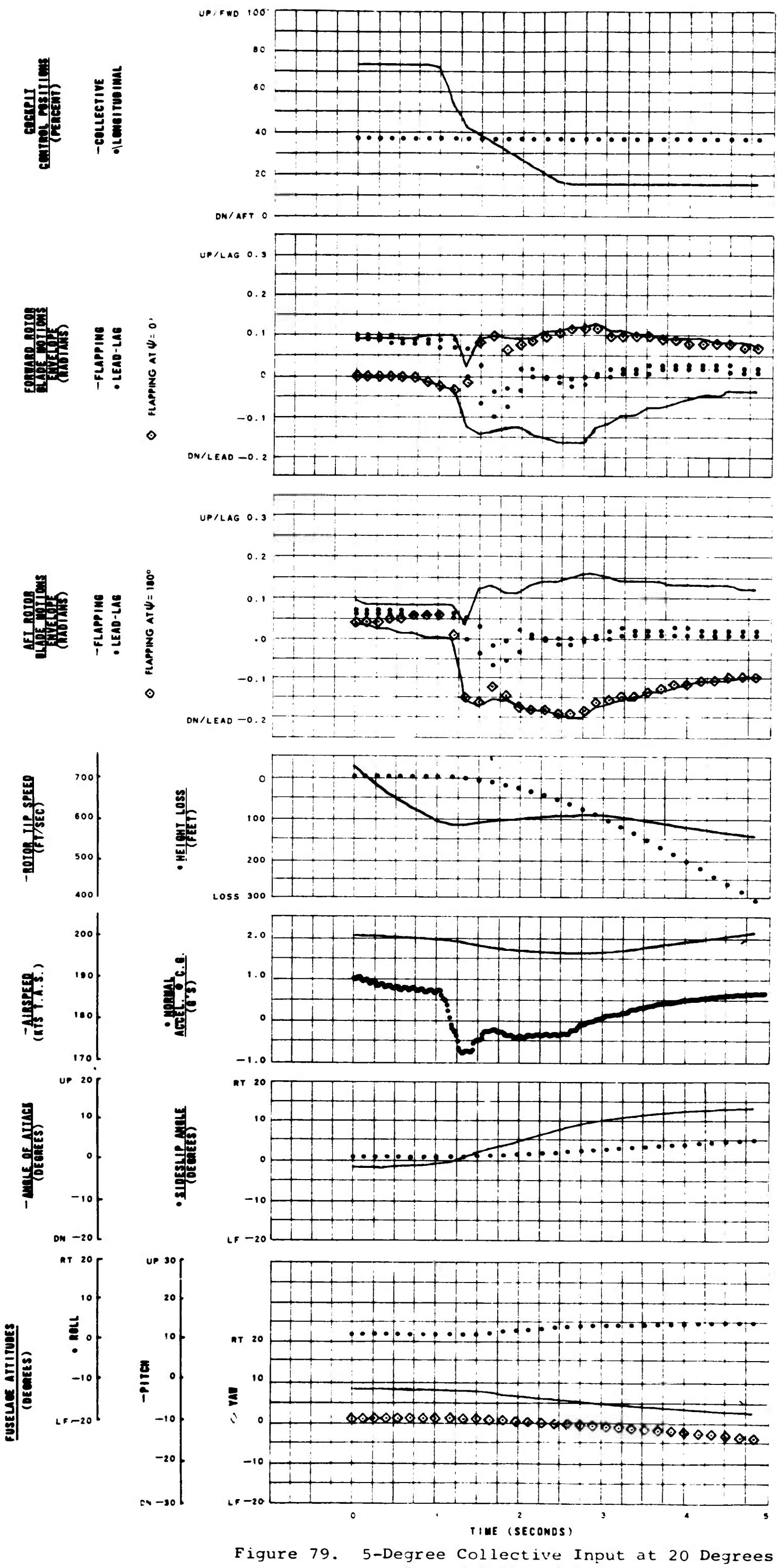

AIRSPEED	200 KT
GROSS WEIGHT	30,000 LB
C. G.	5 IN FWD
SEA LEVEL, STANDARD DAY	
TIP SPEED	723 FPS
TIP MACH NO	0.95
DRAG/LIFT	0.15
BLADE TWIST	—4 DEG
LOCK NO	4.38
LONG CYCLIC PITCH	
FWD ROTOR	8 DEG FWD
AFT ROTOR	8 DEG FWD
SWASHPLATE	
CATHEDRAL	2.5 DEG
ROTOR OVERLAP	35%
RELATIVE AFT ROTOR HEIGHT	8%
HINGE OFFSET	5%

Figure 79. 5-Degree Collective Input at 20 Degrees per Second followed by 5 Degrees at 4 Degrees per Second, 1.0-Second Delay.

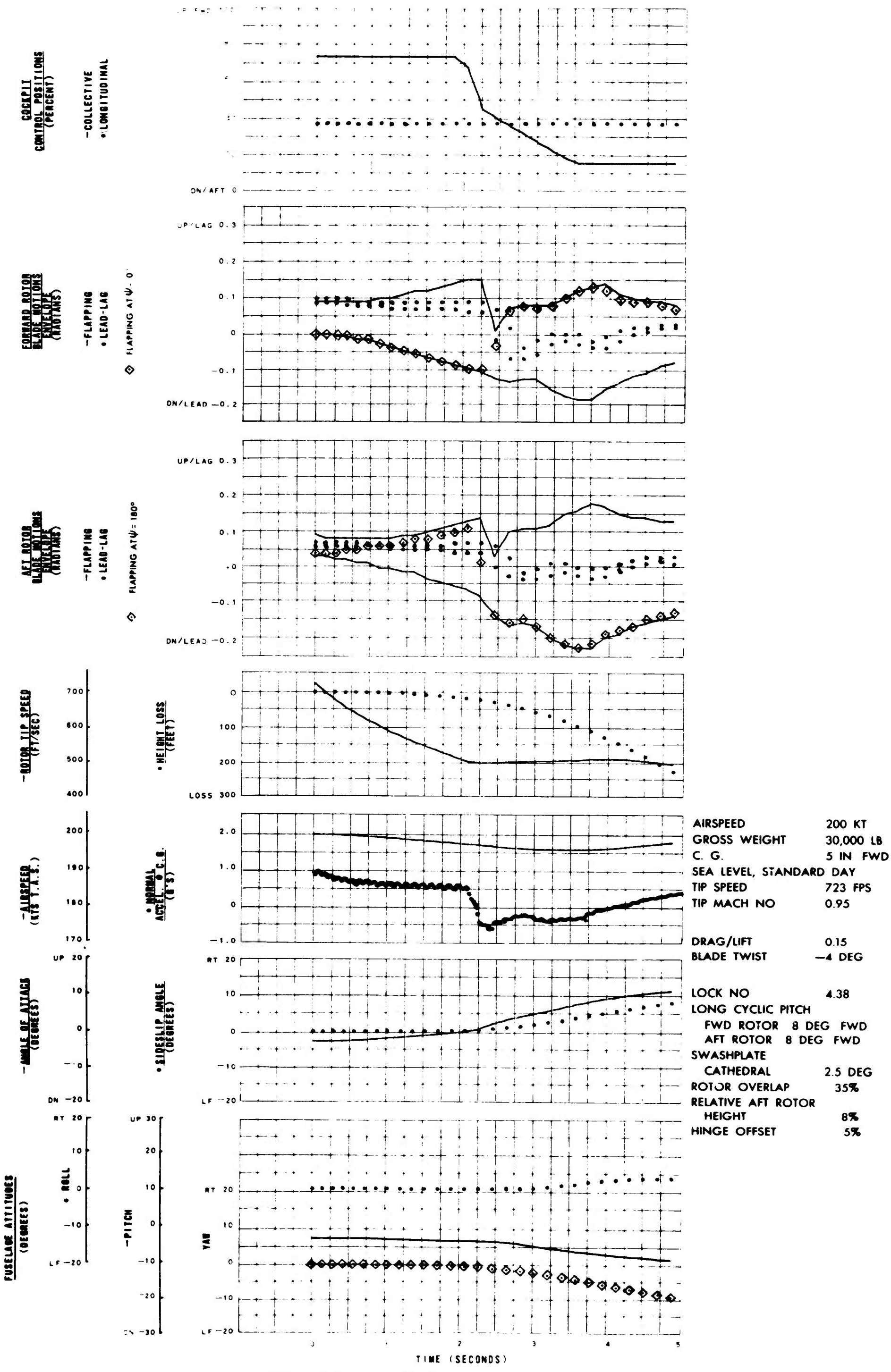

Figure 80. 5-Degree Collective Input at 20 Degrees per Second followed by 5 Degrees at 4 Degrees per Second, 2.0-Second Delay.

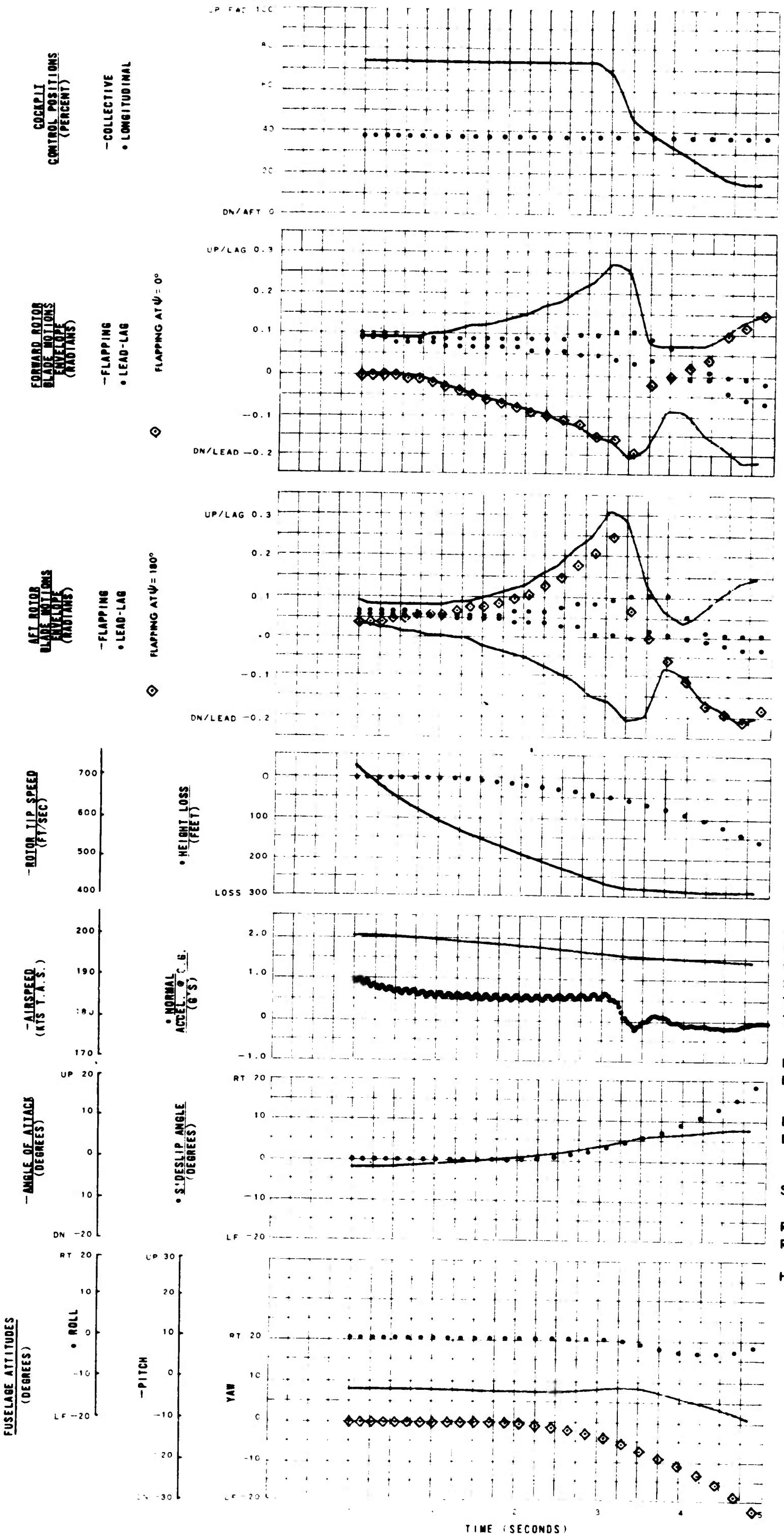

AIRSPEED	200 KT
GROSS WEIGHT	30,000 LB
C. G.	5 IN FWD
SEA LEVEL, STANDARD DAY	
TIP SPEED	723 FPS
TIP MACH NO	0.95
DRAG/LIFT	0.15
BLADE TWIST	—4 DEG
LOCK NO	4.38
LONG CYCLIC PITCH	
FWD ROTOR	8 DEG FWD
AFT ROTOR	8 DEG FWD
SWASHPLATE	
CATHEDRAL	2.5 DEG
ROTOR OVERLAP	35%
RELATIVE AFT ROTOR HEIGHT	8%
HINGE OFFSET	5%

Figure 81. 5-Degree Collective Input at 20 Degrees per Second followed by 5 Degrees at 4 Degrees per Second, 3.0-Second Delay.

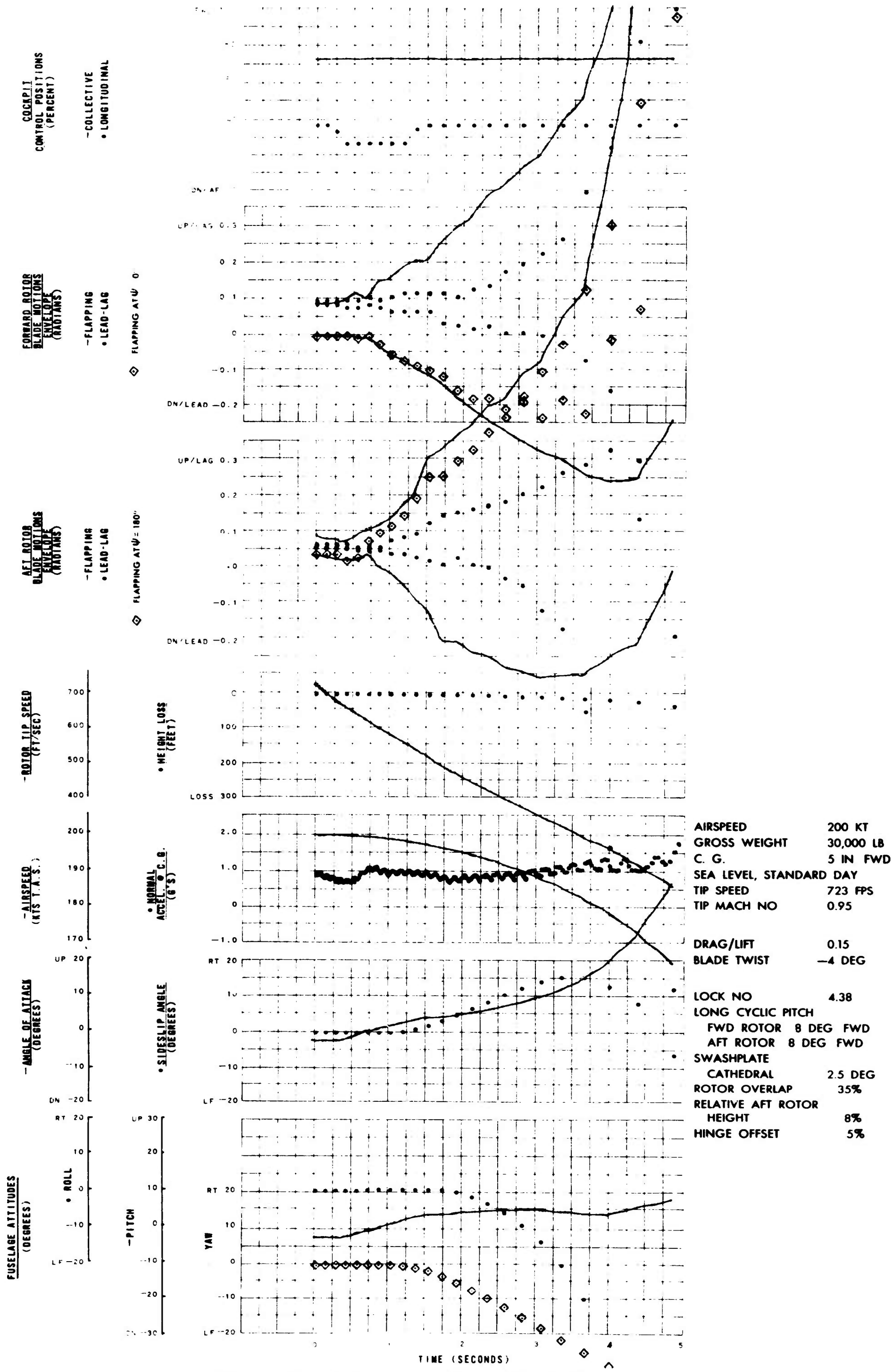

AIRSPEED	200 KT
GROSS WEIGHT	30,000 LB
C. G.	5 IN FWD
SEA LEVEL, STANDARD DAY	
TIP SPEED	723 FPS
TIP MACH NO	0.95
DRAG/LIFT	0.15
BLADE TWIST	-4 DEG
LOCK NO	4.38
LONG CYCLIC PITCH	
FWD ROTOR	8 DEG FWD
AFT ROTOR	8 DEG FWD
SWASHPLATE	
CATHEDRAL	2.5 DEG
ROTOR OVERLAP	35%
RELATIVE AFT ROTOR HEIGHT	8%
HINGE OFFSET	5%

Figure 82. 1 Degree per Rotor Aft Differential Collective Pulse Input of 1.0-Second Duration, 0.2-Second Delay.

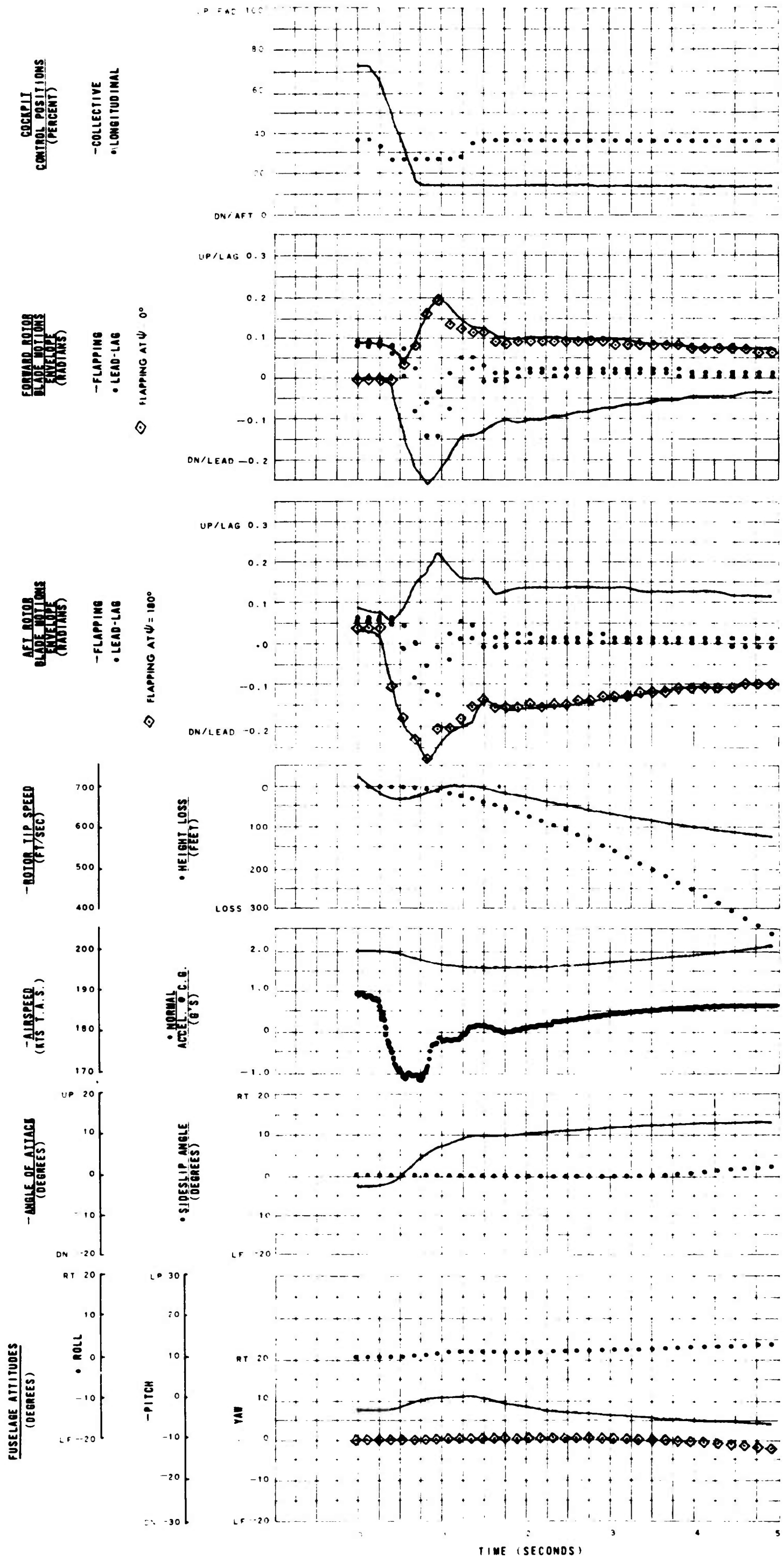

AIRSPEED	200 KT
GROSS WEIGHT	30,000 LB
C. G.	5 IN FWD
SEA LEVEL, STANDARD DAY	
TIP SPEED	723 FPS
TIP MACH NO	0.95
DRAG/LIFT	0.15
BLADE TWIST	−4 DEG
LOCK NO	4.38
LONG CYCLIC PITCH	
FWD ROTOR	8 DEG FWD
AFT ROTOR	8 DEG FWD
SWASHPLATE	
CATHEDRAL	2.5 DEG
ROTOR OVERLAP	35%
RELATIVE AFT ROTOR HEIGHT	8%
HINGE OFFSET	5%

Figure 83. 1 Degree per Rotor Aft Differential Collective Pulse Input of 1.0-Second Duration, 0.2-Second Delay, with Collective Input of 10 Degrees at 20 Degrees per Second.

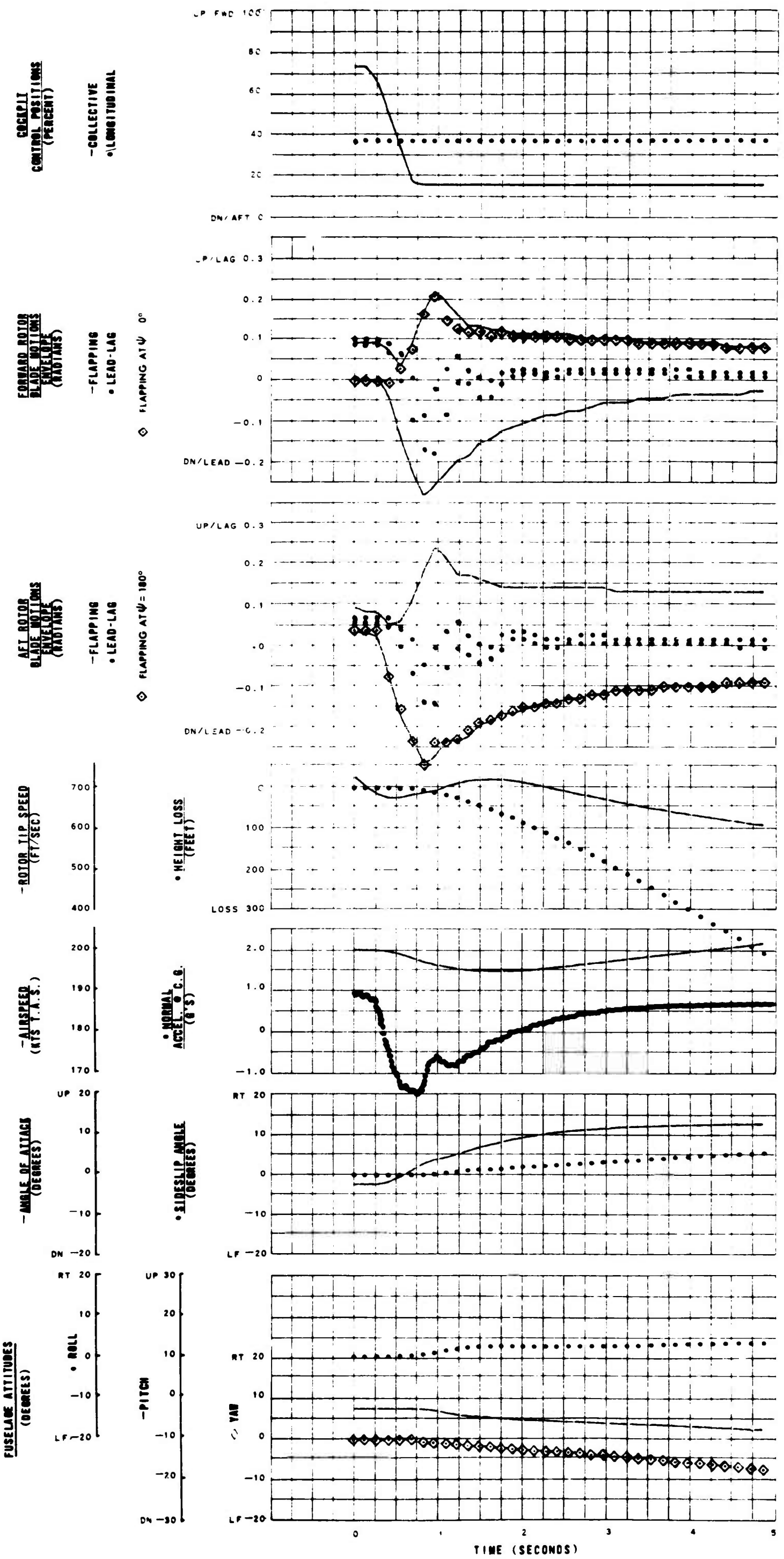

AIRSPEED	200 KT
GROSS WEIGHT	30,000 LB
C. G.	5 IN FWD
SEA LEVEL, STANDARD DAY	
TIP SPEED	723 FPS
TIP MACH NO	0.95
DRAG/LIFT	0.15
BLADE TWIST	–4 DEG
LOCK NO	4.38
LONG CYCLIC PITCH	
FWD ROTOR	8 DEG FWD
AFT ROTOR	8 DEG FWD
SWASHPLATE	
CATHEDRAL	2.5 DEG
ROTOR OVERLAP	35%
RELATIVE AFT ROTOR HEIGHT	8%
HINGE OFFSET	5%

Figure 84. 10–Degree Collective Input at 20 Degrees per Second, 0.2-Second Delay.

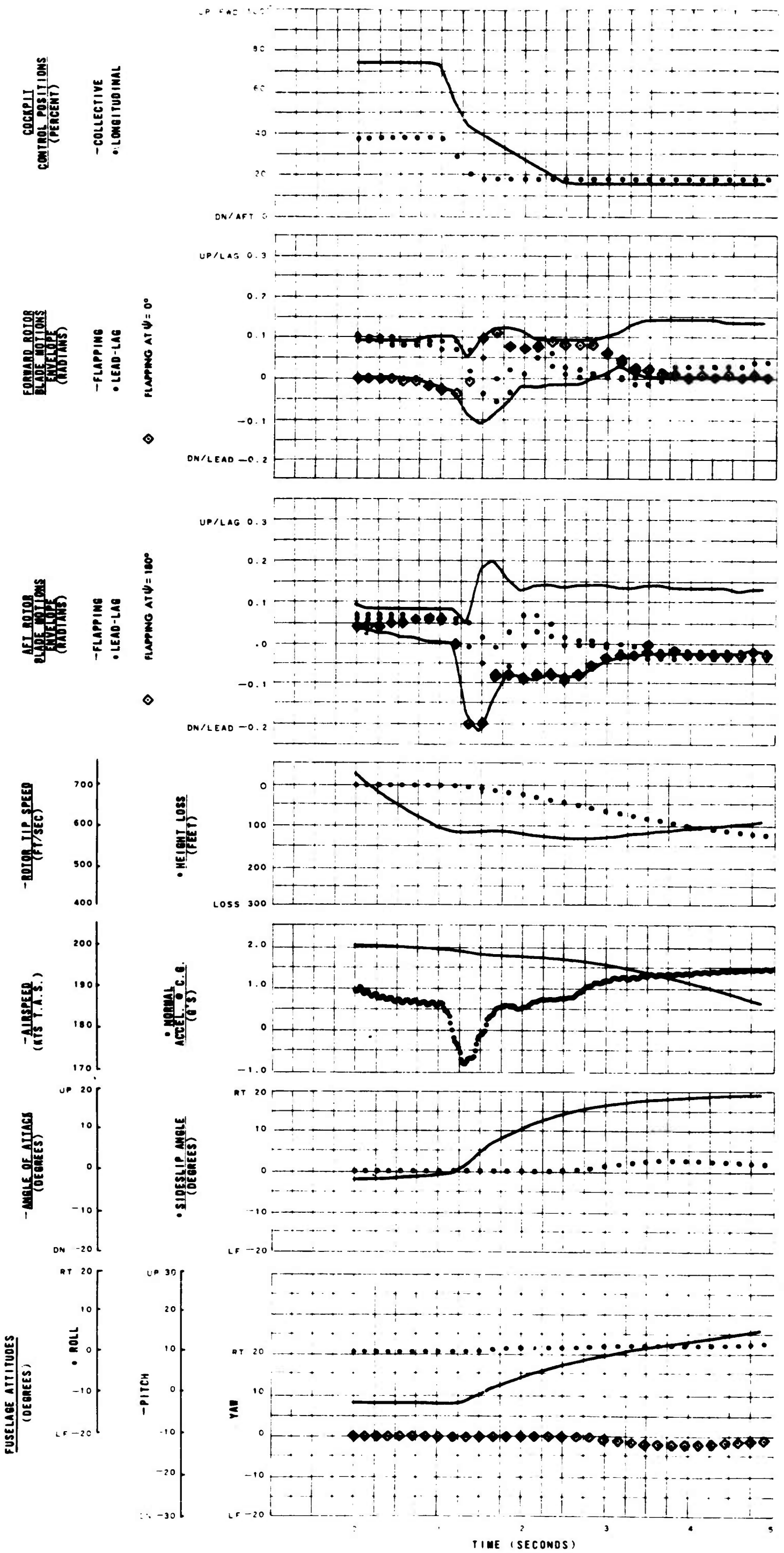

AIRSPEED	200 KT
GROSS WEIGHT	30,000 LB
C. G.	5 IN FWD
SEA LEVEL, STANDARD DAY	
TIP SPEED	723 FPS
TIP MACH NO	0.95
DRAG/LIFT	0.15
BLADE TWIST	—4 DEG
LOCK NO	4.38
LONG CYCLIC PITCH	
FWD ROTOR	8 DEG FWD
AFT ROTOR	8 DEG FWD
SWASHPLATE	
CATHEDRAL	2.5 DEG
ROTOR OVERLAP	35%
RELATIVE AFT ROTOR HEIGHT	8%
HINGE OFFSET	5%

Figure 85. 5-Degree Collective Input at 20 Degrees per Second followed by 5 Degrees at 4 Degrees per second with Simultaneous Longitudinal Stick Step of 2 Degrees per Rotor, 1.0-Second Delay.

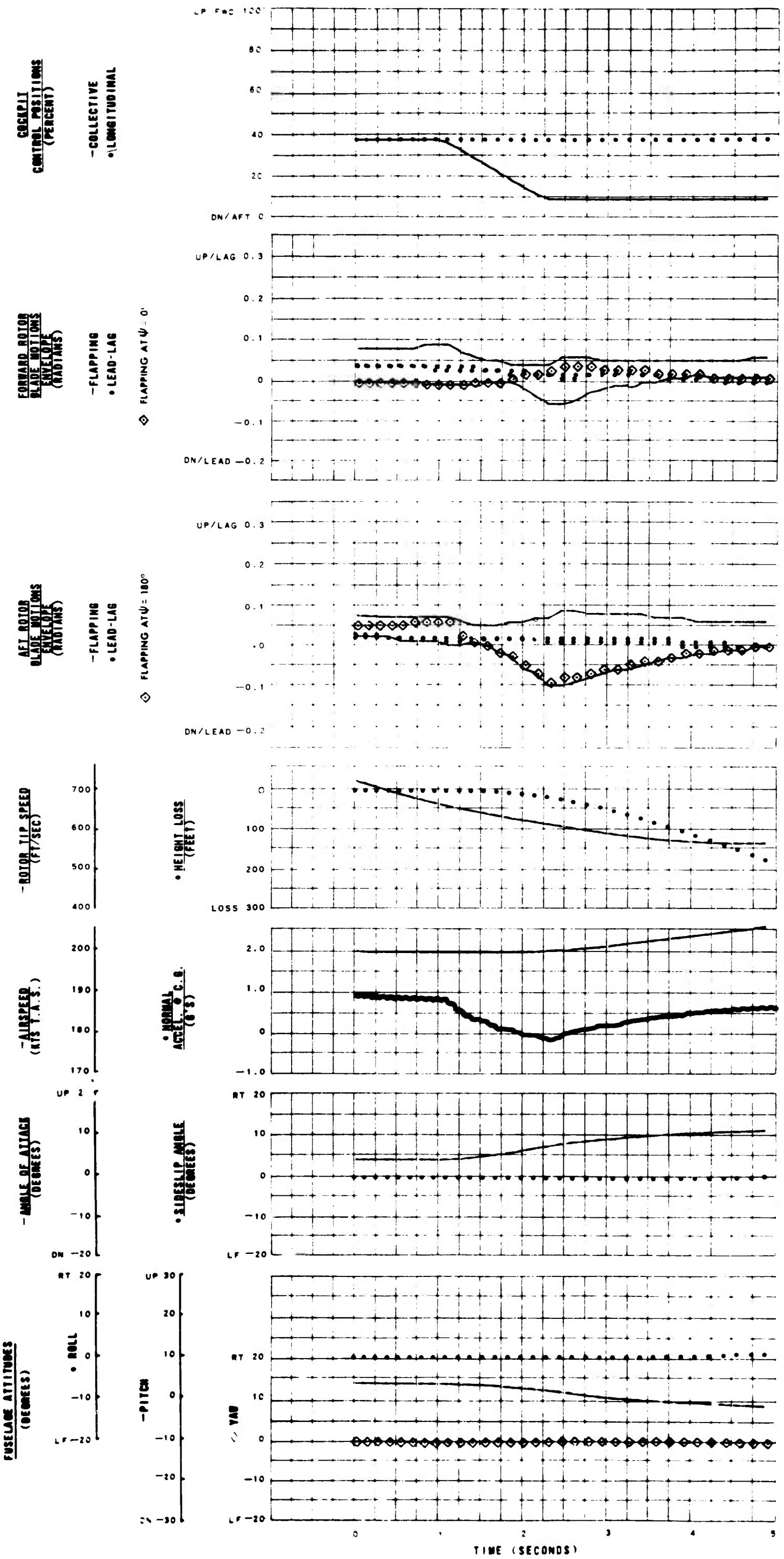

AIRSPEED	200 KT
GROSS WEIGHT	30,000 LB
C. G.	5 IN FWD
SEA LEVEL, STANDARD DAY	
TIP SPEED	723 FPS
TIP MACH NO	0.95
DRAG/LIFT	0.0
BLADE TWIST	0 DEG
LOCK NO	4.38
LONG CYCLIC PITCH	
FWD ROTOR	4 DEG FWD
AFT ROTOR	4 DEG FWD
SWASHPLATE CATHEDRAL	2.5 DEG
ROTOR OVERLAP	35%
RELATIVE AFT ROTOR HEIGHT	8%
HINGE OFFSET	5%

Figure 86. Complete Power Failure at 200 Knots with Collective Input of 5 Degrees at 4 Degrees per Second, 1.0-Second Delay, Configuration 4.

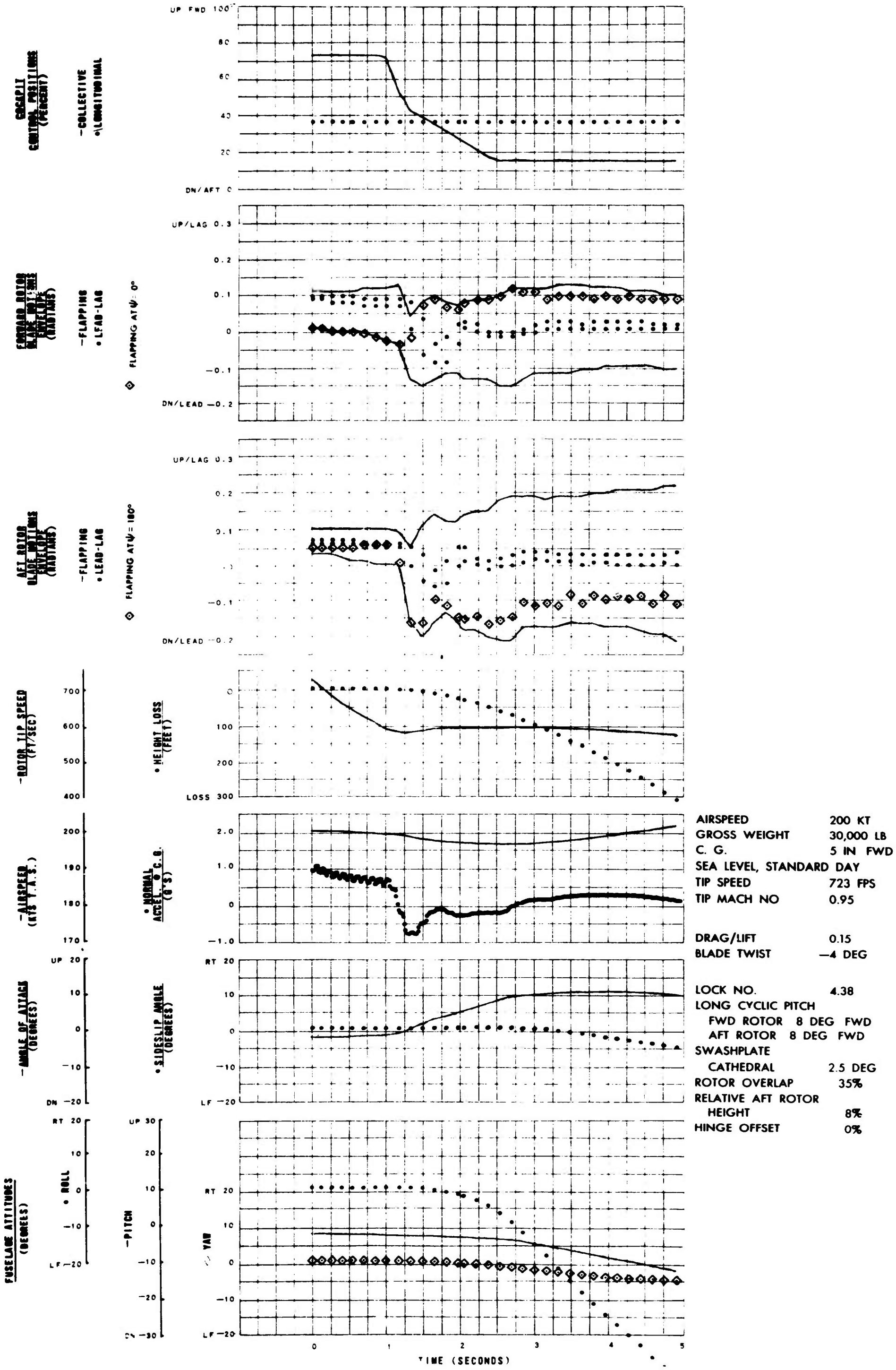

AIRSPEED	200 KT
GROSS WEIGHT	30,000 LB
C. G.	5 IN FWD
SEA LEVEL, STANDARD DAY	
TIP SPEED	723 FPS
TIP MACH NO	0.95
DRAG/LIFT	0.15
BLADE TWIST	—4 DEG
LOCK NO.	4.38
LONG CYCLIC PITCH	
FWD ROTOR	8 DEG FWD
AFT ROTOR	8 DEG FWD
SWASHPLATE	
CATHEDRAL	2.5 DEG
ROTOR OVERLAP	35%
RELATIVE AFT ROTOR HEIGHT	8%
HINGE OFFSET	0%

Figure 87. Configuration 3.

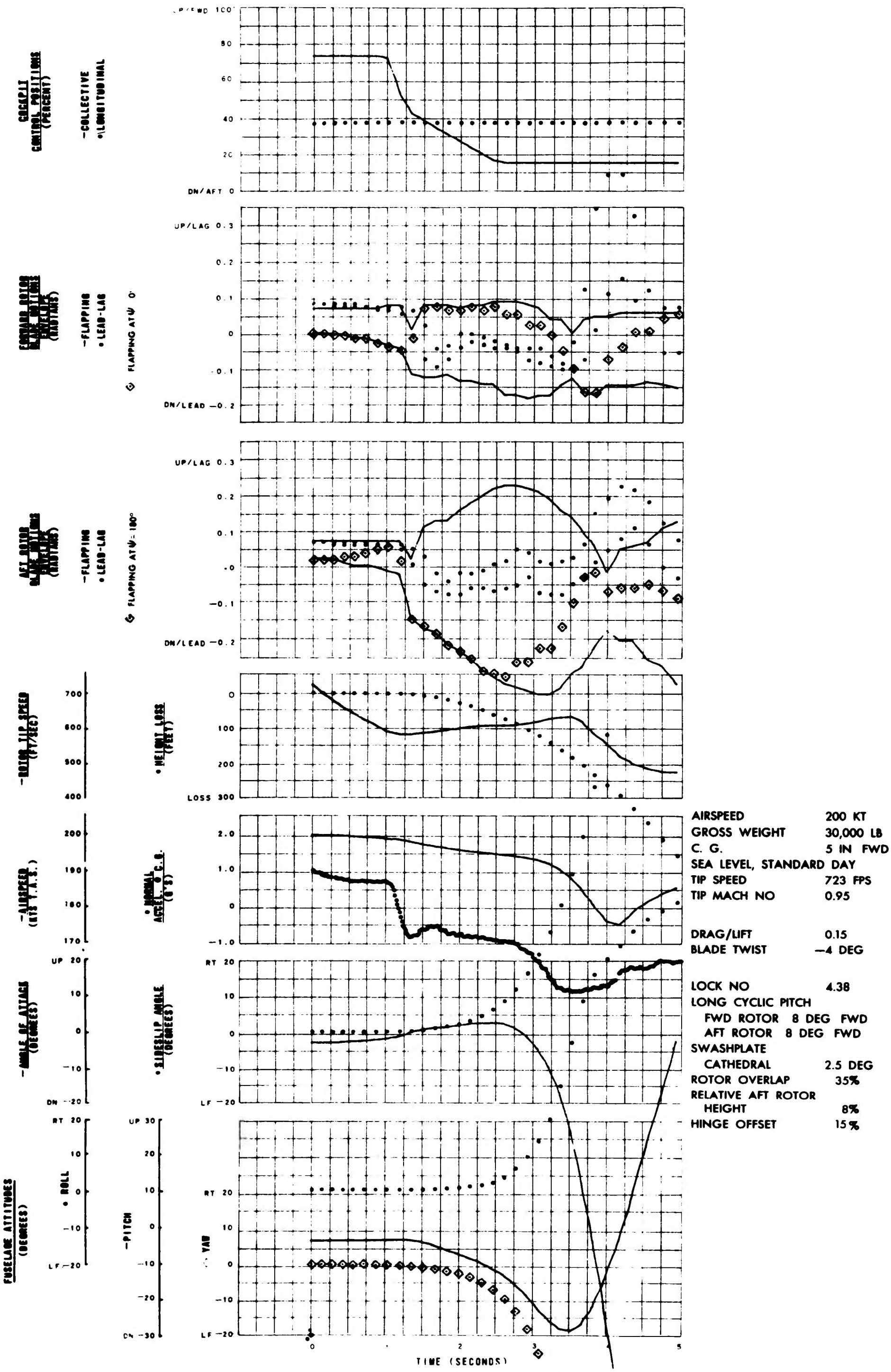

Figure 88. Configuration 11.

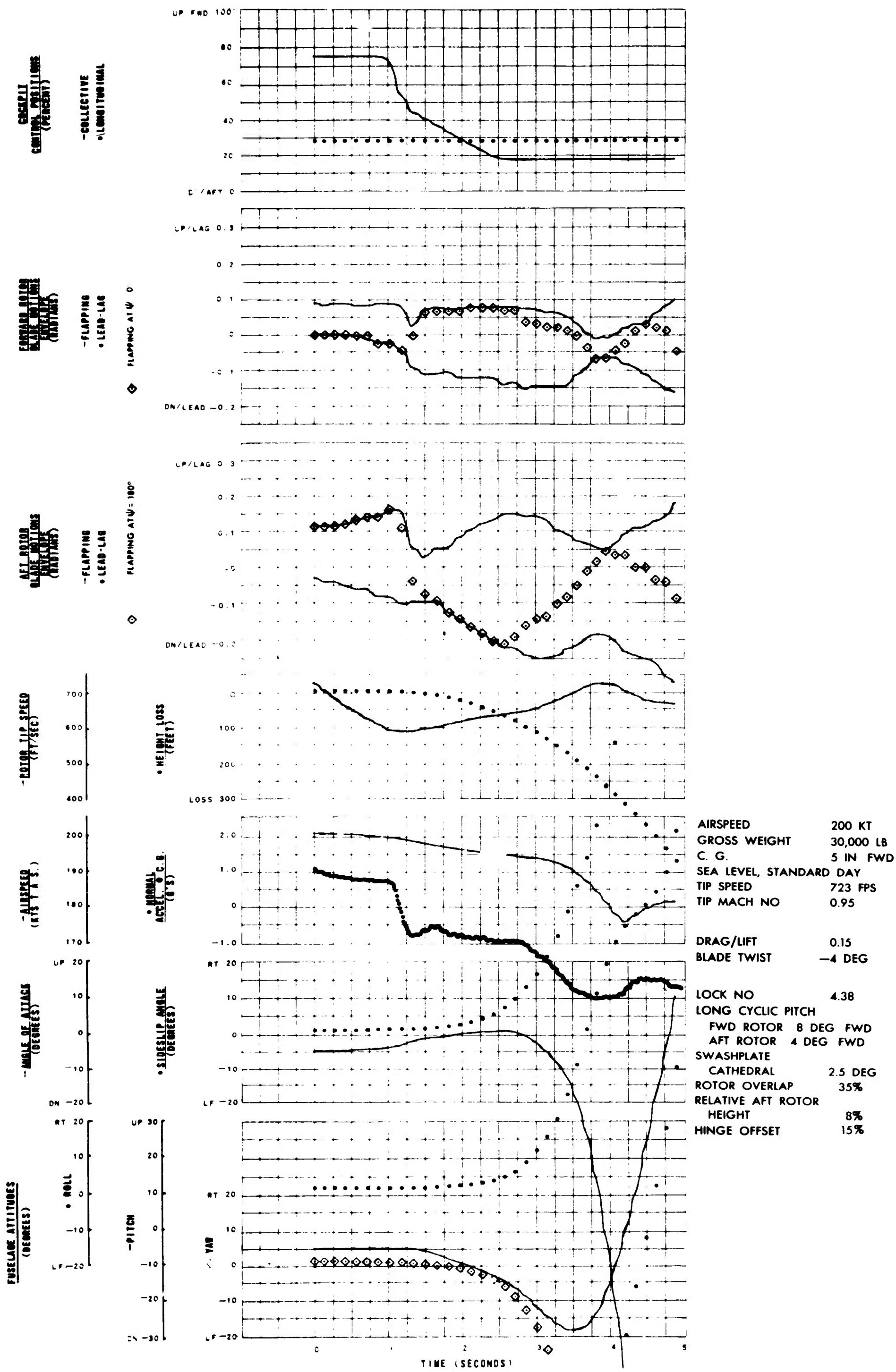

AIRSPEED	200 KT
GROSS WEIGHT	30,000 LB
C. G.	5 IN FWD
SEA LEVEL, STANDARD DAY	
TIP SPEED	723 FPS
TIP MACH NO	0.95
DRAG/LIFT	0.15
BLADE TWIST	−4 DEG
LOCK NO	4.38
LONG CYCLIC PITCH	
FWD ROTOR	8 DEG FWD
AFT ROTOR	4 DEG FWD
SWASHPLATE CATHEDRAL	2.5 DEG
ROTOR OVERLAP	35%
RELATIVE AFT ROTOR HEIGHT	8%
HINGE OFFSET	15%

Figure 89. Configuration 11 Modified to have 4-Degree Forward Cyclic on Aft Rotor.

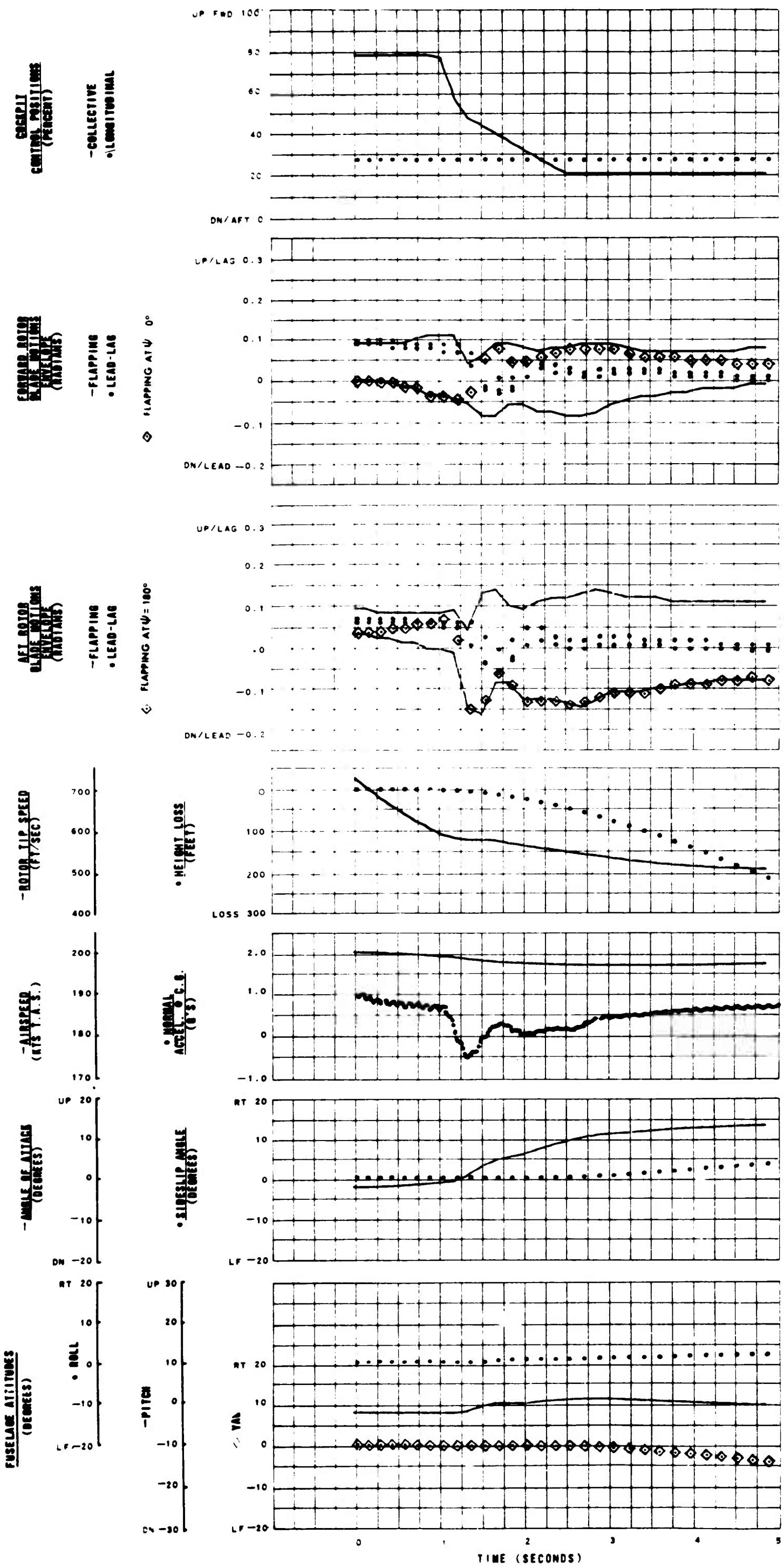

AIRSPEED	200 KT
GROSS WEIGHT	30,000 LB
C. G.	5 IN FWD
SEA LEVEL, STANDARD DAY	
TIP SPEED	723 FPS
TIP MACH NO	0.95
DRAG/LIFT	0.15
BLADE TWIST	−4 DEG
LOCK NO	4.38
LONG CYCLIC PITCH	
FWD ROTOR	8 DEG FWD
AFT ROTOR	8 DEG FWD
SWASHPLATE	
CATHEDRAL	2.5 DEG
ROTOR OVERLAP	35%
RELATIVE AFT ROTOR HEIGHT	8%
HINGE OFFSET	5%

TIP PATH PLANE CONTROLLER
30-DEG PITCH—CONE

Figure 90. Configuration 19.

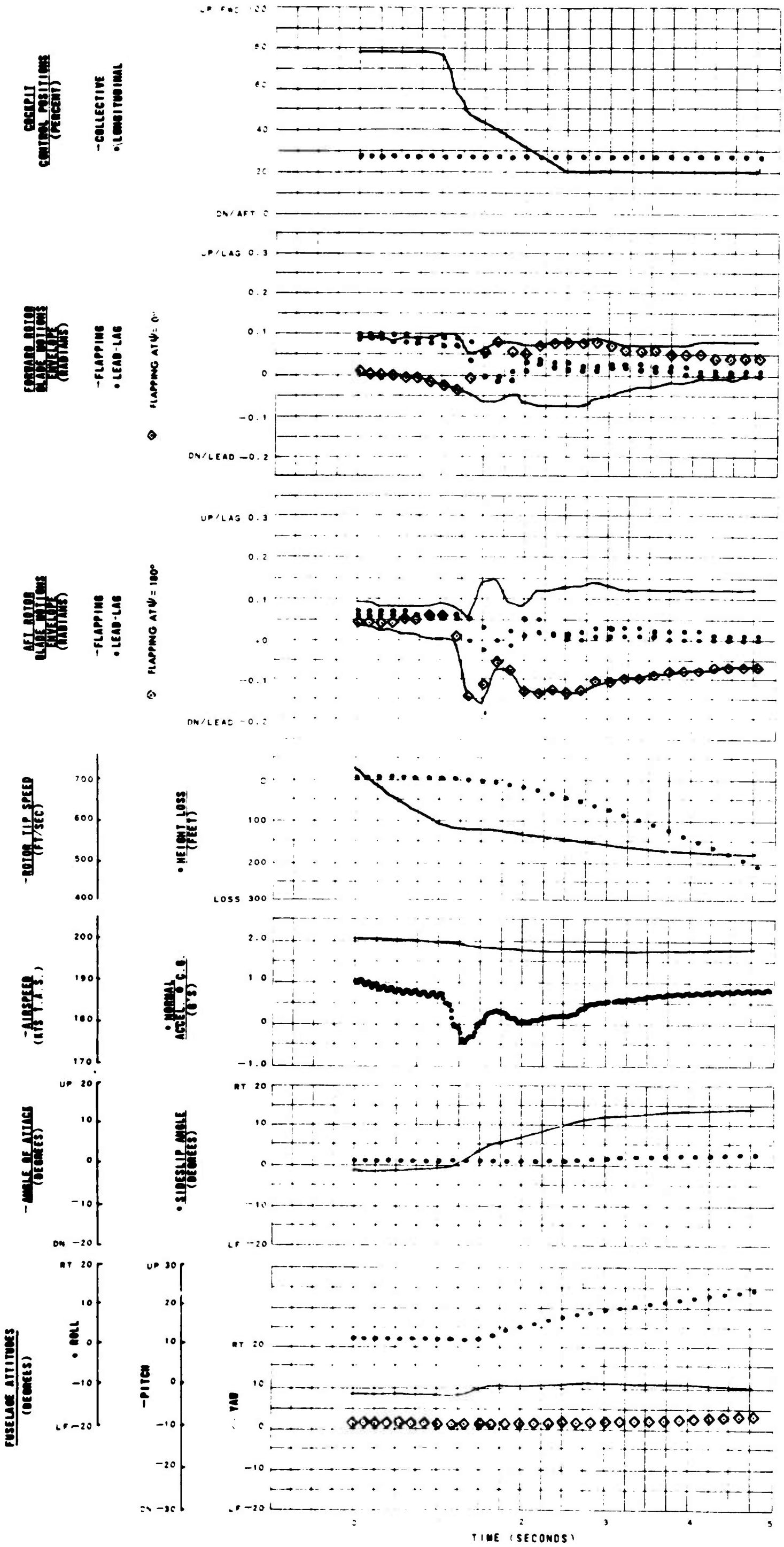

AIRSPEED	200 KT
GROSS WEIGHT	30,000 LB
C. G.	5 IN FWD
SEA LEVEL, STANDARD DAY	
TIP SPEED	723 FPS
TIP MACH NO	0.95
DRAG/LIFT	0.15
BLADE TWIST	−4 DEG
LOCK NO	4.38
LONG CYCLIC PITCH	
FWD ROTOR	8 DEG FWD
AFT ROTOR	8 DEG FWD
SWASHPLATE	
CATHEDRAL	2.5 DEG
ROTOR OVERLAP	35%
RELATIVE AFT ROTOR HEIGHT	8%
HINGE OFFSET	5%
DELTA THREE	30 DEG

Figure 91. Configuration 16.

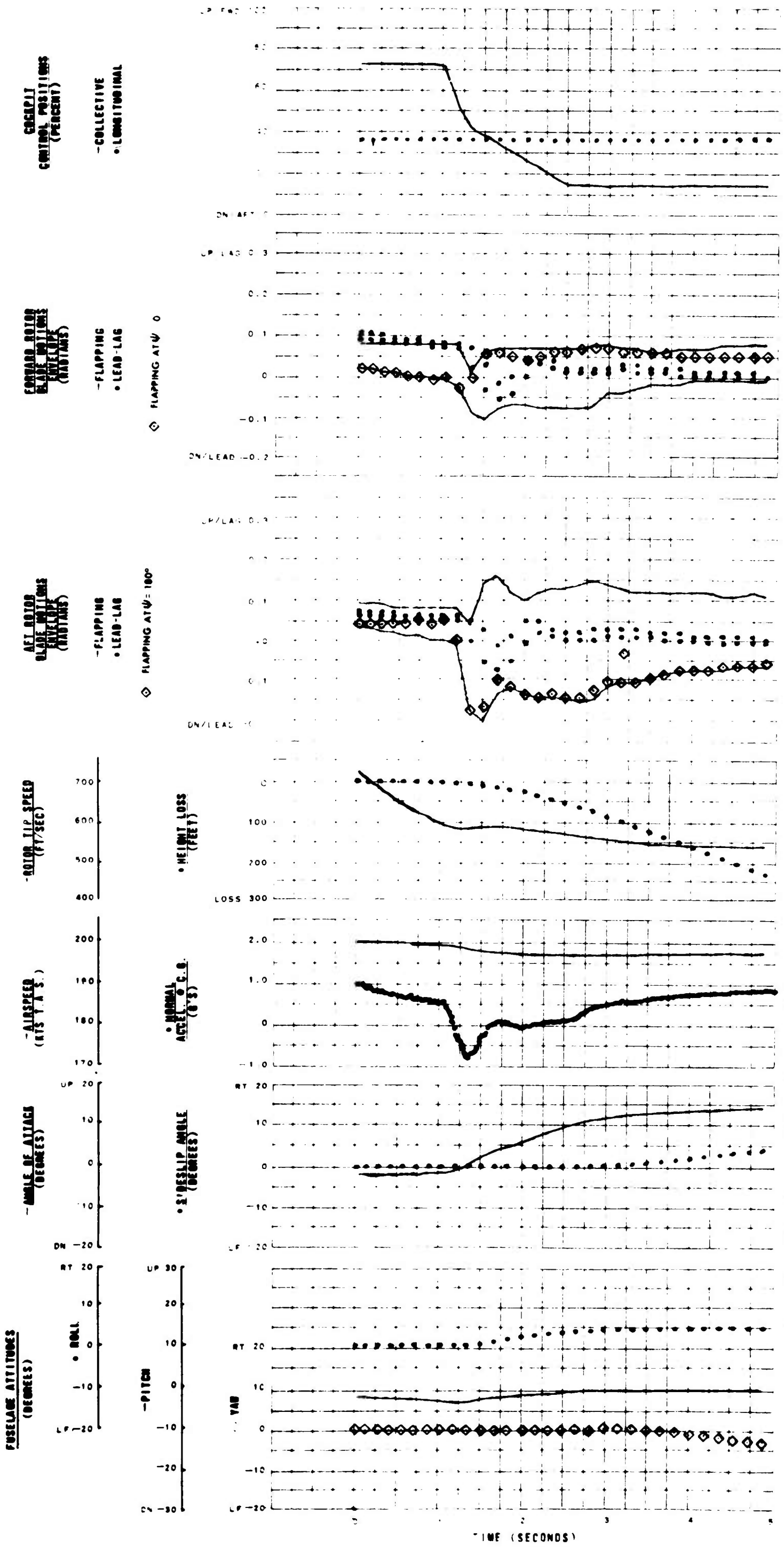

Figure 22. Configuration 22.

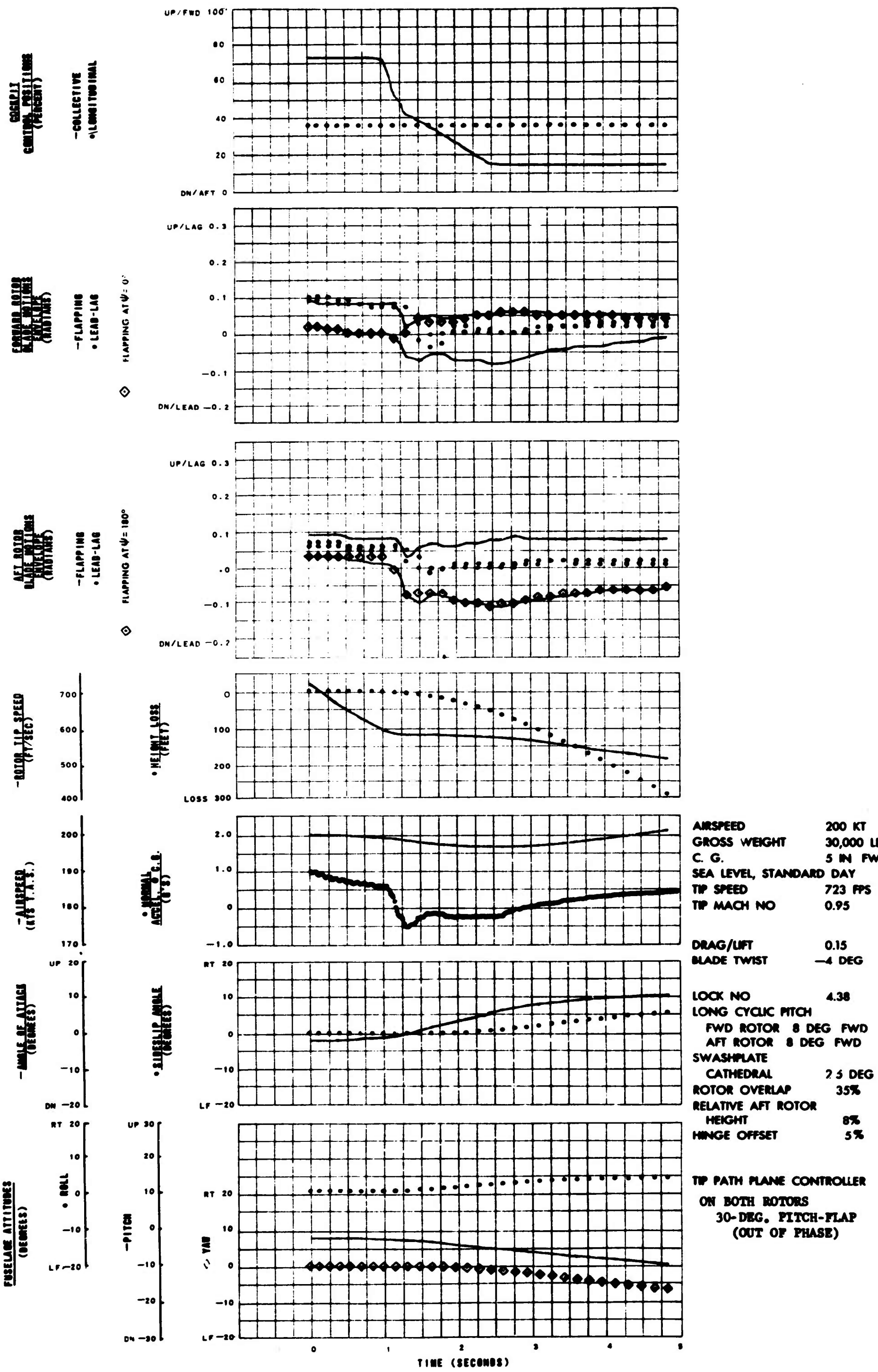

AIRSPEED	200 KT
GROSS WEIGHT	30,000 LB
C. G.	5 IN FWD
SEA LEVEL, STANDARD DAY	
TIP SPEED	723 FPS
TIP MACH NO	0.95
DRAG/LIFT	0.15
BLADE TWIST	−4 DEG
LOCK NO	4.38
LONG CYCLIC PITCH	
FWD ROTOR	8 DEG FWD
AFT ROTOR	8 DEG FWD
SWASHPLATE	
CATHEDRAL	2.5 DEG
ROTOR OVERLAP	35%
RELATIVE AFT ROTOR	
HEIGHT	8%
HINGE OFFSET	5%

TIP PATH PLANE CONTROLLER
ON BOTH ROTORS
30-DEG. PITCH-FLAP
(OUT OF PHASE)

Figure 93. Configuration 22 Modified to have 30-Degree Pitch-Flap Out-of-Phase Coupling on Aft Rotor.

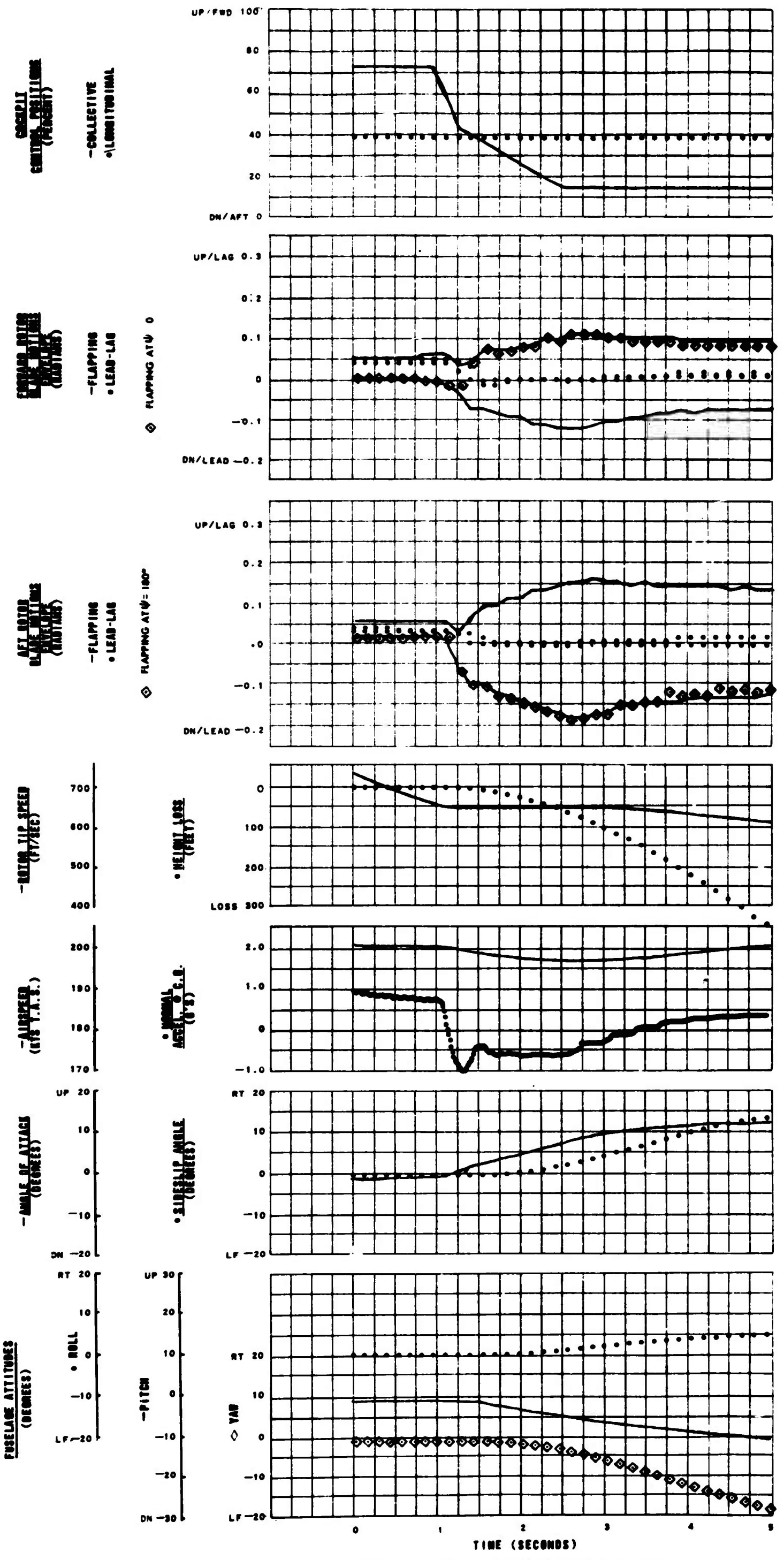

Figure 94. Configuration 28.

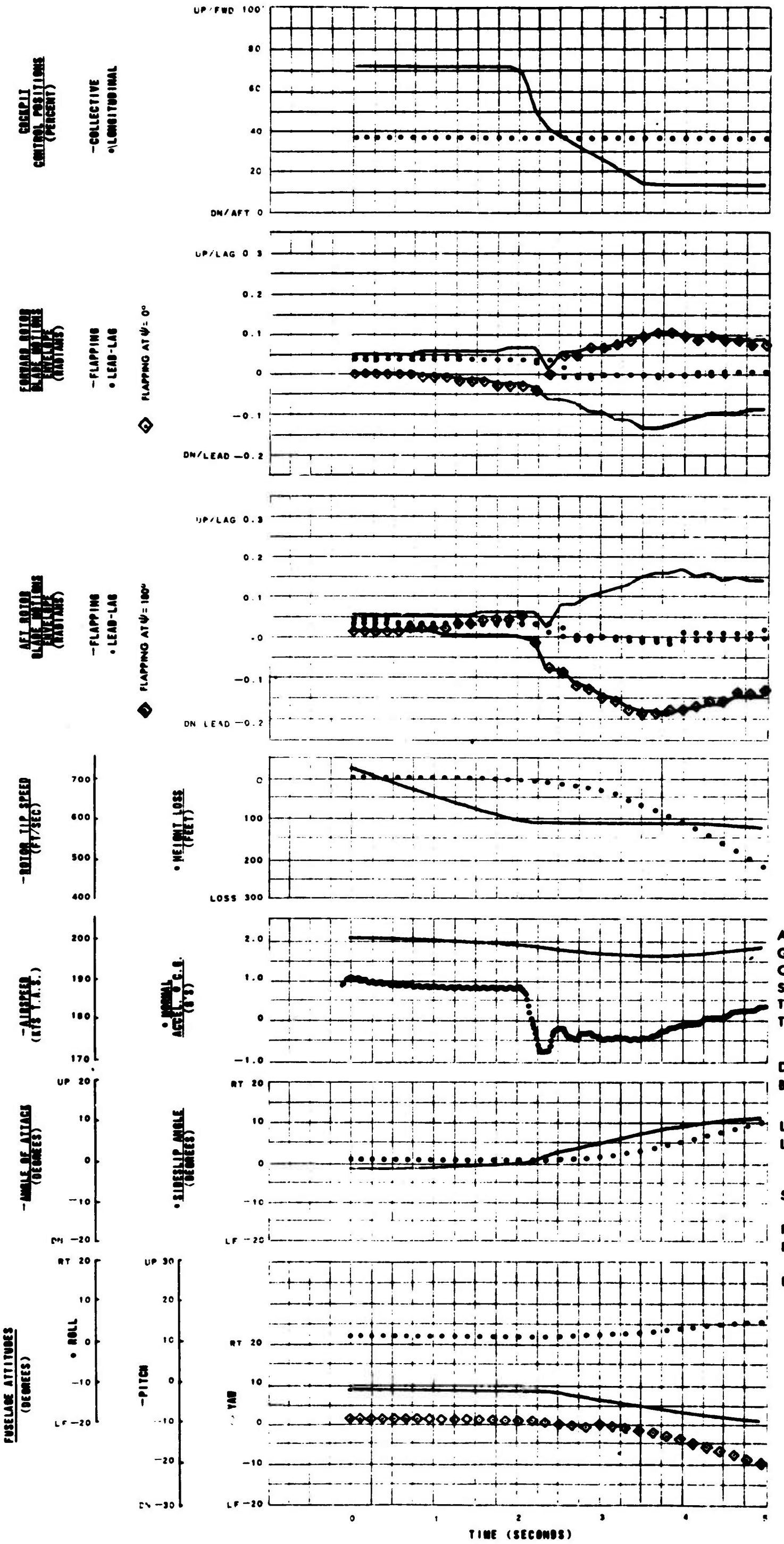

AIRSPEED	200 KT
GROSS WEIGHT	30,000 LB
C. G.	5 IN FWD
SEA LEVEL, STANDARD DAY	
TIP SPEED	723 FPS
TIP MACH NO	0.95
DRAG/LIFT	0.15
BLADE TWIST	–4 DEG
LOCK NO	2.19
LONG CYCLIC PITCH	
FWD ROTOR	8 DEG FWD
AFT ROTOR	8 DEG FWD
SWASHPLATE CATHEDRAL	2.5 DEG
ROTOR OVERLAP	35%
RELATIVE AFT ROTOR HEIGHT	8%
HINGE OFFSET	5%

Figure 95. Configuration 28 except that Control Input is Delayed 2 Seconds.

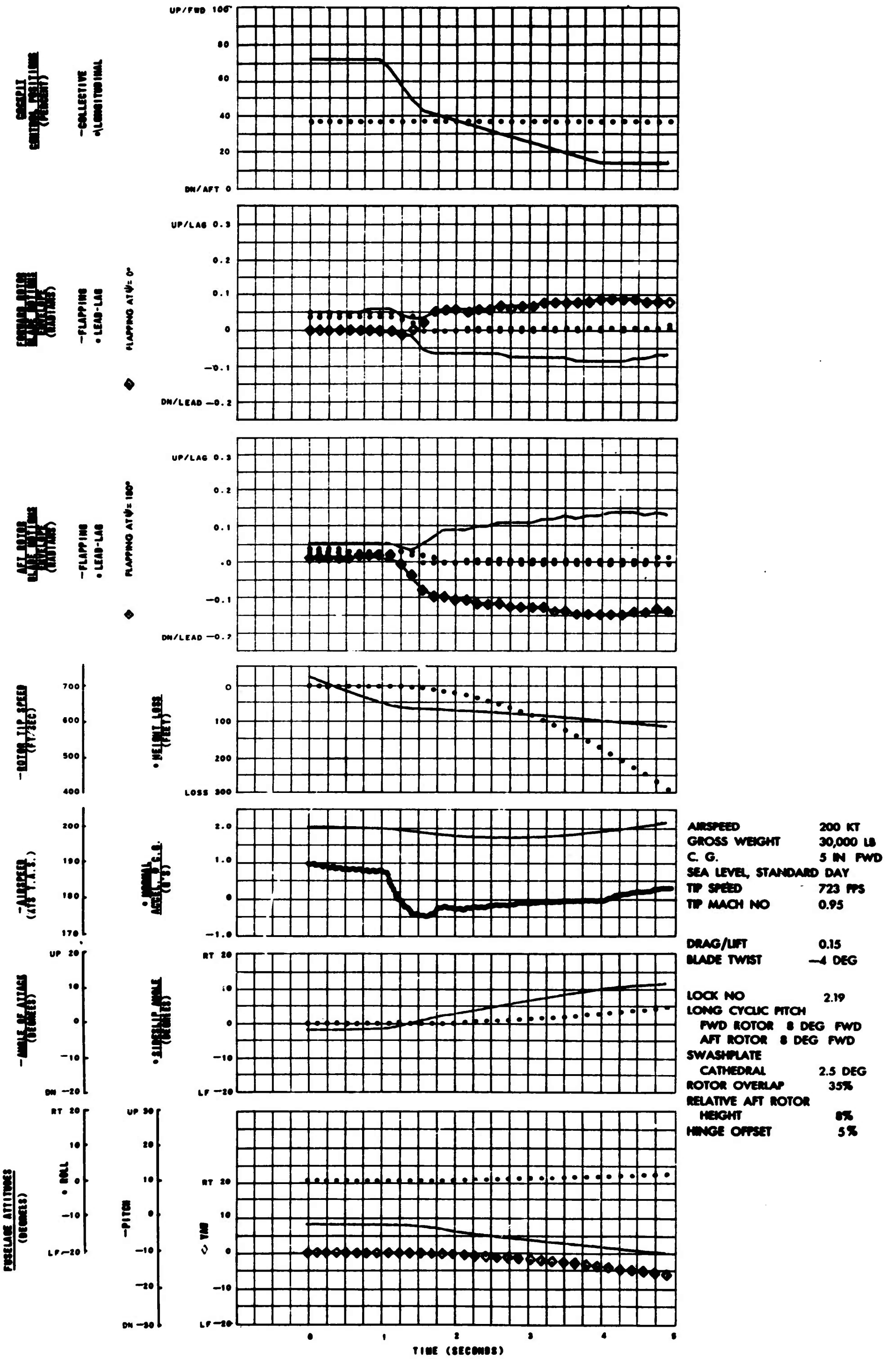

AIRSPEED	200 KT
GROSS WEIGHT	30,000 LB
C. G.	5 IN FWD
SEA LEVEL, STANDARD DAY	
TIP SPEED	723 FPS
TIP MACH NO	0.95
DRAG/LIFT	0.15
BLADE TWIST	—4 DEG
LOCK NO	2.19
LONG CYCLIC PITCH	
FWD ROTOR	8 DEG FWD
AFT ROTOR	8 DEG FWD
SWASHPLATE	
CATHEDRAL	2.5 DEG
ROTOR OVERLAP	35%
RELATIVE AFT ROTOR	
HEIGHT	8%
HINGE OFFSET	5%

Figure 96. Configuration 28 Except That Control Input Rate is Reduced by One-Half.

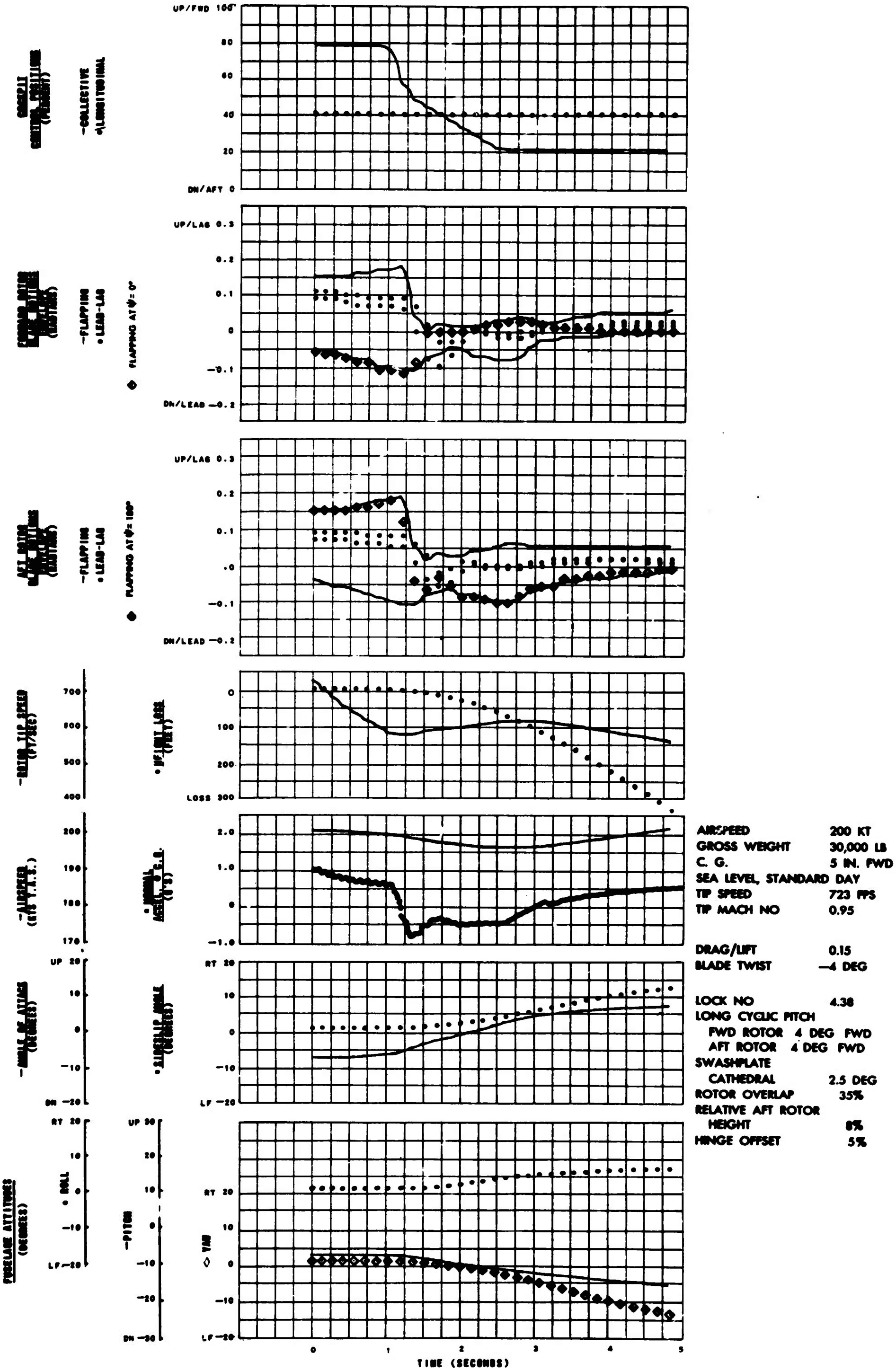

AIRSPEED	200 KT
GROSS WEIGHT	30,000 LB
C. G.	5 IN. FWD
SEA LEVEL, STANDARD DAY	
TIP SPEED	723 FPS
TIP MACH NO	0.95
DRAG/LIFT	0.15
BLADE TWIST	—4 DEG
LOCK NO	4.38
LONG CYCLIC PITCH	
FWD ROTOR	4 DEG FWD
AFT ROTOR	4 DEG FWD
SWASHPLATE	
CATHEDRAL	2.5 DEG
ROTOR OVERLAP	35%
RELATIVE AFT ROTOR	
HEIGHT	8%
HINGE OFFSET	5%

Figure 97. Configuration 30

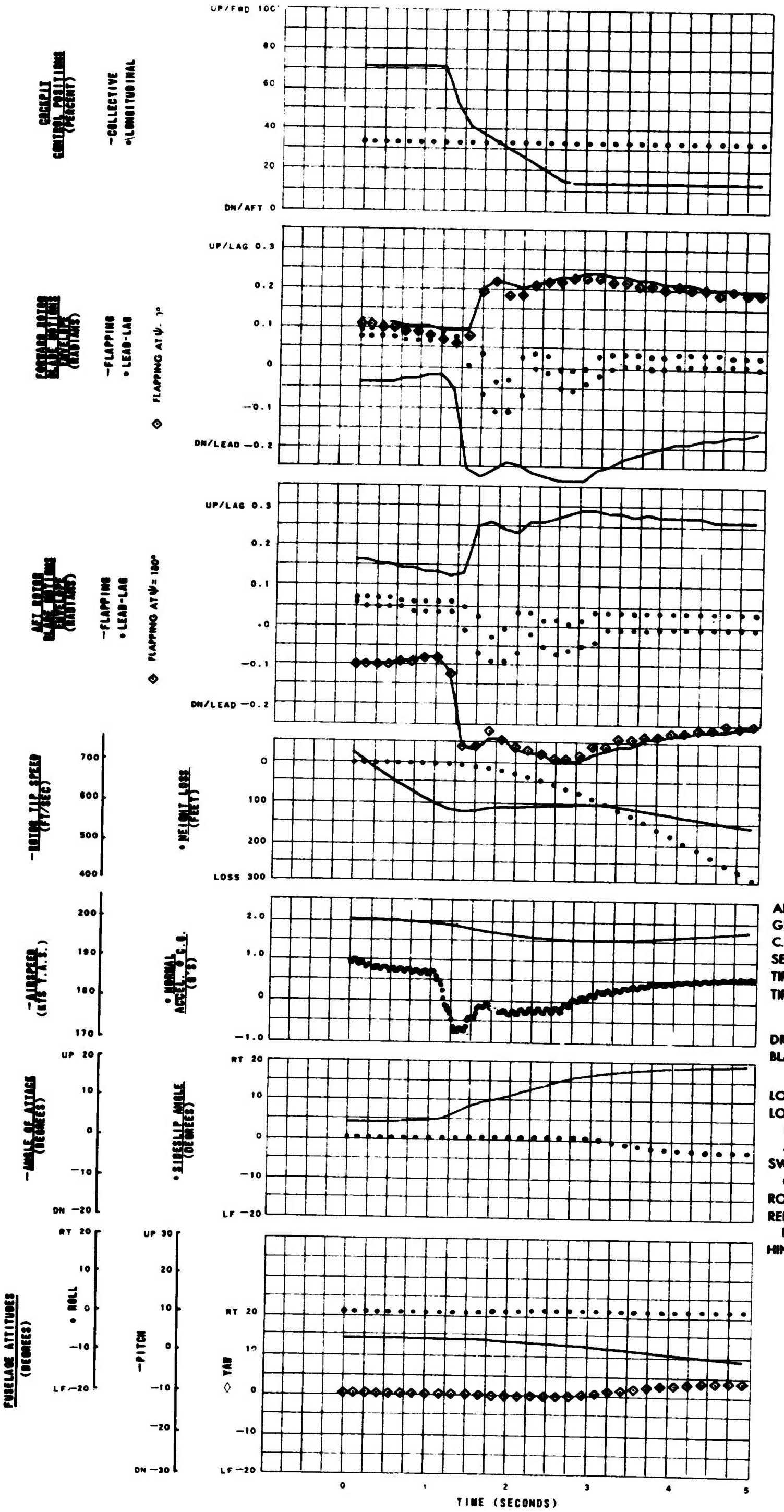

AIRSPEED	200 KT
GROSS WEIGHT	30,000 LB
C. G.	5 IN FWD
SEA LEVEL, STANDARD DAY	
TIP SPEED	723 FPS
TIP MACH NO	0.95
DRAG/LIFT	0.15
BLADE TWIST	—4 DEG
LOCK NO	4.38
LONG CYCLIC PITCH	
FWD ROTOR 14 DEG FWD	
AFT ROTOR 14 DEG FWD	
SWASHPLATE CATHEDRAL	2.5 DEG
ROTOR OVERLAP	35%
RELATIVE AFT ROTOR HEIGHT	8%
HINGE OFFSET	5%

Figure 98. Configuration 32.

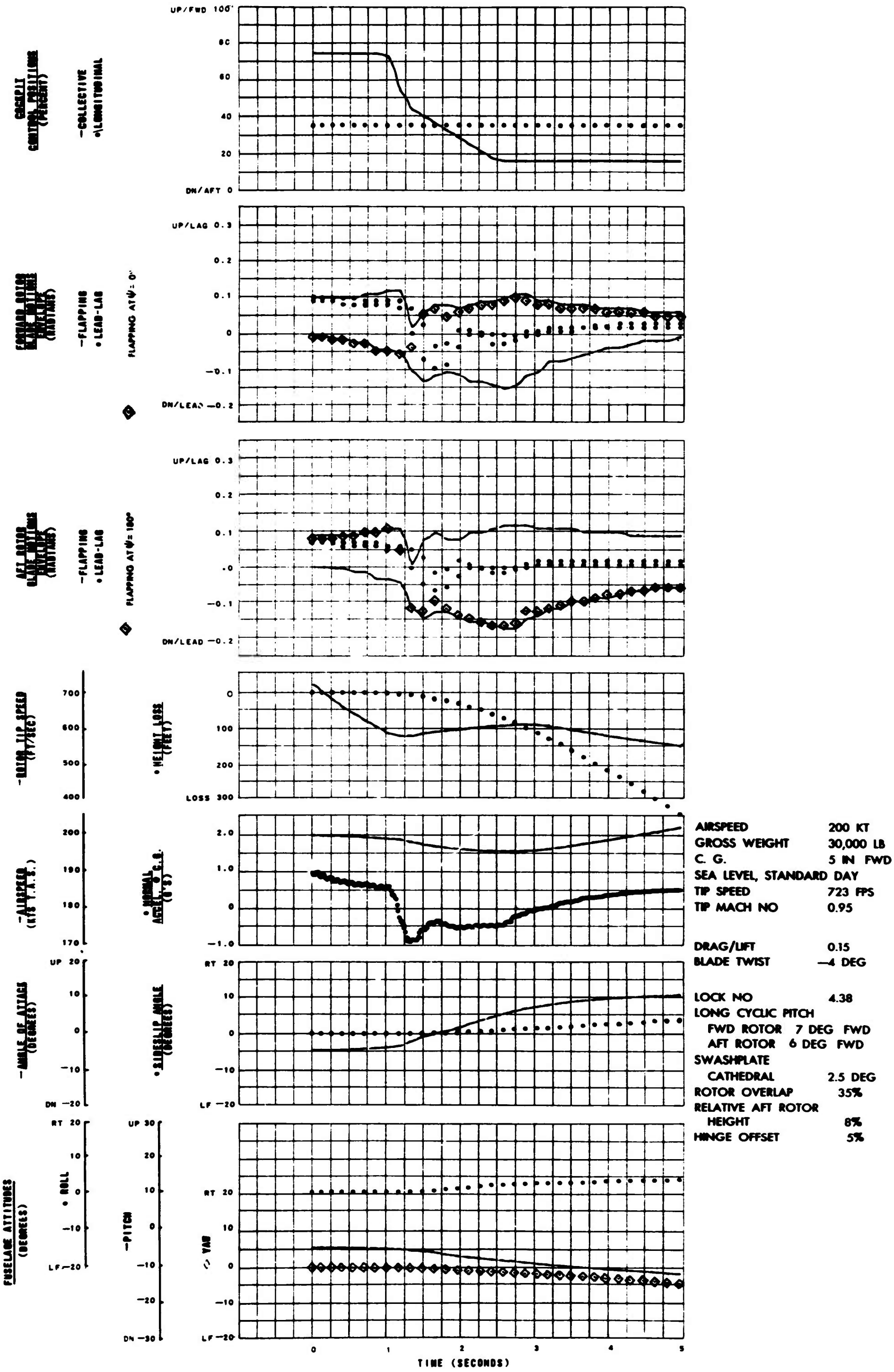

Figure 99. Configuration 6 Modified to have 7-Degree Forward Cyclic on Forward Rotor and 6-Degree Forward Cyclic on Aft Rotcr.

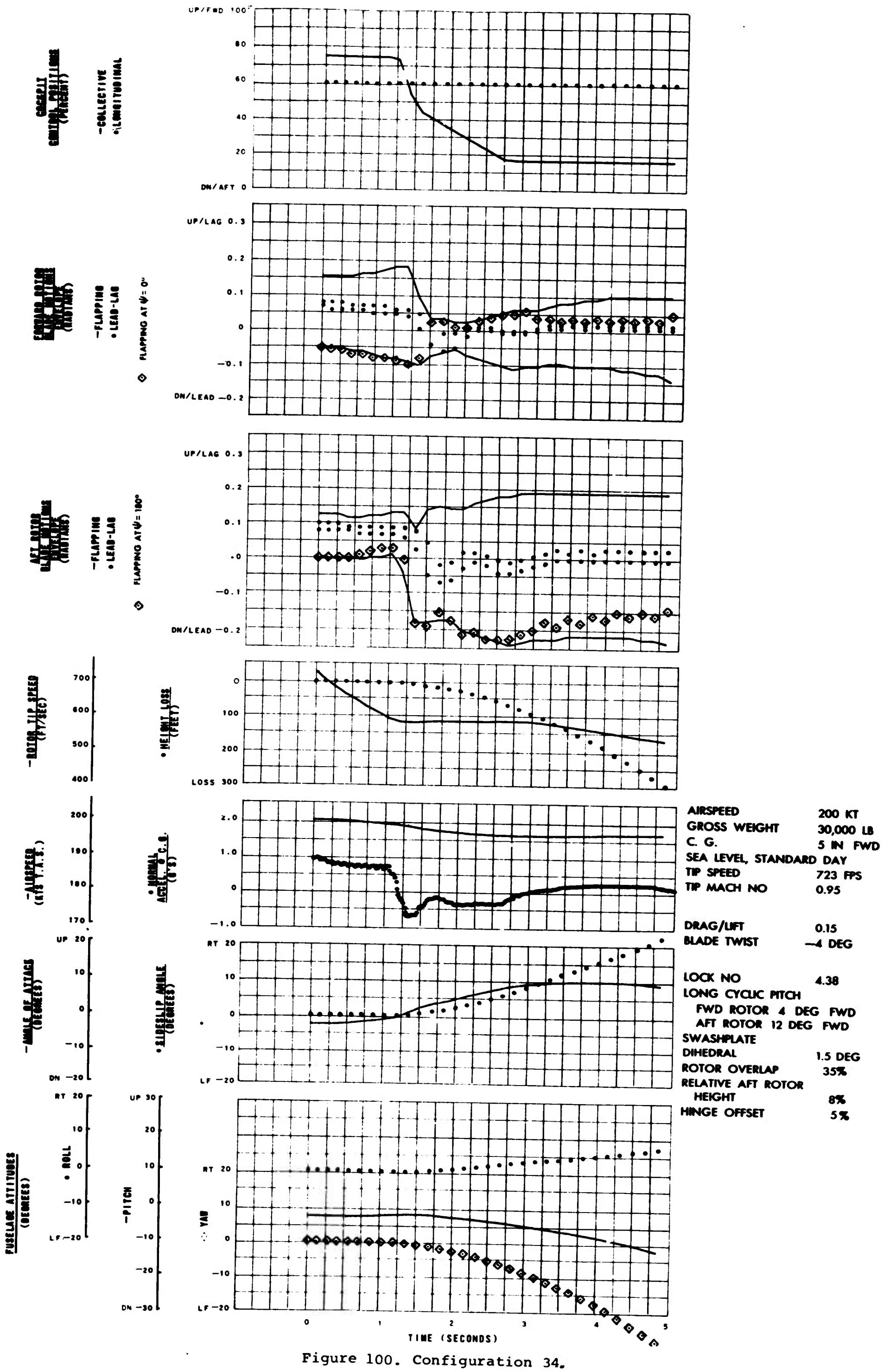

AIRSPEED	200 KT
GROSS WEIGHT	30,000 LB
C. G.	5 IN FWD
SEA LEVEL, STANDARD DAY	
TIP SPEED	723 FPS
TIP MACH NO	0.95
DRAG/LIFT	0.15
BLADE TWIST	—4 DEG
LOCK NO	4.38
LONG CYCLIC PITCH	
FWD ROTOR	4 DEG FWD
AFT ROTOR	12 DEG FWD
SWASHPLATE DIHEDRAL	1.5 DEG
ROTOR OVERLAP	35%
RELATIVE AFT ROTOR HEIGHT	8%
HINGE OFFSET	5%

Figure 100. Configuration 34.

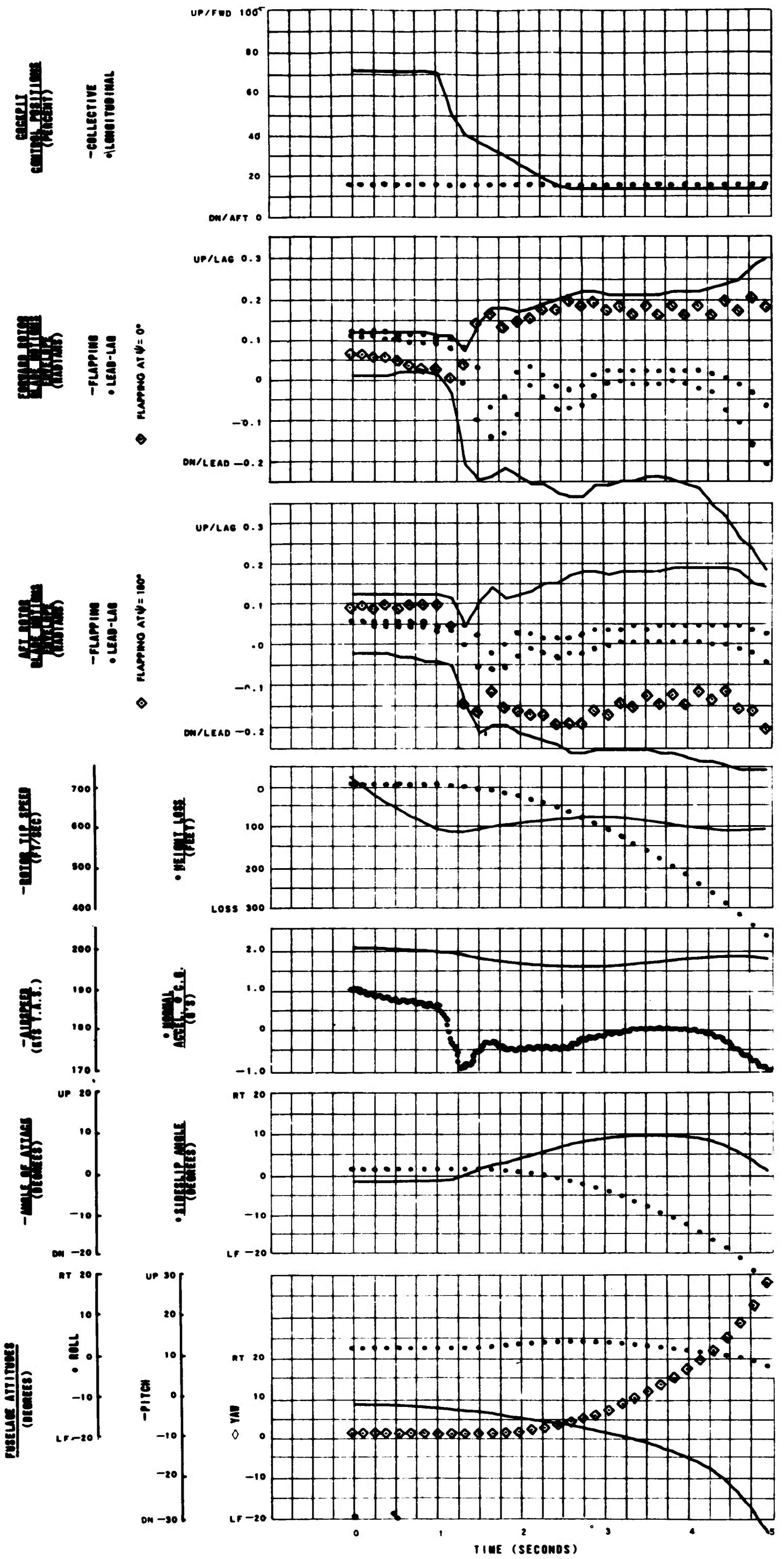

AIRSPEED	200 KT
GROSS WEIGHT	30,000 LB
C. G.	5 IN FWD
SEA LEVEL, STANDARD DAY	
TIP SPEED	723 FPS
TIP MACH NO	0.95
DRAG/LIFT	0.15
BLADE TWIST	—4 DEG
LOCK NO	4.38
LONG CYCLIC PITCH	
FWD ROTOR	12 DEG FWD
AFT ROTOR	4 DEG FWD
SWASHPLATE	
CATHEDRAL	6.5 DEG
ROTOR OVERLAP	35%
RELATIVE AFT ROTOR HEIGHT	8%
HINGE OFFSET	5%

Figure 101. Configuration 35

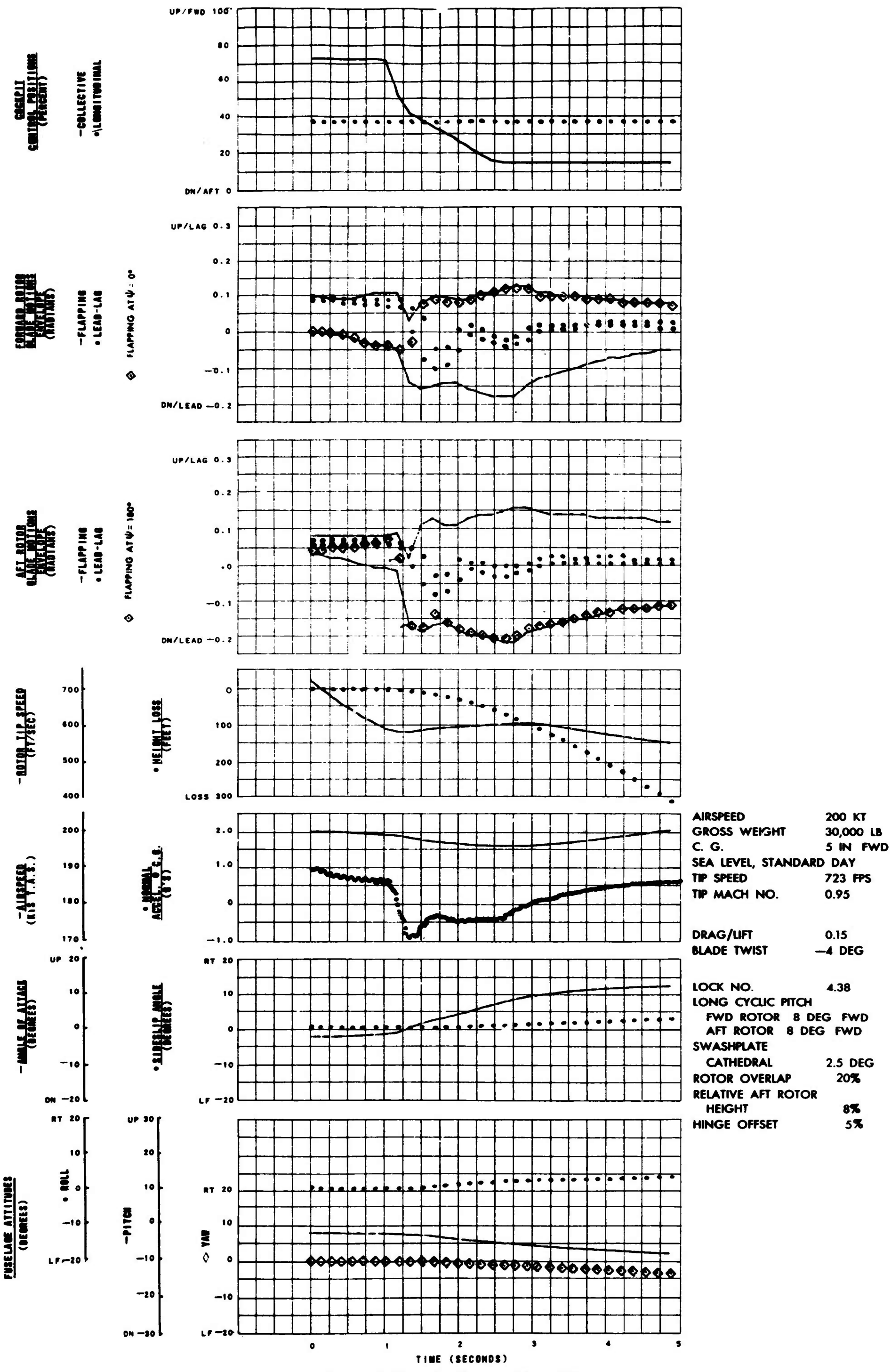

AIRSPEED	200 KT
GROSS WEIGHT	30,000 LB
C. G.	5 IN FWD
SEA LEVEL, STANDARD DAY	
TIP SPEED	723 FPS
TIP MACH NO.	0.95
DRAG/LIFT	0.15
BLADE TWIST	—4 DEG
LOCK NO.	4.38
LONG CYCLIC PITCH	
FWD ROTOR	8 DEG FWD
AFT ROTOR	8 DEG FWD
SWASHPLATE	
CATHEDRAL	2.5 DEG
ROTOR OVERLAP	20%
RELATIVE AFT ROTOR HEIGHT	8%
HINGE OFFSET	5%

Figure 102. Configuration 38.

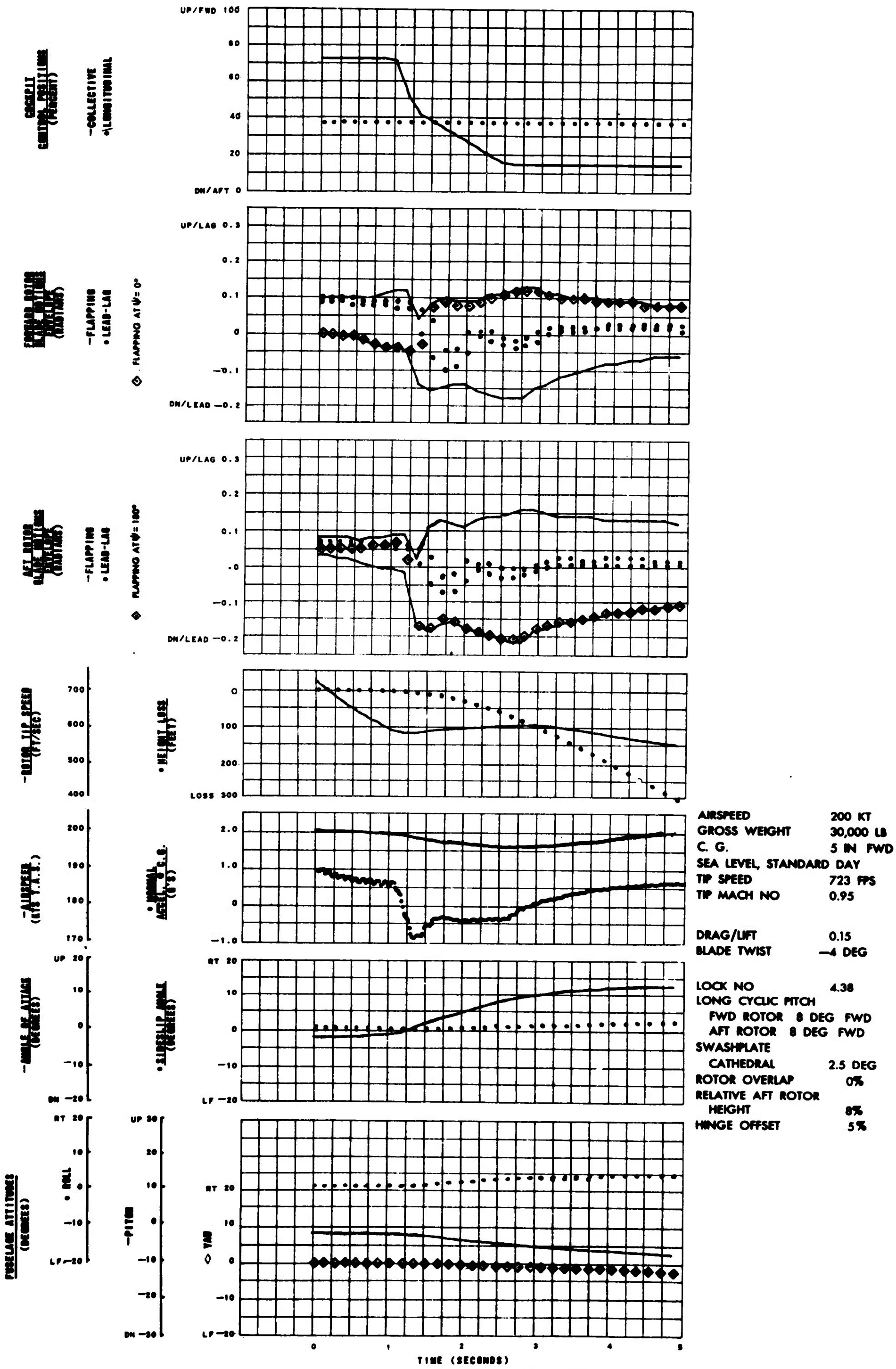

AIRSPEED	200 KT
GROSS WEIGHT	30,000 LB
C. G.	5 IN FWD
SEA LEVEL, STANDARD DAY	
TIP SPEED	723 FPS
TIP MACH NO	0.95
DRAG/LIFT	0.15
BLADE TWIST	—4 DEG
LOCK NO	4.38
LONG CYCLIC PITCH	
FWD ROTOR	8 DEG FWD
AFT ROTOR	8 DEG FWD
SWASHPLATE	
CATHEDRAL	2.5 DEG
ROTOR OVERLAP	0%
RELATIVE AFT ROTOR HEIGHT	8%
HINGE OFFSET	5%

Figure 103. Configuration 40.

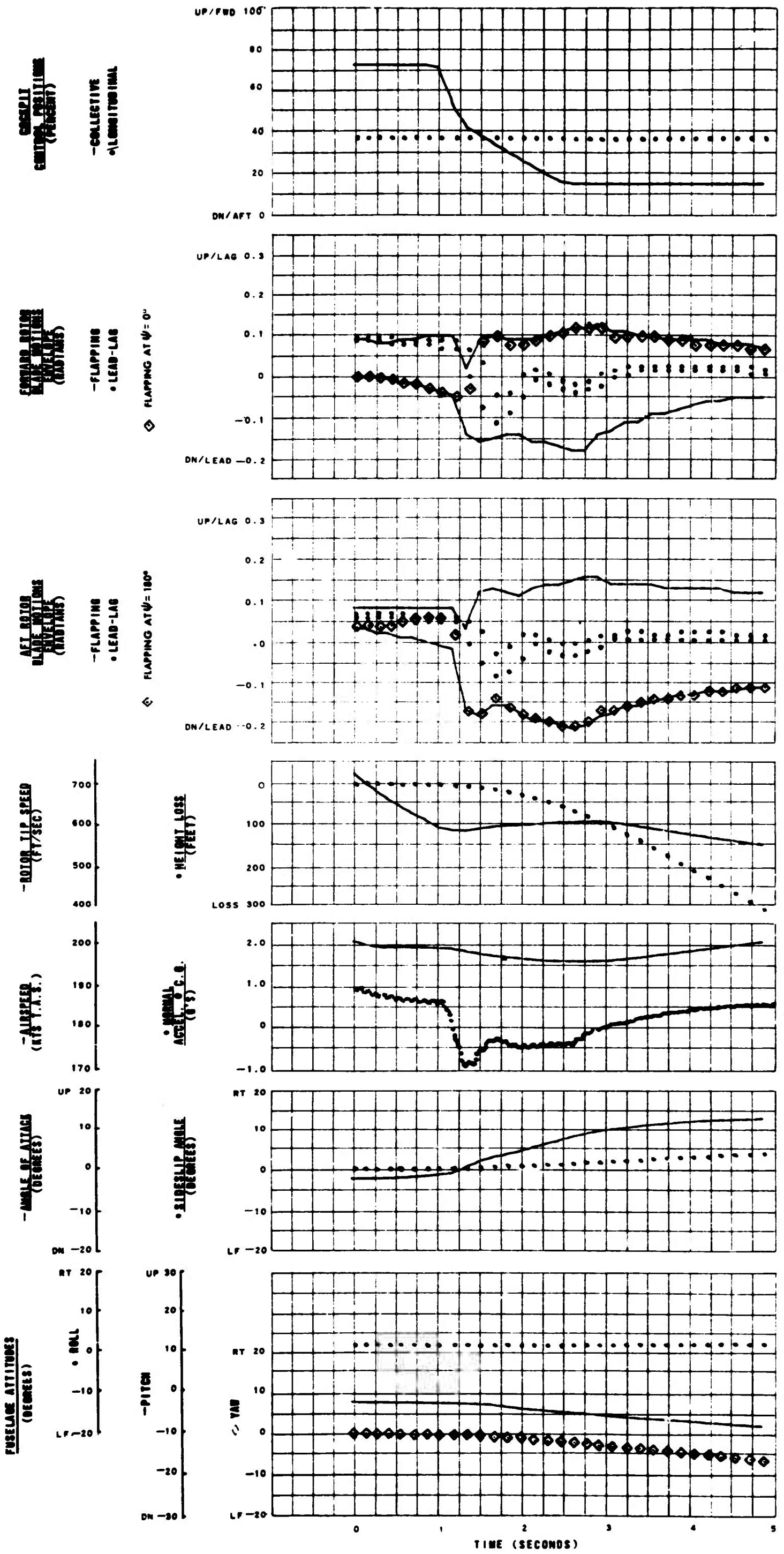

AIRSPEED	200 KT
GROSS WEIGHT	30,000 LB
C. G.	5 IN FWD
SEA LEVEL, STANDARD DAY	
TIP SPEED	723 FPS
TIP MACH NO	0.95
DRAG/LIFT	0.15
BLADE TWIST	−4 DEG
LOCK NO	4.38
LONG CYCLIC PITCH	
FWD ROTOR	8 DEG FWD
AFT ROTOR	8 DEG FWD
SWASHPLATE	
CATHEDRAL	2.5 DEG
ROTOR OVERLAP	35%
RELATIVE AFT ROTOR HEIGHT	20%
HINGE OFFSET	5%

Figure 104. Configuration 42.

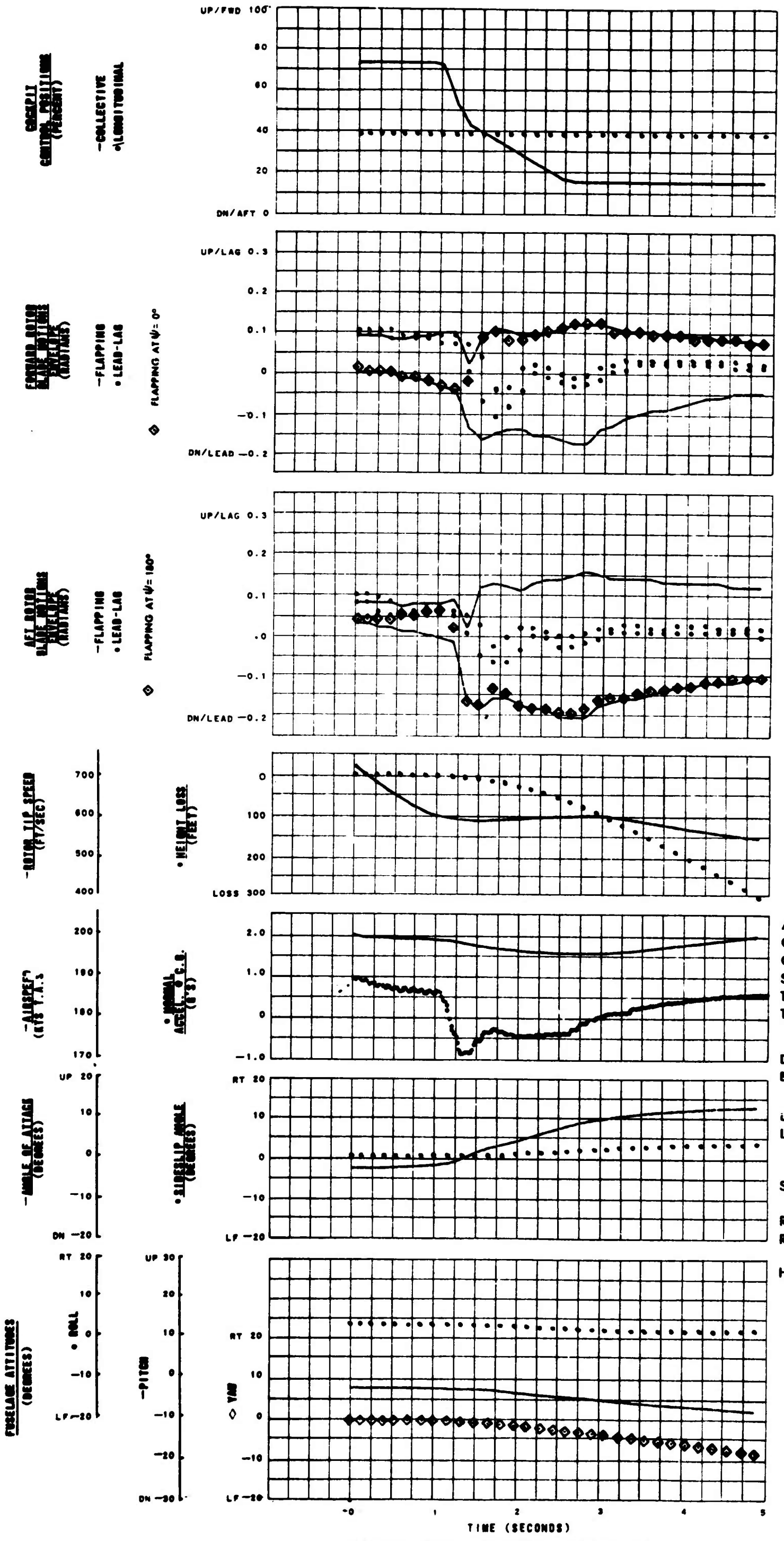

AIRSPEED	200 KT
GROSS WEIGHT	30,000 LB
C. G.	5 IN FWD
SEA LEVEL, STANDARD DAY	
TIP SPEED	723 FPS
TIP MACH NO	0.95
DRAG/LIFT	0.15
BLADE TWIST	—4 DEG
LOCK NO	4.38
LONG CYCLIC PITCH	
FWD ROTOR	8 DEG FWD
AFT ROTOR	8 DEG FWD
SWASHPLATE CATHEDRAL	2.5 DEG
ROTOR OVERLAP	35%
RELATIVE AFT ROTOR HEIGHT	30%
HINGE OFFSET	5%

Figure 105. Configuration 44.

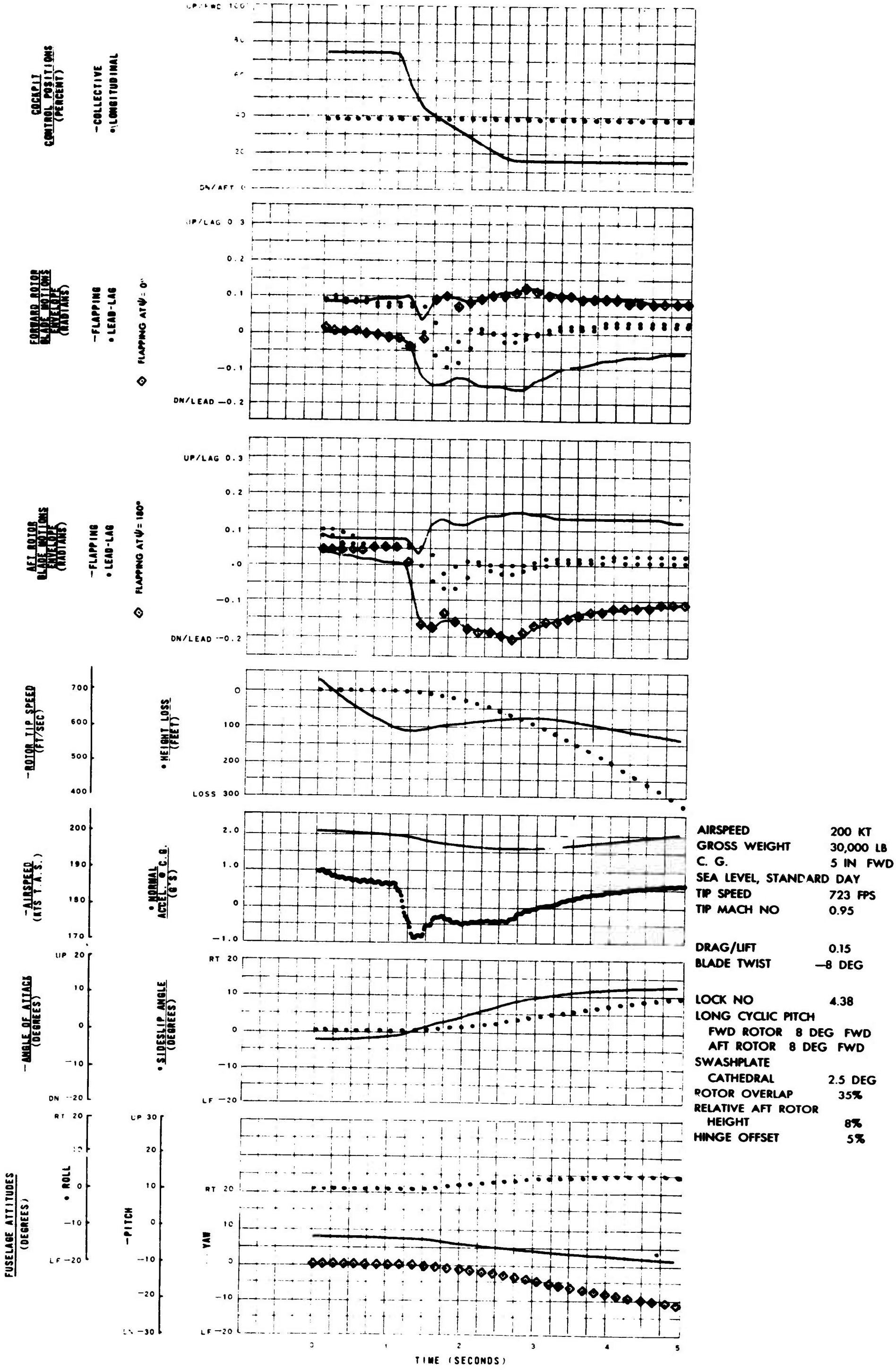

AIRSPEED	200 KT
GROSS WEIGHT	30,000 LB
C. G.	5 IN FWD
SEA LEVEL, STANDARD DAY	
TIP SPEED	723 FPS
TIP MACH NO	0.95
DRAG/LIFT	0.15
BLADE TWIST	—8 DEG
LOCK NO	4.38
LONG CYCLIC PITCH	
FWD ROTOR	8 DEG FWD
AFT ROTOR	8 DEG FWD
SWASHPLATE CATHEDRAL	2.5 DEG
ROTOR OVERLAP	35%
RELATIVE AFT ROTOR HEIGHT	8%
HINGE OFFSET	5%

Figure 106. Configuration 7.

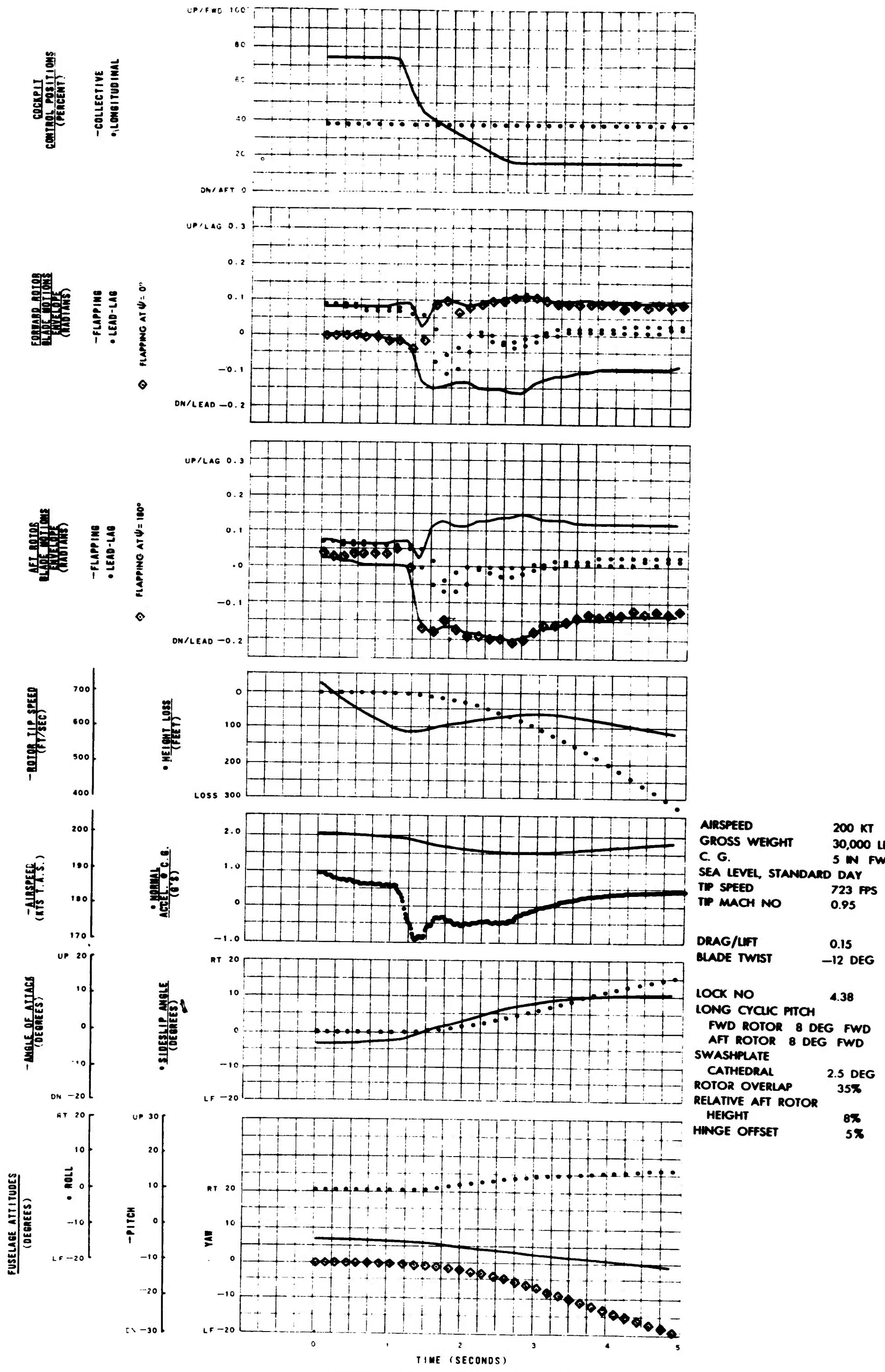

Figure 107. Configuration 8.

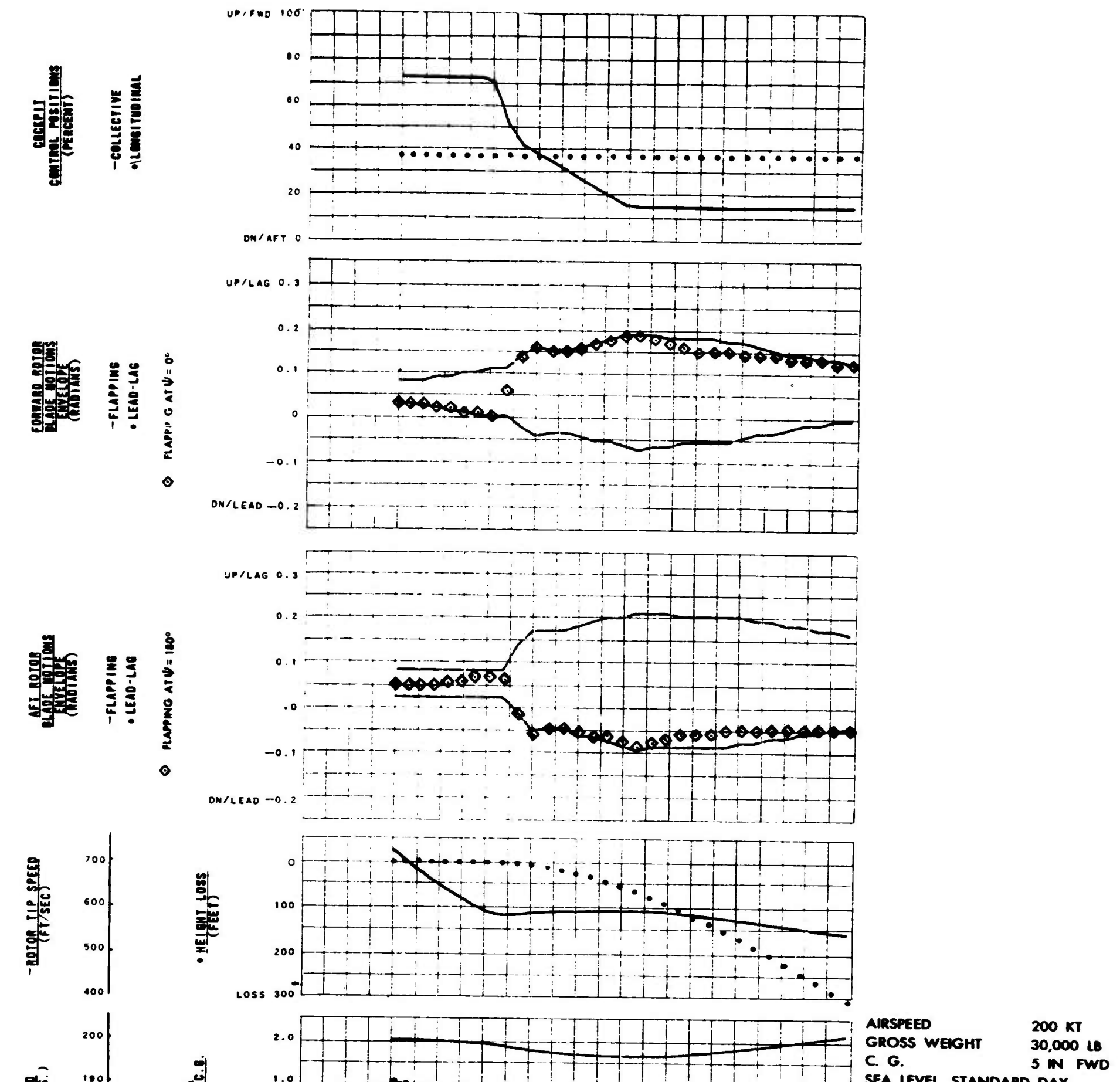

Figure 108. Configuration 14.

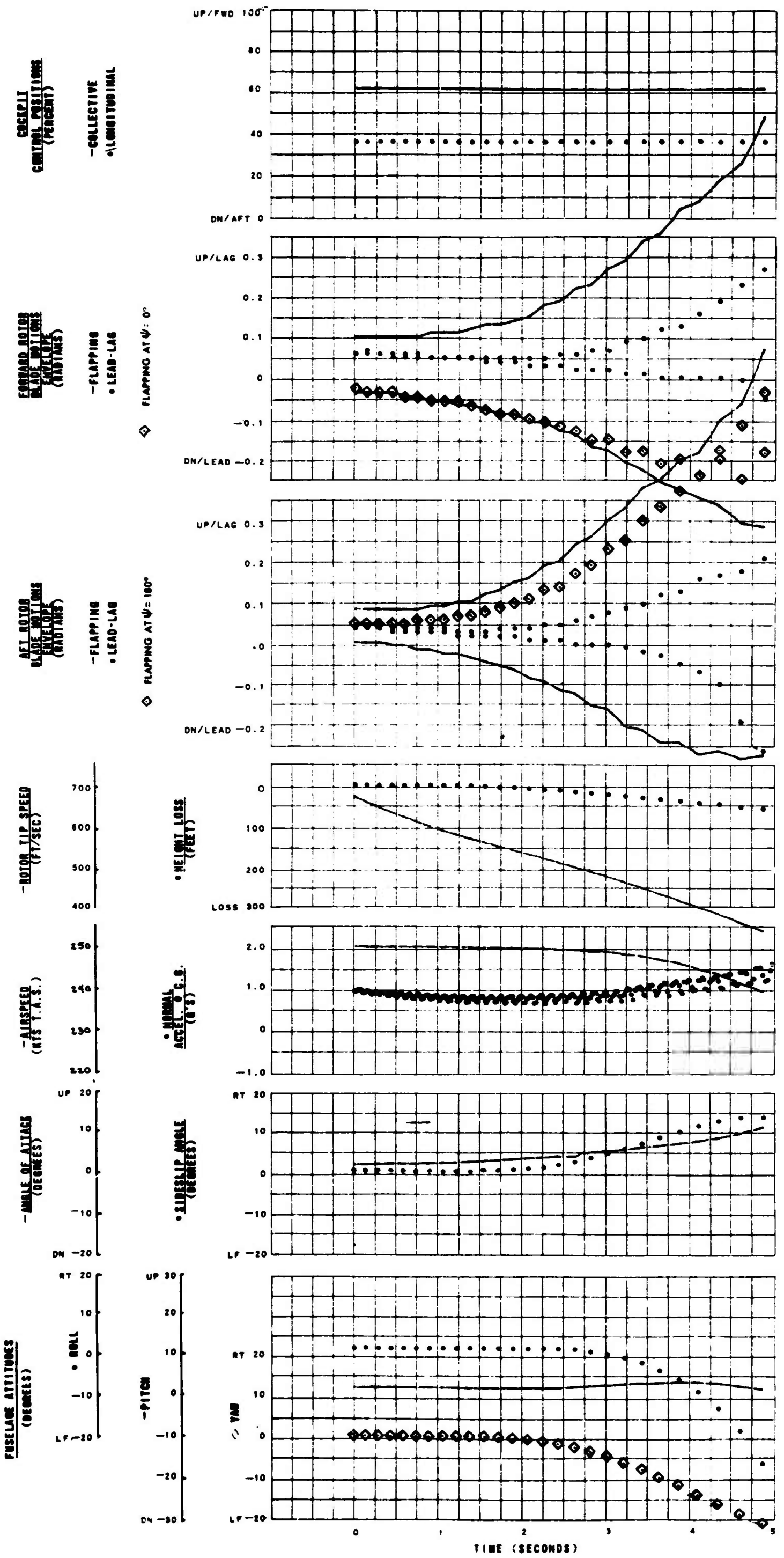

AIRSPEED	250 KT
GROSS WEIGHT	30,000 LB
C. G.	5 IN. FWD
SEA LEVEL, STANDARD DAY	
TIP SPEED	668 FPS
TIP MACH NO	0.975
DRAG/LIFT	0.0
BLADE TWIST	—12 DEG
LOCK NO	4.38
LONG CYCLIC PITCH	
FWD ROTOR	8 DEG FWD
AFT ROTOR	8 DEG FWD
SWASHPLATE CATHEDRAL	2.5 DEG
ROTOR OVERLAP	35%
RELATIVE AFT ROTOR HEIGHT	8%
HINGE OFFSET	5%

Figure 109. Configuration 45 -- No Control Input.

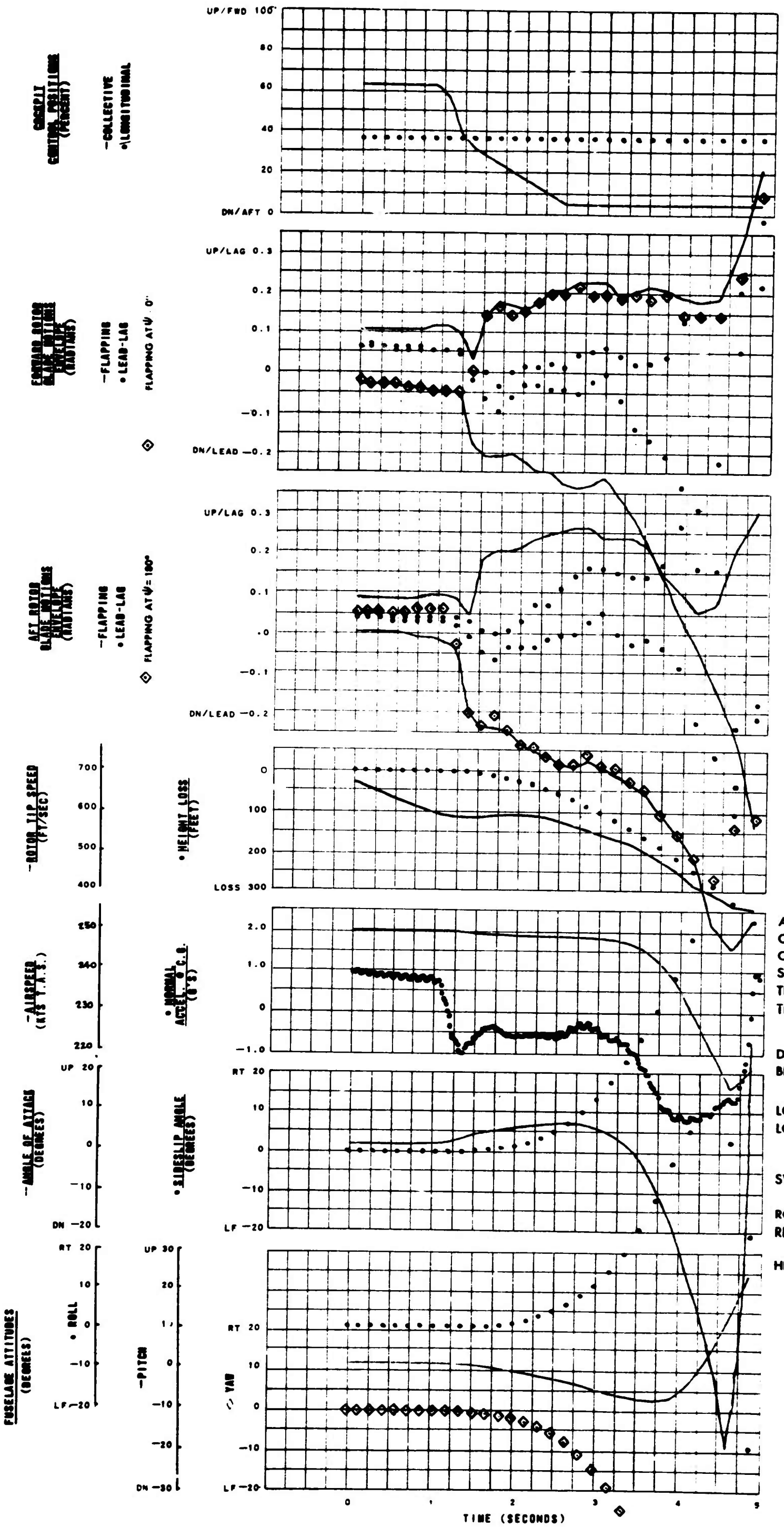

AIRSPEED	250 KT
GROSS WEIGHT	30,000 LB
C. G.	5 IN FWD
SEA LEVEL, STANDARD DAY	
TIP SPEED	668 FPS
TIP MACH NO	0.975
DRAG/LIFT	0.0
BLADE TWIST	—12 DEG
LOCK NO	4.38
LONG CYCLIC PITCH	
FWD ROTOR	8 DEG FWD
AFT ROTOR	8 DEG FWD
SWASHPLATE	
CATHEDRAL	2.5 DEG
ROTOR OVERLAP	35%
RELATIVE AFT ROTOR HEIGHT	8%
HINGE OFFSET	5%

Figure 110. Configuration 45 -- 5-Degree Input at 20 Degrees per Second followed by 5 Degrees at 4 Degrees per Second, 1.0-Second Delay Time.

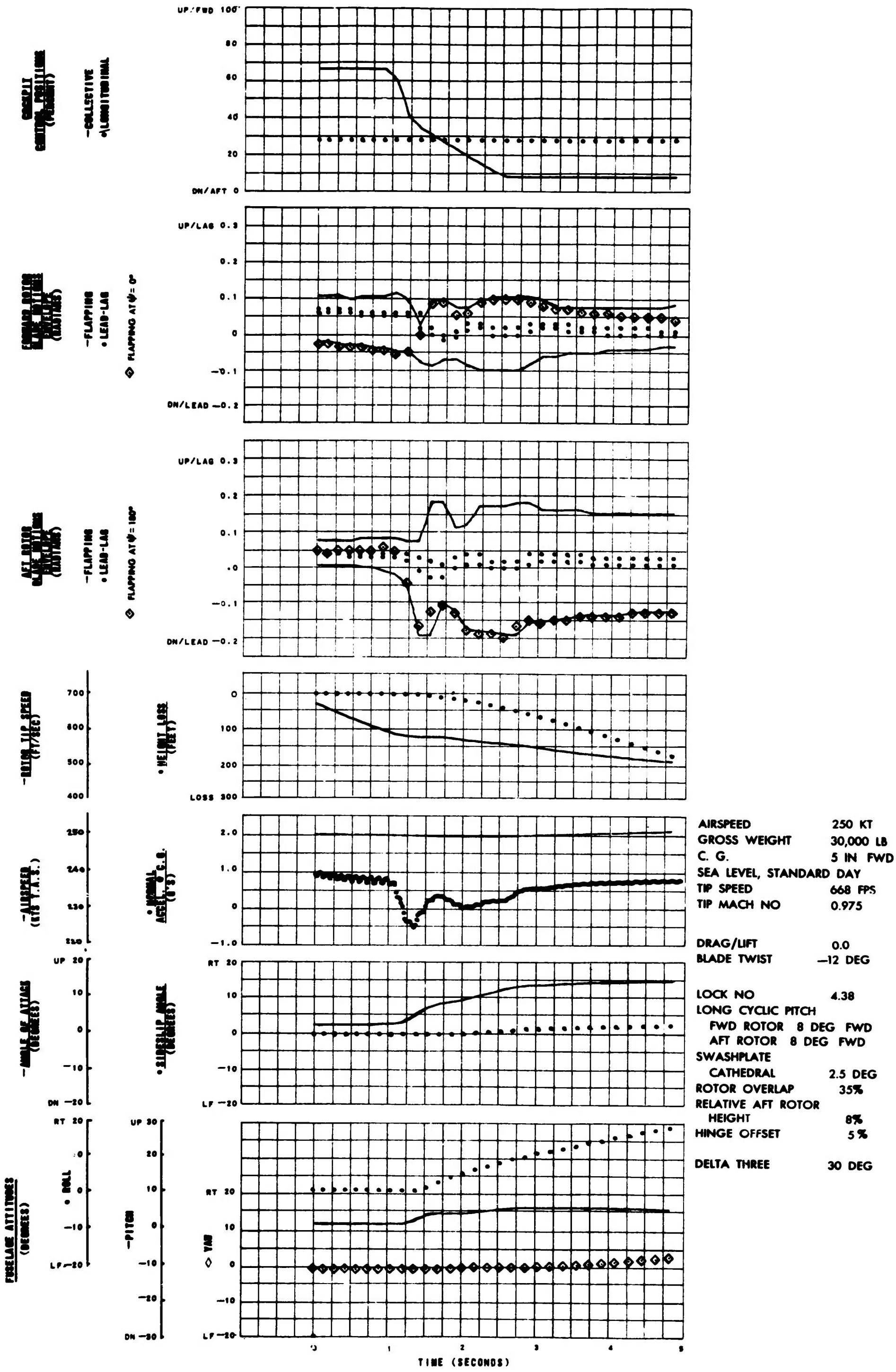

AIRSPEED	250 KT
GROSS WEIGHT	30,000 LB
C. G.	5 IN FWD
SEA LEVEL, STANDARD DAY	
TIP SPEED	668 FPS
TIP MACH NO	0.975
DRAG/LIFT	0.0
BLADE TWIST	—12 DEG
LOCK NO	4.38
LONG CYCLIC PITCH	
FWD ROTOR	8 DEG FWD
AFT ROTOR	8 DEG FWD
SWASHPLATE	
CATHEDRAL	2.5 DEG
ROTOR OVERLAP	35%
RELATIVE AFT ROTOR HEIGHT	8%
HINGE OFFSET	5%
DELTA THREE	30 DEG

Figure 111. Configuration 46 -- 5-Degree Input at 20 Degrees per Second followed by 5 Degrees at 4 Degrees per Second, 1.0-Second Delay Time.

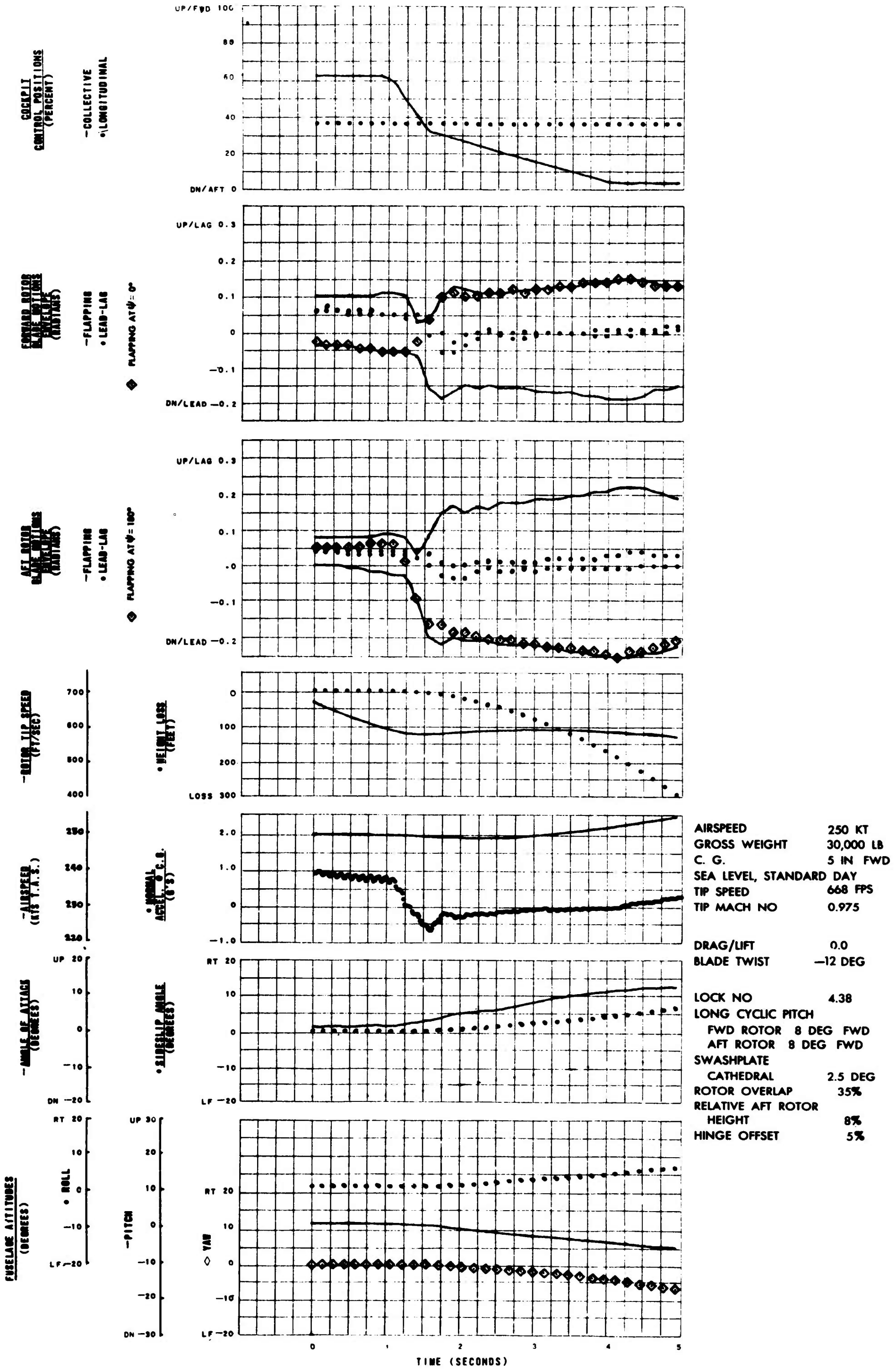

AIRSPEED	250 KT
GROSS WEIGHT	30,000 LB
C. G.	5 IN FWD
SEA LEVEL, STANDARD DAY	
TIP SPEED	668 FPS
TIP MACH NO	0.975
DRAG/LIFT	0.0
BLADE TWIST	—12 DEG
LOCK NO	4.38
LONG CYCLIC PITCH	
FWD ROTOR	8 DEG FWD
AFT ROTOR	8 DEG FWD
SWASHPLATE	
CATHEDRAL	2.5 DEG
ROTOR OVERLAP	35%
RELATIVE AFT ROTOR HEIGHT	8%
HINGE OFFSET	5%

Figure 112. Configuration 45 -- 5-Degree Input at 10 Degrees per Second followed by 5 Degrees at 2 Degrees per Second, 1.0-Second Delay Time.

Unclassified

Security Classification

DOCUMENT CONTROL DATA - R&D

(Security classification of title, body of abstract and indexing annotation must be entered when the overall report is classified)

1. ORIGINATING ACTIVITY (Corporate author)	2a. REPORT SECURITY CLASSIFICATION
The Boeing Company Vertol Division	Unclassified 2b. GROUP

3. REPORT TITLE

Study of Tandem Rotor Helicopter Dynamics Following Power Failure at High Speed

4. DESCRIPTIVE NOTES (Type of report and inclusive dates)

Final report on study conducted between 1 July 1964 and 31 March 1965

5. AUTHOR(S) (Last name, first name, initial)

Davis, J. M. Leone, P. F.
Kannon, J. F. McCafferty, H. A.

6. REPORT DATE	7a. TOTAL NO. OF PAGES	7b. NO. OF REFS
November 1965	288	7

8a. CONTRACT OR GRANT NO.	9a. ORIGINATOR'S REPORT NUMBER(S)
DA 44-177-AMC-239(T) b. PROJECT NO. Task 1D121401A14203 c. d.	USAAVLABS Technical Report 65-72 9b. OTHER REPORT NO(S) (Any other numbers that may be assigned this report) R-383

10. AVAILABILITY/LIMITATION NOTICES

Distribution of this document is unlimited.

11. SUPPLEMENTARY NOTES	12. SPONSORING MILITARY ACTIVITY
	US Army Aviation Materiel Laboratories Fort Eustis, Virginia

13. ABSTRACT

This report covers a parametric study of tandem rotor helicopter dynamics following power failure at high speed (200 knots plus).

It was concluded that complete loss of power on a high-speed helicopter results in hazardous flight conditions. Installation of auxiliary propulsion and incorporation of high-inertia rotor blades greatly relieve the situation by increasing the time available for the pilot to initiate recovery. Installation of a collective pitch rate limiter and an engine failure warning horn are recommended, to assist the pilot in taking corrective action. Provided collective pitch inputs are limited to safe values, no serious problems arise in the structural design of rotor blades to meet the conditions encountered in recovery from high-speed power failure. Dualization of engines and fuel systems provides an adequate margin of safety against sudden and complete power failure.

DD FORM 1 JAN 64 1473

Unclassified

Security Classification

Unclassified

Security Classification

14. KEY WORDS	LINK A		LINK B		LINK C	
	ROLE	WT	ROLE	WT	ROLE	WT
Helicopter Dynamics Following Power Failure						

INSTRUCTIONS

1. ORIGINATING ACTIVITY: Enter the name and address of the contractor, subcontractor, grantee, Department of Defense activity or other organization *(corporate author)* issuing the report.

2a. REPORT SECURITY CLASSIFICATION: Enter the overall security classification of the report. Indicate whether "Restricted Data" is included. Marking is to be in accordance with appropriate security regulations.

2b. GROUP: Automatic downgrading is specified in DoD Directive 5200.10 and Armed Forces Industrial Manual. Enter the group number. Also, when applicable, show that optional markings have been used for Group 3 and Group 4 as authorized.

3. REPORT TITLE: Enter the complete report title in all capital letters. Titles in all cases should be unclassified. If a meaningful title cannot be selected without classification, show title classification in all capitals in parenthesis immediately following the title.

4. DESCRIPTIVE NOTES: If appropriate, enter the type of report, e.g., interim, progress, summary, annual, or final. Give the inclusive dates when a specific reporting period is covered.

5. AUTHOR(S): Enter the name(s) of author(s) as shown on or in the report. Enter last name, first name, middle initial. If military, show rank and branch of service. The name of the principal author is an absolute minimum requirement.

6. REPORT DATE: Enter the date of the report as day, month, year; or month, year. If more than one date appears on the report, use date of publication.

7a. TOTAL NUMBER OF PAGES: The total page count should follow normal pagination procedures, i.e., enter the number of pages containing information.

7b. NUMBER OF REFERENCES: Enter the total number of references cited in the report.

8a. CONTRACT OR GRANT NUMBER: If appropriate, enter the applicable number of the contract or grant under which the report was written.

8b, 8c, & 8d. PROJECT NUMBER: Enter the appropriate military department identification, such as project number, subproject number, system numbers, task number, etc.

9a. ORIGINATOR'S REPORT NUMBER(S): Enter the official report number by which the document will be identified and controlled by the originating activity. This number must be unique to this report.

9b. OTHER REPORT NUMBER(S): If the report has been assigned any other report numbers *(either by the originator or by the sponsor)*, also enter this number(s).

10. AVAILABILITY/LIMITATION NOTICES: Enter any limitations on further dissemination of the report, other than those imposed by security classification, using standard statements such as:

(1) "Qualified requesters may obtain copies of this report from DDC."

(2) "Foreign announcement and dissemination of this report by DDC is not authorized."

(3) "U. S. Government agencies may obtain copies of this report directly from DDC. Other qualified DDC users shall request through _____."

(4) "U. S. military agencies may obtain copies of this report directly from DDC. Other qualified users shall request through _____."

(5) "All distribution of this report is controlled. Qualified DDC users shall request through _____."

If the report has been furnished to the Office of Technical Services, Department of Commerce, for sale to the public, indicate this fact and enter the price, if known.

11. SUPPLEMENTARY NOTES: Use for additional explanatory notes.

12. SPONSORING MILITARY ACTIVITY: Enter the name of the departmental project office or laboratory sponsoring *(paying for)* the research and development. Include address.

13. ABSTRACT: Enter an abstract giving a brief and factual summary of the document indicative of the report, even though it may also appear elsewhere in the body of the technical report. If additional space is required, a continuation sheet shall be attached.

It is highly desirable that the abstract of classified reports be unclassified. Each paragraph of the abstract shall end with an indication of the military security classification of the information in the paragraph, represented as *(TS)*, *(S)*, *(C)*, *or (U)*.

There is no limitation on the length of the abstract. However, the suggested length is from 150 to 225 words.

14. KEY WORDS: Key words are technically meaningful terms or short phrases that characterize a report and may be used as index entries for cataloging the report. Key words must be selected so that no security classification is required. Identifiers, such as equipment model designation, trade name, military project code name, geographic location, may be used as key words but will be followed by an indication of technical context. The assignment of links, rules, and weights is optional.

Unclassified

Security Classification